Characterization of a landslide-prone glaciolacustrine clay from the Thompson River Valley near Ashcroft, British Columbia

by

Gael Le Meil

A thesis submitted in partial fulfillment of the requirements for the degree of

Master of Science

in

Geotechnical Engineering

Department of Civil and Environmental Engineering

University of Alberta

© Gael Le Meil, 2017

Abstract

Several large landslides have occurred in the Thompson River Valley near Ashcroft, British Columbia. The movement of these landslides have presented challenges for the operation of the two national railways that traverse this valley. The landslides are multiple retrogressive, translational, slow-moving and occur within glaciolacustrine clay.

In this study, continuous core samples were collected from the Ripley slide (velocity in the order of 80 mm/year; volume 1.0×10^6 m^3) for characterizing the glaciolacustrine clay. The x-ray radiography and logging of the core revealed interbedded silt and clay, interpreted as a glaciolacustrine stratigraphic unit. It includes brown, fat, slickensided clay beds. The glaciolacustrine unit was found to be stiff and heavily overconsolidated ($\sigma'_p \geq 2000$ kPa). The objective of the laboratory tests was to characterize the shear behaviour and strength of the glaciolacustrine clay, in particular the pore water pressure response and development of residual shear strength. Direct shear, ring shear and direct simple shear (DSS) tests were conducted. Test results showed that clay-dominated beds have a greater potential for shear strength reduction than silt-dominated beds. Softening and orientation of platy clay particles in the direction of shear reduce the drained shear strength. After large strains were imposed in the direct shear and ring shear tests, slickenside-like shear surfaces were formed in clay-rich samples. At the Ripley slide, clay beds exhibit a low residual friction angle ($\varphi_r' = 12°$). Low residual shear strength was correlated with high plasticity ($LL = 84\%$).

Plastic clay-rich beds are weak soil horizons. Where they are persistent, they are the preferential location for retrogressive failures to occur. Two such clay beds are responsible for the major landslides of the Thompson River Valley. These clay beds were found to host the Ripley slide's active rupture surfaces (elevations 257.3 and 268.8 m).

Acknowledgements

I am deeply grateful to Dr. M.T. Hendry and Dr. C.D. Martin for their supervision during this thesis work. They have given invaluable ideas and enthusiasm for the development of this project. Their guidance, patience and financial support were essential in achieving the objectives of this research.

Gratitude is extended to the professors of the geotechnical group, who have contributed to my personal and professional development. My interest in geotechnical engineering became greater during my studies at the University of Alberta.

I am sincerely thankful to Christine Hereygers, Gilbert Wong and Lucas Duerksen for providing technical support in the University of Alberta laboratory. I am grateful to Dr. R. Macciotta for his help in this project. I also thank Paul Sully and his colleagues of MEG Technical Services for their collaboration.

My appreciation is extended to Tom Edwards (Canadian National), Eddie Choi (Canadian Pacific) and David Huntley (Geological Survey of Canada) for their collaboration.

This research was made possible through the Railway Ground Hazard Research Program, funded by the Natural Sciences and Engineering Research Council of Canada (NSERC), Canadian Pacific, Canadian National and Transport Canada. The financial support of these organizations is largely appreciated.

I am grateful to colleagues Matthew Schafer, Jeffrey Journault, Eric Leishman and Chris Davies for making friendly my time at the university. I thank my friend Mathieu Estellon for his continuous encouragement. Finally, I thank my parents and my brother for their love and support.

Table of Contents

Chapter 1. Introduction..1

1.1 Context..1
1.2 Objectives..2
1.3 Organization of thesis..3

Chapter 2. Literature Review on Glaciolacustrine Clays..5

2.1 Glaciolacustrine clay..5
2.2 Soil mechanics considerations..8
  2.2.1 Anisotropy..8
  2.2.2 Overconsolidation..8
  2.2.3 Mechanisms of strength loss in stiff fissured clays..11
  2.2.4 Slope instability..11
2.3 Laboratory tests..13
  2.3.1 Sample size..13
  2.3.2 Ring shear..13
  2.3.3 Direct shear..14
  2.3.4 Undrained direct simple shear..14

Chapter 3. Description of the Thompson River Valley Landslides..17

3.1 Thompson River Valley landslides..17
  3.1.1 History..17
  3.1.2 Geology..18
  3.1.3 Landslide mechanism..19
3.2 The Ripley slide..21
  3.2.1 Description..21
  3.2.2 Site investigations..23

Chapter 4. Methodology, from Core Samples to Shear Strength Testing..25

4.1 Field work 25
4.1.1 Drilling 25
4.1.2 Instrumentation 27
4.2 Core usage 28
4.2.1 Preservation 28
4.2.2 X-ray radiography 29
4.2.1 Logging 29
4.2.2 Assessment of sampling disturbance 30
4.2.3 Sample selection 33
4.3 Laboratory testing program 34
4.3.1 Soil classification 34
4.3.2 X-ray diffraction 36
4.3.1 Intact sample preparation 36
4.3.2 Oedometer tests 37
4.3.3 Direct shear tests 38
4.3.4 Ring shear tests 40
4.3.5 Soil extrusion issue 42
4.3.6 Direct simple shear tests 47
Chapter 5. Results: Borehole Stratigraphy and Shear Strength of Soils 52
5.1 Soil description 52
5.1.1 General 52
5.1.2 Borehole stratigraphy 56
5.1.3 Slope inclinometer surveys 59
5.2 Laboratory tests results 60
5.2.1 Index properties 60
5.2.2 Mineralogy 64
5.2.3 Consolidation properties 67
5.2.4 Drained “intact” shear strength 68
5.2.5 Drained residual shear strength 72
5.2.6 Undrained shear strength 76
Chapter 6. Interpretation: Weak Clay Horizons 79

6.1 Stratigraphy 79
6.1.1 Glaciolacustrine Unit 2 79
6.1.2 Till Unit 6 80
6.2 Shear surfaces within glaciolacustrine Unit 2 81
6.2.1 Slickensides 81
6.2.2 Persistence 83
6.3 Shear strength of glaciolacustrine Unit 2 84
6.3.1 Drained intact shear strength 84
6.3.2 Undrained shear strength 85
6.3.3 Operating shear strength 87
6.4 Weak clay horizons of glaciolacustrine Unit 2 93
Chapter 7. Conclusion 95
7.1 Summary 95
7.2 Contributions of the thesis 96
7.3 Implications 96
7.4 Suggestions for further research 97
Bibliography 98
Appendices 106
Appendix A. Table summary of testing program 107
Appendix B. Core photographs and radiographs 108
Appendix C. Core logs 110
Appendix D. X-ray diffractograms 113
Appendix E. Oedometer test time-deformation results 117
Appendix F. Direct shear test results 119
Appendix G. Ring shear test results 136
Appendix H. Mohr-Coulomb strength criteria 147
Appendix I. Direct simple shear test results 153
Appendix J. Direct simple shear (DSS) testing of a very stiff glaciolacustrine clay 157

List of Tables

Table 4.1. Parameters of boreholes 27

Table 4.2. Parameters of the DSS tests 49

Table 5.1. Specific gravity results 64

Table 5.2. Consolidation properties 68

Table 5.3. Compression index estimates 68

Table 5.4. Direct shear test results 70

Table 5.5. Mohr-Coulomb parameters for peak effective shear strength 71

Table 5.6. Ring shear test results 75

Table 5.7. Residual friction angle ϕ_r' 76

Table 5.8. DSS Test S6a results 78

List of Figures

Figure 1.1. Map of southern British Columbia showing the railway network (modified from Natural Resources Canada 2017) and the location of the Thompson River Valley landslides....... 2

Figure 2.1. Extent of glaciolacustrine deposits in British Columbia..7

Figure 2.2. Overconsolidation of clay 9

Figure 2.3. Shear behaviour of normally and over-consolidated clay... 9

Figure 2.4. Shear strains in test specimens 14

Figure 2.5. A DSS-relevant problem..16

Figure 2.6. Difference in stress state between (a) the DSS apparatus and (b) the idealized simple shear..16

Figure 3.1. Generalized stratigraphy of the Thompson River Valley at Ashcroft (modified from Clague and Evans 2003)...18

Figure 3.2. Location of landslides in the Thompson River Valley (modified from Hendry et al. 2015) 22

Figure 3.3. 2016 aerial photograph of the Ripley slide (courtesy of CN) 23

Figure 4.1. Location of boreholes and instrumentation (modified from Hendry et al. 2015)...... 26

Figure 4.2. BH15-01 drilling location, looking north 26

Figure 4.3. (a) On-site core sealing operations; (b) preserved core runs in core box 28

Figure 4.4. X-ray radiographs of (a) lamination (BH15-03 depth 14.5 m) and (b) disturbed core suggesting a twisting motion (BH15-03 depth 15.7 m); numbered lead markers indicate distance from top of core run.. 30

Figure 4.5. Erosion-like superficial disturbance as seen on (a) x-ray radiograph and (b) photograph (BH15-03 depth 10.5 m) 31

Figure 4.6. Core split along glossy surface (BH15-03 depth 12.9 m) 32

Figure 4.7. Drilling-induced slickensides: (a) BH15-03 depth 9.6 m; (b) BH15-03 depth 10.2 m 32

Figure 4.8. Phases of core handling: (a) on-site conditioning; (b) logging; (c) sample selection 33

Figure 4.9. Front-loading oedometer 37

Figure 4.10. Direct shear apparatus 39

Figure 4.11. Ring shear apparatus 41

Figure 4.12. Soil extrusion in the direct shear apparatus 43

Figure 4.13. One-sided soil extrusion on direct shear test Specimen S35_1 44

Figure 4.14. Asymmetrical response on direct shear test S46_1 (gap: 0.20 mm) stress-strain plot 44

Figure 4.15. Soil extrusion in the ring shear apparatus 46

Figure 4.16. Response on ring shear test S250_a stress-strain plot 46

Figure 4.17. DSS apparatus pedestal, bottom platen with pins, stack of confining rings and membrane 48

Figure 4.18. DSS apparatus schematic 48

Figure 4.19. Effective stress paths for DSS tests S6a (1%/hour) and S6b (5%/hour) 51

Figure 5.1. Varves as seen in a photograph and radiograph: (a) BH15-03 depth 12.7 m; (b) BH15-01 depth 9.8 m 53

Figure 5.2. (a) Mottled clay at BH15-03 depth 9.8 m (different soil colors indicated); (b) disrupted bedding at BH15-01 depth 10.7 m; (c) sand lamina at BH15-03 depth 10.7 m (transverse view); (d) contorted sand laminae at BH15-01 depth 7.4 m (contortion underlined) 54

Figure 5.3. Fissured and weathered clay: (a, b) BH15-01 depth 4.7 m; (c) BH15-01 depth 5.7 m 55

Figure 5.4. Slickensides: (a) BH15-03 depth 8.6 m; (b) BH15-03 depth 13.0 m; (c) BH15-03 depth 9.2 m; (d) BH15-01 depth 7.7 m; (e) BH15-01 depth 13.1 m 57

Figure 5.5. Core description of BH15-03 from a depth of 9.0 to 9.7 m (shear zone) 58

Figure 5.6. Cumulative displacement measured from inclinometers installed in 2015.............. 60

Figure 5.7. Results for BH15-03 samples, against depth..61

Figure 5.8. Plasticity chart 62

Figure 5.9. Particle size distribution... 63

Figure 5.10. Activity chart, typical values of common clay minerals (Skempton 1984) plotted for comparison 63

Figure 5.11. S33 (BH15-03 depth 9.1 m) diffractogram: minerals interpreted from reflection peaks are given (with corresponding spacing) 66

Figure 5.12. Oedometer tests on (a) BH13-01 and (b) BH15-03 samples 67

Figure 5.13. Stress-strain results of direct shear tests on BH15-03 intact samples: (a) S38 (depth 10.4 m); (b) S42 (depth 14.2 m)... 69

Figure 5.14. Mohr-Coulomb peak shear strength of samples S31, S33, S38 and S42 72

Figure 5.15. Stress-strain results of ring shear tests on BH15-03 samples: (a) S32 (depth 8.9 m); (b) S33 (depth 9.1 m) 73

Figure 5.16. Multiple-rate ring shear tests on S31 (depth 8.9 m)... 74

Figure 5.17. Variation of the residual shear strength in multiple-rate ring shear tests............... 74

Figure 5.18. Mohr-Coulomb shear strength of Sample S33 76

Figure 5.19. Stress path results of DSS tests on BH13-01 samples: (a) S4 (depth 13.4 m); (b) S6 (depth 17.5 m)... 78

Figure 6.1. Cross-section of the Ripley slide 79

Figure 6.2. BH15-03 results: (a) stratigraphy; (b) slope inclinometer displacement; (c) natural water content; (d) Atterberg limits; (e) residual shear strength derived from direct shear and ring shear tests.. 82

Figure 6.3. Horizon elevation throughout the Thompson River Valley landslides 84

Figure 6.4. Normalized undrained shear strength for the Ripley and other clays 86

Figure 6.5. Ring shear tests S32_a (elevation 269.1 m) and S33_b (elevation 268.9 m) 89

Figure 6.6. Peak to residual shear strength domains for samples S31 (elevation 269.6 m) and S38 (elevation 267.6 m) 90

Figure 6.7. Correlation between PI and residual friction angle 92

Chapter 1. Introduction

1.1 CONTEXT

The stretch of the Thompson River Valley immediately south of Ashcroft, British Columbia, is noted for its numerous large landslides. Thirteen major landslides are located within a 10-km stretch, 12 of which are crossed by railway tracks (Figure 1.1).

The Canadian Pacific (CP) and Canadian National (CN) railways were built through the Thomson River Valley in 1885 and 1915, respectively. Since then, these landslides have posed a challenge to the operation of railways. This section of the Thompson River Valley in southern British Columbia is a major transportation corridor occupied by both of Canada's Class I railroads. The transport of goods between Canada's west coast and the rest of the continent is dependent on this corridor, making it an artery of vital importance for Canada's economy. Landslides in the Thompson River Valley have disrupted rail service many times. The continued movement and potential reactivation of these landslides will continue to challenge railways in the future.

More than a century ago, Stanton (1898) began reporting on landslides that adversely affected the operation of the CP railway. Most slope failures observed at the time were attributed to the excessive irrigation of the farmlands on the terraces located just upslope. Stanton (1898) noted the periodical movement of some slides, suggesting these slides were reactivations.

The semi-arid climate of the southern Interior Plateau of British Columbia means that irrigation is necessary for agriculture. During the 20th century, irrigation practices evolved and became more water-efficient. The ditch-and-furrow flooding method was replaced with the sprinkler technique (Porter et al. 2002). Slope movements have continued to occur, but the triggers and velocities are different. Events of the 20th century and until now have been very slow landslide reactivations, with the exception of the rapid Goddard slide reactivation in 1982 (Eshraghian et al. 2007). Ongoing maintenance is required to ensure that railway tracks are in operating condition, as they lie directly on the surface of the unstable slopes. In response to these hazards, a large amount of geotechnical investigation has been carried out in the area, in order to mitigate the risk associated with the landslides.

The focus of the present study is on the Ripley slide that is slow-moving and relatively small when compared to other Thompson River Valley landslides (velocity in the order of 80 mm/year; volume 1.0 × 10^6 m^3). The landslide is translational and the failure plane is within a glaciolacustrine clay, like the other Thompson River Valley landslides (Eshraghian et al. 2007). The Ripley slide is located on the eastern bank of the river and is traversed by both the CP and CN mainlines. Geotechnical investigation and instrumentation at this particular site were started in 2005, when the landslide was reactivated.

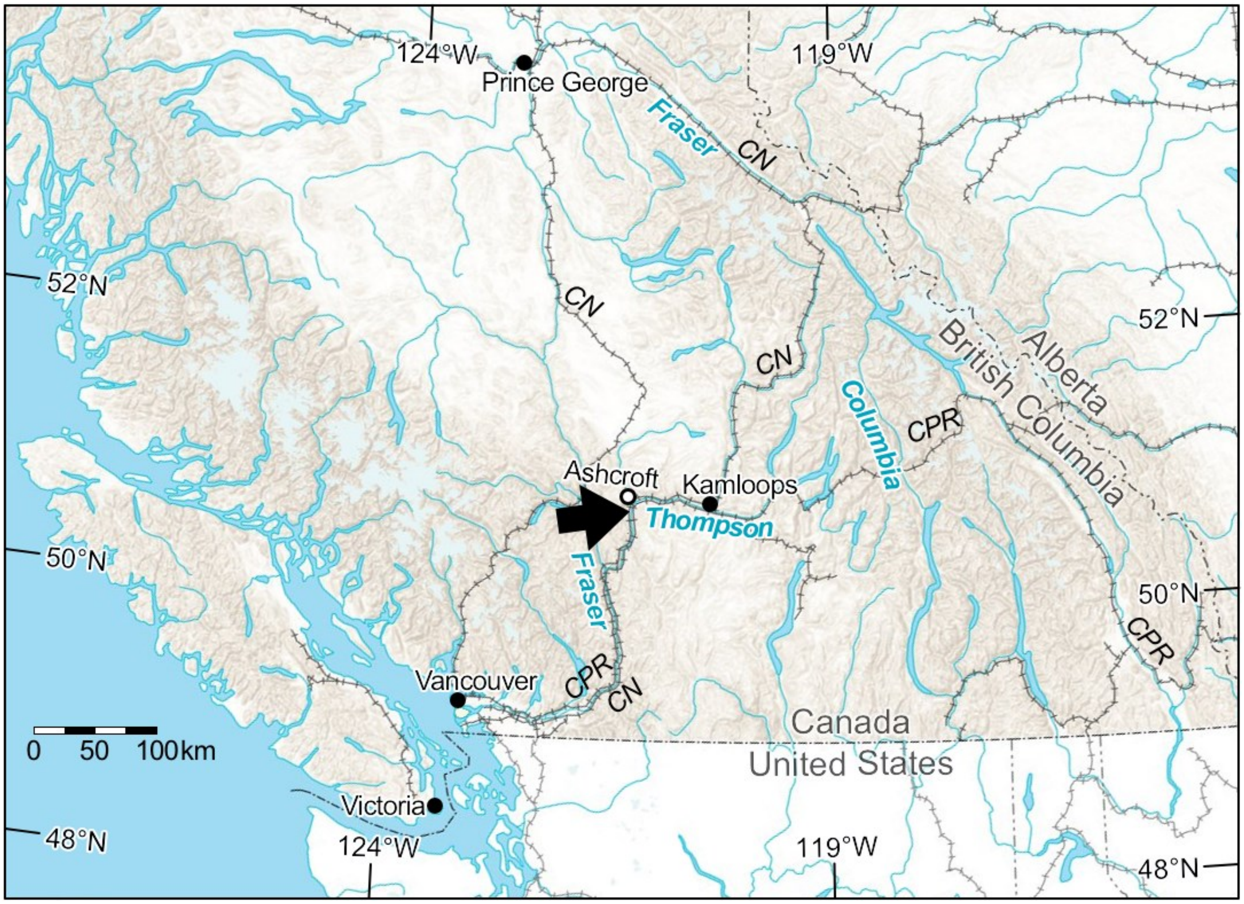
124°W
119°W
Prince George
Fraser
CN
52°N
CN
CN
52°N
British Columbia
Alberta
Columbia
CPR
Ashcroft
Kamloops
Thompson
50°N
Fraser
50°N
CPR
Vancouver
CPR
CN
Canada
United States
0 50 100km
Victoria
48°N
124°W
119°W
48°N

Figure 1.1. Map of southern British Columbia showing the railway network (modified from Natural Resources Canada 2017) and the location of the Thompson River Valley landslides

1.2 OBJECTIVES

The overall objectives of this research program are to characterize soils within the stratigraphy, and evaluate their strengths so as to improve the understanding of why the Ripley slide is sliding on its failure plane, and what strength can be mobilized within the material found at that plane. These results have wider implications as they also inform the understanding of the other landslides within this valley which have been found to be sliding upon what appears to be a common plane within a glaciolacustrine sediment (Eshraghian et al. 2007); this mechanism is similar to that found for other slow-moving landslides in overconsolidated glaciolacustrine clays.

Very little work has been done on these soils, and the properties of the materials have been assumed from the result of geological mapping of the area, and from back calculation of strength from stability analysis of the major landslides. Thus, the goal of this research was to revisit these assumptions and quantify these properties.

The specific research objectives are to:

1. Obtain high quality continuous core samples from the Ripley slide.
2. Define the soil stratigraphy using x-ray radiography and visual logging of the retrieved core. This soil description includes identifiable slickensides and active rupture surfaces.
3. Characterize the overconsolidated glaciolacustrine clay within which the primary failure surface of this landslide is found. This characterization includes the plasticity (Atterberg limits), mineralogy, preconsolidation pressure and permeability.
4. Evaluate the drained peak and residual shear strengths of the overconsolidated glaciolacustrine clay using direct shear and ring shear tests. The ring shear tests were also used to evaluate the effect of the rate of movement.
5. Assess the practicality of the direct simple shear (DSS) apparatus for testing undrained shear strength, and measure the pore pressure response.
6. Compare the laboratory testing results to the properties previously back calculated for these materials and discuss the implications of the testing results on the mechanisms that govern the stability and movement of the Ripley slide and other Thompson River Valley landslides.

1.3 ORGANIZATION OF THESIS

This thesis consists of seven chapters, including this introductory chapter (Chapter 1) and the concluding chapter (Chapter 7).

Chapter 2 presents a review of the literature relevant to this study. This literature review summarizes existing knowledge on the behaviour of stiff and glaciolacustrine clays with respect to strength and slope stability, and discusses the relevant soil properties and laboratory tests.

Chapter 3 presents a review of the Thompson River Valley landslides, with a focus on the geological context, the failure mechanisms, and the recent investigations conducted at the Ripley slide.

Chapter 4 presents the methodology used to evaluate the stress-strain relationship, strength, and generated pore water pressure of the Ripley clay. Also included is information about field work, the use of continuous core samples and laboratory tests. Laboratory test issues that have prompted changes in the methodology are discussed in detail.

Chapter 5 presents the results of laboratory testing, notably the peak and residual shear strength, and the identification of active shear zones.

Chapter 6 presents the interpretation of the glaciolacustrine clay's measured soil properties. In the context of the Ripley slide and the Thompson River Valley landslides, this interpretation highlights the failure mechanism at play in glaciolacustrine clay.

Chapter 2. Literature Review on Glaciolacustrine Clays

2.1 GLACIOLACUSTRINE CLAY

The term glaciolacustrine is a designation for a glacial lake environment. Glaciers are the principal source of sediment for glacial lakes. Glacial lakes are described as sediment sinks because they entrap large quantities of sediments from glacial drainage (Smith and Ashley 1985). A body of still water provides favourable conditions for the deposition of fines at the lake-bottom (Ashley 2002). Strictly speaking, coarse sediment found in the proximity of meltwater discharge points, for instance ice-contact deltas also qualifies as glaciolacustrine (Ashley 2002). However in the following work, glaciolacustrine sediment refers to fine-grained soil deposited at the bottom of glacial lakes.

The size of the lake, the distance from the ice front and the positioning of inflowing glacial streams all influence the deposition of glaciolacustrine sediment (Evans 1982). For instance ice-distal deposits are thinner and more fine-grained than ice-proximal deposits; and, ice-distal deposits are typically richer in clay and whereas ice-proximal deposits are richer in silt or fine sand (Ashley 2002).

Deposition of glaciolacustrine sediment is also characteristically affected by seasonal variations. During the melt season (summer) the coarser silt content settles first. During the non-melt season (winter) the sediment input is stopped. Finer clay content that remains in the suspension settles until the next melt season (Ashley 2002). The facies of rhythmic horizontal lamination associated with alternating silt and clay is typical of glaciolacustrine deposits.

Under ideal conditions a coarse-fine (or silt-clay) couplet reflects one summer-winter cycle. The annual deposit is termed varve (Smith and Ashley 1985). However the sediment input varies from one year to the other. The thickness and gradation of the beds is inconsistent throughout one glaciolacustrine deposit; thus annual cycles of deposition may be difficult to distinguish (Smith and Ashley 1985). In this case the less specific term rythmite describes alternating silt and clay facies.

In the terminology used hereafter, the designation glaciolacustrine clay is not limited to clay beds but encompasses the bulk of glaciolacustrine deposits. An explicit distinction will be made between silt-dominated and clay-dominated beds only when needed.

Glaciolacustrine clays are commonly found in North America and Europe north of the 40th parallel (Terzaghi and Peck 1967). During the Quaternary, glaciations extensively covered Canada (Prest et al. 1968). When the ice sheets retreated, they impounded meltwater drainage, resulting in the creation of many glacial lakes. Some massive and long-lived lakes such as Lake Agassiz resulted in thick (tens of meters) and extensive (hundreds of thousands of square kilometers) glaciolacustrine deposits (Smith and Ashley 1985).

In British Columbia, the Cordilleran Ice Sheet has marked Quaternary geology. According to Ryder et al. (1991) this era saw three glaciations that have led to glaciolacustrine deposits both during advance and retreat phases in southern and central British Columbia. In this area glaciolacustrine deposits are confined to the valleys of British Columbia's Interior Plateau (Evans 1982). The extent of these deposits is illustrated in Figure 2.1.

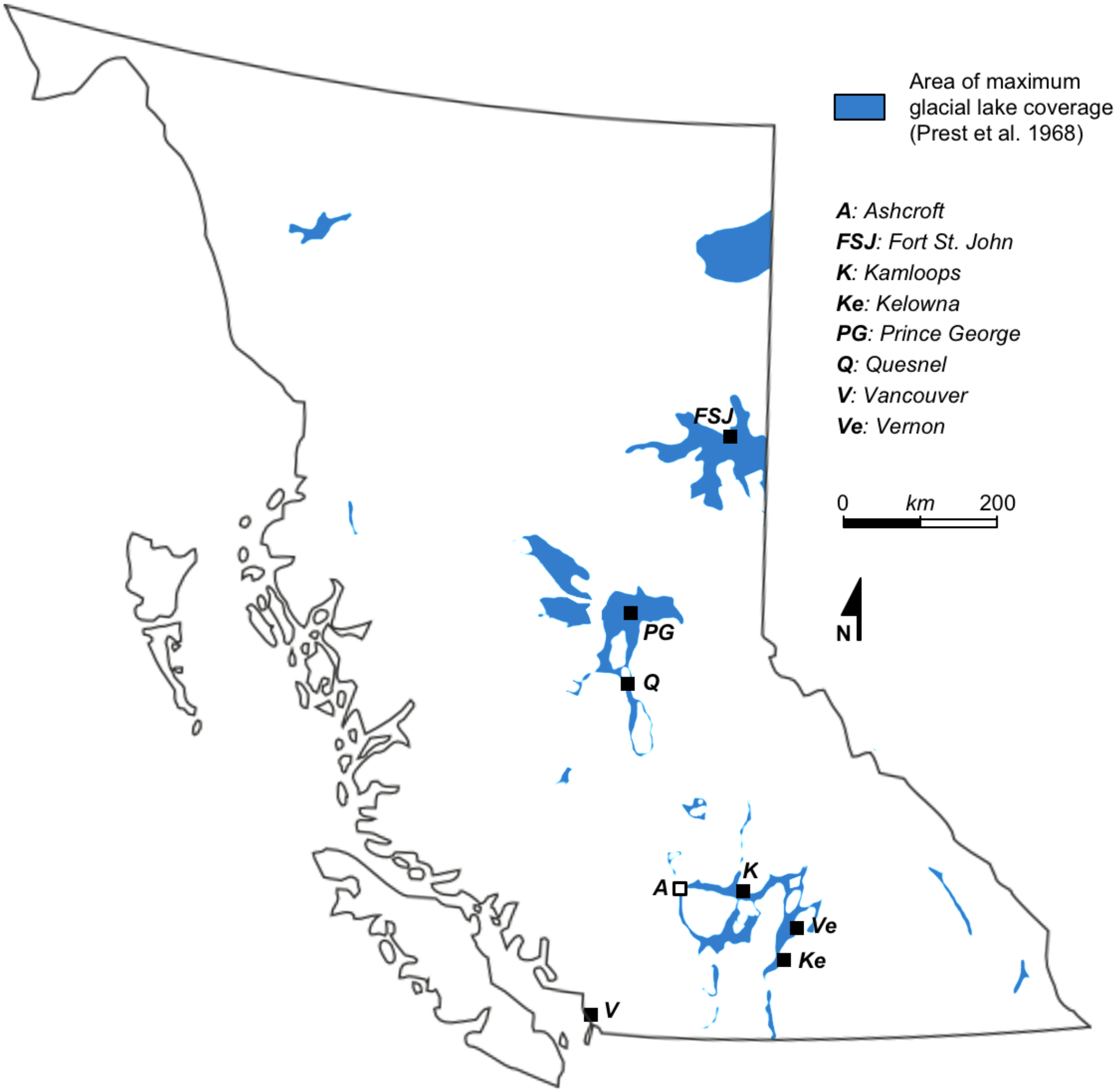
Area of maximum glacial lake coverage (Prest et al. 1968)
A: Ashcroft
FSJ: Fort St. John
K: Kamloops
Ke: Kelowna
PG: Prince George
Q: Quesnel
V: Vancouver
Ve: Vernon
0
km
200
N
FSJ
PG
Q
A
K
Ve
Ke
V

Figure 2.1. Extent of glaciolacustrine deposits in British Columbia

2.2 SOIL MECHANICS CONSIDERATIONS

2.2.1 ANISOTROPY

Terzaghi and Peck (1967) observe that varved clays may show the undesirable properties of both silts and clays. Geotechnical properties of one type of soil govern the behaviour of the bulk of the glaciolacustrine deposit, independently of the other type of soil. Glaciolacustrine soil is inherently anisotropic as it consists of rhythmically bedded soil. Anisotropy reflects on soil properties: for instance shear strength along bedding planes is less than that across bedding planes (Sambhandharaksa 1977). Glaciolacustrine soil is also heterogeneous as its constituents vary from one rythmite to the other: shear strength in a clay bed is less than that in a silt bed and hydraulic conductivity in a clay bed is less than that in a silt bed.

2.2.2 OVERCONSOLIDATION

Overconsolidation is an important characteristic associated with valley fill sediments such as in British Columbia's Interior Plateau. Glaciolacustrine clays have endured glacial advances consecutively to their deposition. Thick ice sheets have exerted considerable loading on the soil (Ryder et al. 1991). As a result the glaciolacustrine clay was consolidated under high normal stresses. During deglaciation and until today, glacial lakes have drained and valley fills have been incised by river erosion and mass wasting (Clague and Evans 2003), thus removing the overburden and unloading the soil. The glaciolacustrine soil, now at shallow depth, is overconsolidated.

The increase of effective stress associated with consolidation causes soil particles to pack in a denser state (Terzaghi and Peck 1967). The process can be quantified in terms of a void ratio and water content decrease. In the overconsolidation process, removal of pressure causes rebound of the clay. The magnitude of void ratio change during rebound is less than during consolidation (Figure 2.2). The packing of soil particles is not fully reversed and therefore the soil is denser in the overconsolidated state than in the normally consolidated state, though both states experience the same effective pressure (Skempton 1964). As the pore space is reduced and the particle packing is denser in overconsolidated clay, the hydraulic conductivity and the compressibility are lower (Mitchell 1976).

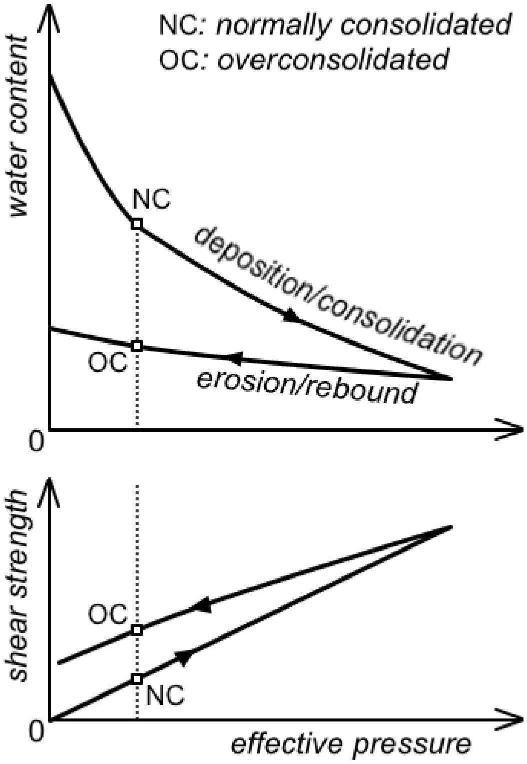
NC: normally consolidated
OC: overconsolidated
water content
NC
deposition/consolidation
OC
erosion/rebound
0
shear strength
OC
NC
0
effective pressure

Figure 2.2. Overconsolidation of clay

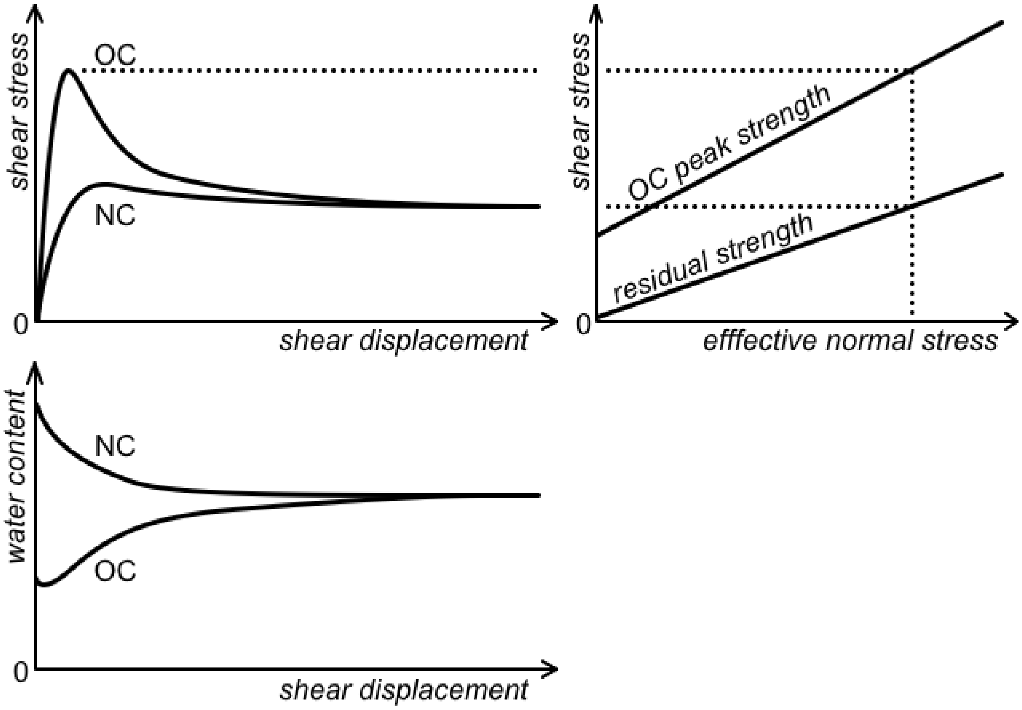
shear stress
OC
NC
0
shear displacement
shear stress
OC peak strength
residual strength
0
efffective normal stress
water content
NC
OC
0
shear displacement

Figure 2.3. Shear behaviour of normally and over-consolidated clay

Overconsolidation is quantified using the overconsolidation ratio (OCR), which is the ratio of the past maximum effective pressure exerted on the soil σ'_p (preconsolidation pressure) to the present effective stress σ' (Equation 2.1).

Equation 2.1. $$OCR = {}^{\sigma'_p}/_{\sigma'}$$

Soil structure, which is defined by both the arrangement of particles (fabric) and interparticle forces, is modified when subject to large overburden (Mitchell 1976). According to Terzaghi and Peck (1967) and Bjerrum (1967) clays inherit an increased number of interparticle bonds from overconsolidation. Therefore, overconsolidated clays exhibit a greater shear strength.

Overconsolidation also induces anisotropy at the scale of fabric (microscopic). When subject to large overburden pressure, platy clay particles develop a preferred orientation, as they tend to align normal to the major principal stress direction (Mitchell 1976). Ladd (1991) has noted that this adds to the macroscopic-scale anisotropy inherent to rhythmically bedded glaciolacustrine clay described above.

Overconsolidation is accompanied by overburden removal but in some cases significant horizontal residual stresses remain in the soil because lateral strain is limited (Terzaghi and Peck 1967). The ratio of horizontal to vertical normal stress increases, leading to anisotropy of the stress system (Kulhawy and Mayne 1990).

The compact arrangement of soil particles in overconsolidated clay is an obstacle to shear strain. Skempton (1964) noted that the cohesion component of effective shear strength that can be mobilized becomes significant after overconsolidation (Figure 2.3). Shear strain encourages soil particles to rearrange into a less dense structure. In drained conditions, it leads to an increase in volume. In undrained conditions, it leads to the generation of negative pore water pressure. This tendency for the soil volume to increase under the effect of shearing is termed dilatancy (Skempton 1970). Dilative shear behaviour is a characteristic of intact heavily overconsolidated clays. The OCR of these clays is typically greater than eight (Terzaghi and Peck 1967). In contrast, contractive behaviour is a characteristic of normally consolidated and lightly overconsolidated clay.

2.2.3 MECHANISMS OF STRENGTH LOSS IN STIFF FISSURED CLAYS

Naturally occurring heavily overconsolidated clays are of stiff consistency and usually contain fissures. The shear strength that can be mobilized in the field is impacted by the soil structure formed by the stiff clay's natural defects. This shear strength is inevitably less than that mobilized in laboratory tests on intact soil specimens too small to contain the large-scale fissured structure. The average strength of the soil mass is misrepresented by the intact strength. Terzaghi (1936) was the first to point out this discrepancy for what he called stiff fissured clays.

The geological history of stiff soils typically includes one or several phases of overburden decrease where the rebound of the clay is associated with the deterioration of interparticle bonds. Weathering accelerates this process in the shallower strata (Bjerrum 1967). Overburden removal also allows for the development of planar fissility parallel to the bedding. Such factors trigger the formation of cracks, fissures and joints within the stiff clay (Morgenstern 1990). Presheared discontinuities may result from considerable forces applied by glacial drag, tectonic movements or from previous landsliding (Morgenstern 1992).

In drained conditions, overconsolidated clays are subject to strength loss because of softening. Imperfections act as stress concentrators within the soil mass. Local over-stressing causes shear strain, which is associated with dilatancy for overconsolidated clays. On a large time scale the water content increases, leading to strain softening. As water reaches open fissures, more softening of the adjoining clay occurs. Through this process stiff clays may develop discontinuities along which the strength is reduced. The fully-softened condition is attained when the shear strength is reduced to that of a normally consolidated clay. The apparent cohesion, a characteristic of intact overconsolidated clay, is lost. Skempton (1964) has widely contributed to the understanding of this mechanism of long-term strength loss.

2.2.4 SLOPE INSTABILITY

The aforementioned aspects of soil behaviour predispose slopes in stiff overconsolidated clays to progressive failure, a model of failure proposed by Bjerrum (1967). Lateral stress release from excavation or erosion from a down-cutting river initiates strain, typically at the toe of the slope. Fissures enhance the process because they open as a result of stress release, so water is able to circulate and cause softening. Local failure progressively migrates from the toe inside the slope.

Eventually progressive failure extends fully along a discontinuity of the natural slope. Strength reduction along the discontinuity is sufficient for failure to occur. Large shear strains impose the orientation of clay particles preferentially in the direction of shear. Therefore the strength is further decreased. The ultimate lower-bound shear strength is called residual strength (Skempton 1985). Along such pre-sheared surfaces, the operative shear strength is the residual strength.

After deglaciation, mass wasting naturally follows the incision of valley fills by rivers (e.g. Ryder 1976, Hutchinson 2001). When a river downcuts through glaciolacustrine soil it leaves slopes vulnerable to instability. Progressive failure is initiated at the lower part of the slope, which is seen to move first. Progressive failure propagates in the direction opposite to the slope face and upslope movement follows. The formation of a failure surface in the direction opposite to the slope face is called retrogression, a mechanism described by Skempton and Hutchinson (1969) among others. In glaciolacustrine soils, retrogression typically occurs along a bed of weak clay (Hungr et al. 2013). The failure surface contained in a weak clay bed is typically subhorizontal, the main scarp is steep and the landslide movement is translational.

Large retrogressive landslides are common in Western Canada. Often they are reactivated old landslides (Evans 1982, Cruden et al. 1997). In the Peace River lowland, river erosion of glaciolacustrine clay triggers these reactivations (Cruden et al. 1993, Cruden et al. 1997). In British Columbia, intermittent reactivations are commonly triggered by weather-related increases in pore water pressure (Evans 1982, Fletcher et al. 2002). Similar cases are found in glaciolacustrine soils elsewhere, e.g., in Estonia (Kohv et al. 2010). Another trigger of landslide activity is heavy rain or irrigation water infiltration causing pressure build-up in glaciolacustrine soil fissures. According to Evans (1982), this type of instability is common in British Columbia's Southern Interior where lateral stress-relief joints are deep at the valley margins but retrogression is limited because the glaciolacustrine soil is silt-dominated, not clay-dominated. In the French Alps, the activity of landslides in low plasticity, heavily overconsolidated glaciolacustrine clay is also dependent on precipitation water infiltrating fissures (Van Genuchten and Van Asch 1988, Giraud et al. 1991).

2.3 LABORATORY TESTS

2.3.1 SAMPLE SIZE

Using laboratory results to explain field behaviour can be misleading. Often the sample size is too small to represent the large-scale fissured structure of stiff clay. The size effect limits the ability for laboratory work to assess the behaviour of a slope (Morgenstern 1980).

Because glaciolacustrine soil is inherently heterogeneous, determining its soil properties is even more complicated. Laboratory results depend on the relative portion of silt and clay layers the specimen holds. Testing large samples yields properties representative of the bulk soil, but it may be only the properties of the clay layer itself that are relevant to slope stability (Lacasse et al. 1977).

2.3.2 RING SHEAR

It is relevant to measure residual shear strength because of the propensity for landslides in overconsolidated glaciolacustrine clay to be reactivations, or failures along pre-sheared surfaces (Morgenstern 1968). The condition of such surfaces is best represented by the drained strength that can be mobilized after large shear displacements. In the laboratory, this condition can be achieved through the ring shear test.

The ring shear apparatus accommodates a ring-shaped specimen. The rotation imposed by the apparatus allows unlimited shear displacement, continuously and in the same direction. This is an advantage over the limited stroke direct shear test. The ring shear test ultimately creates an artificial slickenside and the shear strength decreases to residual strength. Hvorslev (1939) was the first to describe the use of a ring shear apparatus to test soil strength. Modern developments were introduced to show that ring shear apparatuses could successfully measure the residual strength of clays (La Gatta 1970, Bishop et al. 1971, Lupini et al. 1981). Bromhead (1979) proposed a simplified version of the apparatus. The Bromhead-type ring shear apparatus has become available in many soil mechanics laboratories.

Intact clay is difficult to test in the ring shear apparatus given the annular shape and size of the specimen. Remoulded specimens are appropriate to measure the residual shear strength in the ring shear apparatus.

2.3.3 DIRECT SHEAR

The direct shear test is a less straightforward method for measuring the residual strength, but is a simple method for shearing intact samples. The measure of peak strength from a drained direct shear test is indicative of the cohesion of the intact clay (Head 1994). The ensuing post-peak shear response is indicative of the brittleness.

The shear box apparatus as designed by Casagrande in 1932 is widely used to test the strength of soils under direct shear (Head 1994). The soil specimen is contained in a shear box split in half. Under a given normal stress, one half is forced to translate relative to the other half. As seen in Figure 2.4.b, shear is localized along the horizontal plane between the two shear halves. Shear is particularly constrained at the front and rear edges of the box, where failure is thought to occur first before reaching the middle of the specimen. Shear strength is not mobilized simultaneously along the whole rupture surface. Shear stress and strain are not uniform in the direct shear test (Saada and Townsend 1981).

Direct shear tests are performed at a slow rate of shear displacement so conditions remain drained. Effective strength parameters are obtained assuming the imposed stresses are those experienced where the soil fails. Peak and post-peak behaviours of intact soil are measured. The amount of applied shear displacement can be extended through the reversal procedure, and thereby residual strength can be measured too. Early records of this procedure were made at Imperial College in the 1960's and reported by Early and Skempton (1972).

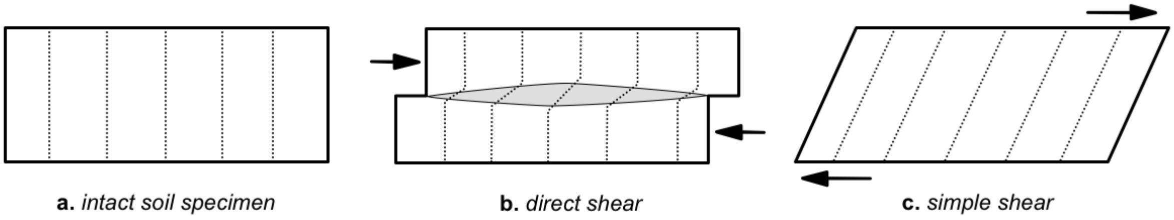
a. *intact soil specimen*
b. *direct shear*
c. *simple shear*

Figure 2.4. Shear strains in test specimens

2.3.4 UNDRAINED DIRECT SIMPLE SHEAR

The undrained strength should provide insight into the glaciolacustrine clay's shear behaviour. Morgenstern (1968) concluded that the stiff clay's undrained shear strength should be valued more as a response than a parameter. This response depends on the loading path experienced by the soil. The laboratory test should attempt to mimic the loading path experienced in-situ, and measure the associated pore water pressure response. Whether the direct simple shear (DSS) test is able to fulfill this task is presented in this study.

Kjellman (1951) initially presented the simple shear apparatus, developed at the Swedish Geotechnical Institute. Bjerrum and Landva (1966) improved the apparatus at the Norwegian Geotechnical Institute (NGI). The NGI-type DSS apparatus has since been beneficial to many geotechnical studies, particularly the characterization of soft soils (Ladd and Edgers 1972, Mayne 1985).

The term “simple shear” refers to a state of plane strain in which points are displaced only in one direction (Saada and Townsend 1981), as illustrated in Figure 2.4.c. Simple shear loading is characterized by the free rotation of the principal stress directions. This loading condition occurs in the field (e.g. in slope stability problems, Figure 2.5): the soil experiences stress and strain increments such that the principal axes are free to rotate. Also, the strength of anisotropic glaciolacustrine clay depends on the orientation of the stresses.

The triaxal test cannot reproduce such a loading condition as it only allows for an exchange between the minor and major principal stress directions, thus predetermining the orientation of the stress condition at failure. On the contrary, the purpose of the DSS test is to apply simple shear strain, so that the loading condition to which a soil element is subjected in-situ is better reproduced (Lau 1988).

Another advantage of the DSS test is the potential for constant-volume DSS tests to measure the undrained response to shear. Dyvik et al. (1987) showed that the change in normal load required to maintain a constant volume during a DSS test is equivalent to the change in pore water pressure. Thus, the DSS provides an effective stress path for a constant-load undrained test.

One disadvantage of the DSS test is that only the average vertical stress and the average shear stress are measured. The complete state of stress remains unknown so one cannot draw Mohr’s circle. De Josselin de Jong (1972), supported by Wroth (1984), showed that two different mechanisms of shear are possible in the DSS test. This leaves the value of undrained shear strength open to interpretation, which is problematic when undrained strength is a design parameter.

The DSS apparatus deforms the specimen in a simple shear fashion but does not impose a state of simple shear stress (Figure 2.6). Resulting non-uniform distributions of shear and normal stresses have been addressed several times in the literature (Prevost and Hoeeg 1976, Airey and

Wood 1987, Grognet 2011). In spite of the criticism that this has raised against the DSS test (La Rochelle 1981, Saada and Townsend 1981), the DSS apparatus is recognized to provide relevant stress-strain relationships for natural clays (Vucetic and Lacasse 1982, Jamiolkowski et al. 1985).

Sambhandharaksa (1977) and De Groot and Lutenegger (2005) have used the DSS to study the strength anisotropy of Connecticut Valley varved clay, a glaciolacustrine soil. DSS tests successfully allowed shearing along the varves, yielding lower undrained shear strength values than those measured in triaxial tests (shearing across the varves).

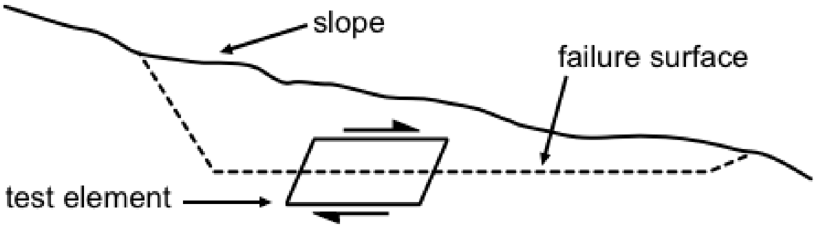
slope
failure surface
test element

Figure 2.5. A DSS-relevant problem

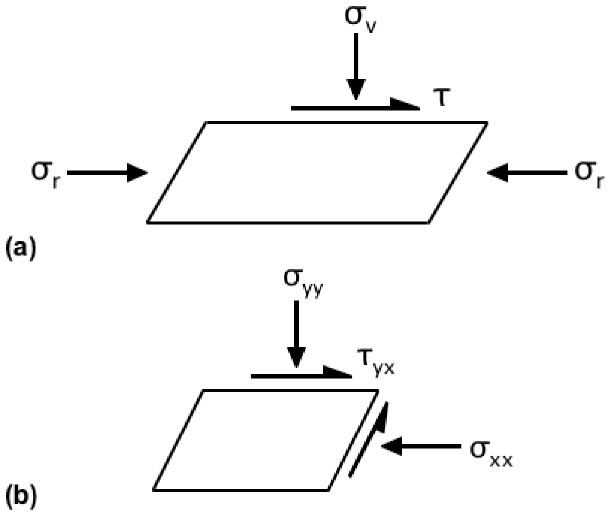
σ_v
τ
σ_r
σ_r
(a)
σ_{yy}
τ_{yx}
σ_{xx}
(b)

Figure 2.6. Difference in stress state between (a) the DSS apparatus and (b) the idealized simple shear

Chapter 3. Description of the Thompson River Valley Landslides

3.1 THOMPSON RIVER VALLEY LANDSLIDES

3.1.1 HISTORY

Thirteen major landslides are located within a 10-km stretch of the Thompson River Valley immediately south of Ashcroft, British Columbia. Historical landslide events have been observed since the 1880s. Records of these events coincide with the construction of the Canadian Pacific (CP) railway through the valley in 1885. Stanton (1898) made the earliest publication on large landslides in the Ashcroft area, describing in detail the North and South slides along with the adverse conditions that these landslides posed to CP operations. He recognized that the water input from irrigation on upland terraces contributed to ongoing landslide activity.

Clague and Evans (2003) described the following significant events of landslide activity. In October 1880 (North slide) a very rapid failure occurred with an estimated volume of 15×10^6 m^3. It dammed the river for the following two days, forming a lake that reached a length of 14 km. In October 1886 (Goddard slide) another very rapid failure occurred and destroyed 575 meters of CP line. In September 1897 (CN50.9 slide) a rapid failure occurred and constricted the river. In August 1921 (Red Hill slide) a very rapid failure occurred, again temporarily damming the river.

The 1880, 1886 and 1897 rapid failures correspond to the most recent retrogressions of the North, Goddard and CN50.9 slides respectively. The most recent retrogressions of the South and Basque slides occurred before 1885 (Eshraghian et al. 2007). The latest retrogressions developed the rearmost, major scarps that can be observed to this day.

Eshraghian et al. (2007) report that reactivations occurred several times for each of the CN50.9, Goddard, North and South slides. In September 1982 (Goddard slide) a rapid reactivation occurred within the original 1886 landslide mass, again damaging the CP line. The volume was estimated at 3×10^6 m^3. With the exception of the Goddard slide in 1982, velocities of the reactivations were observed to be very slow. Increased maintenance of the railway tracks allows CP and Canadian National (CN) to keep operating lines through the Thompson River Valley in spite of the frequent very slow reactivations (Bunce and Chadwick 2012).

3.1.2 GEOLOGY

The Thompson River Valley fill sediments are inherited from the glacial geological history of the area. The last glaciation, the Fraser glaciation, culminated 14,000 years ago. The oldest glaciation revealed by the geology is from the early Pleistocene age. In between those two time periods, at least one glacial advance has occurred (Clague and Evans 2003). The deposits associated with these three glaciations are seen in the Thompson River Valley and have been interpreted by Clague and Evans (2003) to set the geologic framework for the Thompson River Valley landslides.

Amid successive glaciation and interglaciation sequences, till, glaciolacustrine, glaciofluvial and colluvial sediments were deposited. Erosion and mass wasting during interglaciations produced unconformities between the glacial sequences. The resulting stratigraphy is complex, as shown in Figure 3.1. Numbered units refer to the nomenclature that Clague and Evans (2003) established to designate different geological strata.

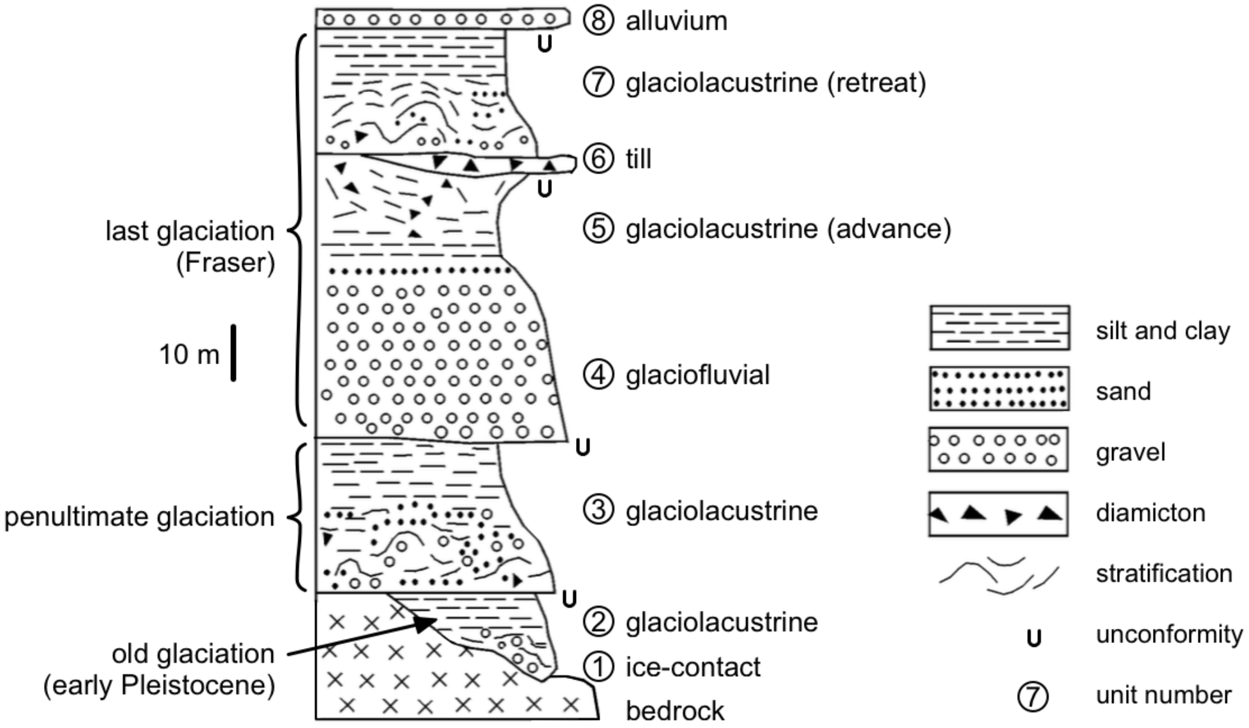

⑧ alluvium
⑦ glaciolacustrine (retreat)
⑥ till
⑤ glaciolacustrine (advance)
④ glaciofluvial
③ glaciolacustrine
② glaciolacustrine
① ice-contact
bedrock
U
last glaciation (Fraser)
10 m
penultimate glaciation
old glaciation (early Pleistocene)
silt and clay
sand
gravel
diamicton
stratification
unconformity
⑦ unit number

Figure 3.1. Generalized stratigraphy of the Thompson River Valley at Ashcroft (modified from Clague and Evans 2003)

The stratigraphy sequence introduced above is usually incomplete for a given site of the Thompson River Valley. According to Eshraghian et al. (2007) the stratigraphy of the landslides does not comprise units 4, 5 and 7. Landslides are located at the bottom of the broad Thompson River Valley, where the flow of meltwater deeply incised the Quaternary fill during the glacial advance and retreat surrounding the Fraser glaciation. As a result not all units associated with the Fraser glaciation exist at the landslide locations.

Within this stratigraphy Unit 2 and Unit 3 distinguish themselves because they are fine-grained plastic sediment with potentially low permeability. These sediments are of glaciolacustrine origin, meaning they have been deposited in a glacial lake environment. Glaciers blocked regional drainage, creating large lakes in valleys like the Thompson River Valley (Evans 1982). Current-day Kamloops Lake is a remnant of the Thompson-Deadman glacial lake that occupied the valley as far south as Spences Bridge following the climax of the Fraser glaciation (Johnsen and Brennand 2004).

Unit 2 is interpreted as glaciolacustrine because it shows silt and clay couplets of thickness ranging from less than one centimeter to several tens of centimeters. Unit 2 dates from the early Pleistocene glaciation and Unit 3 is most likely from the penultimate glaciation (Clague and Evans 2003). Consecutive glacial advances and deposition of more recent units subjected these units to large overburden. In today's deeply incised Thompson River Valley the overburden has been removed. Glaciolacustrine sediments are left at a shallow depth, most likely overconsolidated and stiff.

3.1.3 LANDSLIDE MECHANISM

a. Retrogressions

Using the terminology of Cruden and Varnes (1996), Thompson River Valley landslides can be classified as multiple retrogressive, translational, very slow, earth slides. These qualifiers describe the activity, type of movement, rate of movement and involved material, respectively. Their large size is another characteristic, with volumes ranging between 0.6×10^6 and 15.0×10^6 m^3 (Hendry et al. 2015).

Eshraghian et al. (2007) report that failure surfaces are systematically found within Unit 2 clay layers at the CN50.9, Goddard, North, and South slides. A 2006 investigation of the Ripley slide reported by Hendry et al. (2015) also identified active failure surfaces within Unit 2. A strong potential for progressive failure was found in clay-rich, highly plastic beds located within glaciolacustrine sediment. For reasons explained earlier, bedding-parallel planar fissility and pre-sheared discontinuities also predispose clay beds to failure. Progressive failure along a given bed creates a planar failure surface, which leads to translational movement.

The river down-cutting and eroding of the valley slopes initiates strain at the toe of the slope. When a deeper bed of high plasticity clay is reached, retrogression is triggered, eventually forming a new bedding-parallel rupture surface. Two such distinct rupture surfaces are known to exist in Unit 2 at different landslide locations (Eshraghian et al. 2007). Deeper retrogressions may occur in the future as a result of the river down-cutting through deeper clay beds of Unit 2. Landslide movement is periodically reactivated at very slow velocities along the existing rupture surfaces.

b. Controls on stability

Stanton (1898) identified irrigation as one cause of slope instability in the area. The ditch-and-furrow system was the irrigation technique used in the late 1800s. It flooded the upland terraces above the landslides with large volumes of water. High pore water pressure developed in the glaciolacustrine soil as a result of heavy irrigation and triggered major landslides (Porter et al. 2002, Clague and Evans 2003). The sprinkler system, a more water efficient irrigation technique, was adopted in the 1960s. Major landslide events have not occurred since then, except for the 1982 Goddard slide. However, very slow reactivations at several locations of the Thompson River Valley have made for ongoing landslide activity.

Porter et al. (2002) have measured artesian pore pressure beneath the toe of the CN50.9 and North slides. They attribute artesian pressure to a confined aquifer in the fractured bedrock overlain by low permeability glaciolacustrine soil. Bishop (2008) supports the theory that regional groundwater flow leads to elevated pore water pressure at the bottom of the valley sediment sequence, which is confined by the less pervious Unit 2. Excess pore water pressure reduces the effective stresses, contributing to lower stability of the slopes.

There are three ways in which the Thompson River has been suggested to affect the stability of slopes:

1. First, Thompson River level fluctuations affect the pore water pressure within the slope. Eshraghian et al. (2008) have conducted transient seepage analysis to show that during river drawdown the groundwater level in the slope decreases. Latency between the decrease in the river level and the decrease in the groundwater level causes excess pore

water pressure in the slope. Seepage is oriented towards the river until the end of the drawdown period. Excess pore water pressure dissipates until the groundwater level comes to equilibrium with the river level. At the Ripley slide, Schafer (2016) used piezometer data to measure the differential pressure, the excess pore water pressure at the Ripley slide shear surface. Schafer showed a strong correlation between the differential pressure and the landslide velocity. This confirms the drawdown effect. When the river rises during spring and summer snowmelt, the Ripley slide stops. It accelerates again following river drawdown in the fall. According to Eshraghian et al. (2008), it is mainly the toe of the slope that is affected by the Thompson River seasonal fluctuations. Drawdown effects are felt less upslope and where the rupture surface is deeper.

2. Second, the toe load of the water mass against the slope contributes to stability (Porter et al. 2002, Eshraghian et al. 2008). Seasonally, as the Thompson River level decreases, so does the buttressing effect of the water mass.
3. Third, river erosion contributes to ongoing landslide activity. Riverbank erosion progressively changes the geometry of a slope until it becomes unstable. As reported by Porter et al. (2002), construction of toe berms at the CN50.9 slide and South slide successfully slowed movements by preventing riverbank erosion.

At first, the Thompson River's impacts on stability are felt only at the toe of the slope. However, it is the whole slope that becomes less stable when movement starts occurring at the toe.

Consistent with the Thompson River's fluctuations is the seasonal pattern of landslide activity. The river drawdown in the fall coincides with historical records that show most landslides occur in the fall (Porter et al. 2002). Eshraghian et al. (2008) also report increased rates of movement following the onset of river drawdown in the fall.

3.2 THE RIPLEY SLIDE

3.2.1 DESCRIPTION

The focus of the present study is the Ripley slide, which is located approximately 10 km south of the town of Ashcroft, on the east side of the Thompson River (Figure 3.2). Both CP and CN tracks cross the slide over a length of approximately 220 m. The landslide volume is estimated at 1.0×10^6 m^3 (Hendry et al. 2015). It is relatively small compared to other slides in the area.

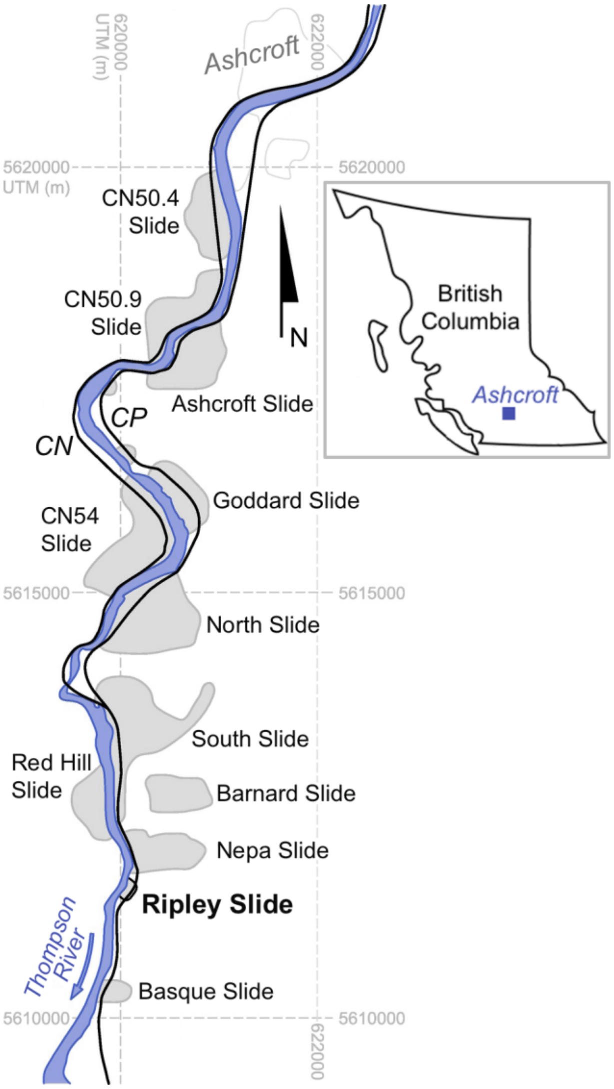
620000
UTM (m)
622000
Ashcroft
5620000
UTM (m)
5620000
CN50.4
Slide
CN50.9
Slide
N
British
Columbia
Ashcroft
Ashcroft Slide
CP
CN
Goddard Slide
CN54
Slide
5615000
5615000
North Slide
South Slide
Red Hill
Slide
Barnard Slide
Nepa Slide
Ripley Slide
Thompson
River
Basque Slide
5610000
5610000
622000

Figure 3.2. Location of landslides in the Thompson River Valley (modified from Hendry et al. 2015)

In 1951, a shift in the fence line upslope of the CP track enabled Charles Ripley to identify slope movement (Leonoff and Klohn Leonoff Ltd. 1994). This is the earliest record of what is now known as the Ripley slide. Until 2005 the slide was of little concern because inactive or very slow movement allowed regular railway maintenance to realign tracks frequently enough for rail operations to remain undisturbed and safe (Bunce and Chadwick 2012). In 2005, CP constructed a second track (siding) across the Ripley slide, requiring upslope cuts and the construction of a lock-block retaining wall (Figure 3.3). Two slope inclinometers installed before construction sheared off within 17 months. Deformations of the slope and of the lock-block retaining wall were noticed soon after construction. By 2007 more frequent maintenance operations were needed to realign the tracks. Tension cracks had developed, making the back scarp of the landslide largely apparent. Optical survey monitoring in 2007 revealed that the landslide velocity was 25 to 180 mm/year (Bunce and Chadwick 2012).

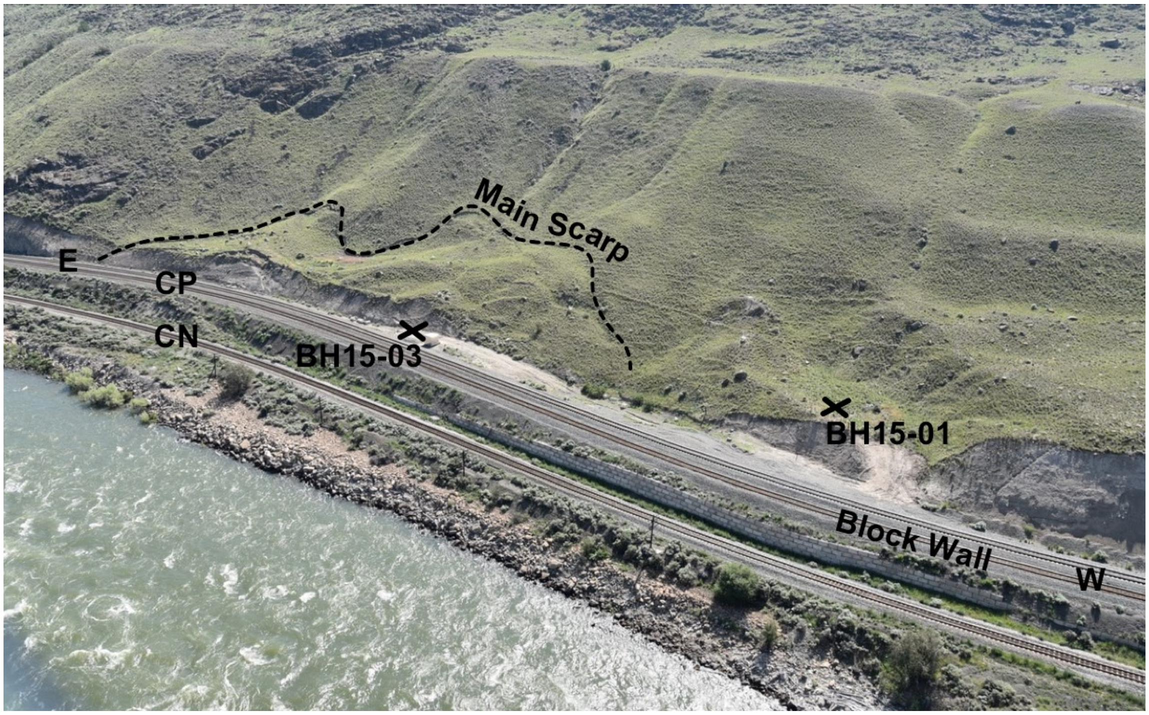

Figure 3.3. 2016 aerial photograph of the Ripley slide (courtesy of CN)

3.2.2 SITE INVESTIGATIONS

Hendry et al. (2015) reported on data from the 2005 geotechnical investigation commissioned by CP before the rail siding was constructed: one inclinometer revealed displacement along two distinct shear surfaces at elevations of 256.5 and 267.4 m; piezometers reveal an upward hydraulic gradient. These findings are similar to those reported by other studies about landslides in the Thompson River Valley (Porter et al. 2002, Eshraghian et al. 2007).

Three GPS units were installed by CP in 2008 at three different locations of the slide, providing a system to continuously monitor deformations (Bunce and Chadwick 2012). Depending on the GPS station the measured average annual velocity was 90 to 120 mm/year between 2008 and 2013. Hendry et al. (2015) compared GPS-measured velocity and river elevation to find that landslide movement accelerates during river drawdown.

Instrumentation was enhanced in 2013 when one ShapeAccelArray (SAA) and five grouted-in vibrating-wire piezometers were installed to measure slope deformations and pore water pressures against depth (Schafer et al. 2015). Also in 2013, the Geological Survey of Canada (GSC) started to use Interferometric Synthetic Aperture Radar (InSAR) technology on the Ripley site to monitor deformations (Huntley and Bobrowsky 2014, Journault et al. 2016). Ground-based LiDAR was used to obtain detailed mapping of the slope surface (Hendry et al. 2015).

Chapter 4. Methodology, from Core Samples to Shear Strength Testing

4.1 FIELD WORK

4.1.1 DRILLING

As part of this thesis and the thesis by Schafer (2016), a campaign of drilling and instrumentation was conducted in February 2015. Five boreholes were drilled at different locations of the site (Figure 4.1, Figure 4.2) through the valley fill material and until bedrock was reached, thus complementing the 2013 campaign.

To fulfill laboratory testing of intact soil specimens, continuous core samples were retrieved while drilling. In 2013, continuous core samples were retrieved from borehole BH13-01 and shipped to the University of Alberta in Edmonton. However, only a few of the samples were conditioned for limited moisture loss. In 2015, boreholes BH15-01 and BH15-03 were drilled for continuous core samples. The core has a diameter of 63.5 mm (2.5”). Borehole parameters are given in Table 4.1.

Continuous core samples make it possible to inspect entirely the variable glaciolacustrine sediment, including the sparse, narrow seams of clay that potentially control slope stability. Bromhead (2013) reports that such small but key features are only found occasionally, often by chance.

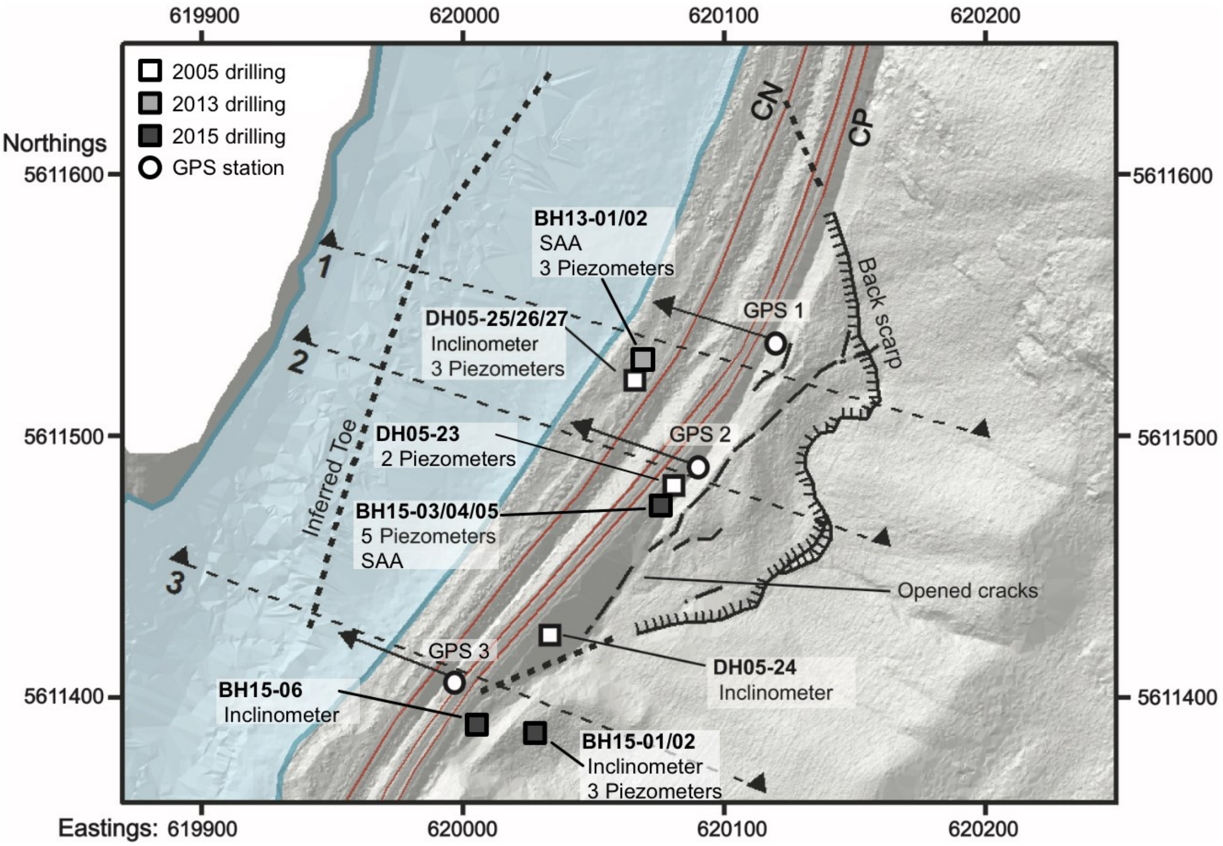
619900
620000
620100
620200
□ 2005 drilling
▨ 2013 drilling
■ 2015 drilling
○ GPS station
Northings
5611600
5611500
5611400
CN
CP
BH13-01/02
SAA
3 Piezometers
1
2
3
GPS 1
DH05-25/26/27
Inclinometer
3 Piezometers
Back scarp
Inferred Toe
DH05-23
2 Piezometers
GPS 2
BH15-03/04/05
5 Piezometers
SAA
Opened cracks
GPS 3
DH05-24
Inclinometer
BH15-06
Inclinometer
BH15-01/02
Inclinometer
3 Piezometers
Eastings: 619900
620000
620100
620200

Figure 4.1. Location of boreholes and instrumentation (modified from Hendry et al. 2015)

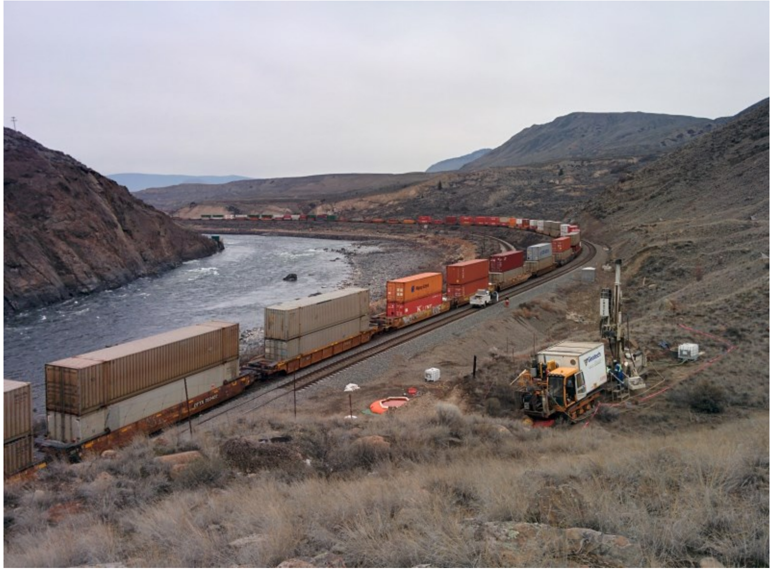

Figure 4.2. BH15-01 drilling location, looking north

Table 4.1. Parameters of boreholes

approx. elevation (m.a.s.l)	BH13-01	BH15-01	BH15-03
top of borehole	273	282	278
start of core recovery	269.2	278.6	273.2
bedrock surface	242.5	266.8	261.2
end of borehole	235.5	264.3	260.1

4.1.2 INSTRUMENTATION

In order to monitor deformations, three boreholes were fitted with slope inclinometer casings. Slope inclinometer surveys are accurate for measuring displacements and the depth of the active shear plane. For each survey, inclinometer readings were taken with a depth interval of 0.30 m (1 foot). One inclinometer casing was later equipped with a ShapeAccelArray (SAA) after the shear surface was located. In order to monitor pore water pressures the two remaining boreholes were equipped with grouted-in piezometers.

The settlement of the lock-block retaining wall and measurements from GPS 3 showed a significant vertical component to slope movement near the southern edge of the slide. The two other GPS stations recorded subhorizontal movement. Hendry et al. (2015) hypothesized the existence of a secondary sliding mass adjacent and south of the main slide body in order to account for the different slope movements. This prompted locating boreholes BH15-01 and BH15-06 in this portion of the slope.

The objective of the present thesis is to characterize the soil properties. Only the results from the 2015 slope inclinometer surveys are presented in Chapter 5 of this thesis, the objective being to locate the Ripley slide active shear surfaces. Further monitoring of displacements and pore pressures at the Ripley slide is outside the scope. Schafer's thesis (2016) addresses results from the 2013 and 2015 instrumentation campaigns in detail, along with the interpretation of the landslide kinematics.

4.2 CORE USAGE

4.2.1 PRESERVATION

The core from the 2015 drilling campaign was only briefly logged on site. More thorough logging was to take place in Edmonton in the University of Alberta laboratory. This allowed good quality intact samples to be tested in the laboratory. Therefore precautionary measures were taken on site to preserve the integrity of the core during transportation and storage and until the soil description could be completed in the laboratory. Specifically, the aim of core conditioning was to prevent changes in water content. Drying or softening would deteriorate samples of glaciolacustrine clay.

The core was retrieved in five-feet-long runs with a triple-tube drilling system, where the inner tube contains a 1.59-mm (1/16 inch) thick PVC coreliner. Core runs were kept inside the liner and sealed at their ends with wax (a mix of beeswax and melted paraffin). Core loss or rock boulders and cobbles sometimes made the application of wax impossible because no soil was available at the end of the run, so there was nothing to which the wax could adhere. Systematically, the ends of the core runs were closed with layers of plastic wrap and a tight plastic cap (Figure 4.3). After transportation, core boxes were stored in a moisture-controlled room at the University of Alberta. These measures limited moisture loss and disturbance between the time of the core drilling (February 2015) and the time of logging and laboratory testing (2016).

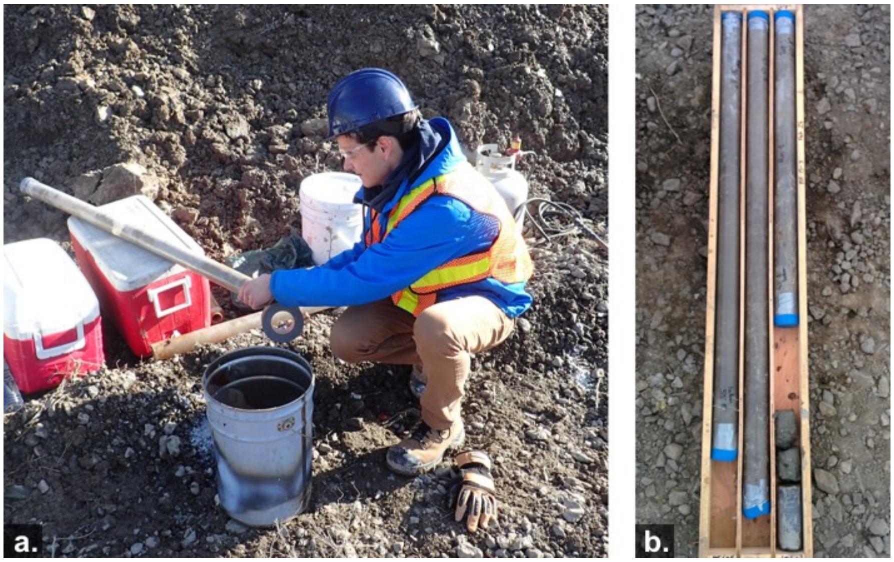

Figure 4.3. (a) On-site core sealing operations; (b) preserved core runs in core box

4.2.2 X-RAY RADIOGRAPHY

X-ray radiography was conducted on both the BH15-01 and BH15-03 cores. X-rays penetrate the core liner so it did not need to be removed, and the sample's condition was maintained. The contrast on x-ray images reflects material density, so subtle features were identified (Figure 4.4.a). A preliminary log of the core was completed after the x-ray image.

According to the ASTM D4452 (2014) standard test procedure, a major application of x-ray radiography is detecting soil disturbance so that the quality of sampling can be assessed. In the case of BH15-01 and BH15-03, the x-ray radiography did not reveal drilling-induced distortion of the bedding. However, it shows where core recovery is only partial.

Fissures within the soil are also clearly seen. The shape of some fissures suggests drilling disturbance (Figure 4.4.b). Other fissures are natural and can be mapped to serve the stratigraphic log. Based on the x-ray image, sample quality was assessed and a preliminary selection of laboratory test specimens was made.

4.2.1 LOGGING

In March 2016, the BH15-03 core was opened for the description and selection of test samples. Logging was not conducted in the field directly after core delivery but in the laboratory. Meticulous logging aims at observing subtle features inherent to the glaciolacustrine soil. Identifying sparse and narrow clay seams is important since they potentially drive slope instability. Logging in the laboratory is relevant when the core condition can be maintained during transportation and storage, which was the case for the Ripley 2015 core.

Observations were compared against the x-ray radiography results. Interestingly, some features are more easily noticed on the x-ray radiography. Bedding is more obvious because the contrast of densities derived from x-ray radiography is strong, while the colour contrast between the beds is not readily visible to the naked eye.

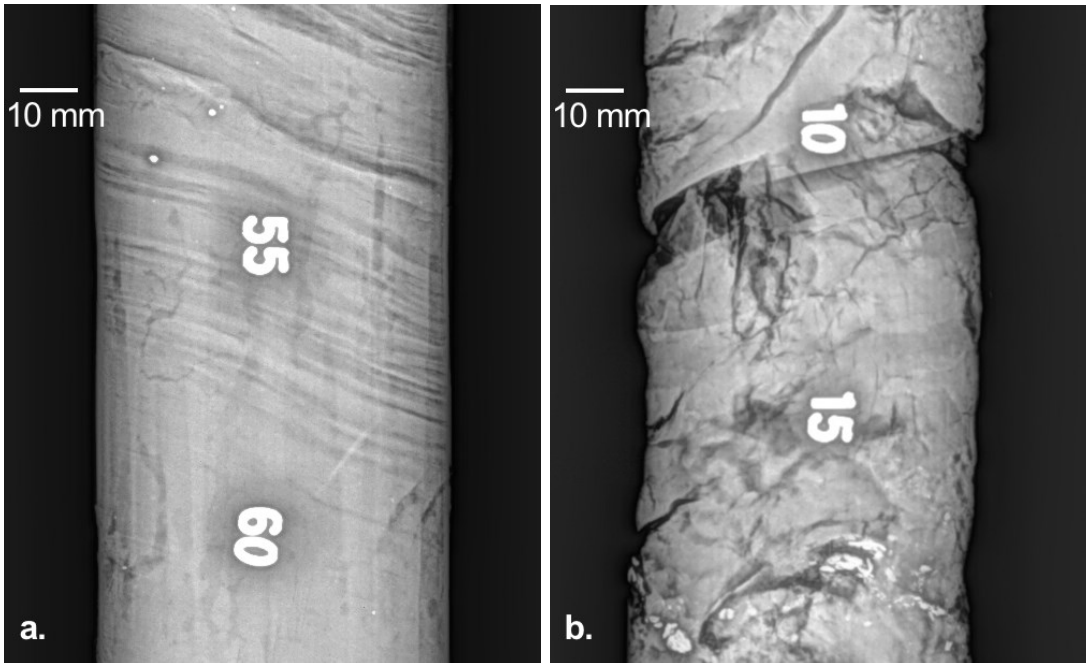

Figure 4.4. X-ray radiographs of (a) lamination (BH15-03 depth 14.5 m) and (b) disturbed core suggesting a twisting motion (BH15-03 depth 15.7 m); numbered lead markers indicate the distance in centimeters from the top of core run

4.2.2 ASSESSMENT OF SAMPLING DISTURBANCE

Prior to the selection of laboratory tests samples, disturbance that the sampling process may have caused to the soil was assessed. Factors of drilling-induced disturbance are stress-relief at the bottom of the borehole, sample travel within the core barrel, and shear against the core edge, for instance (Olson 1986). Moisture migration within the sample is a factor of disturbance during transportation and storage. Samples affected by disturbance may fail to represent the in-situ soil. In the case of clay, disturbance may cause softening, thereby reducing the consistency and the cohesion of the soil (Terzaghi and Peck 1967).

Typically disturbance was apparent in the topmost 20 centimeters of each 152-cm (5 feet) long core run (Figure 4.4.b). This was observed on both x-ray images and when examining the soil itself. X-ray images show cracks. Darker tones show less dense clay (Jamiolkowski et al. 1985), suggesting it suffered swelling. An examination of the core in the laboratory revealed that the topmost part of each core run is less stiff soil. The topmost end of the core run is the part that was pushed first in the core barrel during drilling. Therefore, it suffered more disturbance; associated cracks and deformations have resulted in drilling-induced softening.

Eroded-like surfaces of the core were another drilling-induced feature (Figure 4.5). Such disturbance was attributed to water circulation over the sample surface during the drilling process; it was found to be only superficial.

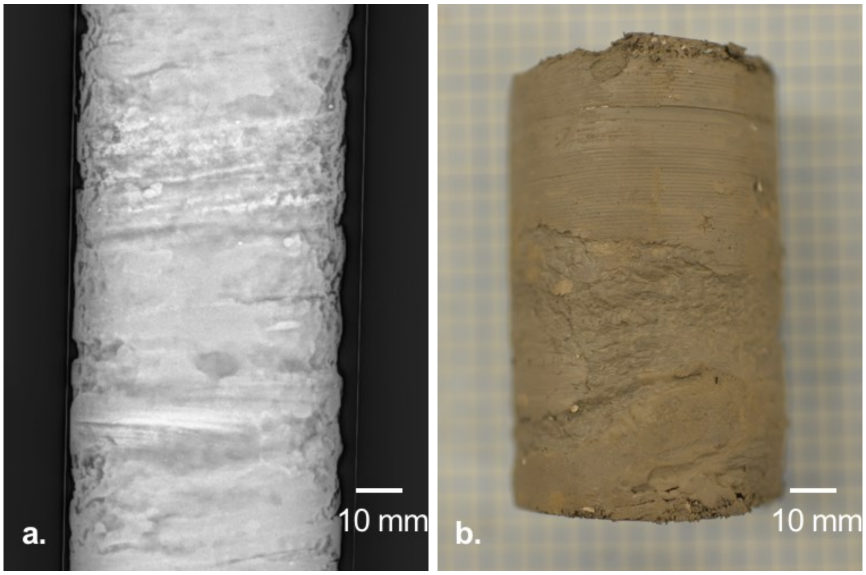

Figure 4.5. Erosion-like superficial disturbance as seen on (a) x-ray radiograph and (b) photograph (BH15-03 depth 10.5 m)

Most of the core was unaffected by the aforementioned forms of disturbance. Selected samples were considered intact and the associated fabric and overconsolidation preserved. Some fissures within the core were another form of drilling-induced disturbance. Because bedding functions as a plane of weakness for the stiff clay, bedding-parallel fissility readily develops and the core is easily split apart in many locations of the glaciolacustrine unit. Splits were observed along fine sand laminae and glossy clay surfaces (Figure 4.6).

Efforts were made to dismiss such features and identify natural fissures and slickensides in particular. Slickensides are polished surfaces that form when clay mineral particles align in the direction of shear displacement (Bromhead 2013). Striae marking the slickenside surface indicate the direction of shear displacement. Linear striae indicate shear displacement so these slickensides are assumed to be natural and their locations were mapped (see Chapter 5). Slickensides with concentric striae indicate a twisting motion of the core during the drilling process (Figure 4.7). They may be drilling-induced fissures or they may be naturally occurring fissures whose appearance was affected by drilling; it is not possible to differentiate one from the other.

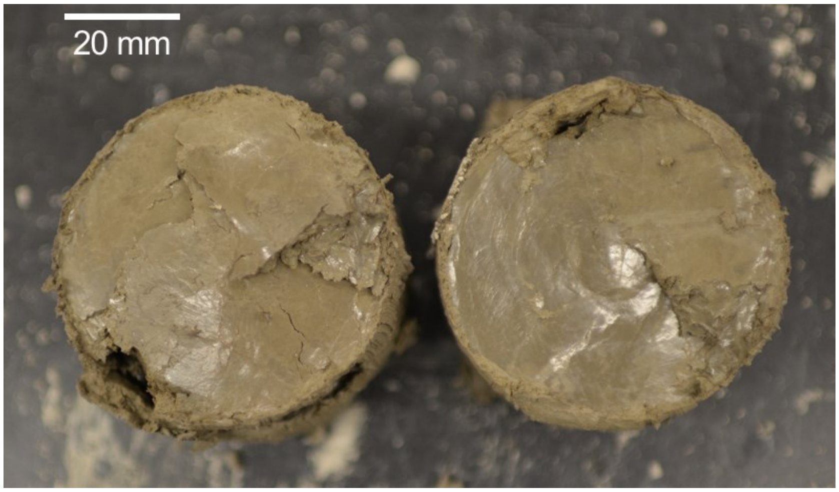

Figure 4.6. Core split along glossy surface (BH15-03 depth 12.9 m)

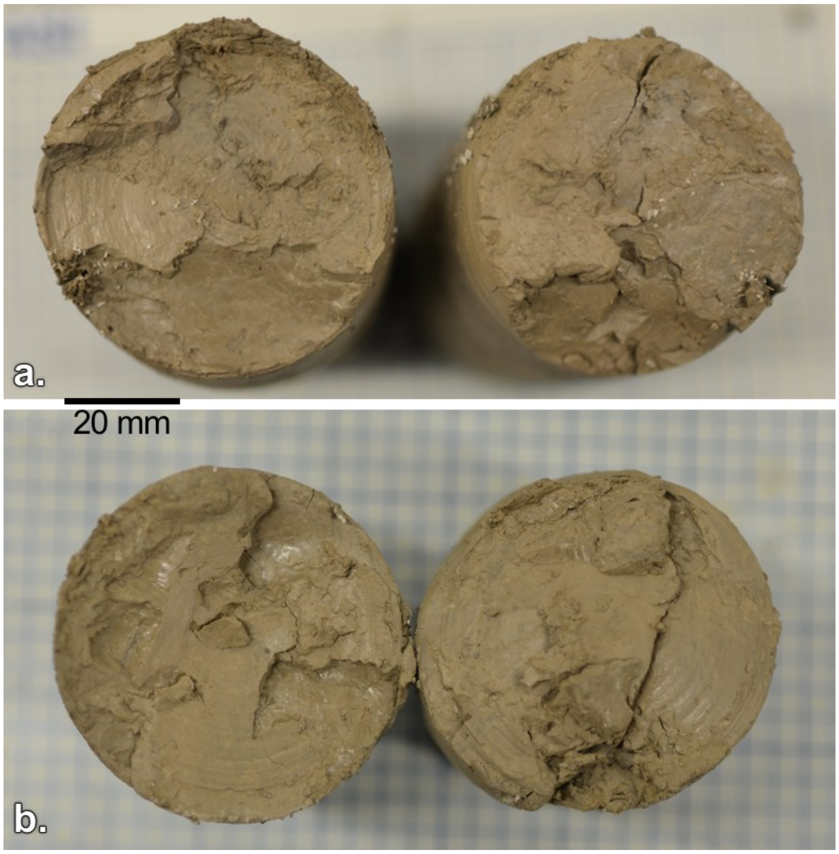

Figure 4.7. Drilling-induced slickensides: (a) BH15-03 depth 9.6 m; (b) BH15-03 depth 10.2 m

4.2.3 SAMPLE SELECTION

Small samples were collected every 20 centimeters on average to measure the water content. The detailed profile of the water content (see Chapter 5) does not show any variation that could result from disturbance or moisture loss during the 13-month-long storage period (February 2015 to March 2016).

Samples for direct shear and oedometer tests were selected based on the x-ray images and visual inspection to identify the most intact material (Figure 4.8). Large samples were used so that multiple specimens could be obtained from each sample to provide the most consistent results. Clay-rich components of the borehole sequence were isolated and used as test samples. However they make up a tiny proportion of the core, so supply for this material was limited. Obtaining samples that are both large and homogeneous proved difficult, so test results had to be interpreted in light of the heterogeneous nature of glaciolacustrine sediment.

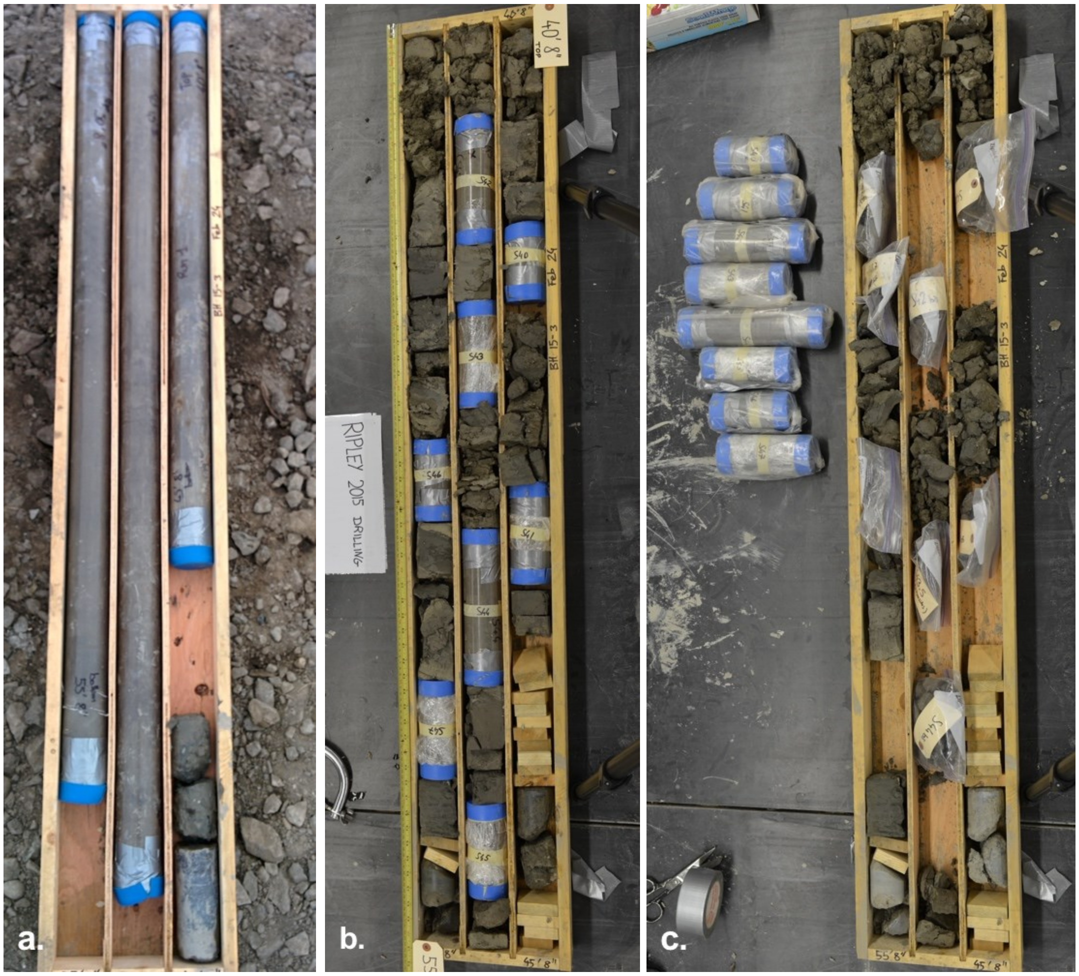

Figure 4.8. Phases of core handling: (a) on-site conditioning; (b) logging; (c) sample selection

4.3 LABORATORY TESTING PROGRAM

This section describes the tests conducted in the laboratory. Information on the laboratory equipment is provided. Test procedures are detailed, with an emphasis on methods specific to stiff or glaciolacustrine soil. Test parameters are briefly summarized in this section. Additional details about the test parameters are presented in the Appendices.

Deficiencies that were encountered during the testing program are discussed. Some test results are presented in this section in order to illustrate methodology issues: soil extrusion in both the direct shear and ring shear tests (see Section 4.3.5); slippage at the soil-platen interface in the direct simple shear (DSS) test (see Section 4.3.6.a). Methods modified in consequence are detailed.

4.3.1 SOIL CLASSIFICATION

The following properties were tested for soil classification:

- Particle size analysis in order to characterize the clay content (grain size <0.002 mm);
- Atterberg limits (plastic limit and liquid limit) in order to characterize the plasticity, a property relevant to clayey soil;
- Specific gravity in order to characterize soil solids density, required for calculating the void ratio during oedometer tests.

a. Sample preparation

Aggregates of soil particles should be broken down because index tests rely on the behaviour of individual particles. Heavily overconsolidated clays can present diagenetic bonding or induration that cause aggregation. During the air-drying process bonding between the clay particles becomes stronger as well. According to the ASTM standard procedure (ASTM D4318 2010), a mortar and pestle should be used to grind the soil until the aggregates of soil particles are broken up into separate grains. When disaggregation is difficult Stark and Hussain (2013) suggest that ball or disc milling be used instead. This facilitates disaggregation but potentially modifies the texture and gradation of the soil, biasing index properties results. Mudstones, claystones or shales present significant diagenetic bonding so ball or disc milling is necessary for disaggregation. It is also tempting to use milling for dried-up heavily overconsolidated clay such as the Ripley clay, but the standard mortar and pestle procedure was preferred here. With a sustained pounding and grinding effort, it satisfied the break-up of the soil into separate grains and did not bias index properties.

b. Particle size analysis

In the hydrometer test for particle size analysis, the sample is dispersed into a slurry and placed in a sedimentation jar, following the ASTM D422 (2007) standard test method.

The hydrometer reads the density of the slurry. Fine soil particles stay longer in the suspension before settling at the bottom of the jar with the rest of the sediment. As a result, it takes longer for the slurry density to decrease. In order to span smaller particle sizes, hydrometer readings should be extended over a longer time. In the case of the Ripley clay, given the relatively high proportion of fines, hydrometer tests lasted at least four days.

A total of eight particle size analysis tests were done on the BH13-01 samples, spanning depths from 8.5 to 27.5 m. On the BH15-03 samples, five particle size analysis tests were done, spanning depths from 12.8 to 16.2 m.

c. Atterberg limits

In the Atterberg limits test, the prepared sample was rehydrated with distilled water so that the water content is close to the liquid limit. The soil was left to cure for at least 16 hours and mixed again until moisture is equally absorbed across the sample. It is possible to proceed to the liquid limit test only after the rehydrated mixture has a consistency representative of the water content (ASTM D4318 2010).

Atterberg limits results are sensitive to the operator running the test because of the numerous manual operations involved in the test procedure: the use of the grooving tool and the hand-operated cup device in the liquid limit test, and the hand-rolling of soil into threads in the plastic limit test. The operator's habits and judgement influence these operations. When preparing samples, assessing whether the degree of disaggregation or rehydration is sufficient also depends on the operator. The same operator with the same tools conducted all the present tests, ensuring that the results would be coherent for the different samples.

From BH13-01, 11 samples were tested for Atterberg limits, spanning depths from 8.5 to 27.5 m. From BH15-03, 14 samples were tested, spanning depths from 7.6 to 16.2 m.

d. Specific gravity

Specific gravity tests were conducted following the ASTM D854 (2014) standard procedure. For each sample the test was repeated two or three times. Repeated results systematically fell within a 0.04 range.

The objective is not to characterize the soil in terms of the specific gravity property but to obtain a range of specific gravity values required for calculating the void ratio in oedometer tests. Four samples from BH13-01 were tested. Three samples from BH15-03 were tested.

4.3.2 X-RAY DIFFRACTION

X-ray diffraction (XRD) is a method used to identify clay minerals. A diffractogram captures reflections of various intensities, a function of the spatial configuration of the atomic planes. A particular clay mineral is identified based on a recognizable reflection pattern.

Aggregates of air-dried soil were destroyed using a mortar and pestle in order to maximize the detection of clay-size particles. As a way to shorten sample preparation, hydrometer analysis for segregating the clay-size fraction (<2 μm) was not conducted. Instead the sample passed through the No. 200 (75 μm) sieve, after which a powder sample was ready for XRD.

Non-clay minerals are largely seen on the diffractograms since the samples are not limited to the clay-size fraction. The diffraction patterns of the clay minerals remain easily distinguished because the clay fraction among these samples is large, according to particle size analyses results (see Chapter 5).

From BH15-03 four samples were analyzed with XRD, spanning depths from 8.4 to 16.2 m.

4.3.1 INTACT SAMPLE PREPARATION

Oedometer, direct shear and DSS tests were conducted on intact samples. Cylindrical-shaped specimens with diameters of 50 mm and heights of 19 mm were obtained from the 63.5-mm diameter core samples. Trimming to a smaller diameter allowed the elimination of the outermost part of the core, which was the most vulnerable to disturbance. The use of a wire saw allowed for cautious trimming so the cutting ring was easily pushed into the soil. Unlike a razor blade, a wire saw does not offer a surface for the sticky clay to attach to, which results in fewer disturbances. A razor blade was only used to trim the more silty specimens.

The supply of intact samples was limited and therefore direct shear tests had to be conducted first. Non-intact samples lose their intact soil properties but still qualify for ring shear tests and index properties tests conducted on remoulded soil specimens.

4.3.2 OEDOMETER TESTS

The objective of the oedometer tests was to study the stress history of the Ripley clay. The preconsolidation stress σ'_p of the soil was determined using Casagrande's method (Casagrande 1936). In order to define the virgin compression curve the normal stress had to be increased incrementally to a maximum of 7000 to 9000 kPa.

In a front-loading oedometer (Wykeham Farrance model "24251", Figure 4.9), the vertical force was applied by a counter balance 11:1 ratio lever loading system. The vertical displacement was measured with a 25-mm range linear variable displacement transducer (LVDT), with an accuracy of 0.2%.

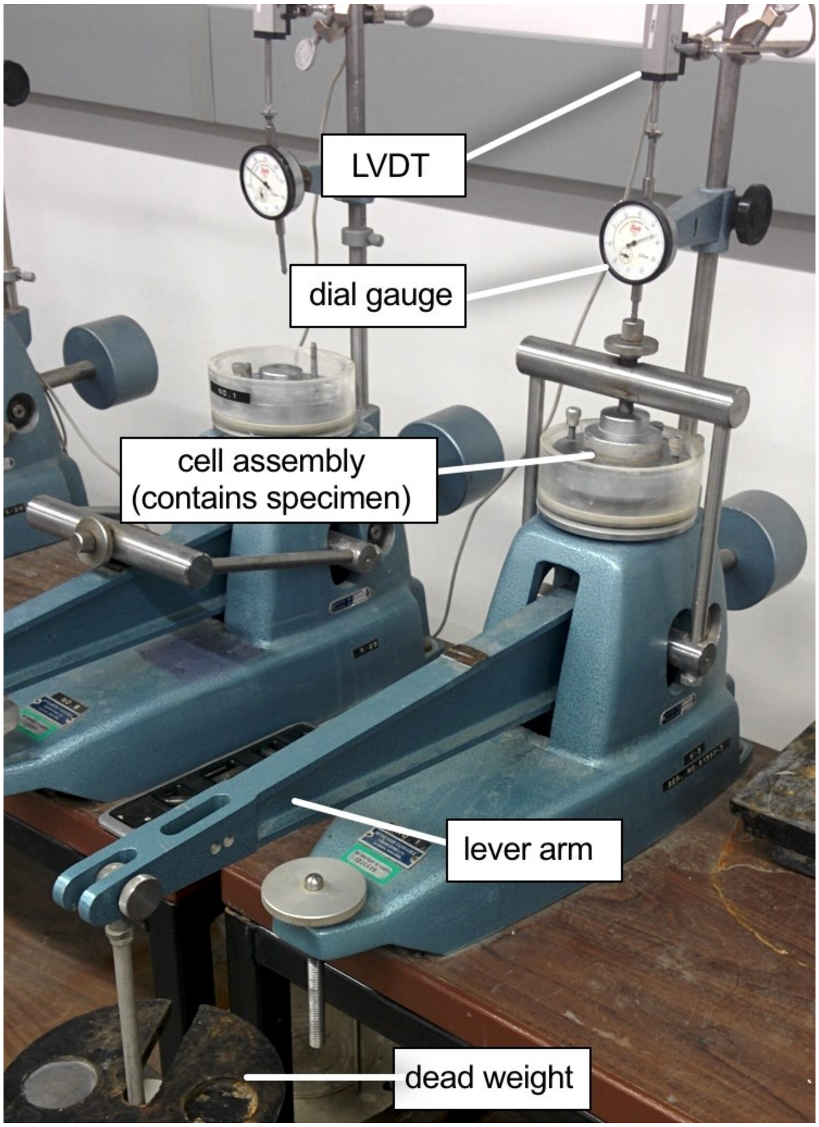

Figure 4.9. Front-loading oedometer

Overconsolidated clay tends to swell when the soil specimen in the water bath is inundated and subject only to a small normal load. Therefore the water bath was only filled with distilled water after a load increment higher than 400 kPa. Under small increments of normal stress, the clay is still in its overconsolidated range so consolidation may occur fast enough that two load increments can be applied in one day. Larger load increments were applied every 24 hours with a load increment ratio (*LIR*) of 1, following the ASTM D2435 (2011) standard procedure.

A sequence of successive load decrements was also achieved for each test after virgin compression was reached, with an LIR of 1 or 2. The unloading phase improves the distinction between recompression and virgin compression curves, and thereby also improves the interpretation of the consolidation properties.

Time-deformation properties of the soil were interpreted from the Log Time method (or Casagrande method). Time-deformation properties provide precious knowledge that can be used to select the appropriate shear strain rate in the drained shear tests (Head 1994).

Eight one-dimensional consolidation tests were conducted in total.

4.3.3 DIRECT SHEAR TESTS

The direct shear test serves to determine both the peak and residual strength of intact clay. Shear strength loss from peak to residual, and the span of displacement necessary for this strength loss, are two quantities that define brittleness, a characteristic relevant to the formation of shear failure surfaces within stiff overconsolidated soil. To characterize brittleness, it is necessary to preserve the intact fabric of the heavily overconsolidated clay. Therefore direct shear tests should rely on the best available samples.

Direct shear tests were conducted with a Karol-Warner Co. model “2001D” apparatus (Figure 4.10). The shear force was measured with a ±6.7-kN capacity S-type load cell, with an accuracy of 0.02%. The vertical force was applied by a 6.7-kN capacity pneumatic loading system and measured with an accuracy of 0.25%. The vertical displacement and the shear displacement were measured with 25-mm range LVDTs, with an accuracy of 0.2%.

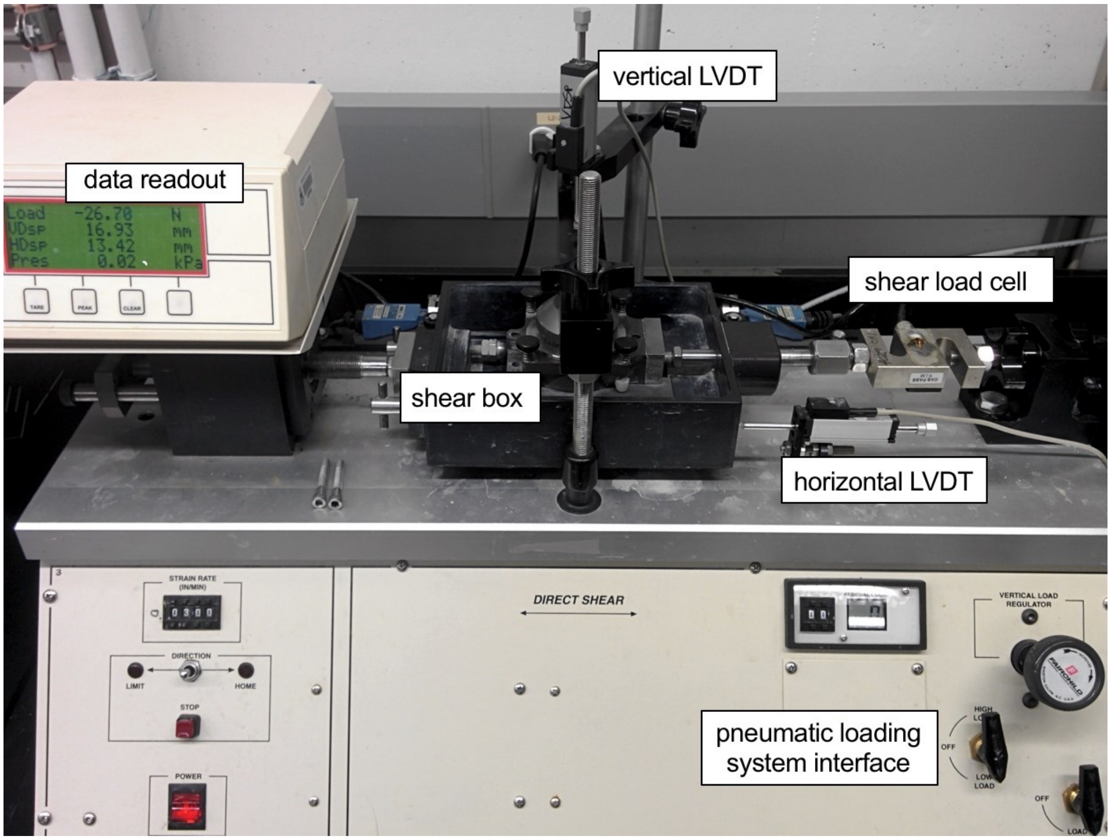
vertical LVDT
data readout
Load -26.70 N
VDsp 16.93 mm
HDsp 13.42 mm
Pres 0.02 kPa
shear load cell
shear box
horizontal LVDT
STRAIN RATE (IN/MIN)
DIRECTION
LIMIT
HOME
STOP
POWER
DIRECT SHEAR
VERTICAL LOAD REGULATOR
pneumatic loading system interface
HIGH LOAD
OFF
LOW LOAD

Figure 4.10. Direct shear apparatus

The specimen is consolidated back under a normal load, in the range of the stresses experienced by the sample before being retrieved from the field.

According to the sample depths and recorded water table level (Schafer 2016), the representative in-situ vertical effective stress σ' is 120 to 220 kPa. Specimens were sheared under normal stresses ranging from 130 to 400 kPa so the Mohr-Coulomb failure envelope could be determined accurately.

In the drained direct shear test, the chosen shear strain rate is one that is slow enough to ensure that shear-induced pore water pressures dissipate. Time-deformation data from the oedometer tests was used to compute the time required to achieve 50 percent consolidation t_{50}. This parameter depends on sample overconsolidation. The reference value for t_{50} was based on a high consolidation load increment, i.e. in the normally consolidated range. Then the time to failure was estimated following Equation 4.1 (ASTM D3080 2011).

Equation 4.1. $t_f = 50 \times t_{50}$

Distance to failure d_f (defined as the amount of shear displacement required to reach peak strength in the direct shear test) can be as low as 1.5 mm for this brittle soil. The displacement rate was chosen following Equation 4.2. For the majority of the tests the shear displacement rate was set equal to 0.013 mm/min.

Equation 4.2. $$\dot{d} = {}^{d_f}\!/_{t_f}$$

Residual strength is mobilized after significant shear displacement, thus requiring an adapted procedure called a reversal direct shear test: when the stroke limit is reached (7 mm approximately), the direction of displacement is reversed. With multiple reversals it is possible to extend shear displacement to amounts where the shear strength reaches a lower-bound ultimate value known as residual strength.

In the reversal procedure the soil is alternatively sheared in two directions, which may delay or even prevent the platy clay particles from maintaining an aligned position. Consequently, most tests take an additional amount of displacement to reach residual strength. After 60 to 70 mm of shear displacement was accumulated, the shear strength reached a constant value, which was maintained as the shear displacement increased. This ultimate value was taken as the measure of the residual shear strength (Head 1994).

For BH15-03, 25 direct shear tests were run on intact specimens for a total of 11 samples characterized for shear strength with the direct shear apparatus, spanning depths from 7.6 to 16.2 m.

4.3.4 RING SHEAR TESTS

The ring shear apparatus has been specially developed to test the residual strength of soils (see Chapter 2). The Bromhead-type apparatus used in this study holds a ring-shaped specimen with a 70 mm inner diameter and a 100 mm outer diameter. The specimen is 5 mm thick so shear-induced pore water pressures are dissipated quickly, allowing for a larger shear displacement rate.

Ring shear tests were conducted with a Wykeham Farrance model “Torshear” apparatus (Figure 4.11). The vertical force was applied by a counter balance 10:1 ratio lever loading system. The shear force was measured with a pair of 1-kN capacity load cells, with an accuracy of 0.1%.

The vertical displacement was measured with a 10-mm range LVDT, with an accuracy of 0.02%. The shear displacement was measured with an etched scale on the circumference of the base platen, in degrees.

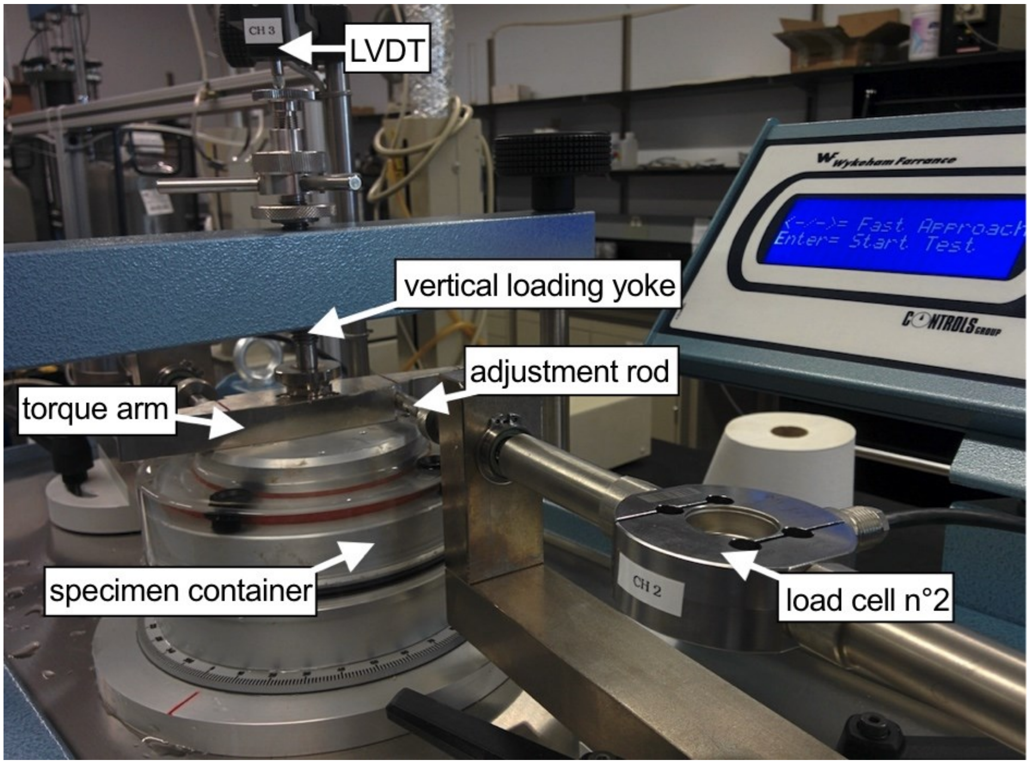
LVDT
vertical loading yoke
adjustment rod
torque arm
specimen container
load cell n°2
CH 3
CH 2
Wykeham Farrance
<-/->= Fast Approach
Enter= Start Test
CONTROLS GROUP

Figure 4.11. Ring shear apparatus

The apparatus complies with the ASTM 6467 (2013) standard procedure upon which this study's tests were based. Specimens of remoulded soil were prepared with the same method as in the index properties tests. The remoulded sample water content was increased at least to the liquid limit, making it easier to mix and cure the soil into a uniform paste. As suggested by Meehan et al. (2007), the test specimens water contents were decreased in order to reduce consolidation settlement. The soil mixture was left to air-dry while mixed regularly to keep a uniform consistency, until a water content near the plastic limit is reached. The test specimen is formed in place by kneading the soil paste into the specimen container in successive layers, avoiding entrapment of air. Then, specimens were consolidated and sheared under normal stresses ranging from 100 to 300 kPa.

According to the ASTM 6467 (2013) standard procedure, the residual strength state is achieved when the plot of the stress-strain relationship becomes parallel to the shear strain axis. In order to comply with this criterion, ring shear tests were run to 60 mm or more of shear displacement. Enough displacement was imposed so that a slickensided surface was fully formed and the residual shear strength of the soil was measured.

The strain rate was chosen to be small enough to ensure drained conditions throughout the test. The guidelines for the direct shear test also apply here. Most of the tests were conducted with a displacement rate of 0.024 mm/min.

Some specimens were tested under different strain rates to investigate rate effects on shear strength. Three different strain rate orders of magnitude were imposed during the same test. The specimen was first sheared at the regular shear strain rate of 0.024 mm/min until residual shear strength was attained. Shear was continued at a 10 times slower rate (0.0024 mm/min). The test lasted three days at this rate in order to achieve 10 mm of shear displacement. The velocity was increased back to the regular rate and then to a 10 times faster rate (0.24 mm/min). Although fast, drained conditions were maintained at this rate, excess pore water pressures were not generated on the already fully formed shear surface.

For each of the three rates, enough strain was imposed along an artificial slickenside to measure the residual strength. The dependence of residual shear strength on strain rate can be assessed using this method.

Rate effects are slight variations in the shear strength. They are accurately measured only in quality ring shear tests where any shear strength bias is eliminated. In particular, soil extrusion must be restricted in spite of the extended shear displacement that multiple-rate tests imply (see Section 4.3.5).

For BH15-03, 16 ring shear tests were run for a total of eight samples characterized for residual shear strength, spanning depths from 7.6 to 16.2 m. Among these tests, four were multiple-rate tests where rate effects were investigated.

4.3.5 SOIL EXTRUSION ISSUE

During both the direct shear and ring shear tests the soil softens at the shear surface. As shear occurs, soil particles loose their bond with the rest of the soil and escape from the specimen container. This phenomenon is referred to as soil extrusion. Extruded soil obstructs the clearance between the moving parts of both apparatuses. An excessive accumulation of extruded soil creates additional friction forces interfering with the measure of shear stress.

a. Direct shear

In the direct shear apparatus, soil is extruded at the gap between the shear box halves. The amount of extruded soil accumulated at the gap depends on the side of the shear box and the direction of shear (Figure 4.12, Figure 4.13). Test results show both sides of the shear box and both shear directions are prone to soil extrusion. It is not possible to quantify the amount of extruded soil that accumulates at the shear box gap versus the amount that simply escapes in the water bath. Therefore, no direct relationship exists between the amount of settlement and the build-up of additional friction forces at the gap of the shear box. However, settlement is an obvious indication of soil extrusion, and an observation of excessive and asymmetrical (depending on the shear direction) settlement during shear is often paired with an asymmetrical shear response as measured by the load cell (Figure 4.14). In the author's opinion, excessive soil extrusion during shear is the cause of misleading, asymmetrical measurements of the shear load in the direct shear apparatus.

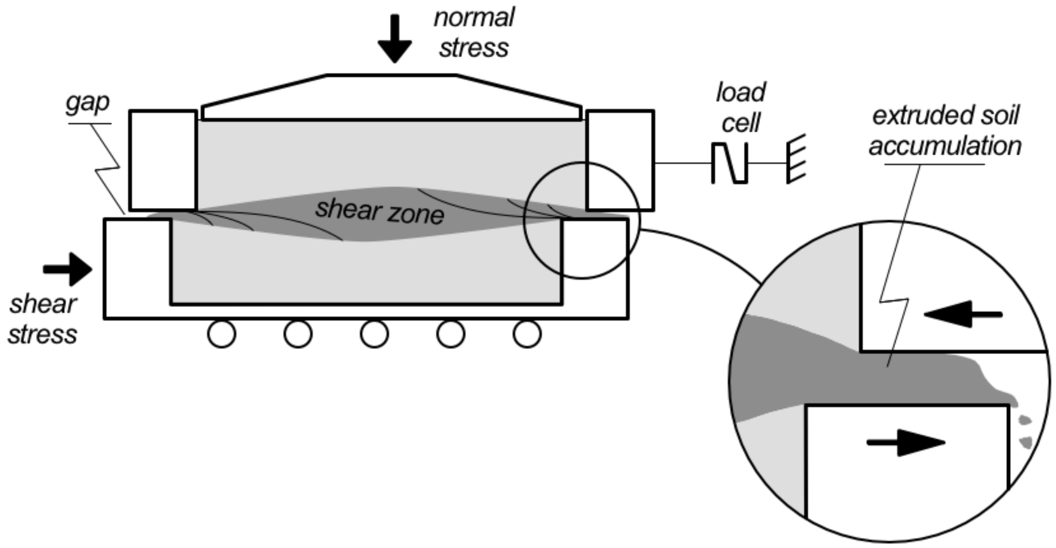

Figure 4.12. Soil extrusion in the direct shear apparatus

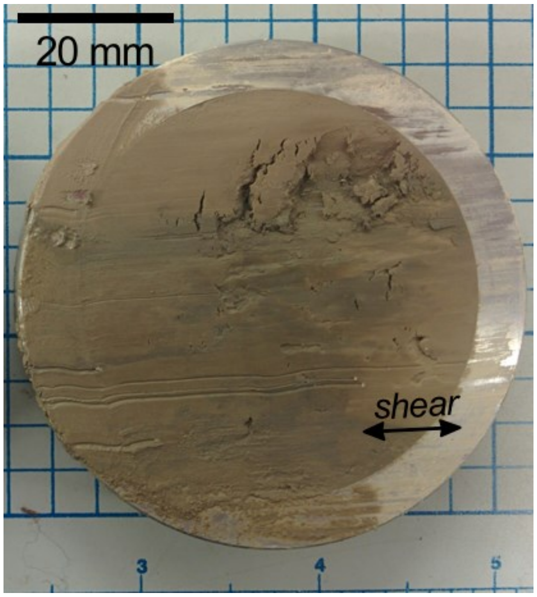

Figure 4.13. One-sided soil extrusion on direct shear test Specimen S35_1

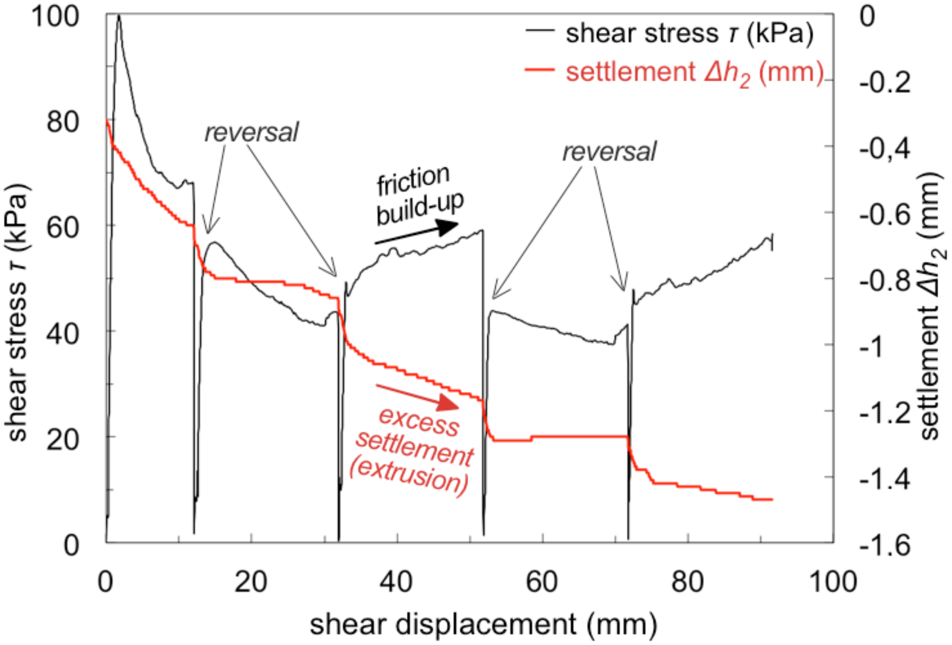

Figure 4.14. Asymmetrical response on direct shear test S46_1 (gap: 0.20 mm) stress-strain plot

In order to prevent excessive soil extrusion, the gap between the shear box halves should be limited. On the University of Alberta apparatuses, four gap screws need to be rotated to lift the upper shear box half away from the lower shear box half. Keeping apart the edges of the shear box halves and inserts ensures that the horizontal shear load is transmitted through the soil itself. The guideline found in the literature (Head 1994, ASTM D3080 2011) is to adjust the gap to the diameter of the largest soil particle of the specimen. Hence soil particles are not crushed between the halves of the shear box and no undesired frictional force is created. For fine-grained soils in particular the guideline is to set the gap to 0.50 mm.

However, particle size analysis (see Chapter 5) suggests that particles 0.10 mm or larger are rare in the tested soil. Tests that were run with a gap of 0.40 mm or more showed significant soil extrusion during the shear stage, and often this was more pronounced in one of the shear directions. Such tests yield strength results that are difficult to interpret because the difference between the two shear directions is not negligible (Figure 4.14).

In order to resolve this issue the gap was set to less than 0.20 mm. Most of the tests were run with a gap of 0.10 mm, corresponding to 1/8 of a turn of the gap screw. The passage of soil particles between the halves of the shear box was allowed but limited. Particular care was taken to even the gap all around the shear box, so that one side of the shear box was not more prone to soil extrusion than the other. In order for the gap to remain uniform and constant, it was decided not to back out the four gap screws after the gap was set, after the consolidation stage.

These measures limited soil extrusion. In tests S250_3, S32_1, S33_1, S35_1 and S46_1, soil extrusion was not limited sufficiently, so an asymmetrical response was still observed. In this case, the residual shear strength was chosen equal to the average shear strength measured over both shear directions.

b. Ring shear

In the ring shear apparatus, soil extruded during shear accumulates between the specimen container and the top platen (Figure 4.15). The top platen settles during the consolidation stage, leaving only a narrow gap at the perimeter of the specimen container for extruded soil to escape. The top platen settles again as the soil is progressively extruded, worsening the effects. Settlement becomes significant after a certain amount of shear displacement, as does the accumulation of extruded soil. Parasitic friction forces become non negligible (Figure 4.16). According to Stark and Vettel (1992), the total settlement should not exceed 0.75 mm in order to minimize wall friction.

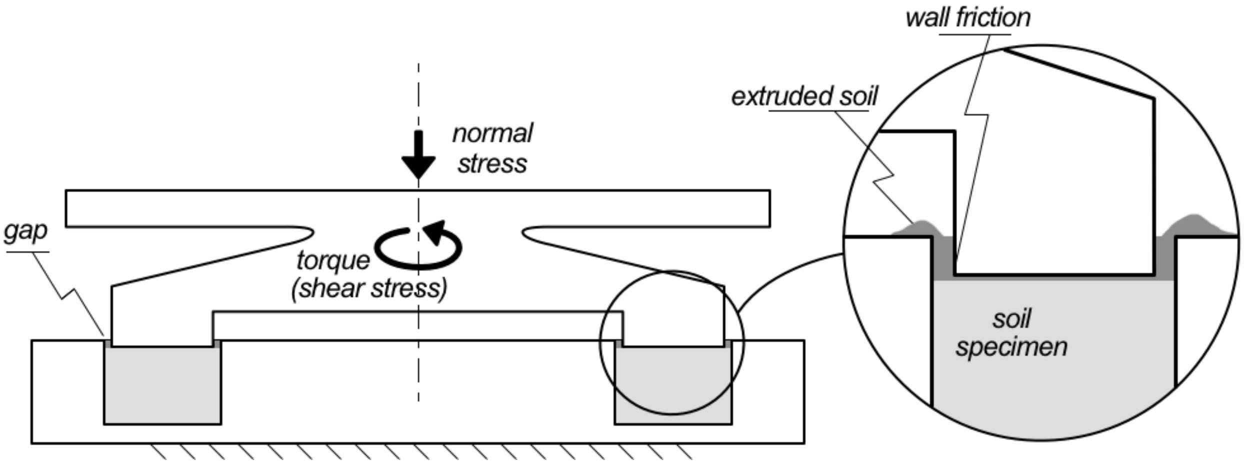
wall friction
extruded soil
normal
stress
gap
torque
(shear stress)
soil
specimen

Figure 4.15. Soil extrusion in the ring shear apparatus

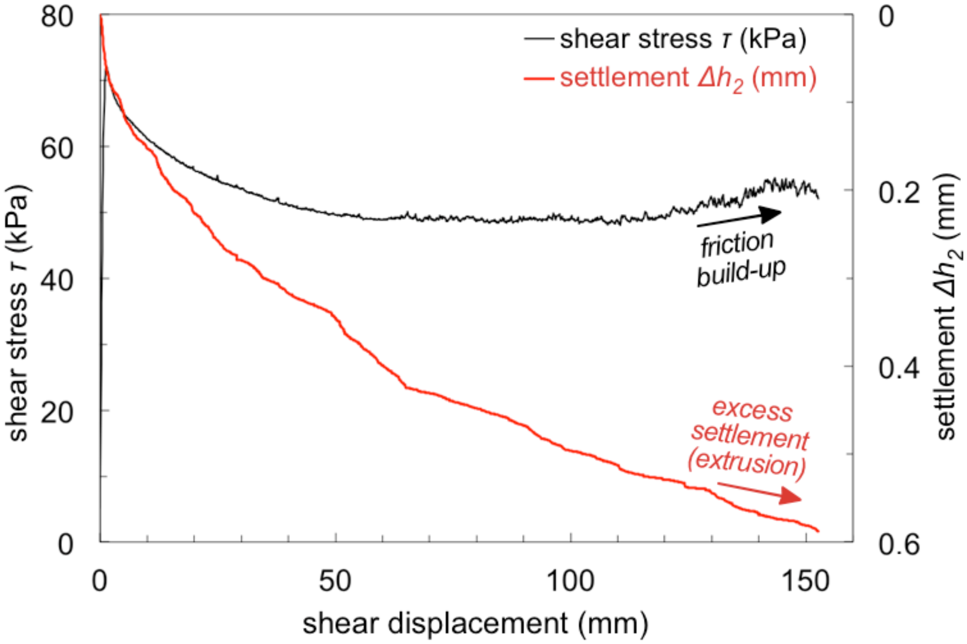

Figure 4.16. Response on ring shear test S250_a stress-strain plot

In order to limit the settlement of the top platen, clay specimens were prepared with special care. As mentioned in Section 4.3.4, the remoulded sample water content should be decreased before placing a specimen in the specimen container. Harris and Watson (1997) and Meehan et al. (2007) suggest remoulding the sample at a water content near the plastic limit.

The consolidation load applied to the test specimen should be preferably low and applied in small increments to limit settlement. Test procedures such as the ASTM D6467 (2013) standard procedure recommend the multi-stage method where the same test specimen is consolidated and sheared under different normal stresses. This method is time-efficient because after one test the shear strength is known for several normal stresses. However, settlement and soil extrusion become excessive as the same test specimen is subject to multiple stages of consolidation and shear. This study did not use the multi-stage method, preferring instead to apply a single normal load for each test.

The formation of a pre-sheared surface at a high strain rate before the consolidation stage drastically reduces the amount of strain needed to attain residual strength in the subsequent shearing stage. The pre-shearing stage is time-saving, but a high strain rate can result in significant soil extrusion (Harris and Watson 1997). The present study did not employ the pre-shearing method.

4.3.6 DIRECT SIMPLE SHEAR TESTS

The constant-volume DSS test imitates undrained conditions. The change in normal load required to maintain constant volume is interpreted as the change in pore water pressure in undrained, constant load conditions. The DSS test yields the effective stress path and the pore water pressure response, giving insight on the shear behaviour of heavily overconsolidated glaciolacustrine clay (see Chapter 2).

DSS tests were conducted at a laboratory of MEG Technical Services (Richmond, British Columbia) with a GDS Instruments model “EMDCSS” apparatus. This NGI-type apparatus complies with the ASTM 6528 (2007) standard procedure. Intact clay specimens were trimmed to a height of 16 mm and a diameter of 48.5 mm. A rubber membrane reinforced by stacked rigid rings held the intact specimen and provided lateral confinement for a K_o condition, while allowing uniform simple shear deformation (Figure 4.17, Figure 4.18).

By default the apparatus is equipped with porous ceramic platens with grooves 1 mm deep and 2 mm wide, transverse to the shear direction in order to interlock with the soil. Platens must provide a no-slip boundary condition at the top and bottom end of the specimen, such that applied horizontal displacement is entirely transmitted to the soil in the form of shear strain. During an early series of tests conducted by Schafer (2014), this setup failed to ensure a no-slip condition at the soil-platen interface. Later tests used platens modified with conical pins (height: 1.9 mm; base diameter: 1.9 mm; spaced every 6.0 mm) to provide a better interlock with the clay (Figure 4.17).

The normal force and shear force were measured with 5-kN capacity load cells, with an accuracy of 0.1%. The shear displacement was measured with a 15-mm range LVDT, with an accuracy of 0.1%. In addition, a high resolution vertical LVDT (range: 2.5 mm; accuracy: 0.1%) was used for feedback to the normal force actuator in order to maintain a constant specimen height during the test (active height control).

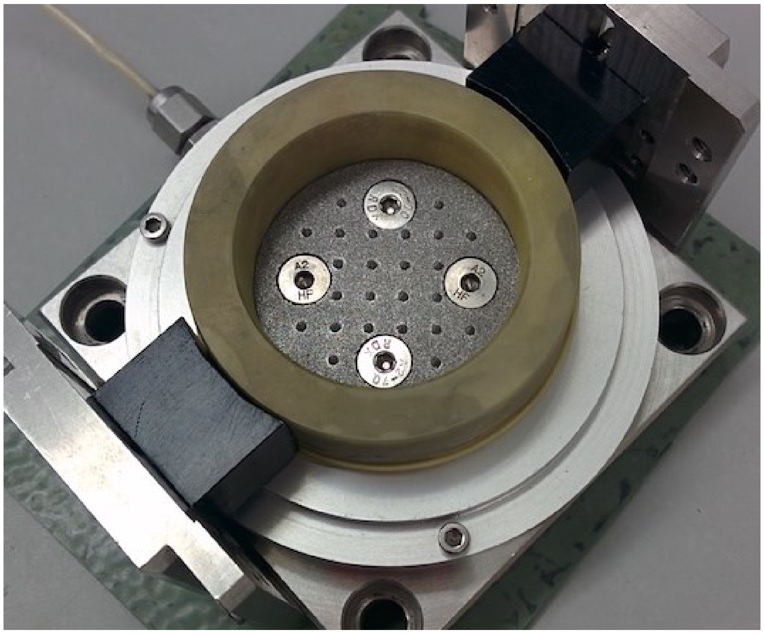

Figure 4.17. DSS apparatus pedestal, bottom platen with pins, stack of confining rings and membrane

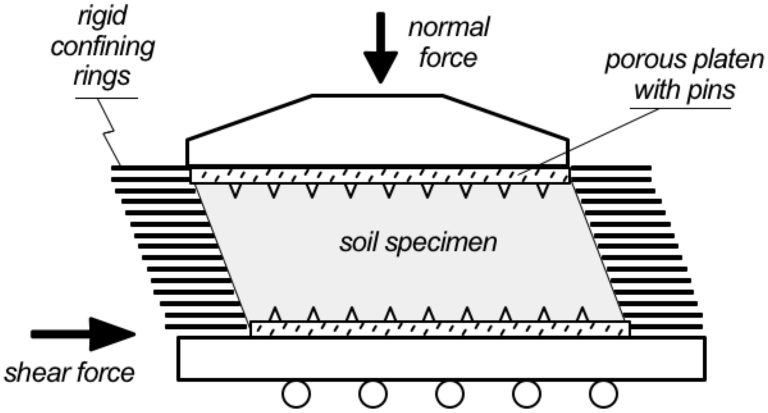
rigid confining rings
normal force
porous platen with pins
soil specimen
shear force

Figure 4.18. DSS apparatus schematic

Consolidation prior to shear under high normal stress as in the SHANSEP technique (Ladd 1991) is inappropriate here because mechanical overconsolidation would destroy the natural structure of the clay. The objective is to characterize the undrained shear response inherited by the natural preconsolidation process of stiff glaciolacustrine clay. Hence the clay is simply reconsolidated to the estimated in-situ vertical stress σ'_v as in the recompression technique (Bjerrum 1973).

Results raised concern that the pore water pressure response depended on the shear strain rate. Early tests were performed at a shear strain rate $\dot{\gamma}$ of 5 %/hour (0.013 mm/min). Other tests were performed at lower strain rates (Table 4.2) in order to investigate this matter.

Nine DSS tests were run using samples S4 and S6 from borehole BH13-01 at a depth of 13.4 m and 17.5 m, respectively. Additional detail is provided in Table 4.2.

Table 4.2. Parameters of the DSS tests

Sample	Test	Shear strain rate $\dot{\gamma}$ (%/h)	Consolidation load σ'_{v0} (kPa)	Applied shear strain γ (mm)	Amount of slippage $\gamma_{slippage}$ (mm)
S4	S4a	5	300	3.2	1.8
	S4b	5	500	3.2	1.8
	S4c	5	200	3.0	2.7
	M4a[1]	5	300	3.2	>2.5
	M4b[1]	5	500	3.2	>2.5
S6	S6a	1	300	1.9	1.5
	S6b	5	300	3.2	2.2
	S6c	5	300	3.2	>2.5
	S6d	0.5	300	3.2	>2.5

[1] tests by Schafer (2014) using the default platens

a. Issues

i. Slippage

Questions were raised as to whether the apparatus could transfer, entirely, the applied shear force to the soil specimen without slippage at the soil-platen interface. The Ripley slide clay well exceeds the stiffness of soil typically tested with the NGI-type DSS apparatus. The greater shear force necessary to strain the specimen exceeds the friction that can be mobilized at the soil-platen interface, thus causing slippage.

As described previously, the slippage issue called for modification of the platens. Work on stiff soils by Burn (1968, on Leda Clay) and Lau (1988, on Cowden Till and London Clay) suggested that adding protruding pins would improve the friction at the soil-platen interface, thereby limiting slippage. As reported in Table 4.2, slippage was not eliminated but limited.

ii. Non-uniform simple shear

Protruding pins of the platens disturb the clay in the boundary zone of the specimen. Slippage adds disturbance when pins cut through the soil of the boundary zone. The shear strength decreases in the boundary zone, becoming that of softened clay. The boundary zone of the specimen becomes a preferential zone in which shear can occur (Tests S4a, S4b and S6b). The boundary zone clay is not dilative anymore and subsequent undrained shear generates contractive behaviour.

Fully drained conditions are essential to the constant-volume DSS test in order to simulate undrained conditions. Dissipated pore pressures are associated with a volumetric response of the soil. In the constant-volume test, the volumetric response is resisted by a change in normal stress, which simulates the change in pore water pressure of undrained conditions. The strain rate must be low enough for any shear-induced pore pressures to dissipate. Figure 4.19 presents Test S6a ($\dot{\gamma}$ = 1 %/hour) with a dilative behaviour and considerably larger undrained shear strength, the expected response for heavily overconsolidated clay. It indicates that a fast strain rate ($\dot{\gamma}$ = 5 %/hour) may prevent shear-induced pore pressure from dissipating. The distribution of effective stress cannot equilibrate across the specimen. The resulting stress non-uniformity contributes to failure in the boundary zone.

When large non-uniformities cause the soil to fail by default in the boundary zone, the response is by no means that of uniform simple shear and the observed behaviour is not that of heavily overconsolidated glaciolacustrine clay. Le Meil et al. (2016) discuss these technical matters in more depth (see Appendix J).

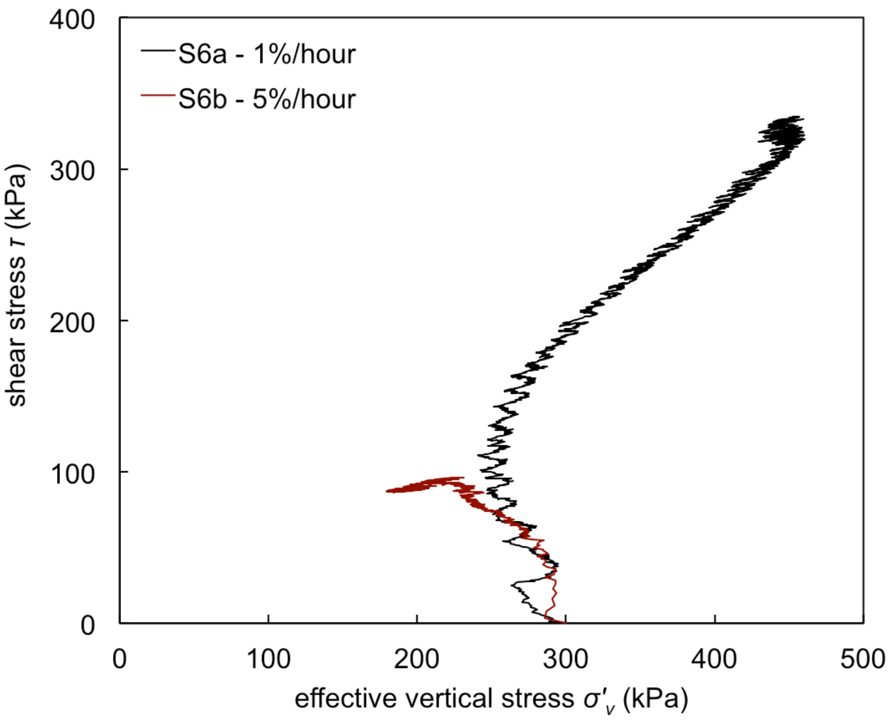

Figure 4.19. Effective stress paths for DSS tests S6a (1%/hour) and S6b (5%/hour)

Chapter 5. Results: Borehole Stratigraphy and Shear Strength of Soils

5.1 SOIL DESCRIPTION

5.1.1 GENERAL

a. Interbedded silt and clay

Alternating silt and clay were observed in the core. At natural water content, silt-rich beds are typically grey and of low to medium plasticity, whereas clay-rich beds are brown and of high plasticity. Where silt and clay beds alternate, the facies is referred to as interbedded silt and clay. This facies is characteristic of glaciolacustrine soil. Interbedding is well distinct when in the form of centimetre-thick contrasted beds called varves (Figure 5.1). Note the sharp contact between the silt and clay beds in Figure 5.1.a. However, in Figure 5.1.b, the varve fines upward and sharp contact is made only atop the light brown clay.

A variety of color tones is observed within the interbedded silt and clay. Clay appears mottled where reddish and light brown tones coexist (Figure 5.2.a). Bed thickness varies from a few tens of centimetres to one millimetre or less, at which point the beds are called laminae. Often beds are not distinct because they are composed of multiple laminae varying gradually in color tone or grain size (see Appendix B). Hence, lesser plasticity silt subtly grades into higher plasticity clay; the interbedded facies is not recognized readily.

Bedding is made more complex when inclined or contorted. Figure 5.2.b illustrates disrupted bedding.

Occasionally sand intersects the silt and clay sequence in the form of millimetre-thick laminae (Figure 5.2.c). More rare occurrences of gravel are also recorded.

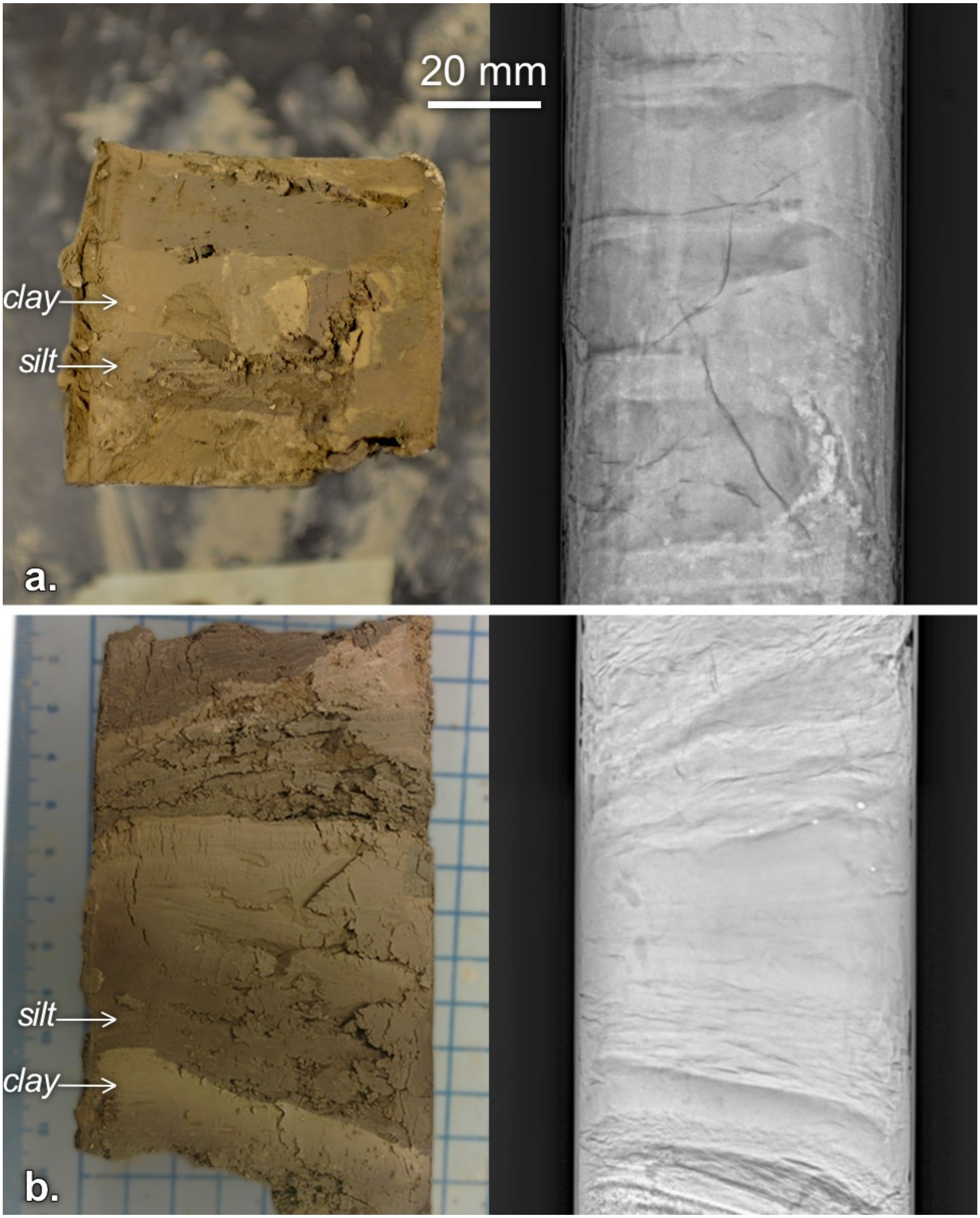
20 mm
clay
silt
a.
silt
clay
b.

Figure 5.1. Varves as seen in a photograph and radiograph: (a) BH15-03 depth 12.7 m; (b) BH15-01 depth 9.8 m

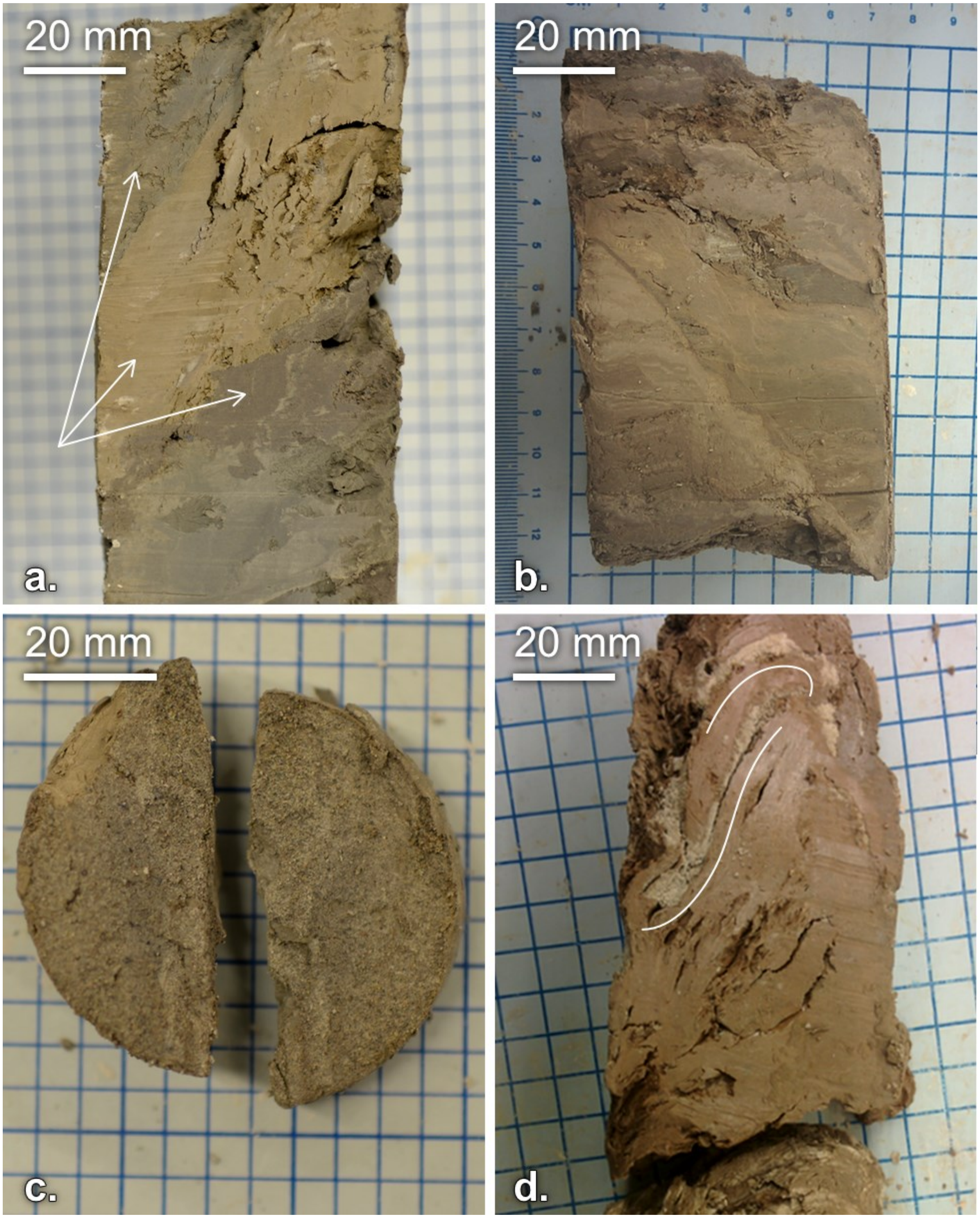

Figure 5.2. (a) Mottled clay at BH15-03 depth 9.8 m (different soil colors indicated); (b) disrupted bedding at BH15-01 depth 10.7 m; (c) sand lamina at BH15-03 depth 10.7 m (transverse view); (d) contorted sand laminae at BH15-01 depth 7.4 m (contortion underlined)

b. Units

The interbedded silt and clay described above constitute a recognizable unit of the core sequence. Another unit, of silty clay, overlies the interbedded silt and clay. In terms of grain size, the soil content is similar between both units. The absence of bedding in the shallower unit of silty clay is the main difference from the unit of interbedded silt and clay. The unit of silty clay has a medium to stiff consistency whereas the interbedded silt and clay have a very stiff consistency, except for some clay-rich beds. Shallower soil is also appreciably more contorted (Figure 5.2.d) and fissured (Figure 5.3). Gypsum precipitates (size ≤1 centimetre) exist in the fissures of the shallower soil, in particular where reddish color tones are prevalent (Figure 5.3). Some cobbles intersect the silty clay unit.

Fine-grained dark grey to olive rock interpreted as andesite underlies the unit of interbedded silt and clay (see Appendix B). Fractures infilled with clay and gravel exist near the contact with the interbedded silt and clay. Otherwise the rock is massive. It constitutes bedrock.

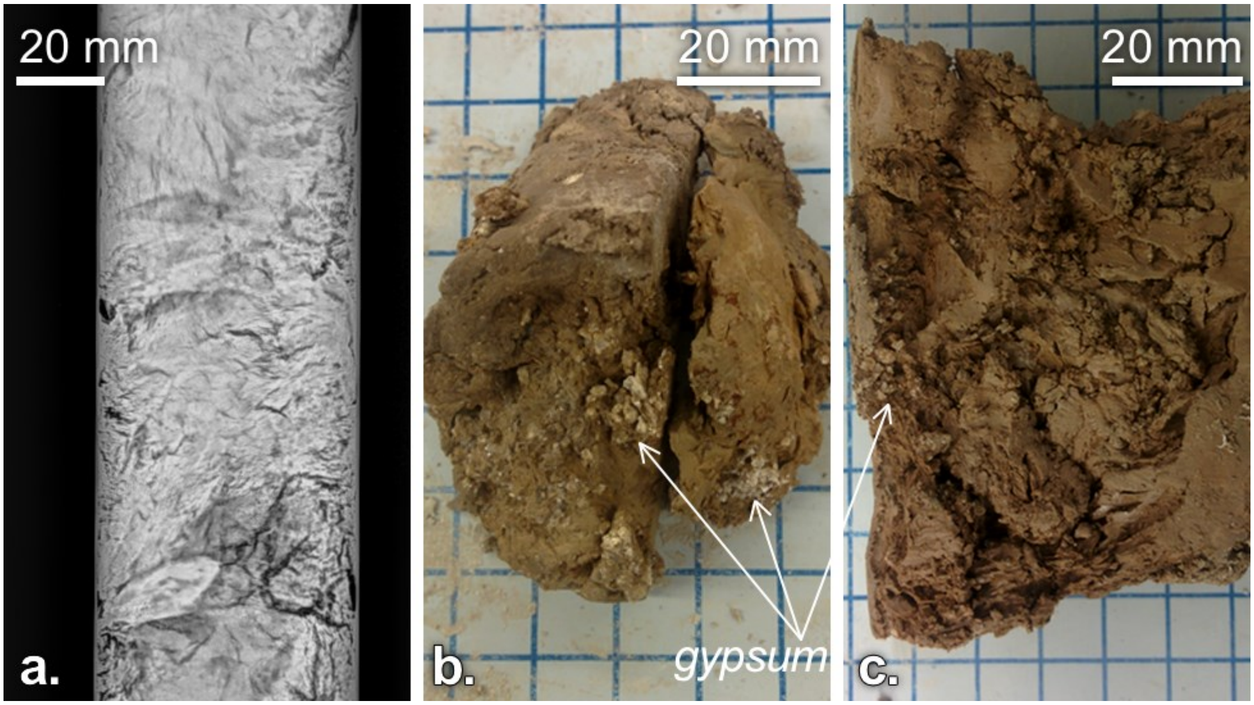

Figure 5.3. Fissured and weathered clay: (a, b) BH15-01 depth 4.7 m; (c) BH15-01 depth 5.7 m

c. Slickensides

Some fissures exhibit polished-like surfaces known as slickenslides. The polished-like aspect is the consequence of clay mineral particles aligned in the same direction. Slickensides are found at several locations in the core, often within clay-rich beds of the interbedded silt and clay unit. Figures 5.4 and 5.5 depict slickensides hosted in high plasticity light brown clay. Slickensides are also marked by linear striae such as those shown in Figures 5.4.b, 5.4.d and 5.4.e. Slickensides are observed to dip 10 to 30°.

5.1.2 BOREHOLE STRATIGRAPHY

Complete core logs for BH15-03 and BH15-01 are presented in Appendix C.

a. Borehole BH15-03

From a depth of 0.0 to 4.8 m, a borehole was advanced using ODEX drilling. No core was retrieved. Drill cuttings consist of crushed cobbles, silt and clay.

From a depth of 4.8 to 6.4 m, the core was only partially recovered and consists of fine-grained dark grey to olive rock interpreted as andesite. It is heavily fractured.

From a depth of 6.4 to 7.7 m, the core is brown silty clay of medium plasticity. No bedding structure is apparent. Andesite cobbles and traces of sand are observed at different locations. Slickensides are observed at depths of 7.1 and 7.3 m.

From a depth of 7.7 to 10.8 m, the core is interbedded silt and clay with a stiff consistency. Figure 5.2.a depicts mottled clay at a depth of 9.8 m. Traces of sand are apparent (Figure 5.2.c). Slickensides are observed at depths of 8.6 (Figure 5.4.a), 9.2 (Figure 5.4.c) and 9.5 m (Figure 5.5).

From a depth of 10.8 to 12.4 m, the core is only partially recovered and consists of andesite rock. Fractures are infilled with clay and some sand.

From a depth of 12.4 to 16.8 m, the core is interbedded silt and clay with a very stiff consistency. Varves are distinct at a depth of 12.7 m (Figure 5.1.a). A slickenside is observed at a depth of 13.0 m (Figure 5.4.b).

From a depth of 16.8 to 18.0 m (end of borehole), the core is massive andesite interpreted as bedrock.

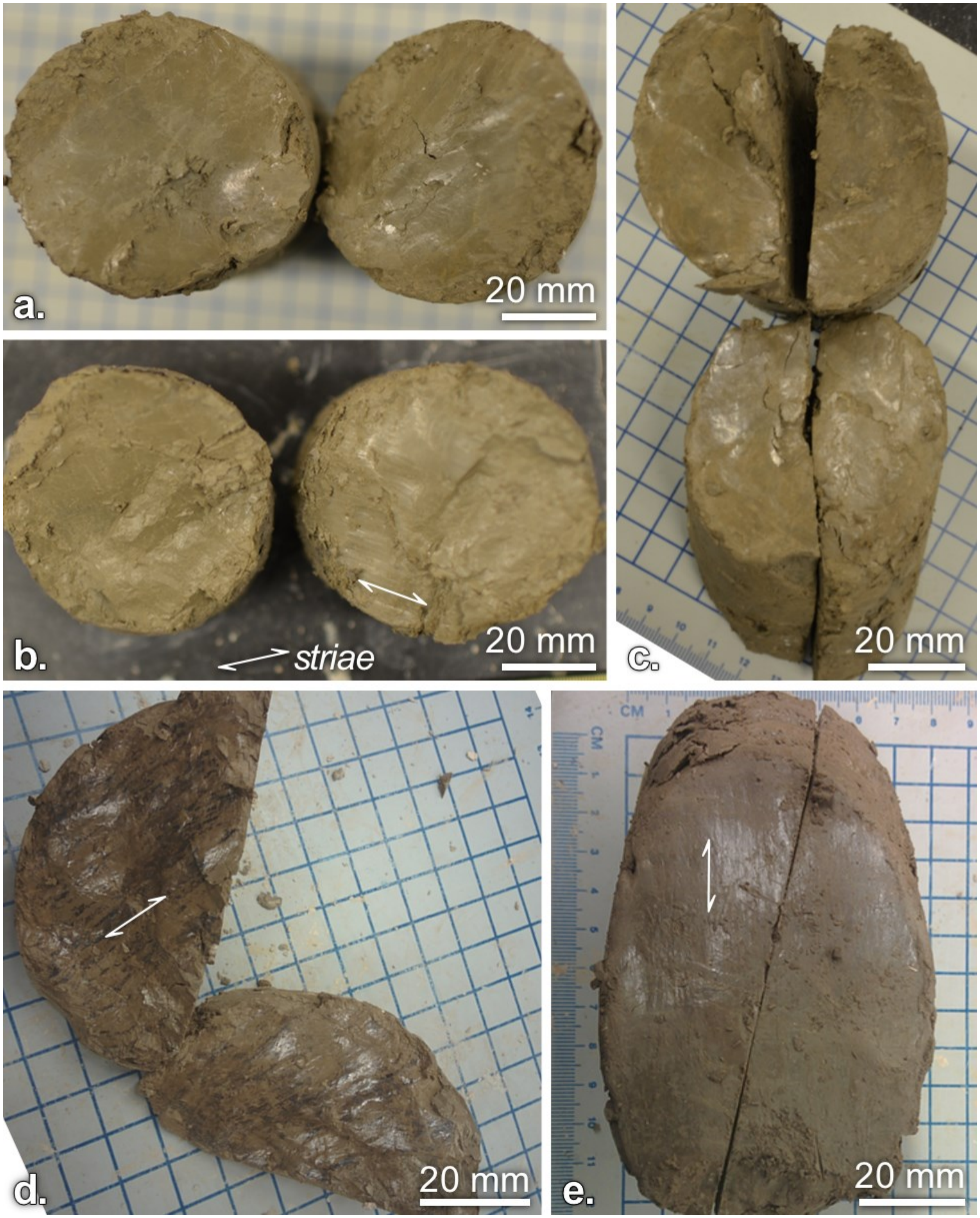
a.
20 mm
b.
striae
20 mm
c.
20 mm
d.
20 mm
e.
20 mm

Figure 5.4. Slickensides: (a) BH15-03 depth 8.6 m; (b) BH15-03 depth 13.0 m; (c) BH15-03 depth 9.2 m; (d) BH15-01 depth 7.7 m; (e) BH15-01 depth 13.1 m

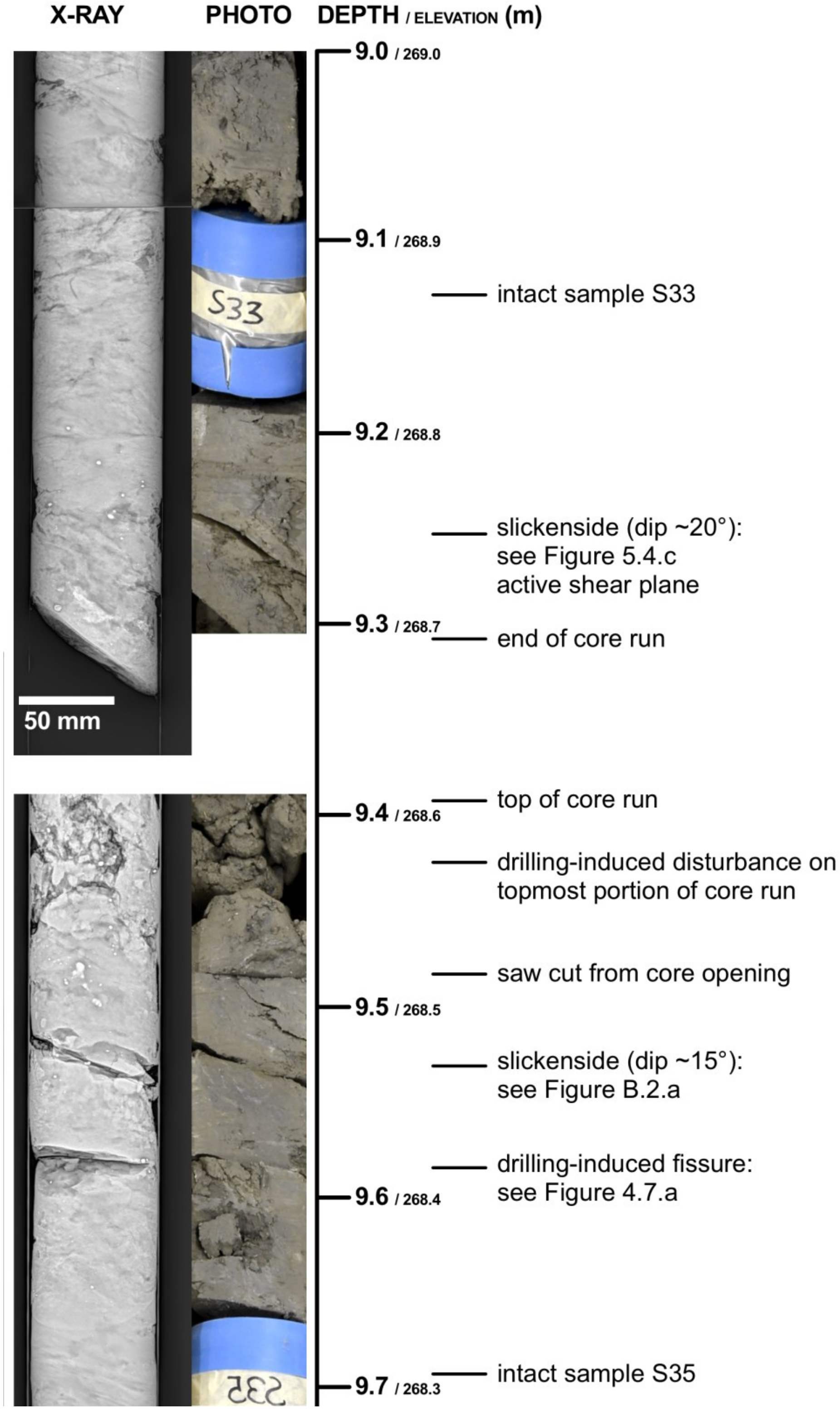
X-RAY
PHOTO
DEPTH / ELEVATION (m)
9.0 / 269.0
9.1 / 268.9
intact sample S33
S33
9.2 / 268.8
slickenside (dip ~20°):
see Figure 5.4.c
active shear plane
9.3 / 268.7
end of core run
50 mm
9.4 / 268.6
top of core run
drilling-induced disturbance on
topmost portion of core run
saw cut from core opening
9.5 / 268.5
slickenside (dip ~15°):
see Figure B.2.a
drilling-induced fissure:
see Figure 4.7.a
9.6 / 268.4
intact sample S35
9.7 / 268.3
S35

Figure 5.5. Core description of BH15-03 from a depth of 9.0 to 9.7 m (shear zone)

b. Borehole BH15-01

From a depth of 0.0 to 3.4 m, a borehole was advanced using ODEX drilling. No core was retrieved. Drill cuttings consist of silt and clay.

From a depth of 3.4 to 8.6 m, the core is silty clay with medium plasticity, and a medium to stiff consistency. It is mottled with tones varying from light brown to reddish to dark grey. Traces of sand are apparent, in the form of contorted laminae at a depth of 7.4 m (Figure 5.2.d). Gypsum precipitates are observed at different locations, coincident with fissures (Figure 5.3). A slickenside with dark-coloured striae is observed at a depth of 7.7 m (Figure 5.4.d).

From a depth of 8.6 to 15.2 m, the core is interbedded silt and clay with a very stiff consistency. Centimetre-thick varves are distinct at depths of 9.0, 9.8 (Figure 5.1.b) and 13.0 m. Fine sand laminae occur at different locations. Slickensides are observed at depths of 10.1, 12.0, 12.7, 13.1 (Figure 5.4.e) and 13.8 m.

From a depth of 15.2 to 18.6 m (end of borehole), the core is only partially recovered and consists of massive andesite interpreted as bedrock.

5.1.3 SLOPE INCLINOMETER SURVEYS

Inclinometer surveys were conducted on the Ripley slide from the end of February 2015. Surveys did not reveal any movement at boreholes BH15-01 and BH15-06 (Figure 5.6). Inclinometer surveys at BH15-03 have recorded 8 mm of displacement at an approximate depth of 9.0 m (elevation 269 m) over a 132-day period.

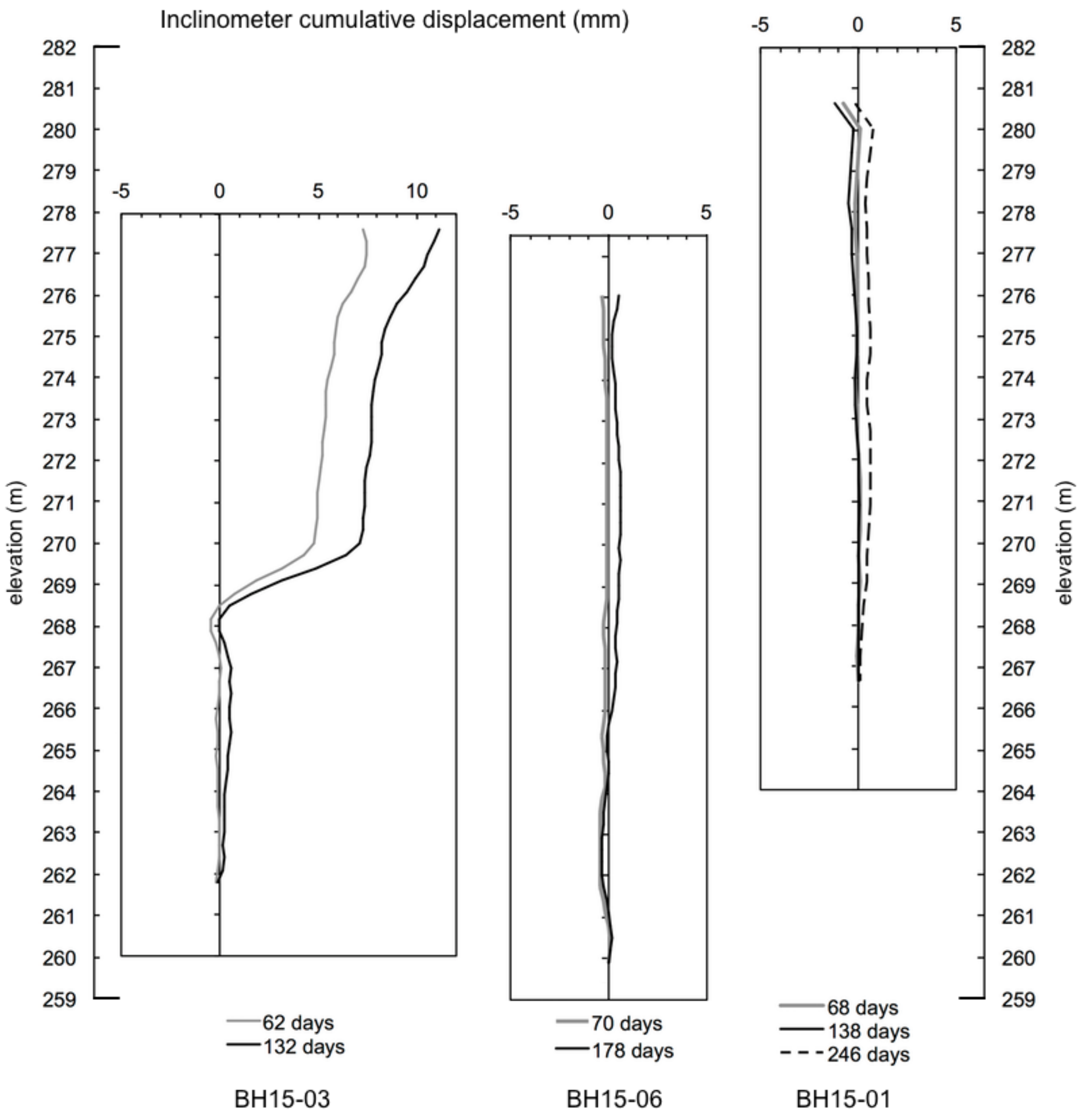

Figure 5.6. Cumulative displacement measured from inclinometers installed in 2015

5.2 LABORATORY TESTS RESULTS

5.2.1 INDEX PROPERTIES

a. Water content

The natural water content was measured on the preserved core of borehole BH15-03. Results range from 24 to 46%. The mean natural water content is 33% (Figure 5.7).

b. Atterberg limits

Atterberg limits were tested on both BH13-01 and BH15-03 samples. The plastic limit is between 17 and 28%. The liquid limit is between 32 and 84%. Results are plotted in the plasticity chart (Figure 5.8). The soil is classified as fat clay (CH) or lean clay (CL), depending on the sample.

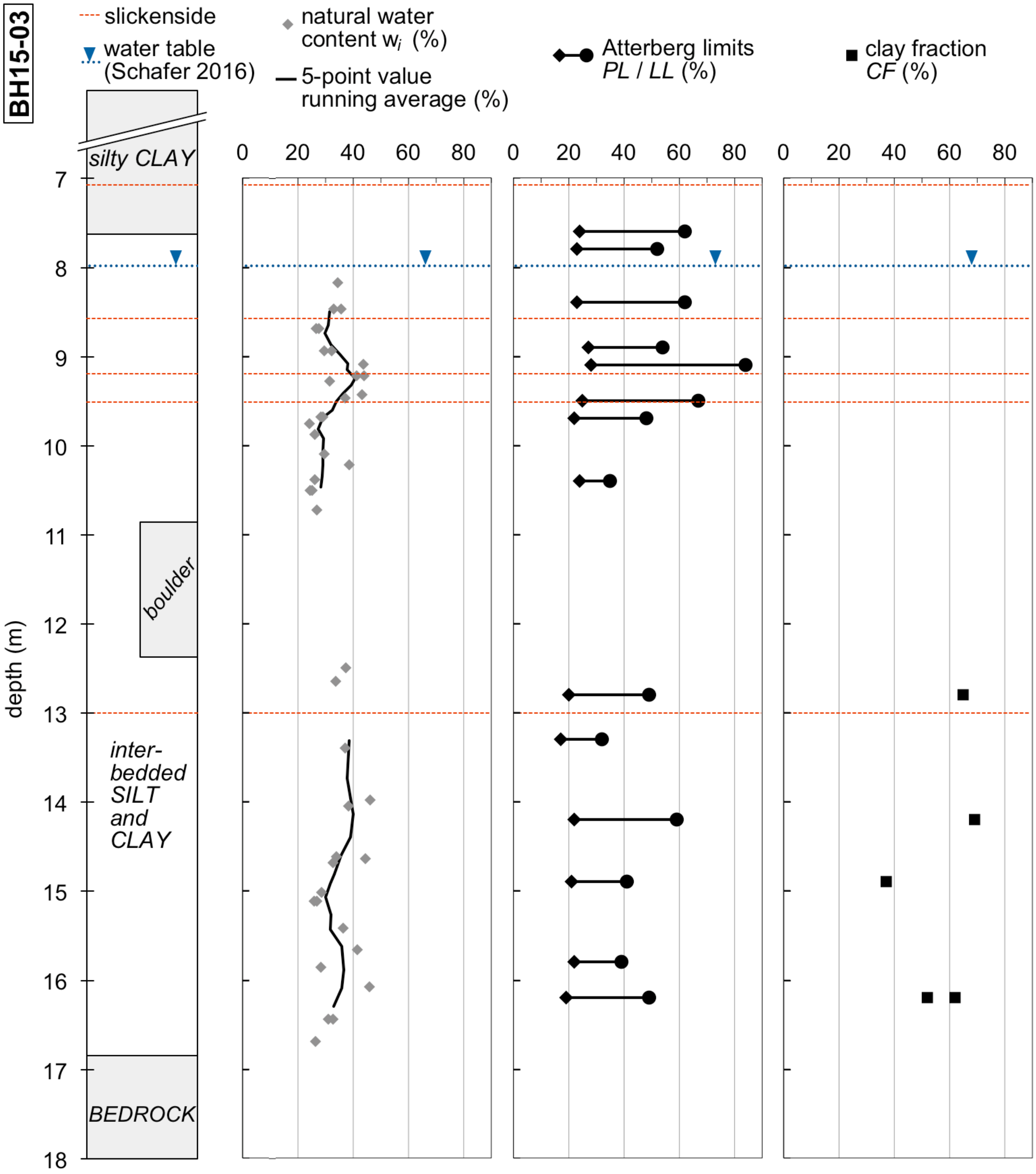

Figure 5.7. Results for BH15-03 samples, against depth

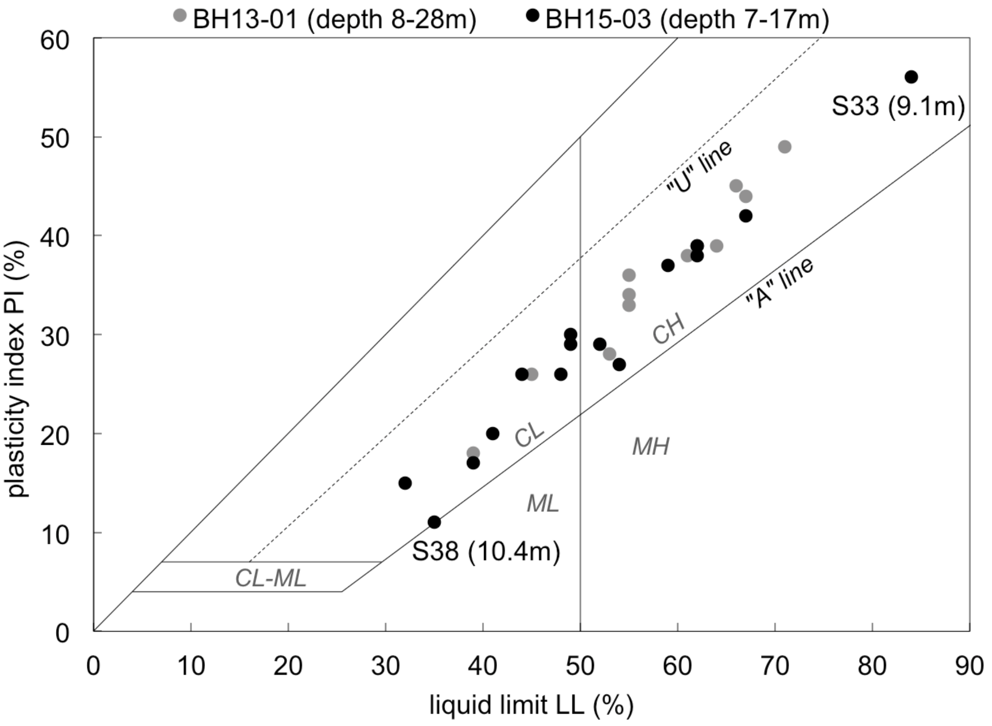

Figure 5.8. Plasticity chart

c. Particle size analysis

The clay fraction is defined as the fraction of soil finer than 0.002 mm, in percentages. After a particle size analysis, the mean clay fraction among tested samples was 58%. The clay fraction ranges from 37 to 77%. The remaining soil fraction is mostly silt-size particles between 0.002 and 0.063 mm. A marginal fraction consists of coarse particles over 0.063 mm. Figure 5.9 illustrates the particle size distribution.

The activity of the clay (A) links plasticity and the clay fraction (Equation 5.1). Activity can be determined for 12 samples where both quantities are measured. Results are plotted in Figure 5.10. The mean activity of the Ripley clay is 0.60. The approximate correlation between plasticity and clay fraction suggests that the clay mineralogy remains consistent across Unit 2 (see Section 5.2.2). The span of the Atterberg limits does not result from variable mineralogy, but from variable clay fraction, depending on the location of the sample within Unit 2 interbedded silt and clay.

Equation 5.1. $A = {}^{plasticity\ index}/_{clay\ fraction}$

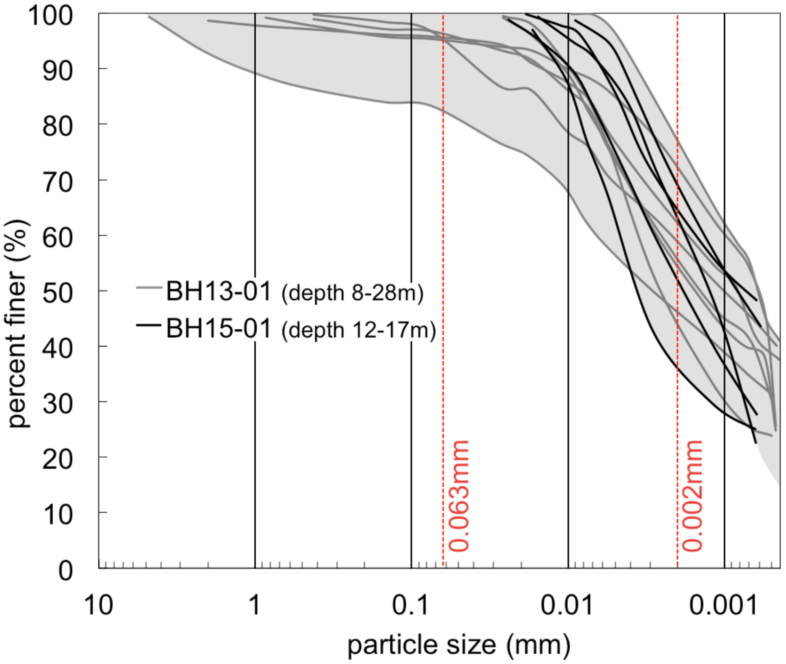

Figure 5.9. Particle size distribution

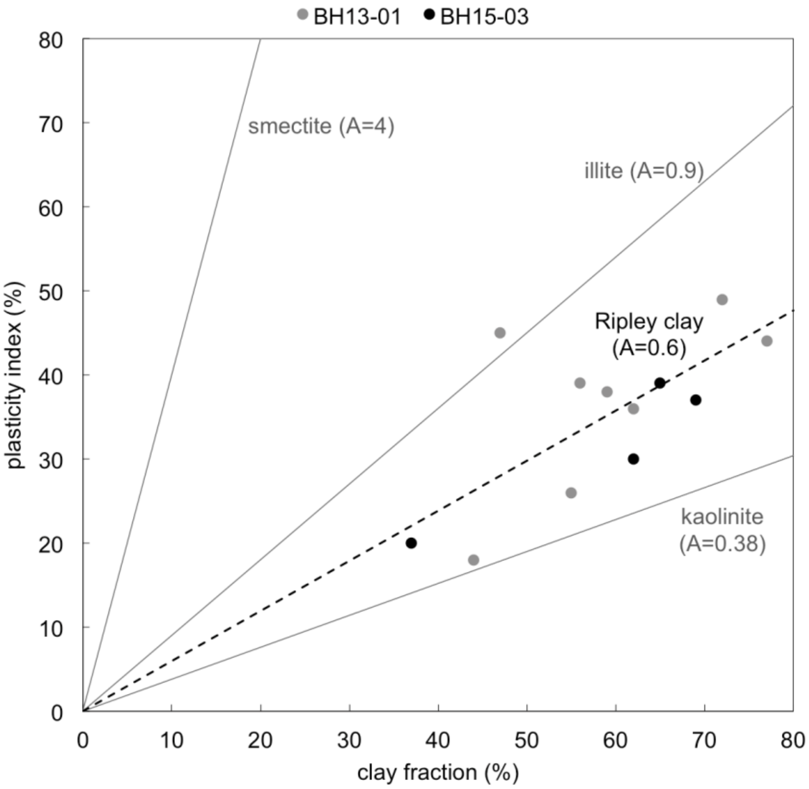

Figure 5.10. Activity chart, typical values of common clay minerals (Skempton 1984) plotted for comparison

d. Specific gravity

Specific gravity results are displayed in Table 5.1.

Table 5.1. Specific gravity results

	Sample	Depth (m)	Specific gravity
BH13-01	S2	12.5	2.84
	S4	13.4	2.82
	S6	17.5	2.82
	S8	25.5	2.82
BH15-03	S40	12.8	2.82
	S41	13.3	2.81
	S44	14.9	2.80

5.2.2 MINERALOGY

Diffractograms yielded by XRD tests reveal patterns of peak reflections. These patterns correspond to particular minerals, allowing for their identification. The diffractogram for Sample S33 (BH15-03 depth 9.1 m) indicates the presence of illite and chlorite for clay minerals, while non-clay minerals such as quartz or feldspar are also detected (Figure 5.11).

Non-clay minerals have well-ordered crystal structures, resulting in sharp and intense reflection peaks. Such is the case for atomic plane spacings of quartz (3.34 and 4.26 Å), feldspar (3.20 Å) or calcite (3.03 Å). Because of the significant presence of these minerals in the samples, peak reflections for clay minerals are comparatively less intense. Some may also be hidden, such as 3.33 Å, a normally prominent reflection for illite hidden by 3.34 Å of quartz.

The structure of clay minerals consists of an arrangement into sheets. Atomic planes, called basal planes, coincide with the planes of sheets. Hence, spacing between basal planes is likely to produce prominent reflection under x-ray diffraction and is characteristic of a given clay mineral. However, clay minerals are typically imperfect crystals and their structure varies from the structure of the perfect clay crystal. Structural disorder leads to broader, less intense basal reflections (Brindley and Brown 1984).

Chlorite is the most readily identified clay mineral. Chlorite structure basal spacing of 14.20 Å produces a distinct first-order reflection. Second-order (7.10 Å), third-order (4.73 Å) and fourth-order (3.55 Å) reflections are apparent reflections corresponding to integral series of basal spacing. Together these reflections form a distinguishable sequence for the identification of chlorite. This clear x-ray pattern of chlorite is attributed to the strong ordering of its sheet structure (Mitchell 1976).

Illite has a basal spacing of 10 Å. In many cases the associated reflection is used for positive identification of illite. In the case of the Ripley clay this reflection is weak. The second-order reflection (5 Å) is insignificant and the third-order reflection (3.33 Å) is masked by a strong quartz reflection. Natural illite is commonly affected by disorder. The structure of illite comprises cations between its sheet-layers. Interlayer cations may be distributed unequally, causing variable basal spacing (Brindley and Brown 1984). Mixed-layer clay minerals are also a source of disorder: crystal structures of illite and smectite are similar so it is common for both sheet-layers to be interstratified. A small amount (<10%) of randomly interstratified smectite layers increases the disorder of illite. In turn, basal reflections are broader.

Other non-basal atomic planes of the crystal structure produce reflections making it possible to identify illite. Spacings 4.48 Å and 2.56 Å produce broad and distinct reflections for the Ripley clay and are characteristic of illite (Mitchell 1976).

For all four samples tested for XRD, the patterns are the same as illustrated in Figure 5.11 for Sample S33. Diffractograms for samples S31, S42 and S46 (BH15-03) are shown in Appendix D. Only the reflection intensities vary from one sample to another. The reflection intensities of S33 are higher for clay minerals and lower for non-clay minerals compared to other samples. This suggests that the clay content (<2 μm) of S33 is larger, but the mineralogy remains the same across all four samples.

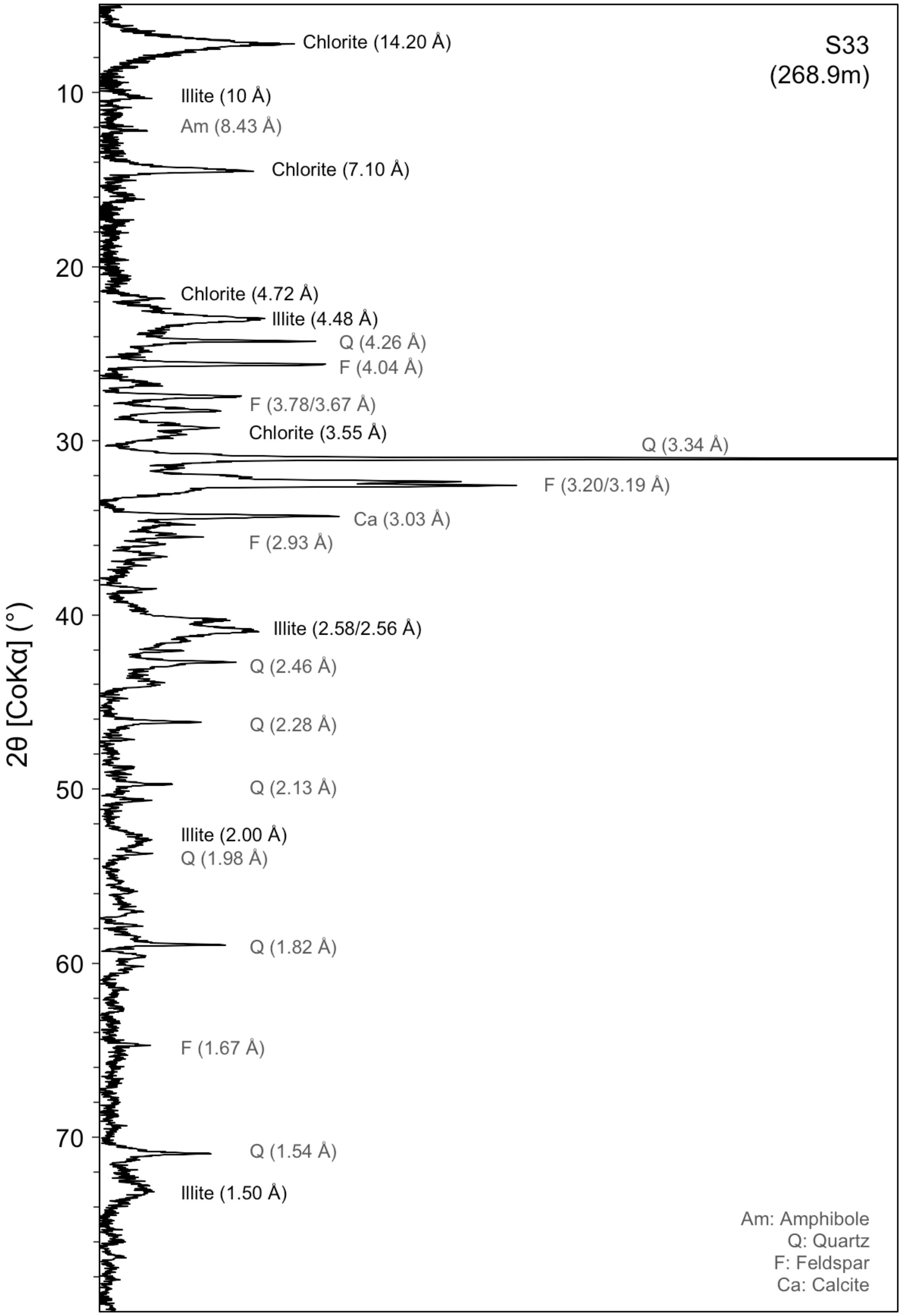

Figure 5.11. S33 (BH15-03 depth 9.1 m) diffractogram: minerals interpreted from reflection peaks are given (with corresponding spacing)

5.2.3 CONSOLIDATION PROPERTIES

Oedometer test results are illustrated in Figure 5.12. Consolidation properties of the Ripley clay are inferred from these test results (Table 5.2). Discrepancies exist among the results. Test S2 exhibits a higher initial void ratio, and is more silty than other samples. Disturbance following the sampling of S2 may have modified the natural density of the soil. In contrast, Test S250 exhibits a low initial void ratio. Unlike other samples from BH15-03, S250 was not sealed inside the PVC coreliner; therefore it lost some moisture during storage. Subsequent shrinkage is unnatural and results in apparent lower compressibility and high overconsolidation. Test S44 appears less compressible because it is more silty. The S44 clay fraction is 37%, compared to 65% for S40 and 62% for S46. Time-deformation records (see Appendix E) also indicate a higher coefficient of consolidation c_v (3.9×10^{-7} m^2/s) for Test S44.

Terzaghi and Peck (1967) proposed a linear relationship between the compressibility and the plasticity of clay (Equation 5.2). Atterberg limits results were used to assess whether oedometer tests conducted in this study are accurate (Table 5.3). Estimated values of the compression index C_c are consistent with with values measured in oedometer tests except for Sample S250, whose compressibility was improperly measured in the oedometer test, as discussed above.

Equation 5.2. $$C_c = 0.009 \times (LL - 10)$$

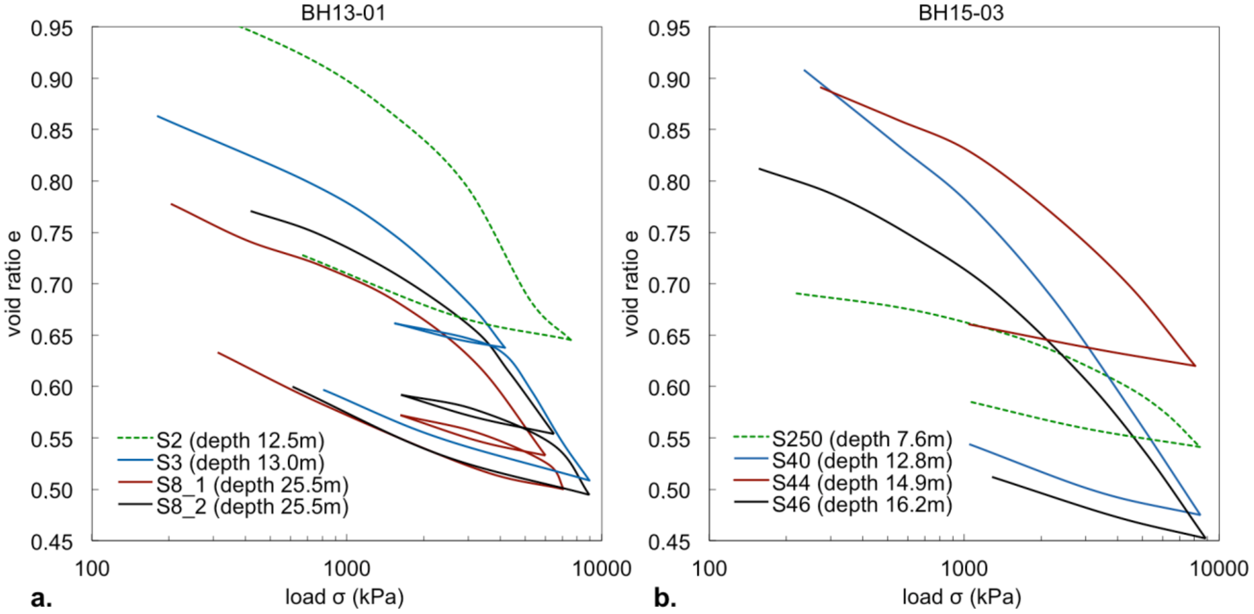

Figure 5.12. Oedometer tests on (a) BH13-01 and (b) BH15-03 samples

Table 5.2. Consolidation properties

	Test	Sample depth (m)	Initial water content w_i (%)	In-situ effective stress estimate σ'_v (kPa)	Preconsolidation stress σ'_p (kPa)	Overconsolidation ratio *OCR*	Compression index C_c	Swelling index C_s	Coefficient of consolidation c_v (m^2/s)
BH13-01	S2	12.5	33	170	2700	16	0.37	0.08	1.1×10^{-7}
	S3	13.0	30	175	2500	14	0.39	0.09	1.6×10^{-8}
	S8_1	25.5	27	300	3500	12	0.36	0.09	1.5×10^{-8}
	S8_2	25.5	27	300	4000	13	0.38	0.09	1.2×10^{-8}
BH15-03	S250	7.6	24	120	4100	34	0.24	0.05	5.1×10^{-8}
	S40	12.8	35	172	1400	8	0.38	0.08	1.4×10^{-7}
	S44	14.9	31	193	2000	10	0.30	0.05	3.9×10^{-7}
	S46	16.2	31	206	2200	11	0.35	0.07	8.2×10^{-8}

Table 5.3. Compression index estimates

	Sample	Liquid limit *LL* (%)	Compression index (Equation 5.2) C_c	Compression index (oedometer test) C_c
BH13-01	S8_2	55	0.41	0.38
BH15-03	S250	62	0.47	0.24
	S40	49	0.35	0.38
	S44	41	0.28	0.30
	S46	49	0.35	0.35

While tests S2 and S250 are considered to be lesser quality because results are biased by a disturbance, other tests provide a reliable characterization of the consolidation properties.

The Ripley clay overconsolidation ratio *OCR* is higher than eight; thus it qualifies as heavily overconsolidated. This is consistent with the significant stiffness of the clay described earlier. The coefficient of consolidation c_v typically ranges from 10^{-8} to 10^{-7} m^2/s.

5.2.4 DRAINED "INTACT" SHEAR STRENGTH

Direct shear tests on the BH15-03 intact samples make it possible to measure the strength of glaciolacustrine soil when intact. Intact shear strength is mobilized under small strains, and corresponds to the peak shear stress measured during the direct shear test. The peak is typically reached after 1.5 to 2.0 mm of shear displacement (8 to 10% of shear strain). Further shear strain following the peak degrades the strength of the sample. Hence, the intact shear strength is not recovered following the reversal of the shear direction. Figure 5.13 plots stress-strain relationships from some tests. Stress-strain plots from all direct shear tests are shown in Appendix F.

Results from all direct shear tests are compiled in Table 5.4. The normalized peak shear strength τ/σ'_n ranges from 0.36 (Test S33_2) to 0.80 (Test S38_1). The mean value is 0.62.

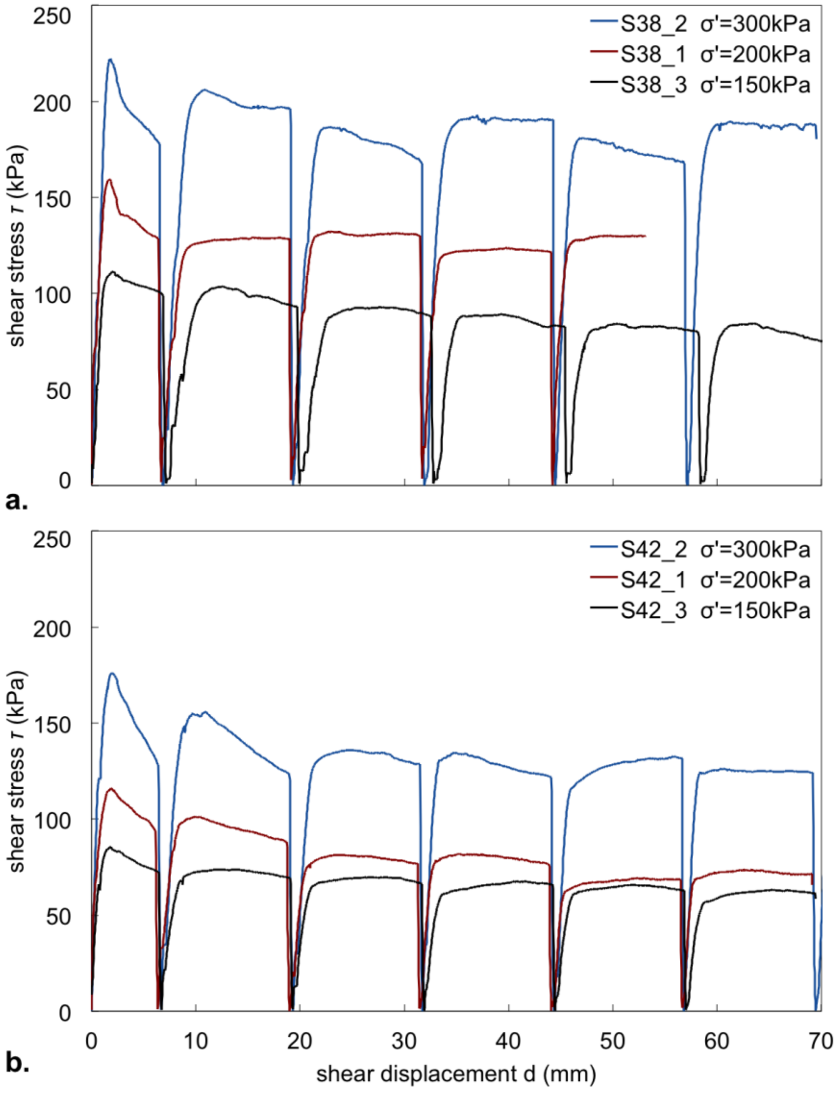

Figure 5.13. Stress-strain results of direct shear tests on BH15-03 intact samples: (a) S38 (depth 10.4 m); (b) S42 (depth 14.2 m)

Table 5.4. Direct shear test results

Test	Sample depth (m)	Normal stress σ'_n (kPa)	Peak shear strength τ (kPa)	Normalized peak shear strength τ/σ'_n	Shear displacement at peak d_{peak} (mm)	Residual shear strength τ_r (kPa)	Normalized residual shear strength τ_r/σ'_n	Residual friction angle φ_r' (°)	Total shear displacement d (mm)
S250_3	7.6	150	101	0.67	1.5	54	0.36	19.8	70
S250_1	7.6	300	176	0.59	1.5	65	0.22	12.2	72
S31_2	8.4	150	85	0.57	1.8	61	0.41	22.1	64
S31_3	8.4	200	105	0.53	1.6	50	0.25	14.0	70
S31_1	8.4	350	172	0.49	2.2	99	0.28	15.8	70
S32_2	8.9	200	132	0.66	1.7	94	0.47	25.2	69
S32_1	8.9	400	250	0.63	2.1	139	0.35	19.2	70
S33_3	9.1	150	70	0.47	1.5	34	0.23	12.8	70
S33_1	9.1	200	102	0.51	1.6	47	0.24	13.2	69
S33_2	9.1	340	121	0.36	2.0	67	0.20	11.1	64
S35_1	9.7	150	100	0.67	1.6	56	0.37	20.5	61
S35_2	9.7	300	198	0.66	1.4	103	0.34	18.9	69
S36_1	10.0	200	154	0.77	1.9	108	0.54	28.4	68
S36_2	10.0	300	230	0.77	1.6	165	0.55	28.8	70
S38_3	10.4	150	110	0.73	2.0	72	0.48	25.6	122
S38_1	10.4	200	159	0.80	1.8	125	0.63	32.0	53
S38_2	10.4	300	222	0.74	1.7	182	0.61	31.2	70
S40_R	12.8	200	-	-	-	55	0.28	15.3	98
S40_1	12.8	250	122	0.49	2.1	105	0.42	22.8	72
S40_2	12.8	350	210	0.60	3.1	188	0.54	28.2	72
S42_3	14.2	150	86	0.57	1.9	63	0.42	22.8	69
S42_1	14.2	200	116	0.58	1.9	71	0.36	19.5	69
S42_2	14.2	300	176	0.59	2.0	125	0.42	22.6	94
S44	14.9	134	95	0.71	3.0	70	0.52	27.6	51
S46_R	16.2	134	-	-	-	57	0.43	23.0	71
S46_1	16.2	134	99	0.74	1.7	39	0.29	16.2	91
S46_2	16.2	200	132	0.66	1.5	56	0.28	15.6	90

For each sample, peak shear strength results are plotted in the shear stress-normal stress space (Figure 5.14). The best fit determines the Mohr-Coulomb strength envelope. The Mohr-Coulomb strength criterion is assumed linear (Equation 5.3); it is a function of the soil cohesion c' and friction angle φ'. Mohr-Coulomb parameters c' and φ' are summarized in Table 5.5.

Equation 5.3. $$\tau = c' + \sigma' \times tan(\varphi')$$

Cohesion c' of the intact soil is measured between 0 and 43 kPa. The peak friction angle φ' is estimated to be between 13 and 37°.

Table 5.5. Mohr-Coulomb parameters for peak effective shear strength

Sample	Depth (m)	Cohesion c' (kPa)	Friction angle φ' (°)	Number of tests
S250	7.6	26	27	2
S31	8.4	19	24	3
S32	8.9	14	31	2
S33	9.1	43	13	3
S35	9.7	2	33	2
S36	10.0	2	37	2
S38	10.4	6	36	3
S40	12.8	0	29	2
S42	14.2	0	30	3
S46	16.2	32	27	2

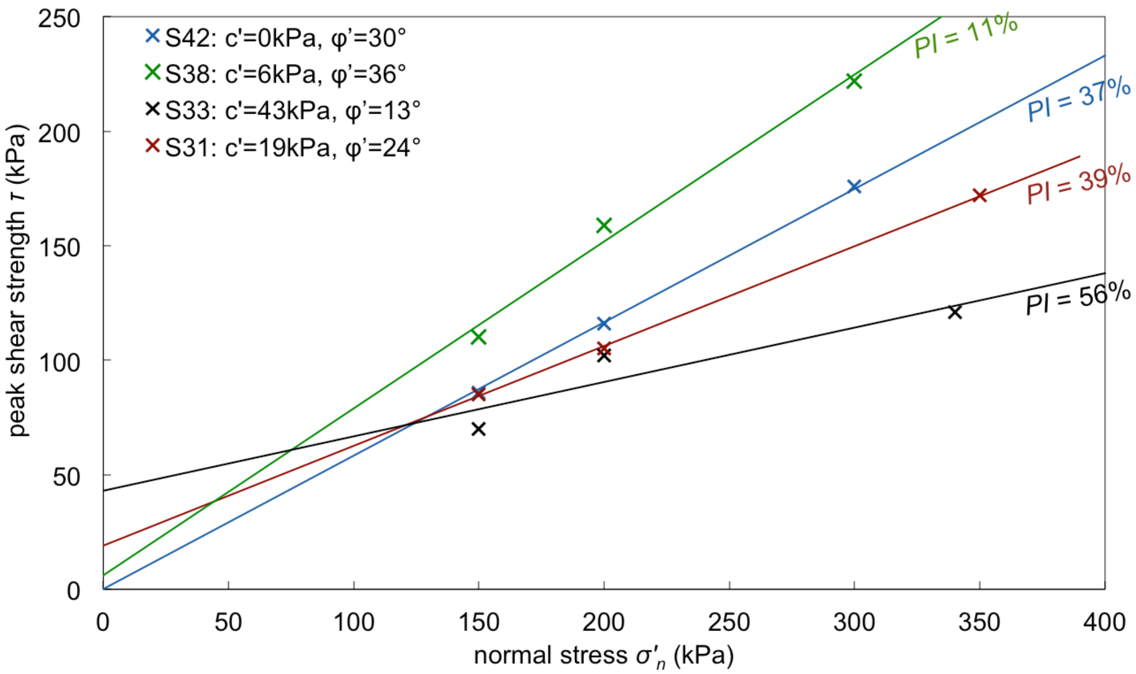

Figure 5.14. Mohr-Coulomb peak shear strength of samples S31, S33, S38 and S42

5.2.5 DRAINED RESIDUAL SHEAR STRENGTH

Ring shear tests on BH15-03 samples make it possible to measure the strength of glaciolacustrine soil after large shear displacements. The lower bound strength value observed during the test is the residual shear strength of the glaciolacustrine soil. The peak in the ring shear test stress-strain relationship is not the intact shear strength because tests are conducted on remoulded specimens. The response to shear strain depends on the sample. For instance, the post-peak strength decrease is less significant for Sample S32 (Figure 5.15.a) than for Sample S33 (Figure 5.15.b). Figure 5.15 also displays direct shear stress-strain relationships for comparison. Stress-strain plots from all ring shear tests are shown in Appendix G.

The dependence of residual shear strength on the strain rate is observed on the stress-strain plots of multiple-rate ring shear tests. Figure 5.16 illustrates multiple-rate tests S31_a and S31_b. Other multiple-rate tests are S32_b (Figure 5.15.a) and S33_c (Figure 5.15.b). Rate effects in the multiple-rate tests are compared in Figure 5.17. A tenfold increase in the strain rate changes the residual shear strength by less than a few per cent.

Results from all ring shear tests are compiled in Table 5.6. The normalized residual shear strength τ_r/σ'_n ranges from 0.20 (Test S33_c) to 0.52 (Test S40_a). The mean value is 0.39.

The Mohr-Coulomb criterion for residual shear strength does not include a component of cohesion *c'*. The residual shear strength is a function of the residual friction angle φ_r' (Equation 5.4). For a given sample, the best fit among direct shear and ring shear tests defines the parameter φ_r' (Figure 5.18, Table 5.7).

The residual friction angle φ_r' is estimated between 12 and 31°. Mohr-Coulomb strength envelopes for all samples are shown in Appendix H.

Equation 5.4. $$\tau_r = \sigma' \times tan(\varphi_r')$$

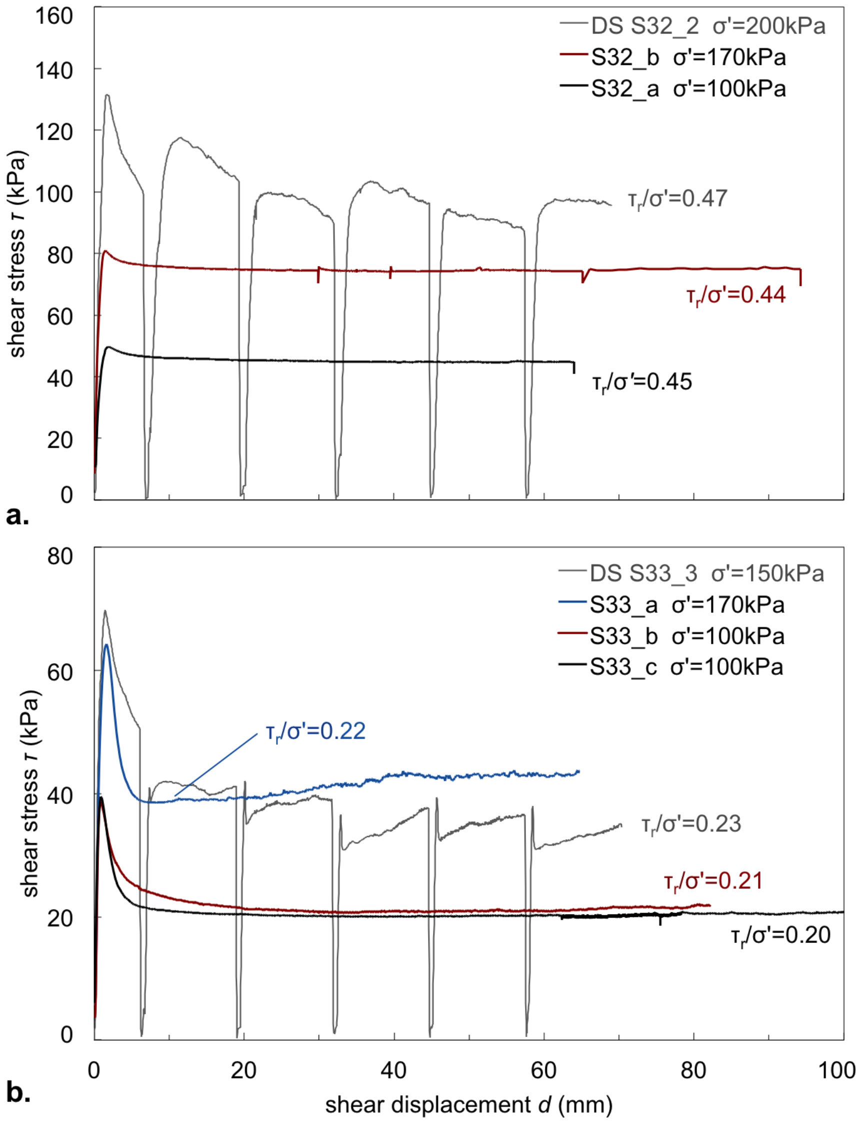

Figure 5.15. Stress-strain results of ring shear tests on BH15-03 samples: (a) S32 (depth 8.9 m); (b) S33 (depth 9.1 m)

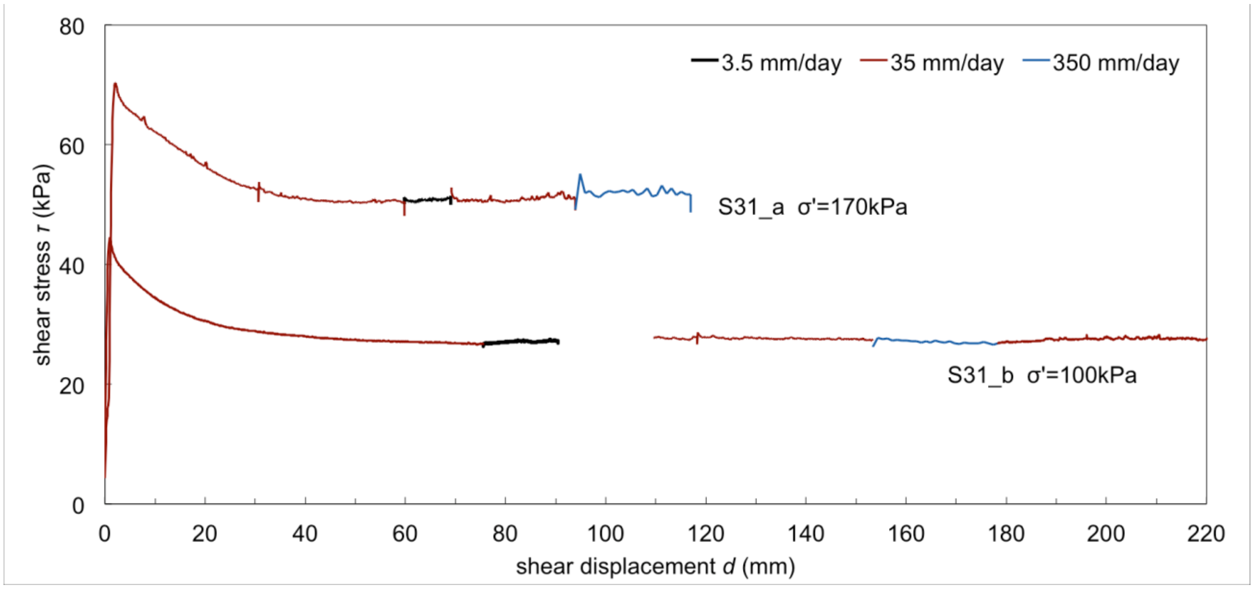

Figure 5.16. Multiple-rate ring shear tests on S31 (depth 8.9 m)

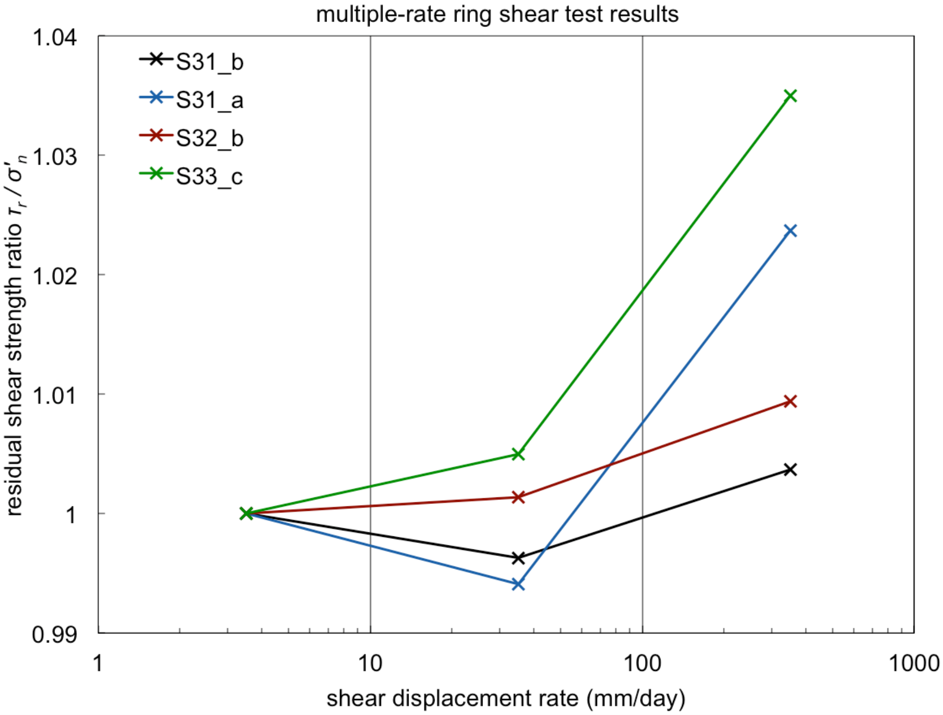

Figure 5.17. Variation of the residual shear strength in multiple-rate ring shear tests

Table 5.6. Ring shear test results

Test	Sample depth (m)	Normal stress σ'_n (kPa)	Residual shear strength τ_r (kPa)	Normalized residual shear strength τ_r/σ'_n	Residual friction angle φ_r' (°)	Total shear displacement d (mm)
S250_a	7.6	170	48	0.28	15.8	152
S31_b^m	8.4	100	27	0.27	15.1	237
S31_a^m	8.4	170	50	0.29	16.4	117
S32_a	8.9	100	45	0.45	24.2	64
S32_b^m	8.9	170	74	0.44	23.5	94
S33_b	9.1	100	21	0.21	11.9	83
S33_c^m	9.1	100	20	0.20	11.3	133
S33_a	9.1	170	38	0.22	12.6	66
S40_a	12.8	100	52	0.52	27.5	64
S40_b	12.8	102	51	0.50	26.6	67
S40_c	12.8	294	140	0.48	25.5	60
S42_a	14.2	200	87	0.44	23.5	196
S44_a	14.9	134	66	0.49	26.2	68
S46_c	16.2	100	48	0.48	25.6	103
S46_a	16.2	134	65	0.49	25.9	96
S46_b	16.2	170	80	0.47	25.2	48

^{m}multiple-rate test

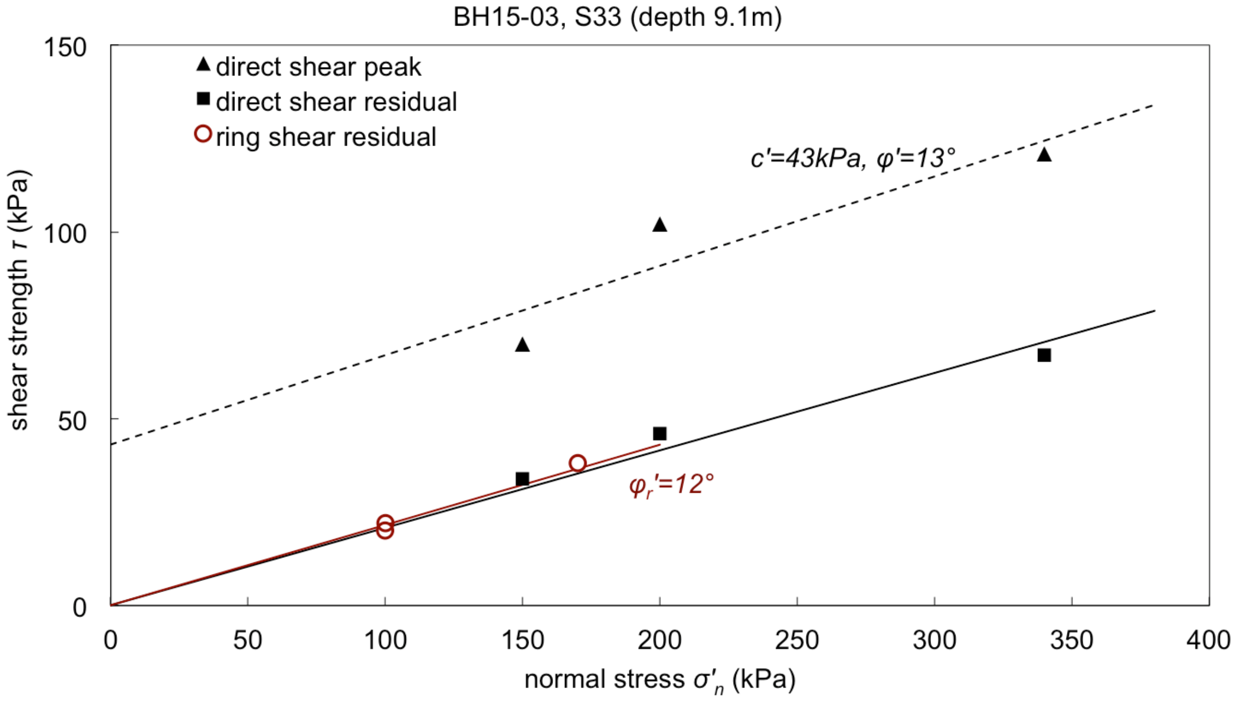

Figure 5.18. Mohr-Coulomb shear strength of Sample S33 (near shear zone)

Table 5.7. Residual friction angle φ_r'

Sample	Depth (m)	Residual friction angle φ_r' (°)	Number of shear tests (*direct*+*ring*)
S250	7.6	15	2+1
S31	8.4	16	3+2
S32	8.9	22	2+2
S33	9.1	12	3+3
S35	9.7	19	2+0
S36	10.0	29	2+0
S38	10.4	31	3+0
S40	12.8	26	3+3
S42	14.2	22	3+1
S44	14.9	26	1+1
S46	16.2	22	3+3

5.2.6 UNDRAINED SHEAR STRENGTH

Constant-volume direct simple shear (DSS) tests yield effective stress paths, which are illustrated in Figure 5.19. Stress-strain responses are plotted in Appendix I. The assumption is made that the maximum shear stress τ_{max} in the DSS test is a measure of the undrained shear strength s_u.

DSS test specimens experience a wide range of soil behaviours. Not all measured behaviours are representative of the response of heavily overconsolidated clay to uniform shear. After accounting for test issues described in Section 4.3.6.a, some test results shall be discarded:

- Tests S4a, S4b and S6b exhibit a large positive pore water pressure change, Δu. This result is consistent with the observation of shear localization in the boundary zone. This suggests that the measured undrained shear strength is that of mechanically softened, contractive clay.
- Tests S4c, M4a, M4b, S6c and S6d exhibit a comparatively small Δu. The imposed shear displacement in these tests does not convert to simple shear strain but results in excessive slippage at the soil-platen interface. The undrained response to simple shear is not experienced.
- Test S6a exhibits a large negative Δu. A comparatively large measure of the undrained shear strength s_u suggests this parameter is well underestimated in other tests. Although singular, the observed dilative soil behaviour is a characteristic of heavily overconsolidated clay. Results for Test S6a are displayed in Table 5.8. The meaning of the other test results is not fully understood and is not interpreted further.

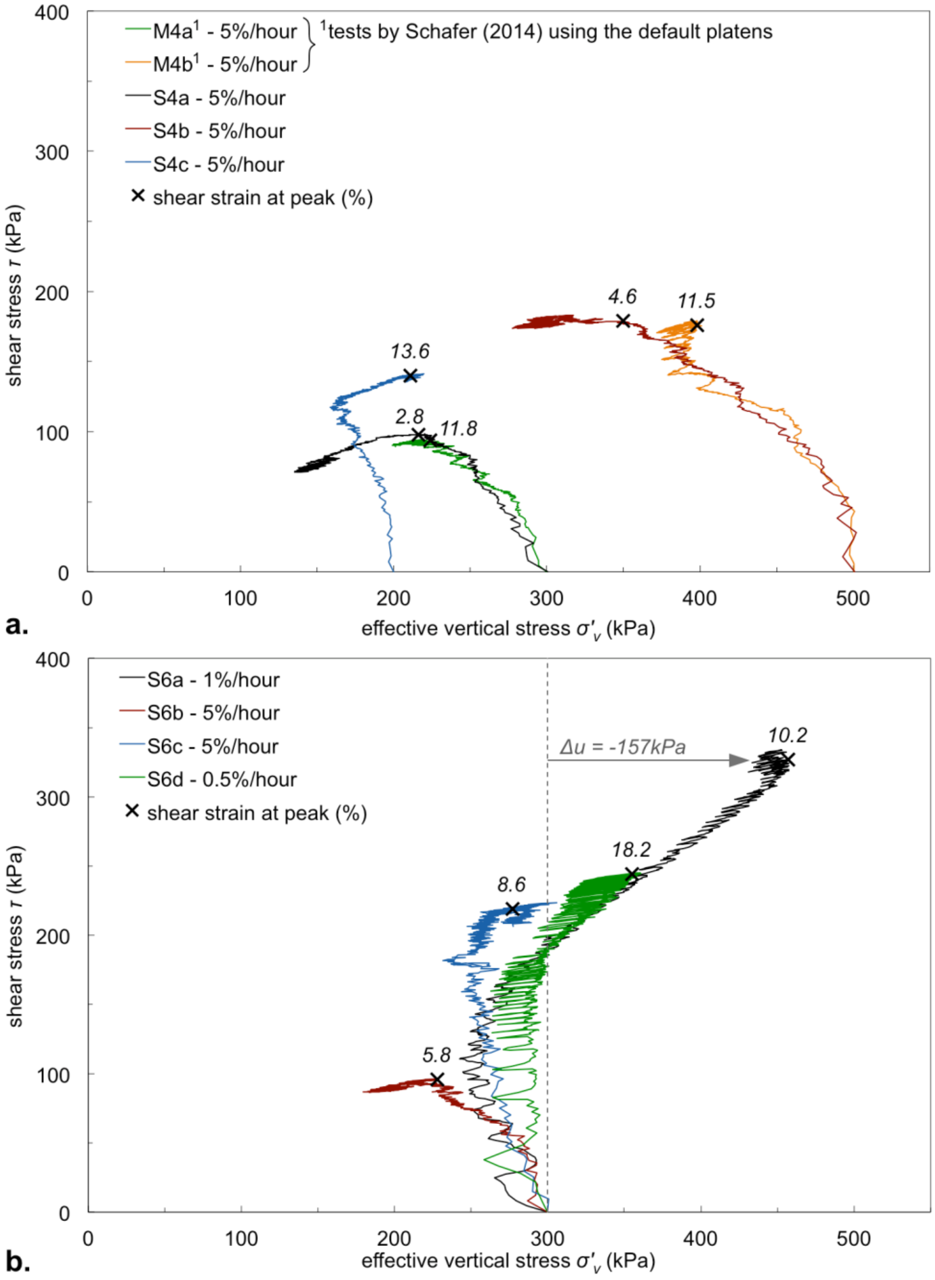

Figure 5.19. Stress path results of DSS tests on BH13-01 samples: (a) S4 (depth 13.4 m); (b) S6 (depth 17.5 m)

Table 5.8. DSS Test S6a results

Test	Sample depth (m)	Consolidation stress σ'_{v0} (kPa)	Undrained shear strength $s_u = \tau_{max}$ (kPa)	Pore water pressure change Δu (kPa)
S6a	17.5	300	327	-157

Chapter 6. Interpretation: Weak Clay Horizons

6.1 STRATIGRAPHY

6.1.1 GLACIOLACUSTRINE UNIT 2

At the location of the 2015 boreholes, the observed unit of interbedded silt and clay is interpreted as Unit 2 of the geological framework set by Clague and Evans (2003). Using the facies of interbedded silt and clay to recognize glaciolacustrine soil, Unit 2 is located at an elevation of between 266.8 and 273.4 m in borehole BH15-01, between 261.2 and 270.3 m in borehole BH15-03.

Schafer (2016) hypothesizes cross-sections of the Ripley slide in accordance with these results. Figure 6.1 presents Cross-section 2 based on the stratigraphy and displacement monitoring at boreholes BH15-03 and BH13-01.

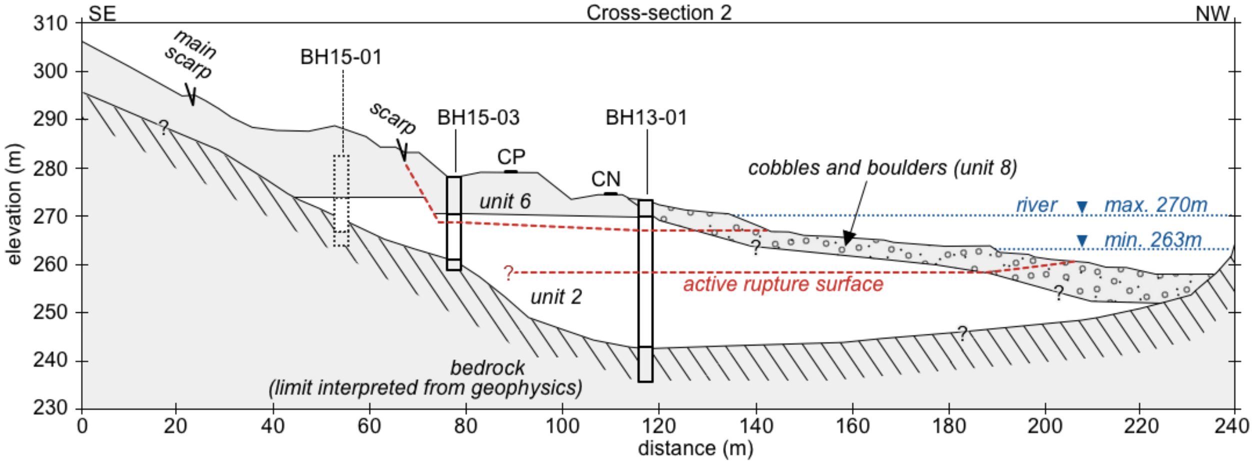
SE
Cross-section 2
NW
main scarp
BH15-01
scarp
BH15-03
BH13-01
CP
CN
cobbles and boulders (unit 8)
river
max. 270m
min. 263m
unit 6
unit 2
?
active rupture surface
bedrock
(limit interpreted from geophysics)
elevation (m)
310
300
290
280
270
260
250
240
230
0
20
40
60
80
100
120
140
160
180
200
220
240
distance (m)

Figure 6.1. Cross-section of the Ripley slide

The varves in the core samples provide information about the deposition regime of Unit 2. A silt-clay couplet that gradually fines upward indicates the transition from a winter to summer regime. The sharp contact with overlying silt (the beginning of a new couplet) marks the beginning of the melt season, a sudden event. The abrupt release of glacial meltwater inputs coarse sediment. Sand laminae intersecting Unit 2 are interpreted as markers of such events.

However, the glaciolacustrine environment evolved over the course of its existence: the distance from the ice front has changed; the meltwater discharge may have increased; melt events may have occured during the winter seasons. As a consequence, Unit 2's deposition regime differs from the idealized model described above. Varves are not necessarily distinct, making difficult the identification of interbedded silt and clay.

The clay minerals contained in Unit 2 are illite and chlorite. Chlorite minerals are derived from rock degradation (Mitchell 1976). The source of glaciolacustrine sediment is likely the erosion of rocks by glacier ice; therefore the presence of chlorite is logical. Illite, an abundant clay mineral, is associated with chlorite. Atterberg limits results plot just above the "A" line on the plasticity chart (Figure 5.8), which is consistent with illite mineralogy (Holtz and Kovacs 1981). Illite and chlorite dominate comparable glaciolacustrine soils such as New Liskeard varved clay and Connecticut Valley varved clay (Sambhandharaska 1977).

Illite and chlorite have a low cation exchange capacity compared to smectite, which was not detected here even in small proportions. Illite and chlorite make for a low-activity non-swelling clay (Mitchell 1976). In this case the cation content of the pore fluid has little influence on the soil behaviour. The use of distilled test water in the laboratory (water baths for consolidation and shear tests, sample remoulding) has only marginally affected the results.

Following its deposition, Unit 2 experienced considerable overburden along with glacial advances. Through the postglacial period until now the Thompson River has incised the valley, leaving the clay heavily overconsolidated. Large preconsolidation stresses ($\sigma'_p \geq 2000$ kPa) measured in oedometer tests underline the stress history of Unit 2. One characteristic associated with heavy overconsolidation is the stiff consistency observed on core samples.

Unit 2 distinguishes itself by the processes that have transformed its structure following deposition. Unlike the overlying till, Unit 2 has not been significantly modified by erosion. Fissures contained in Unit 2 are fewer, presumably deeper and more extensive. The formation of such fissures may result from lateral stress-relief during postglacial valley incision.

6.1.2 TILL UNIT 6

The more recent glaciolacustrine Unit 3 is not found at the boreholes' low elevations. After its deposition, Unit 3 was eroded by the subsequent glaciation or valley incision. Early Pleistocene Unit 2 is unconformably overlain by Unit 6, a till of the Fraser glaciation. Unit 6 till is shallow and blankets the slope. Non-bedded silty clay dominates Unit 6 till. Coarse clasts are often found in Unit 6. Fissures and cracks are numerous and are attributed to the process of till formation, by which glacial drag entrains and reworks sediments. Observations of contorted soil hint at this process, too.

Fissures favour the circulation of surface water. Chemical weathering is accelerated in the shallow soil. Unit 6 displays notable marks of weathering, such as the reddish tone of silty clay. Alternating tones provide the soil with a mottled aspect. Gypsum is a by-product of chemical weathering. Gypsum formation occurs in the fissures. The growth of gypsum precipitates causes volume to increase locally; hence adjacent clay is weakened. Where soil is affected by weathering, gypsum formation may encourage progressive failure (Morgenstern 1970).

6.2 SHEAR SURFACES WITHIN GLACIOLACUSTRINE UNIT 2

6.2.1 SLICKENSIDES

Slickensides exist among Unit 2 discontinuities. The polished-like aspect of the slickenside surface results from the alignment of the platy clay particles in the same direction. Clay particles orient parallel to each other only after significant shear displacement. Some slickensides are marked with striae, a consequence of sustained shear displacement. Slickensides are shear rupture surfaces, thus showing that mass wasting or glacial drag have formed pre-sheared discontinuities in Unit 2.

Mass wasting includes present-day slope instability. More generally, it includes landslides that have accompanied postglacial incision of the Thompson River Valley (Ryder 1976). Failure of stiff clay involves softening, so the water content increases in close proximity to an active slickenside. One indication that shear is no longer occurring is when additional moisture is no longer observed. Another indication is that the surface of the slickenside exhibits a stiff consistency, which is identical to the rest of the sample. Figure 5.4 illustrates “dry” slickensides, at an elevation of 269.4 m in BH15-03 and at elevations of 268.9 and 274.3 m in BH15-01. These slickensides are pre-sheared discontinuities whose origin is hypothesized to be ancient mass wasting or glacial drag. Disrupted bedding at an elevation of 271.3 m in BH15-01 also suggests pre-shearing.

In contrast, the slickenside at the elevation of 268.8 m in BH15-03 is in comparatively softer, wetter clay. This location corresponds to a local maximum in natural water content (Figure

6.2.c). The slope inclinometer surveys at borehole BH15-03 during 2015 reveal an active rupture surface at an approximate elevation of 269.0 m (Figure 6.2.b). However, the dip of mapped slickensides (10 to 30°, Figure 5.5) suggests they do not represent the base shear zone of the landslide, thought to be near horizontal.

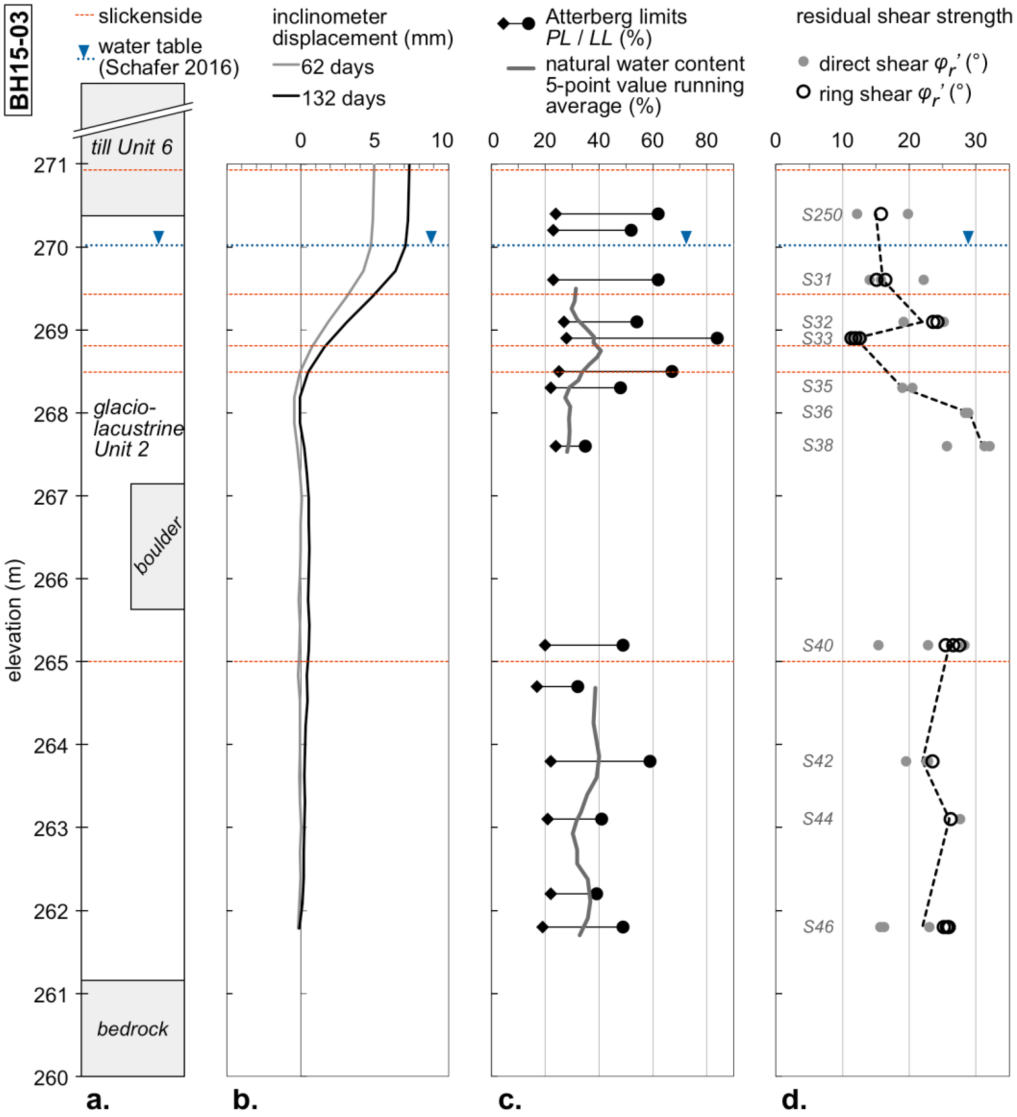

Figure 6.2. BH15-03 results: (a) stratigraphy; (b) slope inclinometer displacement; (c) Atterberg limits and natural water content; (d) residual shear strength derived from direct shear and ring shear tests

6.2.2 PERSISTENCE

According to the slope inclinometer surveys at boreholes BH15-01 and BH15-06, instability does not extend to the southern portion of the slope. The significant vertical component to slope movement reported by Hendry et al. (2015) near the southern edge of the slide does not result from a secondary sliding mass adjacent and south of the main slide body. Instead, Schafer (2016) reports that the lock-block retaining wall and GPS 3 are located near the back scarp of the landslide, along which greater vertical deformation can occur.

The shear rupture surface at an elevation of 268.8 m (BH15-03) is only one of the two rupture surfaces known to be active at the Ripley slide. Hendry et al. (2015) and Schafer (2016) have identified a deeper active rupture surface at elevations of 256.5 m and 257.3 m, respectively. Compared to the aforementioned investigations, borehole BH15-03 is located closer to the south edge of the slide and closer to its crown. At BH15-03 bedrock is shallow (261.2 m) so it prevents retrogression from developing at higher depth. Instead, the bedrock shape controls retrogression. The deeper rupture surface possibly reaches the main scarp upslope, and intersects BH15-03 near the soil-bedrock interface, where the slope inclinometer surveys were not able to record deformations.

The shallower shear surface is a secondary, less active rupture surface, whose shear displacement represents a small fraction of the overall slide movement as measured by the GPS stations. Only 8 mm of displacement along the shallow shear surface were recorded over a 132-day period in 2015.

This makes for a complex landslide geometry, compatible with the multiple retrogressive nature of the landslide. The hypothesized extent of both active rupture surfaces is presented in the Figure 6.1 cross-section.

Similar findings were made in other Thompson River Valley landslides. Porter et al. (2002) and Eshraghian et al. (2007) also recorded the existence of two shear planes at the CN50.9, Goddard, North and South slides. These landslides are approximately aligned along an azimuth of 191°. Figure 6.3 shows that, following this azimuth, the elevations of the shallower and deeper shear planes decrease consistently at rates of 1.7 m/km and 2.6 m/km, respectively. This trend compares to the glacio-isostatic tilt (postglacial rebound): paleogeographic reconstruction from Johnsen and Brennand (2004) shows that the glacio-isostatic tilt in the Thompson River Valley is -1.8 m/km, at an azimuth of 152°; this tilt affected glacial lake-bottom sediments. This suggests that throughout the Thompson River Valley, the landslide rupture surfaces belong to the same, persistent, weak clay horizons.

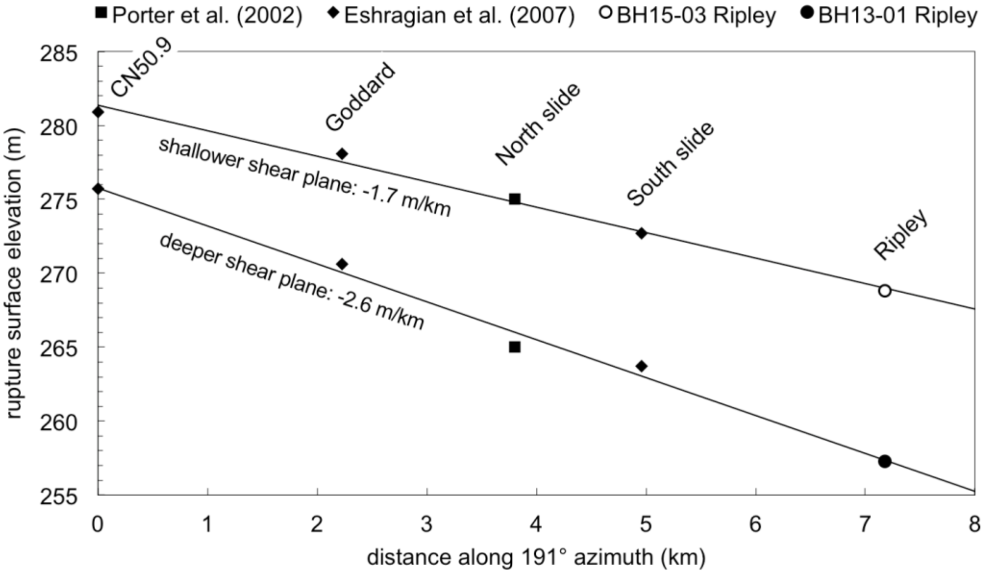

Figure 6.3. Horizon elevation throughout the Thompson River Valley landslides

6.3 SHEAR STRENGTH OF GLACIOLACUSTRINE UNIT 2

6.3.1 DRAINED INTACT SHEAR STRENGTH

For plastic clay-dominated samples S250, S31 and S33 (*PI* > 35%), the Mohr-Coulomb peak shear strength criterion determined from direct shear tests includes a significant cohesion component (*c'* > 15 kPa). The apparent cohesion for Sample S42 is zero, although its measured plasticity index *PI* is 37%. Samples of glaciolacustrine soil may be heterogeneous, so the specimen selected for the Atterberg limits test does not necessarily represent the specimens selected for the direct shear test. The residual shear strength developed at a later stage of direct shear tests on Sample S42 is relatively high (φ_r' = 22°), suggesting that the measured plasticity has been overestimated. A similar discrepancy exists with the direct shear tests on Sample S46. These tests revealed that the apparent cohesion is significant (*c'* = 32 kPa), although the measured plasticity is moderate (*PI* = 30%). The residual shear strength developed at a later stage is relatively low (φ_r' = 18°), suggesting that the measured plasticity has been underestimated.

For low plasticity silt-dominated samples, the cohesion component of the peak shear strength is small. For instance, Sample S38 exhibits little plasticity (*PI* = 11%) and the apparent cohesion *c'* is 6 kPa. The small cohesion is attributed to the presence of a small amount of clay particles. Silt-dominated soil shows a larger friction angle than clay-dominated soil. Figure 5.14 illustrates that Sample S38 (φ' = 36°) mobilizes more shear strength than clay-dominated samples S31 and S33 (φ' = 24° and 13°, respectively) under high normal stresses ($\sigma'_n \geq 70$ kPa), where the contribution of cohesion becomes less important.

The volumetric response was not accurately recorded in the direct shear test because soil extrusion results in excessive settlement (see Section 4.3.5). In the initial 1.5 to 2.0 mm of shear displacement leading to the mobilization of the peak shear strength, vertical deformation is significant (~0.20 mm, see Appendix F) in the following cases:

- The normal stress is high ($\sigma'_n \geq 340$ kPa in S31_1, S32_1, S33_2), thus counteracting dilatancy;
- The gap between the shear box halves is broader (0.20 mm instead of 0.10 mm in S44, S46_1 and S46_2), thus favouring soil extrusion regardless of the particle size;
- The specimen's initial water content is high (w_i = 42% in S33_1, S33_2 and S33_3), thus favouring the loss of bond between the clay particles (softening) and the extrusion of the latter.

Otherwise the vertical deformation is small or negative (<0.10 mm), reflecting the typically dilative behaviour of heavily overconsolidated soil. Direct shear test results do not make it possible to conclude whether the magnitude of dilatancy depends on the clay fraction contained in the sample. Whether silt-dominated or clay-dominated, the Ripley glaciolacustrine soil is seemingly prone to dilatancy when intact.

6.3.2 UNDRAINED SHEAR STRENGTH

The variation of the normalized undrained shear strength s_u/σ'_{vo} with the overconsolidation ratio (*OCR*) for clays has been studied extensively through the use of the SHANSEP technique (Mayne 1988). Jamiolkowski et al. (1985) recommend the following relationship (Equation 6.1) for correlating the undrained shear strength of natural clays measured in the direct simple shear (DSS) test.

Equation 6.1. $$s_u/\sigma'_{v0} = S \times OCR^m \quad \text{where } S = 0.23 \pm 0.04\,;\ m = 0.8$$

Existing DSS data on glaciolacustrine clay is found in the Connecticut Valley (Ladd and Foott 1974) and New Liskeard (Lacasse et al. 1977) varved clays case studies. Dickinson et al. (2016) have investigated a glaciolacustrine clay deposit located at the New Afton mine, just 55 km east of the Ripley slide. DSS and consolidated-undrained triaxial tests indicate that the relationship of Equation 6.1 best represents the undrained shear strength s_u at the New Afton mine.

The DSS Test S6a result is plotted in Figure 6.4 along with the aforementioned cases. This comparison shows that the undrained shear strength measured in the DSS Test S6a is consistent with the overconsolidation of Unit 2. Indeed, overconsolidation confers dilatancy to the Ripley clay. In undrained conditions, dilatancy takes the form of a strong negative pore water pressure response (Δu = -157 kPa in DSS Test S6a). The effective stress increases correspondingly. The undrained shear strength of the Ripley clay well exceeds the drained intact shear strength.

Both the undrained shear response of constant-volume DSS Test S6a and the drained shear response of direct shear tests (see Section 6.3.1) suggest that the Ripley clay is dilative when intact.

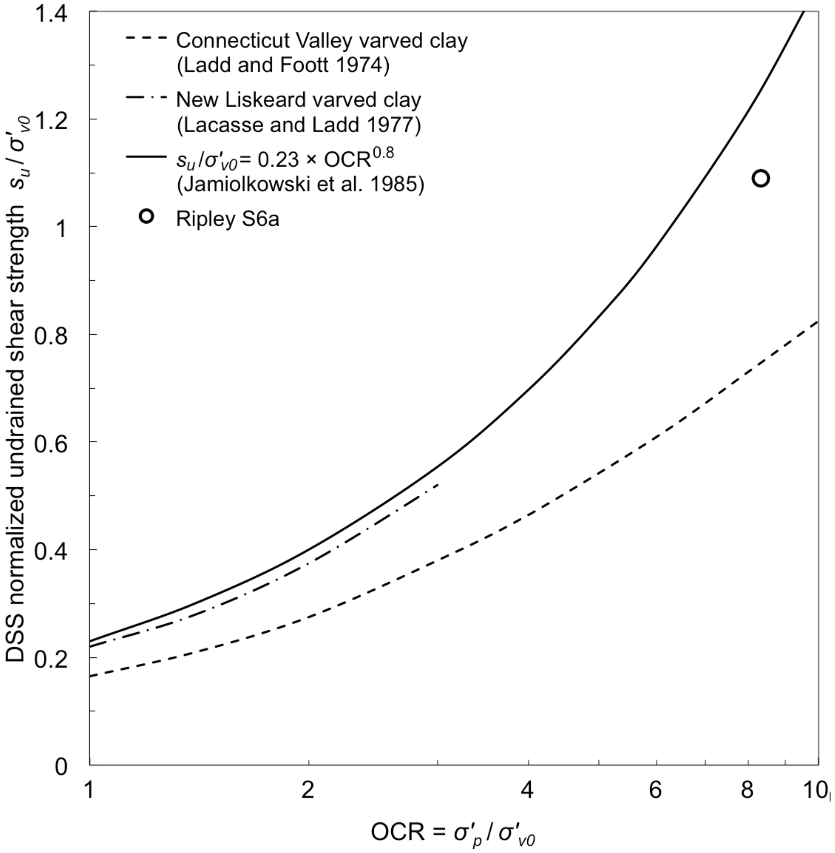

Figure 6.4. Normalized undrained shear strength for the Ripley and other clays

6.3.3 OPERATING SHEAR STRENGTH

a. Drained versus undrained conditions

The vertical permeability k_v of the Ripley clay was estimated based on consolidation data from the oedometer tests (see Appendix E). Under the successive load increments of the oedometer test, the void ratio decreases, as does the permeability. Under large load increments (≥2000 kPa), the clay is normally consolidated and the vertical permeability k_v is on the order of 10^{-9} cm/s. In the overconsolidated range, the vertical permeability k_v is one order of magnitude larger, at 10^{-8} cm/s. Based on this estimation, the Ripley clay is classified as practically impervious (Terzaghi and Peck 1967). The low permeability of the Ripley clay is attributed to the low void ratio inherited from overconsolidation.

The very tight clay raises the prospect of shear-induced pore water pressure. This has motivated the implementation of constant-volume DSS tests in order to assess the pore water pressure response and the undrained shear strength (see Section 6.3.2).

However, the vertical permeability k_v estimated from consolidation data is not representative of the Ripley clay's bulk permeability:

- First, the permeability of glaciolacustrine soil is anisotropic. The horizontal permeability (along the varves) is larger than the vertical permeability (across the varves). The horizontal permeability k_h was not measured in this study. In varved clays, the horizontal permeability k_h is often one order of magnitude larger than the vertical permeability k_v (Mitchell 1976).
- Second, the soil description revealed that fissures and sand laminae intersect the glaciolacustrine silt and clay. Such heterogeneities significantly enhance the soil's bulk permeability.

Unless shear is fast, negative shear-induced pore water pressure tends to draw water into the soil. Consequently the soil swells and excess pore water pressure is dissipated, reducing the strength of heavily overconsolidated clay.

Hendry et al. (2015) report that the Ripley slide velocity $\dot{d}$ reaches a maximum during the seasonal Thompson River drawdown, at 0.6 mm/day. Other reactivated Thompson River Valley landslides are also very slow-moving landslides. Strain rates are slow enough for shear-induced pore water pressure to dissipate. The constant-volume condition is unlikely to be met in the field, and the clay is allowed to swell. The failure mechanism of the glaciolacustrine clay is associated with drained conditions.

b. Softening

The natural water content of the overconsolidated soil initially stands near the plastic limit. In drained conditions, dilatancy causes the water content to increase towards the liquid limit. This is the softening process: the soil consistency changes from stiff to soft, and the soil's cohesion is lost. Eventually, the arrangement of soil particles becomes less dense and non-cohesive. At this stage, the shear strength is the fully softened strength (see Section 2.2.3), the same as if the clay were normally consolidated. A local maximum in the measured water content from the intact core samples (Figure 6.2.c) suggests that softening is localized.

c. Large strains

Further strain mobilizes the friction component of shear strength. Under imposed shear strain, the arrangement of soil particles evolves into the arrangement of least shear resistance. Platy particles present in the shear zone tend to orient parallel to each other, eventually creating an arrangement of least friction.

The post-peak shear behaviour is different in silt-dominated and clay-dominated soil:

- In non-plastic silt, in the absence of platy particles, shear does not generate a preferred particle orientation. Dilatancy essentially yields a less dense arrangement of rotund silt particles, whose friction angle is only marginally decreased. The less dense packing of particles is a reversible type of deformation, because future changes in the stress state will modify the soil density again (Lupini et al. 1981).
- In plastic clay, softening eliminates the cohesion. In the presence of platy particles, further shear also leads to a preferred particle orientation. The decrease in shear strength is significant. In plastic clay, the preferred orientation adopted by the platy particles is an irreversible deformation. This is similar to classical solid mechanics, where irreversible strain is the marker of plasticity.

In short, clay-rich beds of the overconsolidated glaciolacustrine soil offer a greater potential for strength reduction than silt-rich beds. Once strength reduction is established, it is irreversible in clay-rich beds.

In the ring shear tests, the shear strength reduction after large strains is attributed to a decrease of the friction component (the cohesion component is negligible in remoulded specimens). Figure 6.5 illustrates the shear strength reduction in ring shear tests on two different samples. The small decrease in friction in Test Specimen S32_a is attributed to the small fraction of platy clay particles. In contrast, the clay fraction of Sample S33 is large, as suggested by its high plasticity (*PI* = 56%; LL = 84%). In Test S33_b, large strains form a slickenside-like failure surface, leading to a significant decrease in friction.

The difference between the Mohr-Coulomb peak and residual strength criteria also reflects the strength reduction. For instance, Figure 6.6 reveals that the difference between peak and residual strength is larger in the more plastic sample, S31, than in the less plastic sample, S38. These findings support that the post-peak shear behaviour is different in silt-dominated and clay-dominated glaciolacustrine soils.

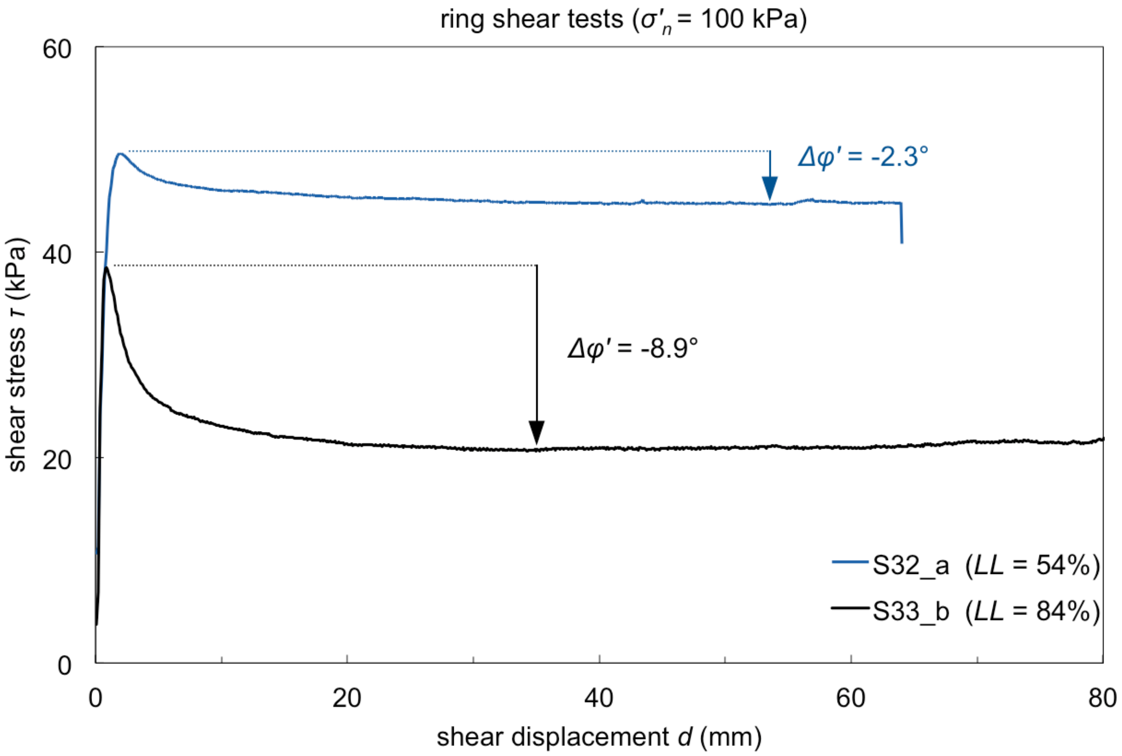

Figure 6.5. Ring shear tests S32_a (elevation 269.1 m) and S33_b (elevation 268.9 m)

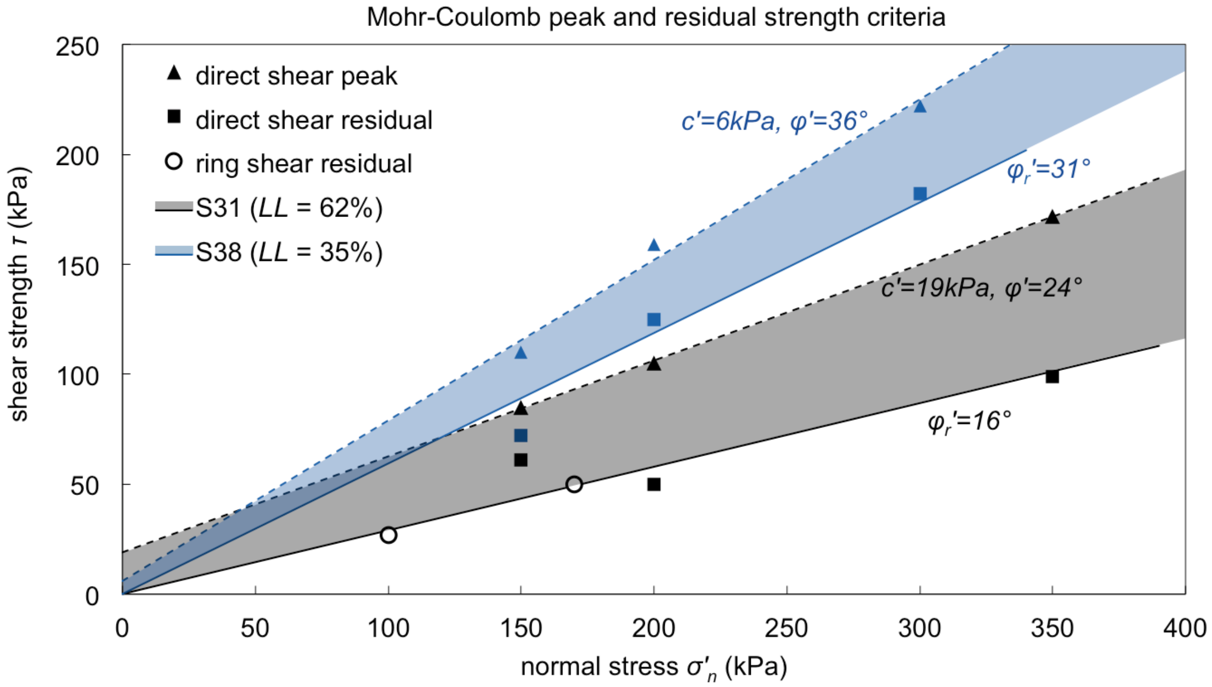

Figure 6.6. Peak to residual shear strength domains for samples S31 (elevation 269.6 m) and S38 (elevation 267.6 m)

In the direct shear tests, strength reduction is nearly complete after a few tens of millimetres of shear displacement. All Ripley clay intact samples require large strains for the residual shear strength to be mobilized (*d* > 20 mm). This is attributed to the coexistence of silt and clay particles. Rotund silt particles interfere with the orientation of platy clay particles in the direction of shear (Lupini et al. 1981). In clay-dominated samples, rotund silt particles cause the shear rupture surface to be discontinuous or undulating. Larger strains are required for the rupture surface to become a continuous and planar slickenside of least strength. When the clay fraction is larger, rotund silt particles are fewer, the difference between peak and residual strength is larger, and the strain required for this difference to be established is smaller. In other words, the soil is more brittle.

Sample S33 (elevation 268.9 m; *LL* = 84%; φ_r' = 12°) is the most brittle, with less than 10 mm of shear displacement required in the ring shear test for the clay to exhibit strong particle orientation. In comparison, samples S250 (elevation 270.4 m; *LL* = 62%; φ_r' = 16°) and S31 (elevation 269.6 m; *LL* = 62%; φ_r' = 17°) are less brittle, with more than 20 mm of shear displacement required in the ring shear test for the clay to exhibit a strong particle orientation.

Slickensides were detected in several clay-rich beds of Unit 2 in boreholes BH15-01 and BH15-03 (see Section 5.1.1). The striae observed on some slickensides reveal that large strains have concentrated at the plane of the slickenside. The polished-like aspect of the slickenside surface is a marker of the preferred particle orientation, now permanently established. Slickensides are shear surfaces along which the soil strength that can be mobilized has reached a minimum: the residual shear strength.

d. Residual friction angle

Shear surfaces similar to natural slickensides were reproduced in the laboratory in clay-dominated samples (Figure F.2, Figure G.2 in Appendices). Both the direct shear and ring shear tests imposed large strains on the samples; thus the residual friction angle was measured.

Clay particles are generally platy but the particle shapes differ depending on the clay mineral. As a result, the residual friction angle depends not only on the quantity of clay-size particles but also on the type of clay mineral. The plasticity index (*PI*) parameter encapsulates information about both the clay fraction (*CF*) and the liquid limit (*LL*) indicative of the clay mineral platyness. An empirical correlation exists between the residual shear strength and the *PI* (Mesri and Shahien 2003). The correlation based on the *PI* shows more scatter than the correlation based on both the *CF* and *LL*, such as developed by Stark and Eid (1994), but it remains a reliable alternative when *CF* data is missing (Eid et al. 2016). Results plotted on Figure 6.7 suggest that such a correlation is true for the Ripley clay.

The residual friction angle φ_r' is also dependent on the effective normal stress, in particular in the low range of normal stresses ($\sigma'_n < 200$ kPa). Clay particles cannot be as effectively oriented at low normal stresses as at higher normal stresses; hence φ_r' tends to decrease when σ'_n increases (La Gatta 1970, Lupini et al. 1981). Figure 6.7 illustrates the empirical correlation from Eid et al. (2016) as a function of the normal stress. The Mohr-Coulomb strength envelope is not linear, and its curvature is pronounced in the low range of normal stresses. In the case of the Ripley clay, the simplifying assumption was made that the strength envelopes were linear. Data was not rich enough to identify curvilinear strength envelopes with accuracy. Moreover, the majority of the tests were conducted under normal stress in the range of Unit 2's in-situ vertical stresses ($120 < \sigma' < 220$ kPa).

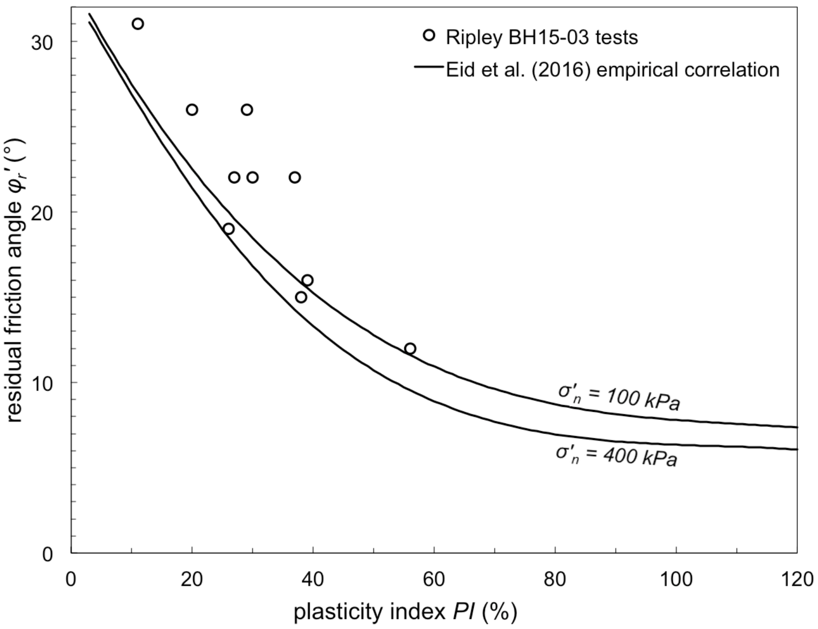

Figure 6.7. Correlation between PI and residual friction angle

The residual shear strength of pure clay (*CF* = 100%) is a lower bound of the residual shear strength of natural soil. According to Chattopadhyay (1972), the residual friction angle of pure illite is 10.2°. The minimum residual friction angle for the Ripley clay is 12° (Sample S33, elevation 268.9 m), which is consistent with the illite and chlorite mineralogy and the non-zero silt content of the Ripley glaciolacustrine soil.

In contrast, for silt-dominated samples, the residual friction angle is 25° or higher.

e. Rate effects

Measurement errors (e.g., parasitic forces induced by wall friction) bias the subtle rate effects. The variability of the rate effects depending on the test is partly attributed to measurement errors (Figure 5.17). Rate effects also increase with plasticity (Wedage 1995); hence the stronger rate effect observed in Test S33_c is attributed to the higher plasticity of Sample S33 (*LL* = 84%).

La Gatta (1970) reports that there exist no rate effects when the shear displacement rate is changed from 8 to 80 mm/day, for three different clays tested in the ring shear apparatus. However the residual shear strength of Cucaracha shale increases by 3.5% when the rate is changed from 80 to 800 mm/day. Wedage (1995) reports that the residual shear strength of

Clearwater shale increases by 3.5% when the rate is increased tenfold, and that rate effects become negligible under 1 mm/day. Viscous effects are a function of velocity, so they become negligible under a certain rate. These findings are consistent with the results of the present study. The average strength increase is 1.8% when the rate is increased tenfold, from 35 to 350 mm/day. However it is near zero when the rate is changed from 3.5 to 35 mm/day (Figure 5.17).

Results of multiple-rate ring shear tests suggest that the strain rate has little effect on the residual shear strength, at least in the range of tested rates (3.5 to 350 mm/day). The Ripley slide current velocity is low enough ($\dot{d} \leq 0.6$ mm/day) that rate effects can be neglected.

6.4 WEAK CLAY HORIZONS OF GLACIOLACUSTRINE UNIT 2

The measurement of geotechnical parameters discussed in the previous section shows variability across glaciolacustrine Unit 2 (Figure 6.2). Plasticity and shear strength depend on the clay fraction, which in turn depends on the considered location in the interbedded silt and clay. This is reflected in the poor reproducibility of direct shear tests (Figure 6.2.d). For instance, the measured residual friction angle ranges from 15.3 to 28.2° for Sample S40 (BH15-03 elevation 265.2 m), and from 15.6 to 23.0° for Sample S46 (BH15-03 elevation 261.8 m). The soil interbedding is preserved in intact specimens; therefore the results are only representative of the bed crossed by the imposed shear plane. Remoulded specimens are made homogeneous so ring shear tests are easily reproducible.

Most of the stratigraphy at the Ripley slide consists of soil comparable to the silt-dominated samples whose residual friction angle is 25° or higher. Beds of brown fat clay are sparse. Often they are narrow, making it difficult to obtain a representative sample. Nonetheless, beds of brown fat clay are recognized for their distinct soil behaviour.

Brown fat clay beds that were characterized in this study correspond to elevations of 270.4 m (S250), 269.6 m (S31) and 268.9 m (S33) in borehole BH15-03. Compared to silt-dominated soil, these beds have a greater potential for shear strength reduction, first through softening and then through the orientation of clay particles in the direction of shear. This makes Unit 2's brown clay beds a preferential location for progressive failure. Retrogression occurs along a bed of weak brown clay, rather than across an adjacent silt bed. Shear strains associated with this failure produce a slickenside, a shear surface along which the shear strength that can be mobilized is the residual shear strength.

From Figure 6.2, the clay bed located at an elevation of 268.8 m in BH15-03 is remarkable. It hosts the active rupture surface of the Ripley slide according to slope inclinometer surveys. This is concurrent with the presence of a slickenside (Figure 5.5). The location also corresponds to a local high in natural water content, indicating that softening is an ongoing process. Nearby Sample S33 (elevation 268.9 m) exhibits the highest plasticity (LL = 84%) and the lowest residual shear strength (φ_r' = 12°) among tested samples.

Similar properties have been measured at other Thompson River Valley landslides. At the North slide, Porter et al. (2002) reported occurrences of brown clay, with a clay fraction often exceeding 70% and a liquid limit as high as 88%. At the South slide, Eshraghian et al. (2007) used direct shear tests to find a residual friction angle φ_r' as low as 13°. Bishop (2008) used ring shear tests to find φ_r' between 10 and 15° in clay-dominated samples. At the Ripley slide, Hendry et al. (2015) used the limit equilibrium method to analyze slope stability, and modeled a clay bed with a φ_r' value of 10.4°.

Such weak clay beds are few but they are persistent, as suggested by Eshraghian et al. (2007) and this study (Figure 6.3). The two same weak clay beds have been found to seat retrogressive failures in several slopes of the Thompson River valley. Thompson River Valley landslides are bedding-controlled because of the singular properties that characterize a small number of Unit 2's clay beds. Bromhead (2013) calls weak clay beds "slide-prone horizons" and remarks that they often have an enhanced smectite content. Such is not the case for the Ripley clay whose mineralogy does not include any smectite. For glaciolacustrine soil, the presence of a slide-prone horizon is only attributed to locally higher clay content. A slide-prone horizon reflects enhanced clay-size sediment input at the time of deposition. For instance, in the event of the glaciolacustrine environment changing from ice-proximal to ice-distal, the input of clay-size sediment is increased (Ashley 2002).

Chapter 7. Conclusion

7.1 SUMMARY

In this thesis, the soil at the Ripley slide was characterized to provide a better understanding of why the Thompson River Valley slopes are vulnerable to failure. More generally, the properties of the Ripley soil, an example of overconsolidated glaciolacustrine clay, were investigated to provide a better understanding of failure in this type of soil.

As part of this study, a campaign of fieldwork was conducted in February 2015. This complemented previous site investigations (2005, 2013) in terms of instrumentation and soil sampling. Continuous core samples were retrieved and conditioned on site for transportation and storage. This provided good quality intact samples for core logging and soil testing in the University of Alberta laboratory. The x-ray radiography of the core proved valuable when selecting laboratory test specimens and identifying features such as fissures (a characteristic of stiff overconsolidated clays) and lamination (a characteristic of glaciolacustrine soils).

The stratigraphy at the Ripley slide was defined in accordance with the existing knowledge about local geology. The unit of interbedded silt and clay was interpreted as glaciolacustrine soil (Unit 2). Beds of brown, fat, slickensided clay were observed in Unit 2.

The glaciolacustrine soil properties were quantified in laboratory tests. The variability of the test results from one sample to another is attributed to the variable clay fraction, a characteristic inherent in glaciolacustrine soil. In oedometer tests, the Ripley clay was found to be heavily overconsolidated. One direct simple shear (DSS) test suggested that significant negative pore water pressure is generated by undrained shear. However, in in-situ, drained conditions, the soil is subject to softening. Consequently, the soil is subject to the loss of cohesion. Measurements taken in the direct shear test showed that cohesion was a significant component of shear strength in Unit 2 clay-dominated beds. The residual shear strength was measured after large strains that were imposed in the ring shear test produced slickenside-like shear surfaces. Results showed that the orientation of clay particles in the direction of shear significantly reduces the strength of clay-dominated beds.

In the present and previous research, landslide movement monitoring showed that two Unit 2 brown fat clay beds host the rupture surfaces of the Ripley slide and other Thompson River

Valley landslides. Soil characterization in this study showed that retrogression occurs preferentially in such beds of glaciolacustrine clay.

7.2 CONTRIBUTIONS OF THE THESIS

The main contributions that this thesis makes are:

- Continuous core samples of glaciolacustrine soil were collected from the Ripley slide (Chapter 3).
- The NGI-type DSS apparatus was shown to be impractical as a method to test the strength of very stiff clays (Chapter 4).
- Limiting soil extrusion was shown to improve the measurement of shear strength in the direct shear and ring shear tests (Chapter 4).
- Glaciolacustrine soil was described, and occurrences of brown, fat, slickensided clay were observed (Chapter 5).
- Plasticity (Atterberg limits), mineralogy, preconsolidation pressure and shear strength were soil properties measured in the laboratory, characterizing the range from clay-dominated to silt-dominated beds of the glaciolacustrine soil (Chapter 5).
- Direct shear, ring shear and DSS tests results provided a comprehensive study of the shear strength of overconsolidated glaciolacustrine soil (Chapter 5).
- Persistent, weak clay horizons in glaciolacustrine Unit 2 were recognized to be responsible for the Thompson River Valley slopes' retrogressive failures (Chapter 6).

7.3 IMPLICATIONS

Soil characterization at the Ripley slide has increased our understanding of the role of glaciolacustrine clay in slope stability issues. The main implications of this study are summarized as follows:

- The intact Ripley soil is characterized as heavily overconsolidated ($OCR \geq 8$) and dilative. Its cohesion represents an important component of the drained shear strength when the clay content is high ($c' > 15$ kPa), in the range of normal stresses experienced in-situ.
- The glaciolacustrine soil is interbedded silt and clay, thus it is heterogeneous. This characteristic is inherited from the mode of deposition of glaciolacustrine soil. Glaciolacustrine clay may be defined by a wide range of soil properties ($37 \leq CF \leq 77\%$;

$32 \leq LL \leq 84\%$). Beds with high clay content are found within the glaciolacustrine soil. These beds may be sparse and narrow, as is the case at the Ripley slide. The clay beds' properties are not representative of the bulk of the soil.

- Clay-rich beds must be recognized for their distinct soil behaviour. Clay beds of glaciolacustrine soil are more brittle than silt beds. Softening and orientation of clay particles in the direction of shear reduce the strength. Clay beds also exhibit low residual shear strength ($\varphi_r' = 12°$). Low residual shear strength is correlated with high plasticity ($LL = 84\%$).
- Plastic, clay-rich beds are weak soil horizons. They are the preferential location in the stratigraphy for failure to occur. Where clay beds are persistent, they host potential retrogressions. Two such clay beds are responsible for major landslides located over a 10-km stretch of the Thompson River Valley.

7.4 SUGGESTIONS FOR FURTHER RESEARCH

In order to complement the present body of work, the research subjects present below may prove to be of interest:

- Improve the DSS test method for stiff overconsolidated clay, in order to investigate further the undrained shear response. A stiffer lateral confinement device should be used to try to limit slippage at the soil-platen interface. For instance, a wire-reinforced membrane may be a suitable alternative to the stacked rigid rings used in this study. Also, samples with the highest clay content should be prioritized over other samples because they are less stiff.
- Develop a model of the Ripley slide compatible with known information about the geometry, soil properties and groundwater regime. The Ripley slide extents are limited by the bedrock; therefore the model should consider a complex landslide geometry.
- Investigate the "healing" of rupture surfaces in glaciolacustrine clay. Thompson River Valley landslides experience seasonal activity, or they are periodically reactivated. The potential for shear strength regain during periods of zero shear displacement is unknown.

Bibliography

Airey, D., & Wood, D. (1987). An evaluation of direct simple shear tests on clay. *Géotechnique , 37* (1), 25-35.

Ashley, G. (2002). Chapter 11: Glaciolacustrine environments. *Modern and Past Glacial Environments* , 335-359.

ASTM. (2011). *D2435. Standard Test Methods for One-Dimensional Consolidation Properties of Soils Using Incremental Loading*. ASTM International.

ASTM. (2011). *D3080. Standard Test Method for Direct Shear Test of Soils Under Consolidated Drained Conditions* . ASTM International.

ASTM. (2007). *D422. Standard Test Method for Particle Size Analysis of Soils*. ASTM International.

ASTM. (2010). *D4318. Standard Test Methods for Liquid Limit, Plastic Limit and Plasticity Index of Soils*. ASTM International.

ASTM. (2014). *D4452. Standard Practice for X-Ray Radiography of Soil Samples*. ASTM International.

ASTM. (2013). *D6467. Standard Test Method for Torsional Ring Shear Test to Determine Drained Residual Shear Strength of Cohesive Soils*. ASTM International.

ASTM. (2007). *D6528. Standard Test Method for Consolidated Undrained Direct Simple Shear Testing of Cohesive Soils*. ASTM International.

ASTM. (2014). *D854. Standard Test Methods for Specific Gravity of Soil Solids by Water Pycnometer*. ASTM International.

Bishop, A., Green, G., Garga, V., Andresen, A., & Brown, J. (1971). A new ring shear apparatus and its application to the measurement of residual strength. *Géotechnique , 21* (4), 273-328.

Bishop, N. (2008). *Geotechnics and hydrology of landslides in Thompson River Valley, near Ashcroft, British Columbia*. M.Sc. thesis, University of Waterloo.

Bjerrum, L. (1967). 3rd Terzaghi Lecture: Progressive failure in slopes of overconsolidated plastic clay and clay shales. *Journal of Soil Mechanics and Foundations Division, ASCE , 93*, 3-49.

Bjerrum, L. (1973). Problems of soil mechanics and construction on soft clays and structurally unstable soils (collapsible expansive and others). *Proc. Eighth Int. Conf. on Soil Mech. and Found. Engng. Moscow , 3*, 111-159.

Bjerrum, L., & Landva, A. (1966). Direct simple-shear tests on a Norwegian quick clay. *Géotechnique , 16* (1), 1-20.

Brindley, G., & Brown, G. (1984). *Crystal structures of clay minerals and their x-ray identification.*

Bromhead, E. (2013). 12th Glossop Lecture: Reflections on the residual strength of clay soils, with special reference to bedding-controlled landslides. *Quarterly Journal of Engineering Geology and Hydrogeology , 46*, 132-155.

Bromhead, E. (1979). A simple ring shear apparatus. *Ground Engineering , 12*, 40-44.

Bunce, C., & Chadwick, I. (2012). GPS monitoring of a landslide for railways. *Landslides and Engineered Slopes: Protecting Society through Improved Understanding* , 1373-1379.

Burn, K. (1968). *Direct Simple Shear Tests on Leda Clay. Internal Report No. 363 of the Division of Building Research*. National Research Council of Canada.

Casagrande, A. (1936). The Determination of the Pre-Consolidation Load and its Practical Significance. *Proceedings 1st ICSMFE , III*, 60.

Chattopadhyay, P. (1972). *Residual shear strength of some pure clay minerals*. Ph.D. thesis, University of Alberta.

Clague, J., & Evans, S. (2003). Geologic Framework of Large Historic Landslides in Thompson River Valley, British Columbia. *Environmental & Engineering Geoscience , 9* (3), 201-212.

Cruden, D., & Varnes, D. (1996). Landslide types and processes. *Transportation Research Board , Special Report 247* (Landslides: investigation and mitigation), 36-75.

Cruden, D., Keegan, T., & Thomson, S. (1993). The landslide dam on the Saddle River near Rycroft, Alberta. *Canadian Geotechnical Journal , 30*, 1003-1015.

Cruden, D., Lu, Z.-Y., & Thomson, S. (1997). The 1939 Montagneuse River landslide, Alberta. *Canadian Geotechnical Journal , 34*, 799-810.

De Groot, D., & Lutenegger, A. (2005). Characterization by sampling and in situ testing - Connecticut Valley varved clay. *Studia Geotechnica et Mechanica , 27* (3-4).

De Josselin de Jong, G. (1972). Discussion to Session II. *Roscoe Memorial Symposium on Stress-Strain Behaviour of Soils* , 258-261.

Dickinson, S., McKane, C., Dugie, M., Savigny, W., & Logue, C. (2016). Characterization of a pre-sheared glaciolacustrine deposit beneath a future tailings dam in South Central British Columbia. *69th Canadian Geotechnical Conference, GeoVancouver 2016*.

Dyvik, R., Berre, T., Lacasse, S., & Raadim, B. (1987). Comparison of truly undrained and constant volume direct simple shear tests. *Géotechnique , 37* (1), 3-10.

Early, K., & Skempton, A. (1972). Investigation of the landslide at Walton's Wood, Staffordshire. *Quarterly Journal of Engineering Geology , 5*, 19-41.

Eid, H., Rabie, K., & Wijewickreme, D. (2016). Drained residual shear strength at effective normal stresses relevant to soil slope stability analyses. *Engineering Geology , 204*, 94-107.

Eshraghian, A., Martin, C., & Cruden, D. (2007). Complex Earth Slides in the Thompson River Valley, Ashcroft, British Columbia. *Environmental & Engineering Geoscience , 13* (2), 161-181.

Eshraghian, A., Martin, C., & Morgenstern, N. (2008). Movement triggers and mechanisms of two earth slides in the Thompson River valley, British Columbia, Canada. *Canadian Geotechnical Journal , 45* (9), 1189-1209.

Evans, S. (1982). Landslides and surficial deposits in urban areas of British Columbia: a review. *Canadian Geotechnical Journal , 19*, 269-288.

Fletcher, L., Hungr, O., & Evans, S. (2002). Contrasting failure behaviour of two large landslides in clay and silt. *Canadian Geotechnical Journal , 39*, 46-62.

Giraud, A., Antoine, P., Van Asch, T., & Nieuwenhuis, J. (1991). Geotechnical problems caused by glaciolacustrine clays in the French Alps. *Engineering Geology , 31*, 185-195.

Grognet, M. (2011). *The boundary conditions in direct simple shear tests: development for peat testing at low vertical stress*. M.Sc. thesis, Delft University of Technology.

Harris, A., & Watson, P. (1997). Optimal procedure for the ring shear test. *Ground Engineering , 30* (6), 26-28.

Head, K. (1994). *Manual of Soil Laboratory Testing Volume 2*. London: Pentech Press.

Hendry, M., Macciotta, R., Martin, C., & Reich, B. (2015). Effect of Thompson River elevation on velocity and instability of Ripley Slide. *Canadian Geotechnical Journal , 52* (3), 257-267.

Holtz, R., & Kovacs, W. (1981). *An introduction to geotechnical engineering*. Englewood Cliffs: Prentice-Hall.

Hungr, O., Leroueil, S., & Picarelli, L. (2013). The Varnes classification of landslide types, an update . *Landslides , 11*, 167-194.

Huntchinson, J. (2001). 4th Glossop Lecture: Reading the Ground: Morphology and Geology in Site Appraisal. *Quarterly Journal of Engineering Geology and Hydrogeology , 34*, 7-50.

Huntley, D., & Bobrowsky, P. (2014). Surficial geology and monitoring of the Ripley Slide, near Ashcroft, British Columbia, Canada. *Geological Survey of Canada , Open File 7531*.

Hvorslev, M. (1939). Torsion shear tests and their place in the determination of the shearing resistance of soils. *Proceedings of the American Society for Testing and Materials , 99*, 999-1022.

Jamiolkowski, M., Ladd, C., Germaine, J., & Lancellotta, R. (1985). New developments in field and laboratory testing of soils. *Proceedings of the 11th International Conference on Soil Mechanics and Foundation Engineering, San Francisco , 1*, 57-154.

Johnsen, T., & Brennand, T. (2004). Late-glacial lakes in the Thompson Basin, British Columbia: paleogeography and evolution. *Canadian Journal of Earth Sciences , 41* (11), 1367-1383.

Journault, J., Macciotta, R., Hendry, M., Charbonneau, F., Bobrowsky, P., Huntley, D., et al. (2016). Identification and quantification of concentrated movement zones within the Thompson River Valley using satellite InSAR. *69th Canadian Geotechnical Conference, GeoVancouver 2016*.

Kjellman, W. (1951). Testing the shear strength of clay in Sweden. *Géotechnique , 2* (3), 225-235.

Kohv, M., Hang, T., Talviste, P., & Kalm, V. (2010). Analysis of a retrogressive landslide in glaciolacustrine varved clay. *Engineering Geology , 116*, 109-116.

Kulhawy, F., & Mayne, P. (1990). *Manual on Estimating Soil Properties for Foundation Design*. Cornell University. Ithaca: EPRI.

La Gatta, D. (1970). *Report on residual strength of clays and clay-shales by rotation shear tests*. Harvard University.

La Rochelle, P. (1981). Limitations of direct simple shear test devices. *ASTM Special Technical Publication* (740), 653-658.

Lacasse, S., Ladd, C., & Barsvary, A. (1977). Undrained behavior of embankments on New Liskeard varved clay. *Canadian Geotechnical Journal , 14* (3), 367-388.

Ladd, C. (1991). 22nd Terzaghi Lecture: Stability evaluation during staged construction. *Journal of Geotechnical Engineering, ASCE , 117* (4), 540-615.

Ladd, C., & Edgers, L. (1972). *Consolidated-undrained direct simple shear tests on saturated clays*. Research Report R 72-82. Department of Civil Engineering, Massachusetts Institute of Technology.

Ladd, C., & Foott, R. (1974). New design procedure for stability of soft clays. *Journal of the Geotechnical Engineering Division , 100* (7), 764-786.

Lau, W. (1988). *Behaviour of clay in simple shear and triaxial tests*. Ph.D. thesis, The City University, London.

Le Meil, G., Hendry, M., & Martin, C. (2016). Direct simple shear (DSS) testing of a very stiff glaciolacustrine clay. *69th Canadian Geotechnical Conference, GeoVancouver 2016*.

Leonoff, C., & Klohn Leonoff Ltd. (1994). *A dedicated team: Klohn Leonoff Consulting Engineers 1951-1991*. Richmond, Canada: Klohn Leonoff Ltd.

Lupini, J., Skinner, A., & Vaughan, P. (1981). The drained residual strength of cohesive soils. *Géotechnique , 31* (2), 181-213.

Mayne, P. (1985). A review of undrained strength in direct simple shear. *Soils and Foundations , 25* (3), 64-72.

Mayne, P. (1988). Determining OCR in clays from laboratory strength. *Journal of Geotechnical Engineering , 114* (1), 76-92.

Meehan, C., Brandon, T., & Duncan, J. (2007). Measuring Drained Residual Strengths in the Bromhead Ring Shear. *Geotechnical Testing Journal , 30* (6), 466-473.

Mesri, G., & Shahien, M. (2003). Residual Shear Strength Mobilized in First-Time Slope Failures. *Journal of Geotechnical and Geoenvironmental Engineering , 129* (1), 12-31.

Mitchell, J. (1976). *Fundamentals of soil behavior*. New York: Wiley.

Morgenstern, N. (1970). Black shale heaving at Ottawa, Canada: Discussion. *Canadian Geotechnical Journal , 7* (2), 114-115.

Morgenstern, N. (1980). Factors affecting the selection of shear strength parameters in slope stability analysis. *Proc. Int. Symp. Landslides New Delhi , 2*, 83-94.

Morgenstern, N. (1990). Instability mechanisms in stiff soils and weak rocks. *Proceedings of the 10th Southeast Asian Geotechnical Conference, Taipei , 2*, 27-36.

Morgenstern, N. (1968). Shear Strength of Stiff Clay. *Proceedings of the Geotechnical Conference Oslo 1967 on shear strength properties of natural soils and rocks , 2*, 59-71.

Morgenstern, N. (1992). The evaluation of slope stability - a 25 year perspective. *Stability and performance of slopes and embankments - II , Geotechnical Special Publication No. 31*.

Natural Resources Canada. (2017). *The Atlas of Canada*. http://atlas.gc.ca/toporama.

Olson, R. (1986). State of the Art: Consolidation Testing. *ASTM Special Technical Publication , 892*, 7-70.

Porter, M., Savigny, K., Keegan, T., Bunce, C., & MacKay, C. (2002). Controls on the stability of the Thompson River landslides. *55th Canadian Geotechnical Conference, Niagara Falls* .

Prest, V., Grant, D., & Rampton, V. (1968). Glacial map of Canada. *Geological Survey of Canada , "A" Series Map 1263A*.

Prevost, J., & Hoeeg, K. (1976). Reanalysis of simple shear soil testing. *Canadian Geotechnical Journal , 13* (4), 418-429.

Ryder, J. (1976). Terrain inventory and quaternary geology Ashcroft, British Columbia. *Geological Survey of Canada , Paper 74-49*.

Ryder, J., Fulton, R., & Clague, J. (1991). The Cordilleran Ice Sheet and the Glacial Geomorphology of Southern and Central British Colombia. *Géographie physique et Quartenaire , 45* (3), 365-377.

Saada, A., & Townsend, F. (1981). State of the Art: Laboratory Strength Testing of Soils. *ASTM Special Technical Publication , 740*, 7-77.

Sambhandharaksa, S. (1977). *Stress-strain-strength anisotropy of varved clays*. D.Sc. thesis, Massachusetts Institute of Technology.

Schafer, M. (2016). *Kinematics and Controlling Mechanics of the Slow Moving Ripley Landslide*. M.Sc. thesis, University of Alberta.

Schafer, M. (2014). *Personal communication. May 21, 2015*.

Schafer, M., Macciotta, R., Hendry, M., Martin, C., Bunce, C., Choi, E., et al. (2015). Instrumenting and Monitoring a Slow Moving Landslide. *68th Canadian Geotechnical Conference, GeoQuébec 2015*.

Skempton, A. (1964). 4th Rankine Lecture: Long-term stability of clay slopes. *Géotechnique , 14* (2), 75-101.

Skempton, A. (1985). Residual strength of clays in landslides, folded strata and the laboratory. *Géotechnique , 35* (1), 3-18.

Skempton, A. (1970). Technical Notes: First-time slides in over-consolidated clays. *Géotechnique , 20* (3), 320-324.

Skempton, A. (1984). The colloidal activity of clays. *Selected papers on soil mechanics* , 60-64.

Skemton, A., & Hutchinson, J. (1969). Stability of natural slopes and embankment foundations. *Proceedings of the 7th International Conference on Soil Mechanics and Foundation Engineering, Mexico , State-of-the-Art Volume*, 291-340.

Smith, N., & Ashley, G. (1985). Proglacial lacustrine environment. *SEPM Short Course , 16*, 135-215.

Stanton, R. (1898). The great land-slides on the Canadian Pacific Railway in British Columbia. *Proceedings of the Institution of Civil Engineers, Session 1897-1898, Part II, Section 1* , 1-46.

Stark, T., & Eid, H. (1994). Drained Residual Strength of Cohesive Soils. *Journal of Geotechnical Engineering , 120* (5), 856-871.

Stark, T., & Hussain, M. (2013). Empirical Correaltions: Drained Shear Strength for Slope Stability Analyses. *Journal of Geotechnical and Geoenvironmental Engineering , 139* (6), 853-862.

Stark, T., & Vettel, J. (1992). Bromhead Ring Shear Test Procedure. *Geotechnical Testing Journal , 15* (1), 24-32.

Terzaghi, K. (1936). Stability of slopes in natural clays. *Proceedings of the 1st International Conference on Soil Mechanics and Foundation Engineering, Cambridge, Mass. , 1*, 161-170.

Terzaghi, K., & Peck, R. (1967). *Soil Mechanics in Engineering Practice, 2nd edition*. New York: Wiley.

Van Genuchten, P., & Van Asch, T. (1988). Factors controlling the movement of a landslide in varved clays near La Mure (French Alps). *Bulletin de la Société Géologique de France , 4* (3), 461-469.

Vucetic, M., & Lacasse, S. (1982). Specimen size effect in simple shear test. *Journal of Geotechnical Engineering , 108* (GT12), 1567-1585.

Wedage, A. (1995). *Influence of rate effects on the residual strength of slopes*. Ph.D. thesis, University of Alberta.

Wroth, C. (1984). 24th Rankine Lecture: The interpretation of in situ soil tests. *Géotechnique , 34* (4), 449-489.

Appendices

APPENDIX A. TABLE SUMMARY OF TESTING PROGRAM

Table A.1. Summary of laboratory tests

Sample		**Tests**						
	Depth (m)	Particle size analysis	Atterberg limits	Specific gravity	Oedometer	Direct shear	Ring shear	Simple shear
Borehole BH13-01								
OR21	8.5	1	1					
OR22	10.9	1	1					
S2	12.5			1	1			
S3	13.0				1			
S4	13.4		1	1				3
OR23	16.0	1	1					
OR24	17.1	1	1					
S6	17.5		1	1				4
OR25	20.6	1	1					
OR27	23.1	1	1					
S8	25.5		1	1	2			
OR28	25.7	1	1					
OR29	27.5	1	1					
	Borehole total	*8*	*11*	*4*	*4*	*0*	*0*	*7*
Borehole BH15-03								
S250	7.6		1	1		2	1	
S257	7.8		1					
S31	8.4		1			3	2	
S32	8.9		1			2	2	
S33	9.1		1			3	3	
S34a	9.5		1					
S35	9.7		1			2		
S36	10.0					2		
S38	10.4		1			3		
S40	12.8	1	3	1	1	3	3	
S41	13.3		1	1				
S42	14.2	1	1			3	1	
S44	14.9	1	1	1	1	1	1	
S45.3	15.8		1					
S46	16.2	2	1		1	3	3	
	Borehole total	*5*	*16*	*4*	*3*	*27*	*16*	*0*
	TOTAL	*13*	*27*	*8*	*7*	*27*	*16*	*7*

APPENDIX B. CORE PHOTOGRAPHS AND RADIOGRAPHS

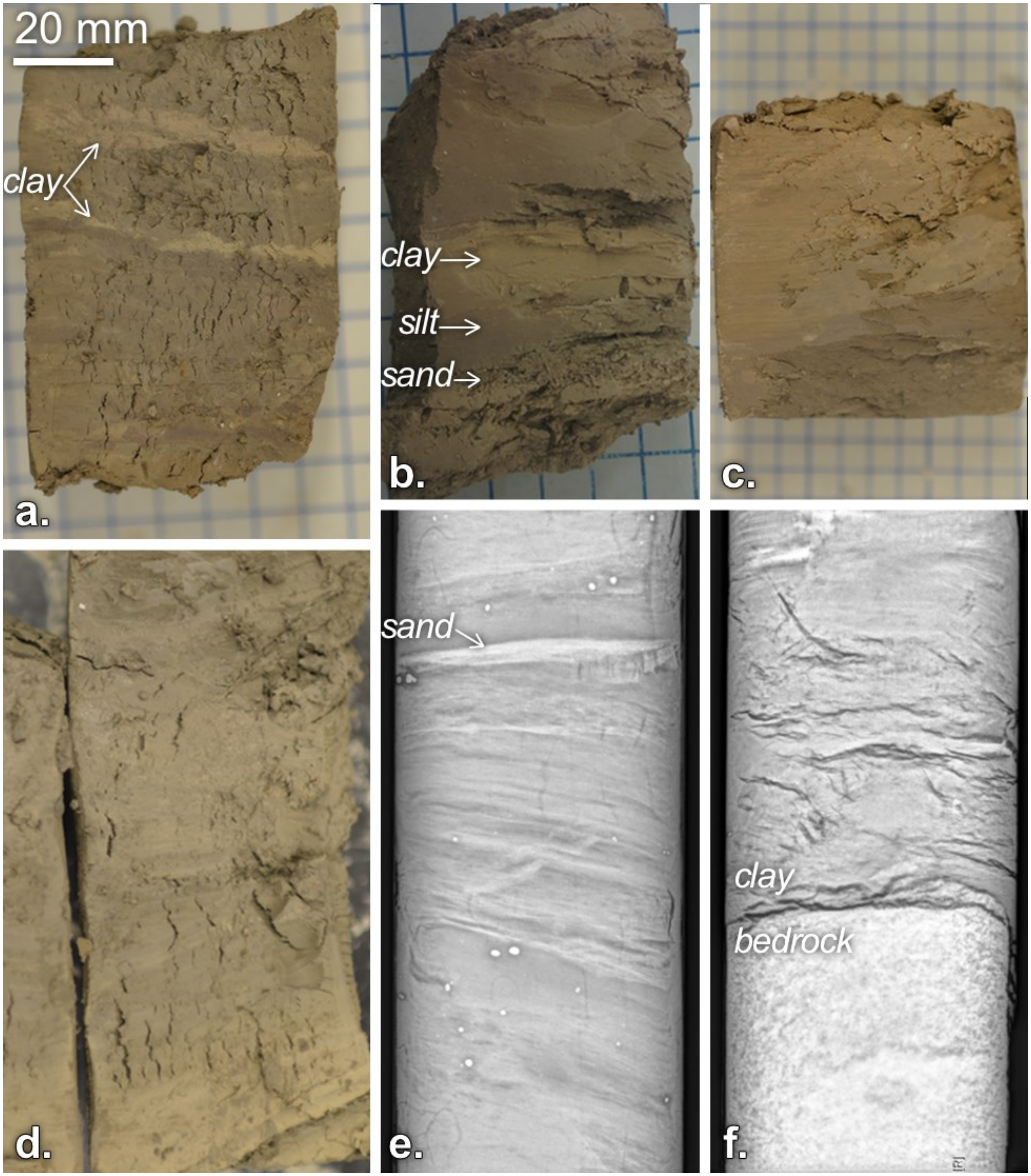
20 mm
clay
a.
clay
silt
sand
b.
c.
d.
sand
e.
clay
bedrock
f.

Figure B.1. (a) Interbedded silt and clay at BH15-03 depth 8.8 m; (b) interbedded silt and clay at BH15-01 depth 9.0 m; (c) grey silt grading into brown clay at BH15-03 depth 10.3 m; (d) brown clay grading into grey silt at BH15-03 depth 16.5 m; (e) laminated soil radiograph at BH15-01 depth 13.0 m; (f) bedrock-clay contact radiograph at BH15-01 depth 15.2 m

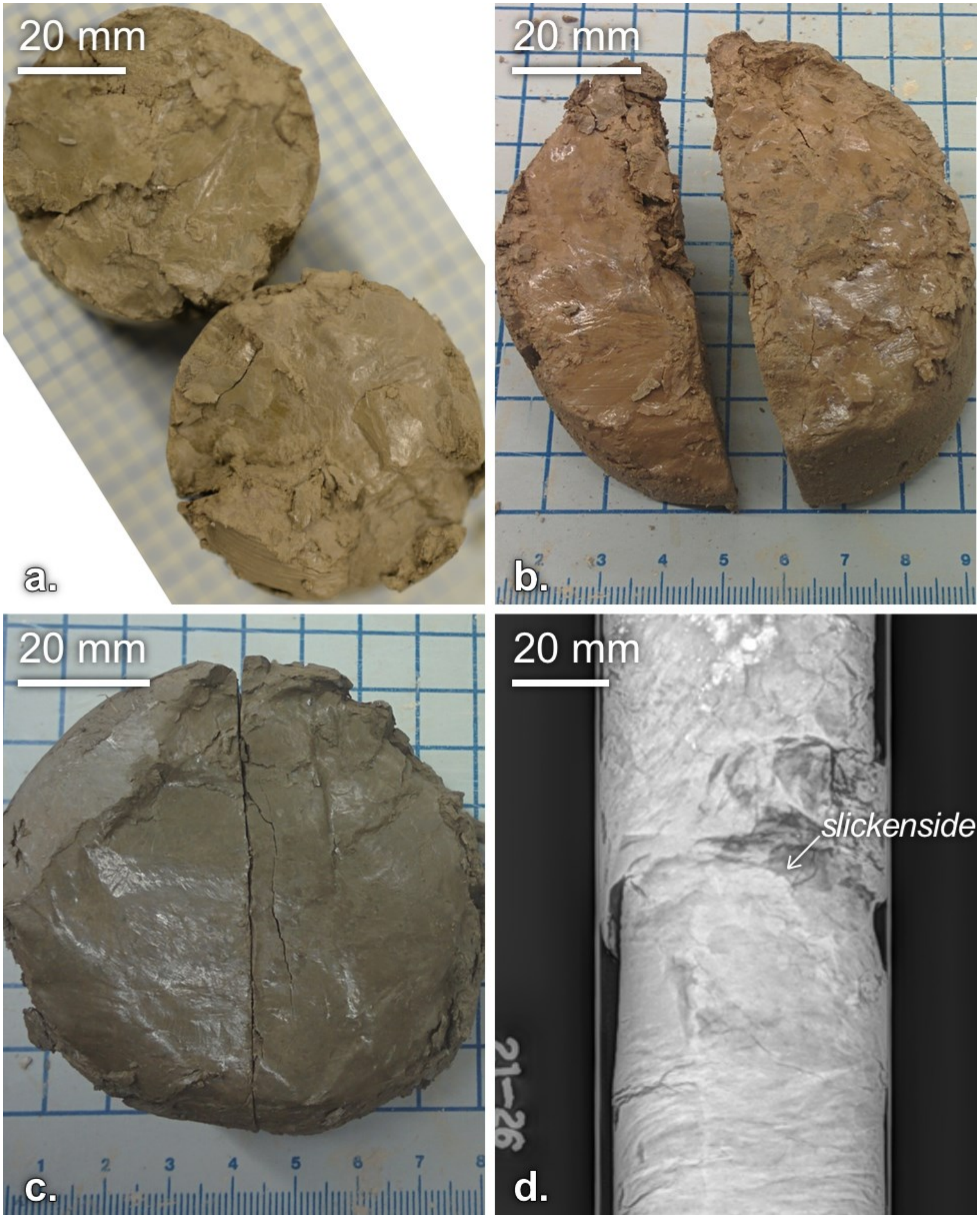
20 mm
a.
20 mm
2 3 4 5 6 7 8 9
b.
20 mm
1 2 3 4 5 6 7 8
c.
20 mm
slickenside
21-26
d.

Figure B.2 Slickensides: (a) BH15-03 depth 9.5 m; (b) BH15-01 depth 10.1 m; (c) BH15-01 depth 12.0 m; (d) BH15-01 depth 7.7 m

APPENDIX C. CORE LOGS

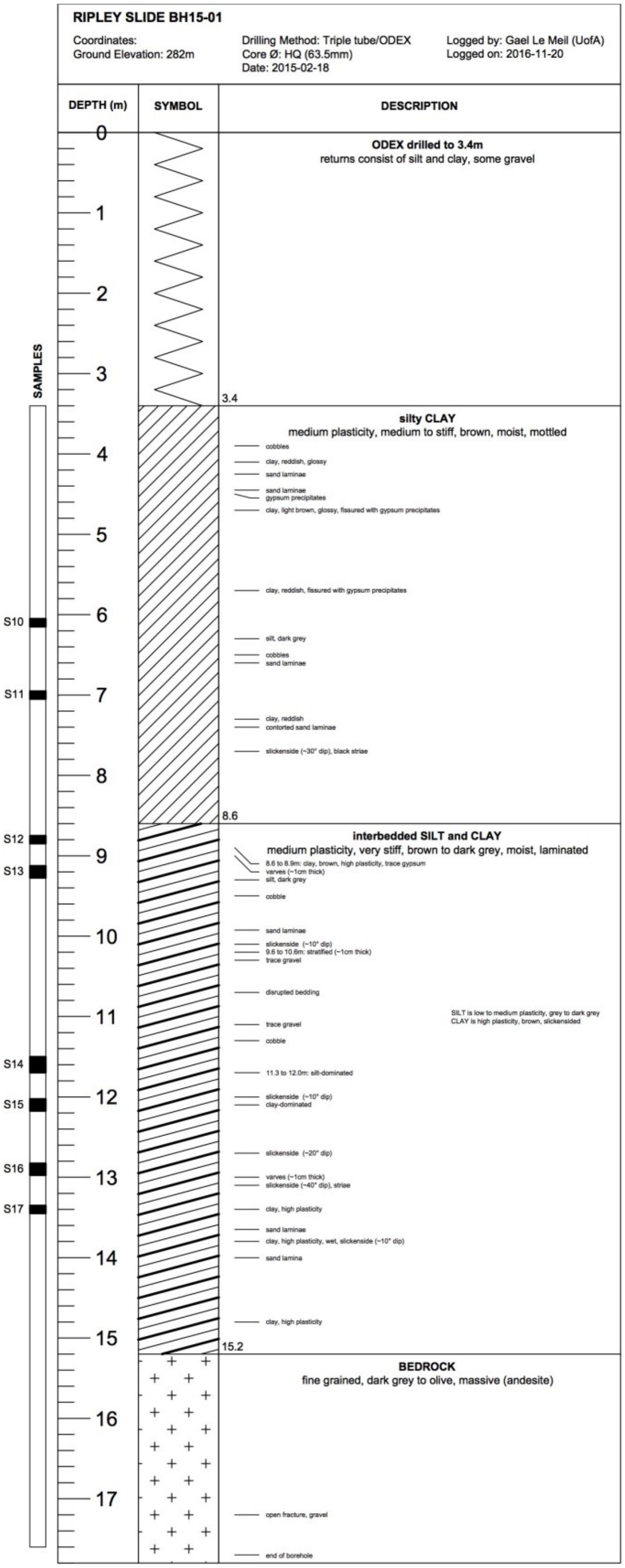
RIPLEY SLIDE BH15-01
Coordinates:
Ground Elevation: 282m
Drilling Method: Triple tube/ODEX
Core Ø: HQ (63.5mm)
Date: 2015-02-18
Logged by: Gael Le Meil (UofA)
Logged on: 2016-11-20
DEPTH (m)
SYMBOL
DESCRIPTION
SAMPLES
0
1
2
3
4
5
6
7
8
9
10
11
12
13
14
15
16
17
S10
S11
S12
S13
S14
S15
S16
S17
ODEX drilled to 3.4m
returns consist of silt and clay, some gravel
3.4
silty CLAY
medium plasticity, medium to stiff, brown, moist, mottled
cobbles
clay, reddish, glossy
sand laminae
sand laminae
gypsum precipitates
clay, light brown, glossy, fissured with gypsum precipitates
clay, reddish, fissured with gypsum precipitates
silt, dark grey
cobbles
sand laminae
clay, reddish
contorted sand laminae
slickenside (~30° dip), black striae
8.6
interbedded SILT and CLAY
medium plasticity, very stiff, brown to dark grey, moist, laminated
8.6 to 8.9m: clay, brown, high plasticity, trace gypsum
varves (~1cm thick)
silt, dark grey
cobble
sand laminae
slickenside (~10° dip)
9.6 to 10.6m: stratified (~1cm thick)
trace gravel
disrupted bedding
SILT is low to medium plasticity, grey to dark grey
CLAY is high plasticity, brown, slickensided
trace gravel
cobble
11.3 to 12.0m: silt-dominated
slickenside (~10° dip)
clay-dominated
slickenside (~20° dip)
varves (~1cm thick)
slickenside (~40° dip), striae
clay, high plasticity
sand laminae
clay, high plasticity, wet, slickenside (~10° dip)
sand lamina
clay, high plasticity
15.2
BEDROCK
fine grained, dark grey to olive, massive (andesite)
open fracture, gravel
end of borehole

Figure C.1. BH15-01 core log

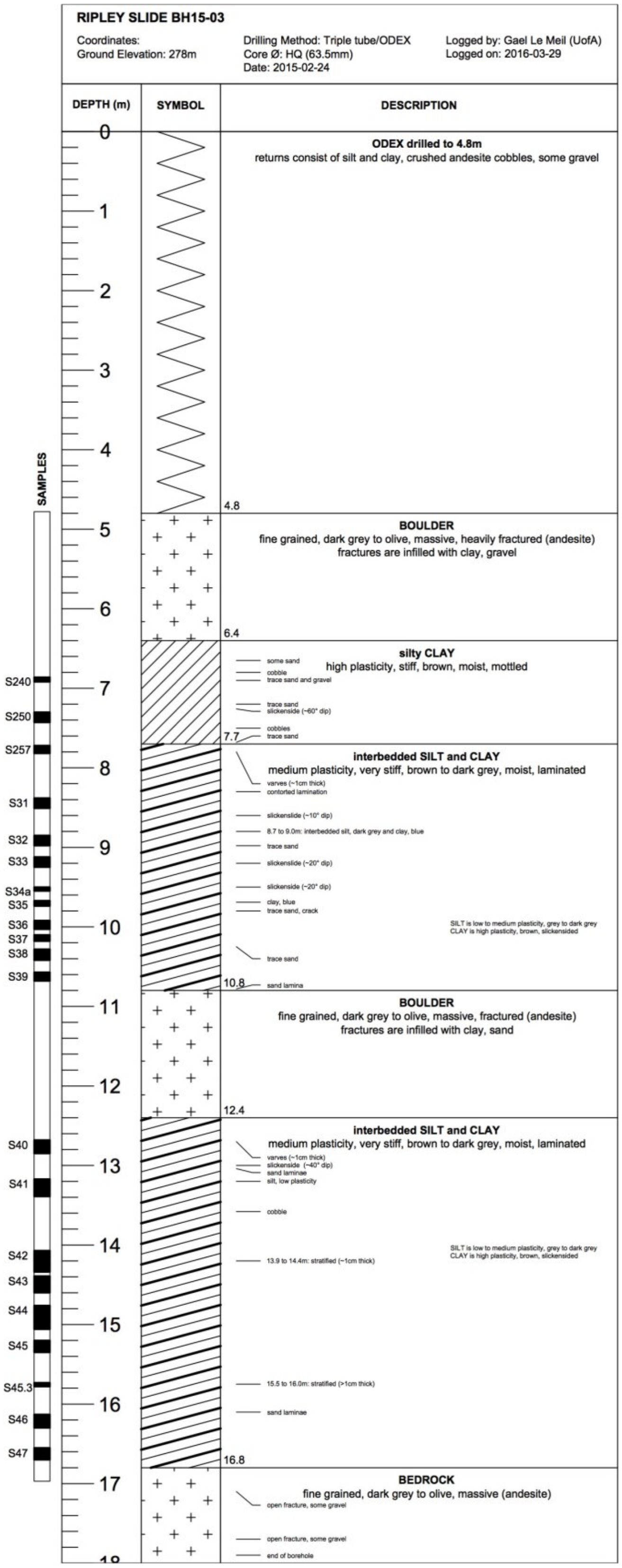
RIPLEY SLIDE BH15-03
Coordinates:
Ground Elevation: 278m
Drilling Method: Triple tube/ODEX
Core Ø: HQ (63.5mm)
Date: 2015-02-24
Logged by: Gael Le Meil (UofA)
Logged on: 2016-03-29
DEPTH (m)
SYMBOL
DESCRIPTION
0
1
2
3
4
5
6
7
8
9
10
11
12
13
14
15
16
17
SAMPLES
S240
S250
S257
S31
S32
S33
S34a
S35
S36
S37
S38
S39
S40
S41
S42
S43
S44
S45
S45.3
S46
S47
ODEX drilled to 4.8m
returns consist of silt and clay, crushed andesite cobbles, some gravel
4.8
BOULDER
fine grained, dark grey to olive, massive, heavily fractured (andesite)
fractures are infilled with clay, gravel
6.4
silty CLAY
high plasticity, stiff, brown, moist, mottled
some sand
cobble
trace sand and gravel
trace sand
slickenside (~60° dip)
cobbles
trace sand
7.7
interbedded SILT and CLAY
medium plasticity, very stiff, brown to dark grey, moist, laminated
varves (~1cm thick)
contorted lamination
slickenslide (~10° dip)
8.7 to 9.0m: interbedded silt, dark grey and clay, blue
trace sand
slickenslide (~20° dip)
slickenside (~20° dip)
clay, blue
trace sand, crack
SILT is low to medium plasticity, grey to dark grey
CLAY is high plasticity, brown, slickensided
trace sand
10.8
sand lamina
BOULDER
fine grained, dark grey to olive, massive, fractured (andesite)
fractures are infilled with clay, sand
12.4
interbedded SILT and CLAY
medium plasticity, very stiff, brown to dark grey, moist, laminated
varves (~1cm thick)
slickenside (~40° dip)
sand laminae
silt, low plasticity
cobble
13.9 to 14.4m: stratified (~1cm thick)
SILT is low to medium plasticity, grey to dark grey
CLAY is high plasticity, brown, slickensided
15.5 to 16.0m: stratified (>1cm thick)
sand laminae
16.8
BEDROCK
fine grained, dark grey to olive, massive (andesite)
open fracture, some gravel
open fracture, some gravel
end of borehole

Figure C.2. BH15-03 core log

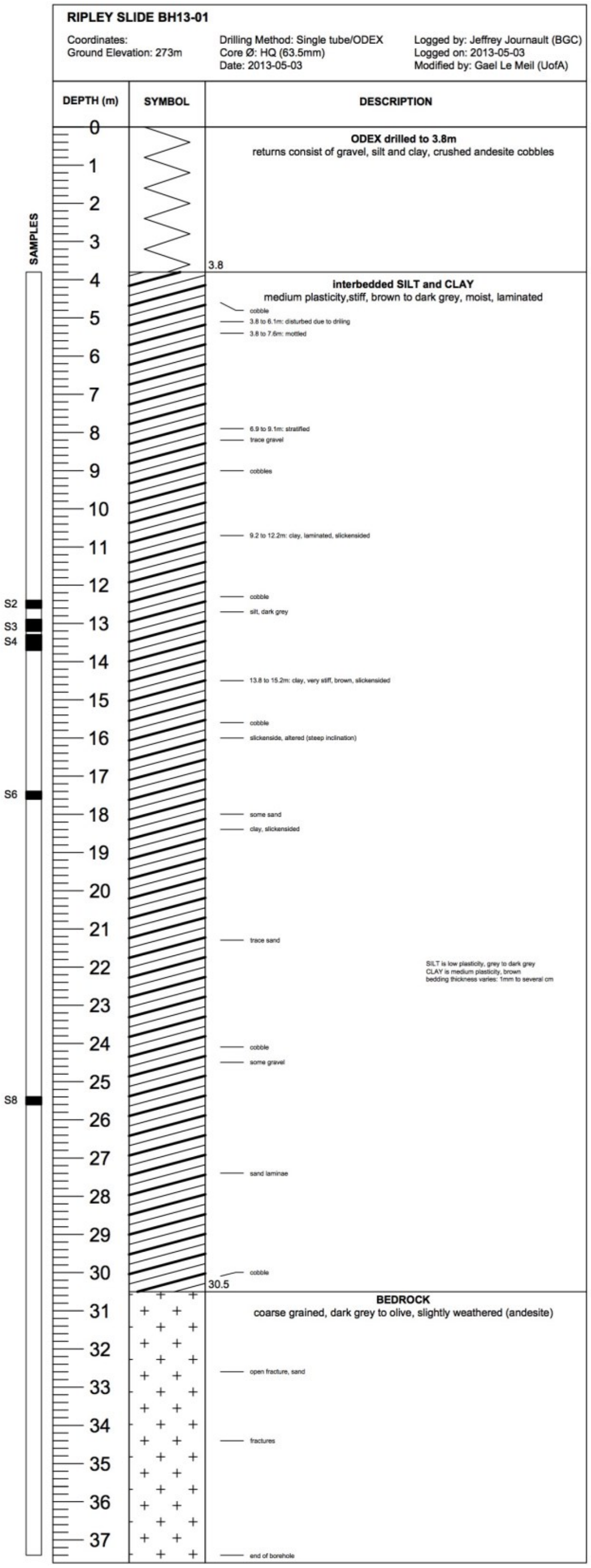
RIPLEY SLIDE BH13-01
Coordinates:
Ground Elevation: 273m
Drilling Method: Single tube/ODEX
Core Ø: HQ (63.5mm)
Date: 2013-05-03
Logged by: Jeffrey Journault (BGC)
Logged on: 2013-05-03
Modified by: Gael Le Meil (UofA)
DEPTH (m)
SYMBOL
DESCRIPTION
SAMPLES
S2
S3
S4
S6
S8
0
1
2
3
4
5
6
7
8
9
10
11
12
13
14
15
16
17
18
19
20
21
22
23
24
25
26
27
28
29
30
31
32
33
34
35
36
37
ODEX drilled to 3.8m
returns consist of gravel, silt and clay, crushed andesite cobbles
3.8
interbedded SILT and CLAY
medium plasticity,stiff, brown to dark grey, moist, laminated
cobble
3.8 to 6.1m: disturbed due to driling
3.8 to 7.6m: mottled
6.9 to 9.1m: stratified
trace gravel
cobbles
9.2 to 12.2m: clay, laminated, slickensided
cobble
silt, dark grey
13.8 to 15.2m: clay, very stiff, brown, slickensided
cobble
slickenside, altered (steep inclination)
some sand
clay, slickensided
trace sand
SILT is low plasticity, grey to dark grey
CLAY is medium plasticity, brown
bedding thickness varies: 1mm to several cm
cobble
some gravel
sand laminae
cobble
30.5
BEDROCK
coarse grained, dark grey to olive, slightly weathered (andesite)
open fracture, sand
fractures
end of borehole

Figure C.3. BH13-01 core log

APPENDIX D. X-RAY DIFFRACTOGRAMS

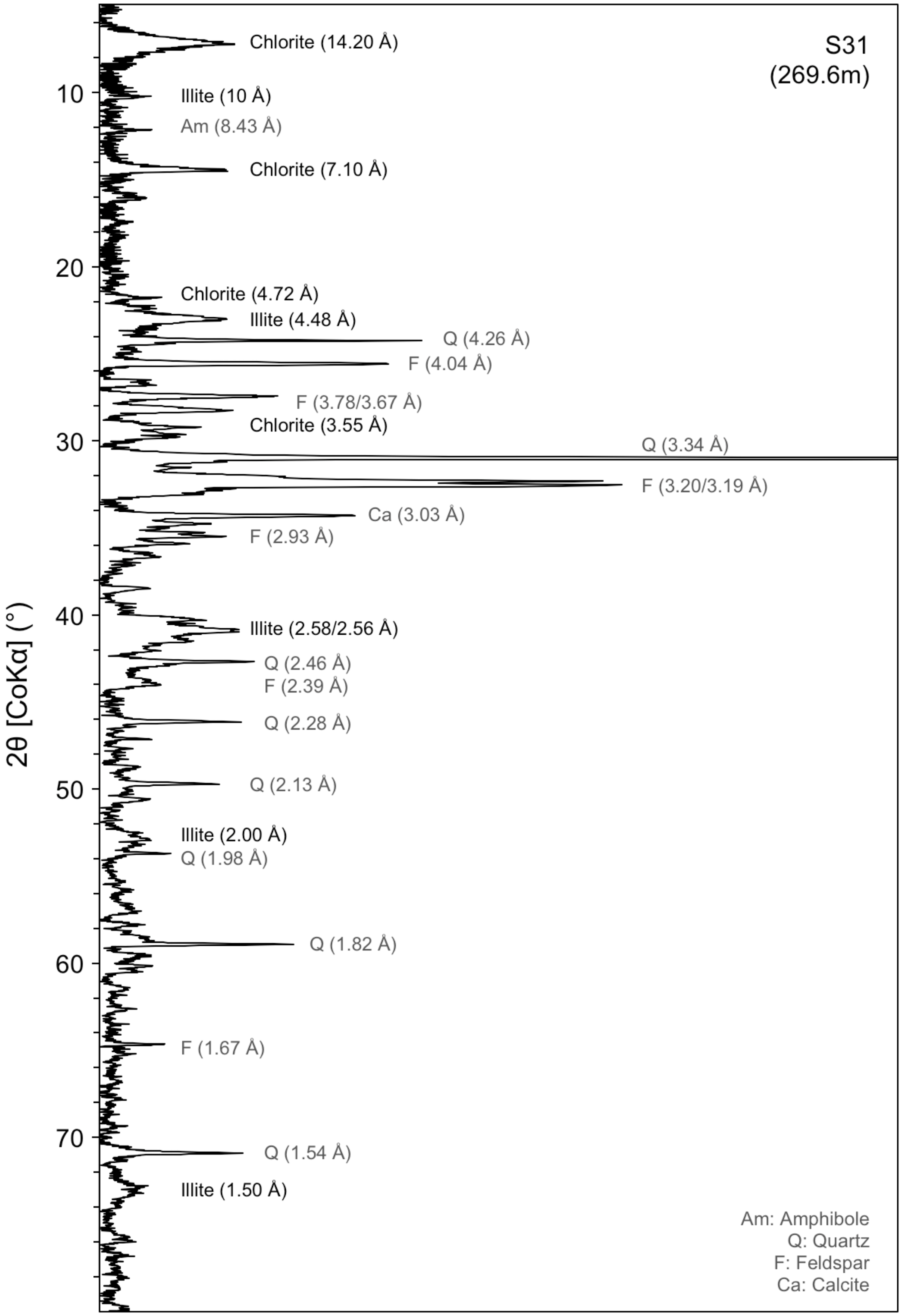

Figure D.1. S31 (BH15-03 depth 8.4 m) diffractogram

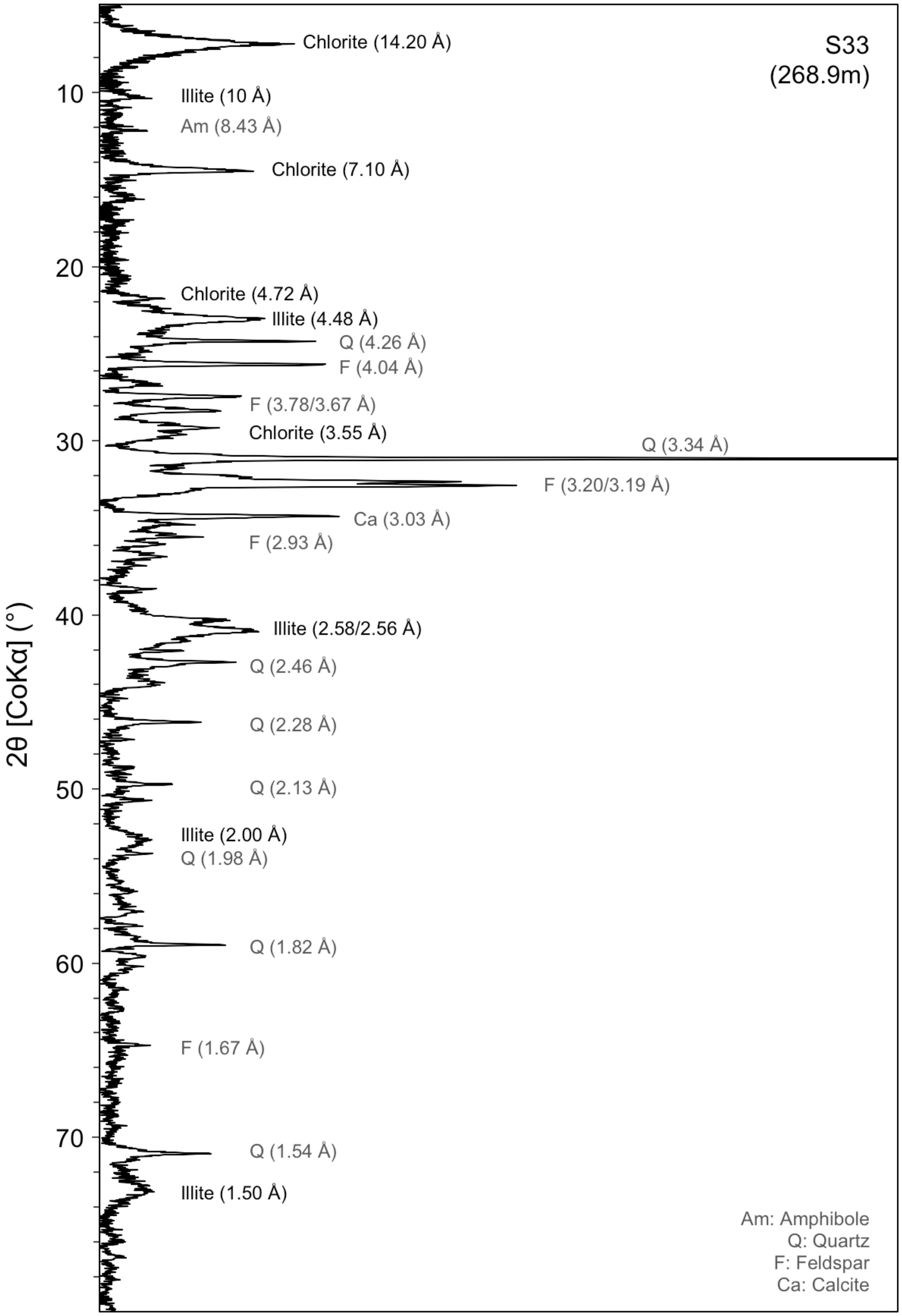

Figure D.2. S33 (BH15-03 depth 9.1 m) diffractogram

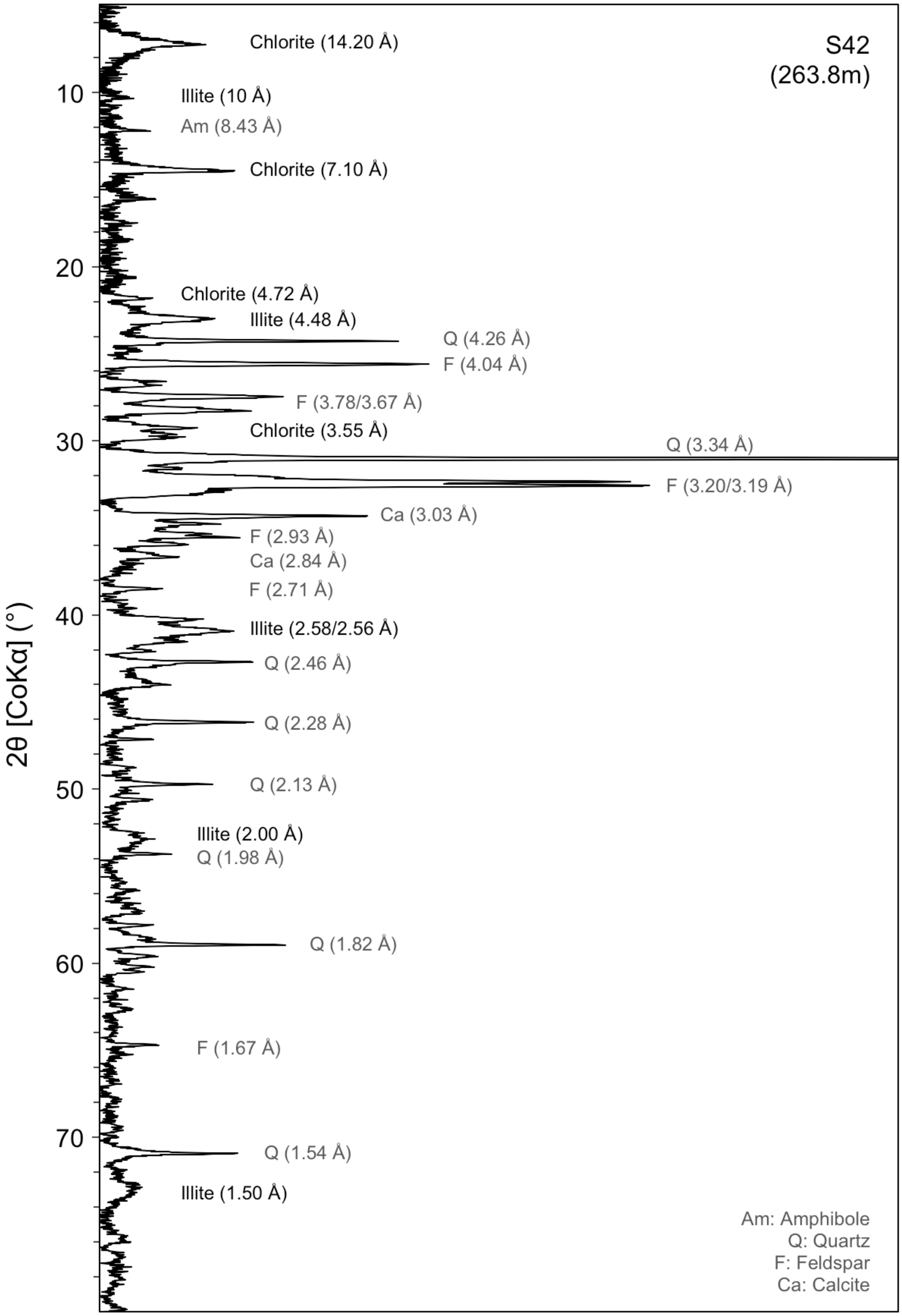

Figure D.3. S42 (BH15-03 depth 14.2 m) diffractogram

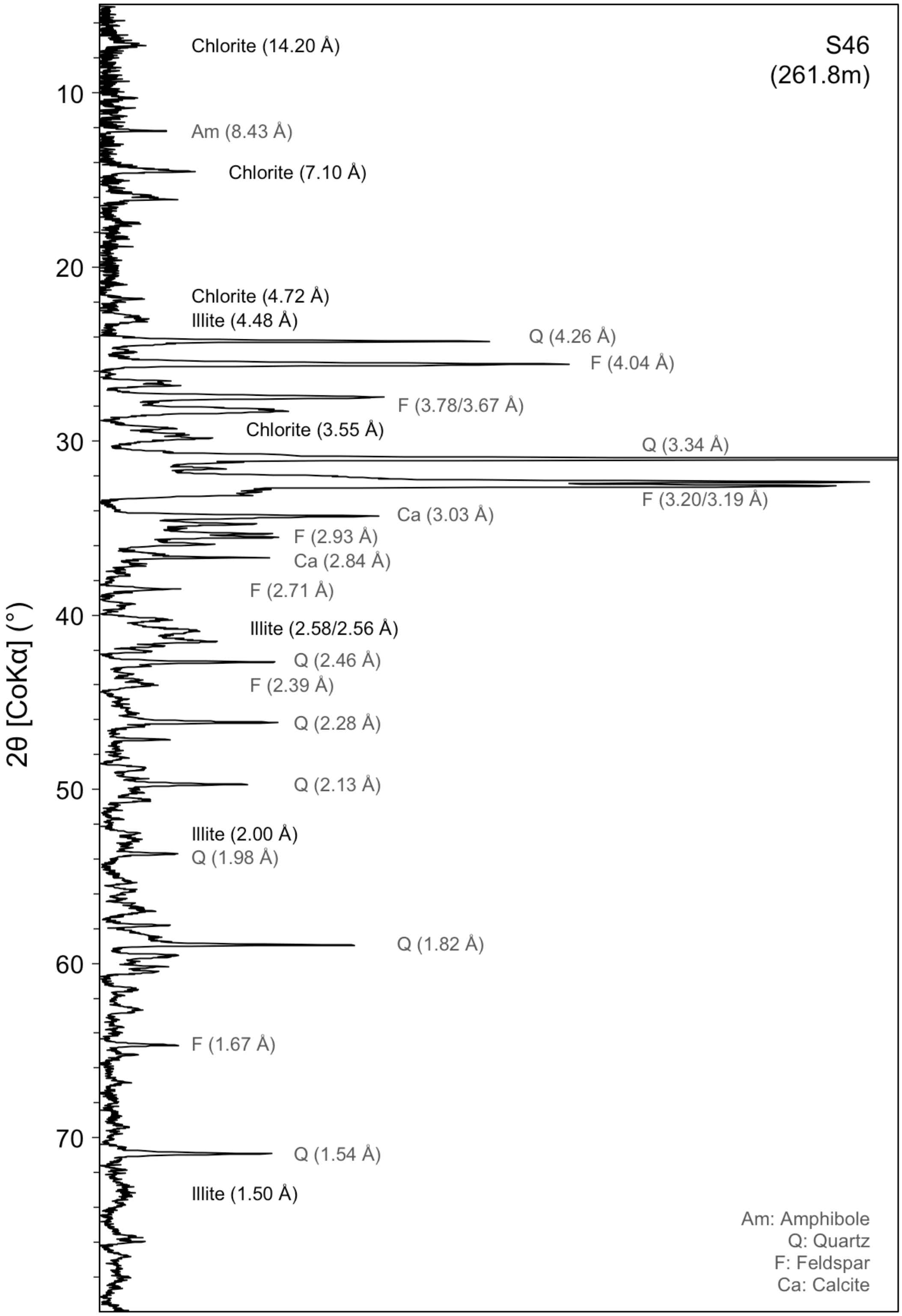

Figure D.4. S46 (BH15-03 depth 16.2 m) diffractogram

APPENDIX E. OEDOMETER TEST TIME-DEFORMATION RESULTS

Table E.1. Oedometer tests on BH13-01 samples

	Test	Sample depth (m)	Initial unit weight γ_0 (kN/m^3)	Initial height H_0 (mm)	Increment load σ'_i (kPa)	Height H_i (mm)	time to 50% consolidation (*log of time* method) t_{50_i} (min)	Coefficient of consolidation of increment c_{v_i} (m^2/s)	Preconsolidation stress σ'_p (kPa)	Overconsolidation ratio of increment OCR_i	Coefficient of consolidation c_v (m^2/s)	Vertical permeability k_v (cm/s)
BH13-01	S2	12.5	18.5	15.1	666	14.6	0.75	2.5×10^{-7}	2700	8		
					1479	14.2	0.4	4.7×10^{-7}		4		
					2926	13.6	0.9	2.1×10^{-7}		2		
					5238	12.8	1.5	1.2×10^{-7}		1	1.1×10^{-7}	2.0×10^{-9}
					7555	12.5	2.0	9.4×10^{-8}		1		
	S3	13	19.0	19.0	733	18.2	1.8	1.6×10^{-7}	2500	7		
					1545	17.7	3.1	9.6×10^{-8}		3		
					2993	17.0	3.6	8.2×10^{-8}		2		
					4166	16.5	9.0	3.3×10^{-8}		1	1.6×10^{-8}	3.3×10^{-10}
					5303	16.1	20	1.5×10^{-8}		1		
					6988	15.6	50	5.9×10^{-9}		1		
					8936	15.3	30	9.9×10^{-9}		1		
	S8_1	25.5	19.7	19.0	402	18.5	3.0	9.9×10^{-8}	3500	17		
					796	18.2	2.4	1.2×10^{-7}		9		
					1587	17.8	2.8	1.1×10^{-7}		4		
					3232	17.2	4.5	6.6×10^{-8}		2		
					6014	16.2	20	1.5×10^{-8}		1	1.5×10^{-8}	2.9×10^{-10}
	S8_2	25.5	19.4	19.0	786	18.3	4.0	7.4×10^{-8}	4000	10		
					1628	17.9	3.5	8.5×10^{-8}		5		
					3178	17.4	4.8	6.2×10^{-8}		3		
					4314	16.9	22	1.3×10^{-8}		2		
					6495	16.3	23	1.3×10^{-8}		1	1.2×10^{-8}	2.0×10^{-10}
					8942	15.7	26	1.1×10^{-8}		1		

Table E.2. Oedometer tests on BH15-03 samples

	Test	Sample depth (m)	Initial unit weight γ_0 (kN/m^3)	Initial height H_0 (mm)	Increment load σ'_i (kPa)	Height H_i (mm)	time to 50% consolidation (*log of time* method) t_{50_i} (min)	Coefficient of consolidation of increment c_{v_i} (m^2/s)	Preconsolidation stress σ'_p (kPa)	Overconsolidation ratio of increment OCR_i	Coefficient of consolidation c_v (m^2/s)	Vertical permeability k_v (cm/s)
BH15-03	S250	7.6	20.1	19.0	532	18.7	1.3	2.3×10^{-7}	4100	15		
					1032	18.6	2.0	1.5×10^{-7}		8		
					2025	18.3	1.5	2.0×10^{-7}		4		
					4116	17.9	1.0	3.0×10^{-7}		2		
					8403	17.2	5.8	5.1×10^{-8}		1	5.1×10^{-8}	4.6×10^{-10}
	S40	12.8	18.8	19.0	546	17.6	2.3	1.3×10^{-7}	1400	5		
					1045	17.1	2.5	1.2×10^{-7}		3		
					2182	16.2	2.0	1.5×10^{-7}		1	1.4×10^{-7}	4.1×10^{-9}
					4493	15.1	2.1	1.4×10^{-7}		1		
					8452	14.2	2.4	1.2×10^{-7}		1		
	S44	14.9	19.2	19.0	2182	17.4	0.64	4.6×10^{-7}	2000	2		
					4422	16.7	0.75	4.0×10^{-7}		1	3.9×10^{-7}	5.8×10^{-9}
					8051	15.9	0.78	3.8×10^{-7}		1		
	S46	16.2	19.4	19.0	311	18.4	2.2	1.3×10^{-7}	2200	14		
					622	17.9	1.8	1.6×10^{-7}		7		
					1284	17.4	3.2	9.3×10^{-8}		3		
					2799	16.6	1.8	1.6×10^{-7}		2		
					5039	15.8	4.6	6.4×10^{-8}		1	8.2×10^{-8}	1.4×10^{-9}
					8857	14.9	3.0	9.9×10^{-8}		1		

APPENDIX F. DIRECT SHEAR TEST RESULTS

Table F.1. Direct shear test parameters

Test	Sample depth (m)	Mass of specimen M_0 (g)	Initial water content w_i (%)	Final water content w_f (%)	Normal stress σ'_n (kPa)	Shear displacement rate (mm/min)	Total shear displacement d (mm)	Consolidation settlement Δh_1 (mm)	Shear settlement Δh_2 (mm)	Gap between shear box halves (mm)
S250_3	7.6	72.7	25	-	150	0.013	70	0.48	1.12	0.10
S250_1	7.6	74.3	28	-	300	0.013	72	0.48	0.71	0.10
S31_2	8.4	73.5	33	33	150	0.013	64	0.39	0.09	0.10
S31_3	8.4	72.1	33	33	200	0.013	70	0.71	0.91	0.10
S31_1	8.4	72.8	35	35	350	0.013	70	1.42	1.04	0.10
S32_2	8.9	74.6	30	30	200	0.013	69	0.72	0.84	0.10
S32_1	8.9	73.4	32	27	400	0.013	70	1.32	1.48	0.10
S33_3	9.1	68.4	42	42	150	0.013	70	0.77	0.75	0.10
S33_1	9.1	69.1	43	42	200	0.013	69	0.74	0.29	0.16
S33_2	9.1	67.7	42	43	340	0.013	64	0.91	1.02	0.10
S35_1	9.7	73.4	32	-	150	0.013	61	0.54	0.64	0.10
S35_2	9.7	74.6	35	30	300	0.013	69	0.69	0.76	0.10
S36_1	10.0	74.8	29	29	200	0.013	68	0.56	1.25	0.10
S36_2	10.0	75.4	28	29	300	0.013	70	0.77	1.24	0.10
S38_3	10.4	76.7	24	25	150	0.013	122	0.42	1.29	0.10
S38_1	10.4	77.8	23	25	200	0.013	53	0.61	1.02	0.16
S38_2	10.4	77.4	24	25	300	0.013	70	0.73	1.19	0.16
S40_R[1]	12.8	73.6	31	32	200	0.030	98	1.05	1.18	0.20
S40_1	12.8	72.6	32	32	250	0.013	72	0.67	0.39	0.10
S40_2	12.8	72.2	31	-	350	0.013	72	1.10	1.36	0.10
S42_3	14.2	72.1	34	35	150	0.013	69	0.68	1.25	0.10
S42_1	14.2	72.1	34	34	200	0.013	69	1.20	1.30	0.16
S42_2	14.2	72.4	35	31	300	0.013	94	1.27	1.25	0.16
S44	14.9	70.0	32	36	134	0.008	51	0.61	1.13	0.20
S46_R[1]	16.2	74.3	28	31	134	0.041	71	0.76	1.12	0.20
S46_1	16.2	73.0	31	31	134	0.008	91	0.67	1.16	0.20
S46_2	16.2	71.1	32	37	200	0.013	90	0.63	1.76	0.20

[1] tests on remoulded specimens

all specimens: diameter ø=50 mm; initial height H_0=19 mm

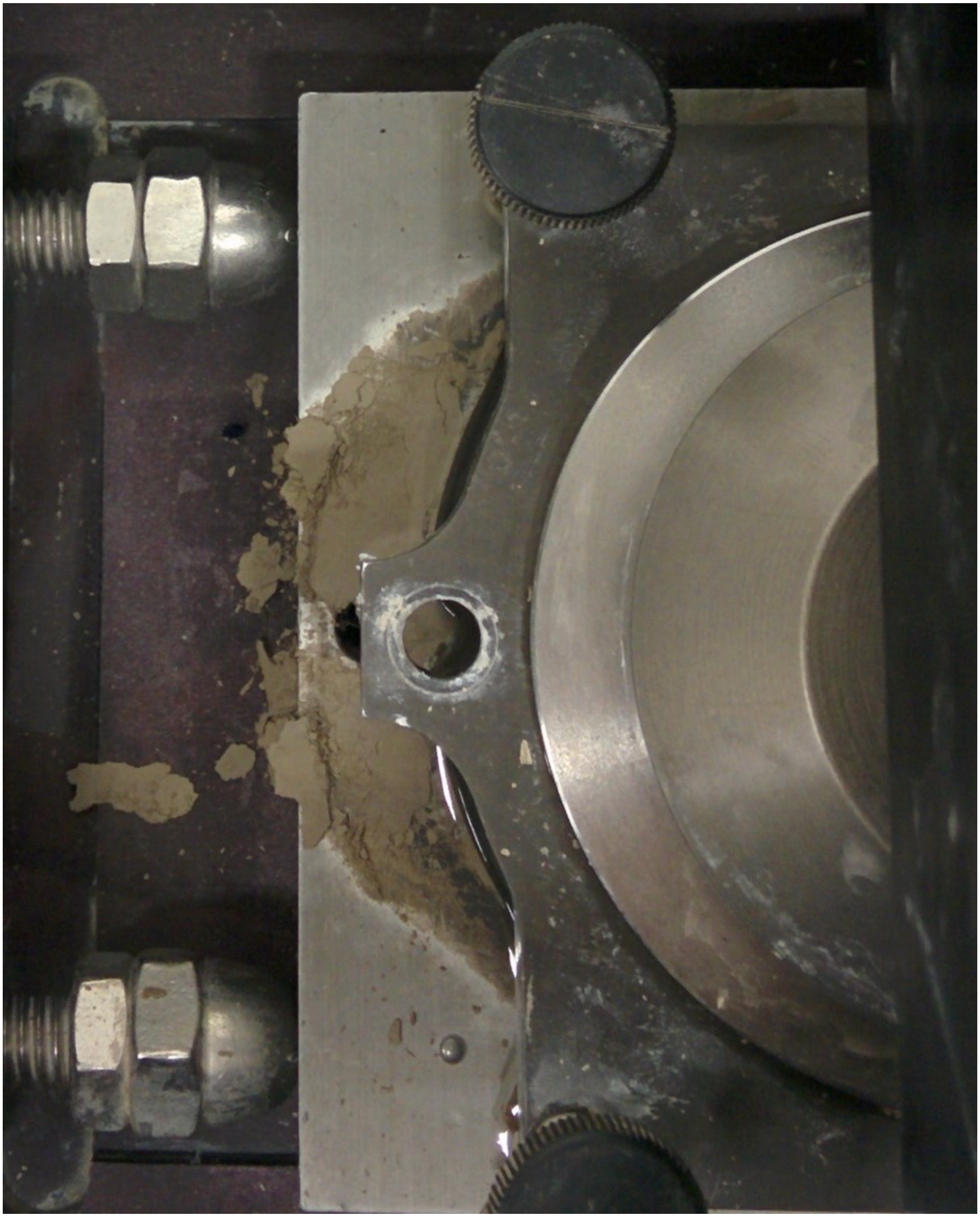

Figure F.1. Soil extrusion at gap between shear box halves in Test S42_2

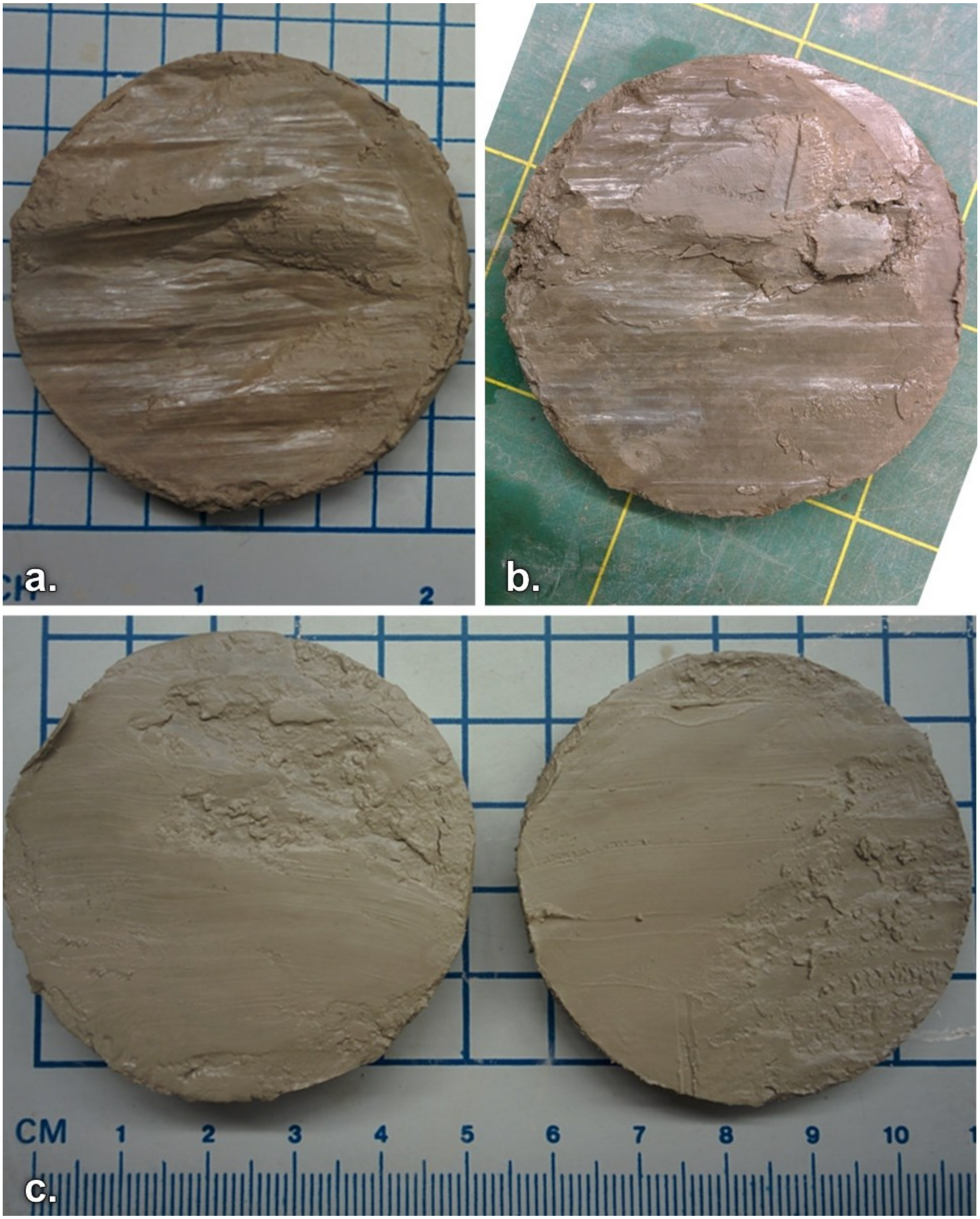
a.
1
2
b.
CM
1
2
3
4
5
6
7
8
9
10
c.

Figure F.2. Shear surfaces: (a) S31_3; (b) S33_1; (c) S40_1

Plots. Direct shear test stress-strain results

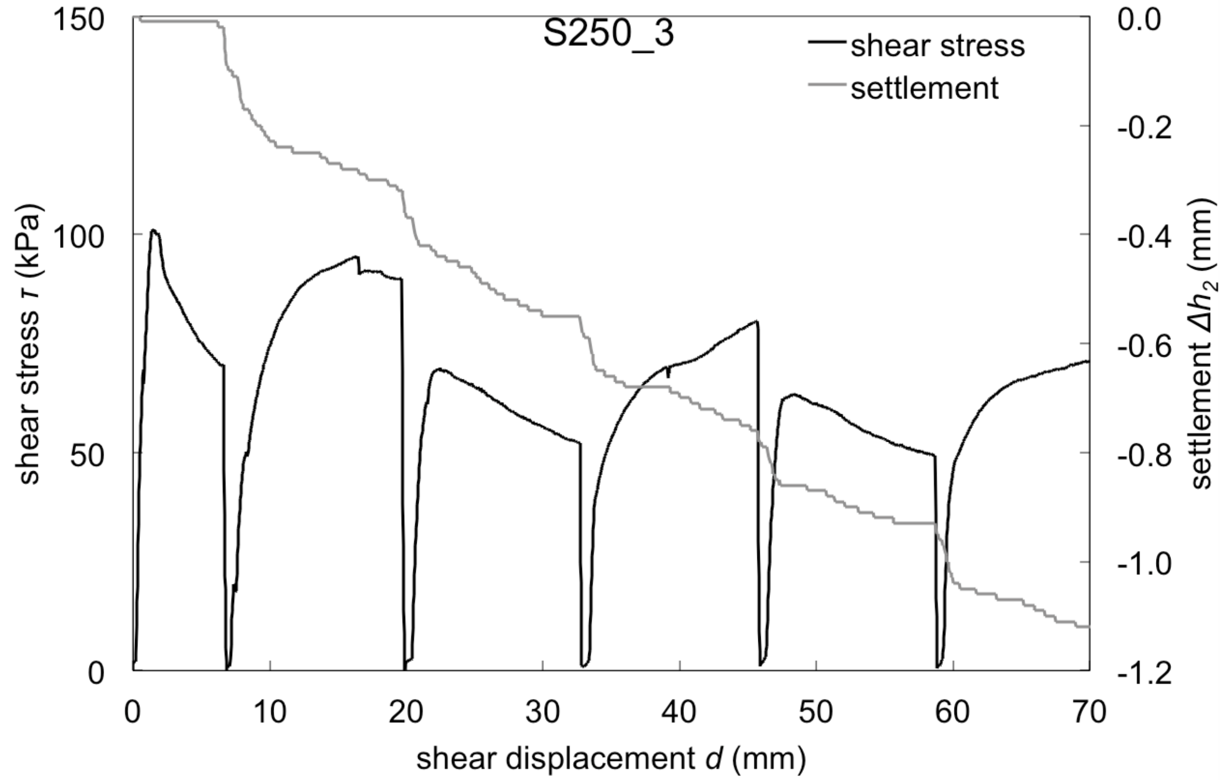

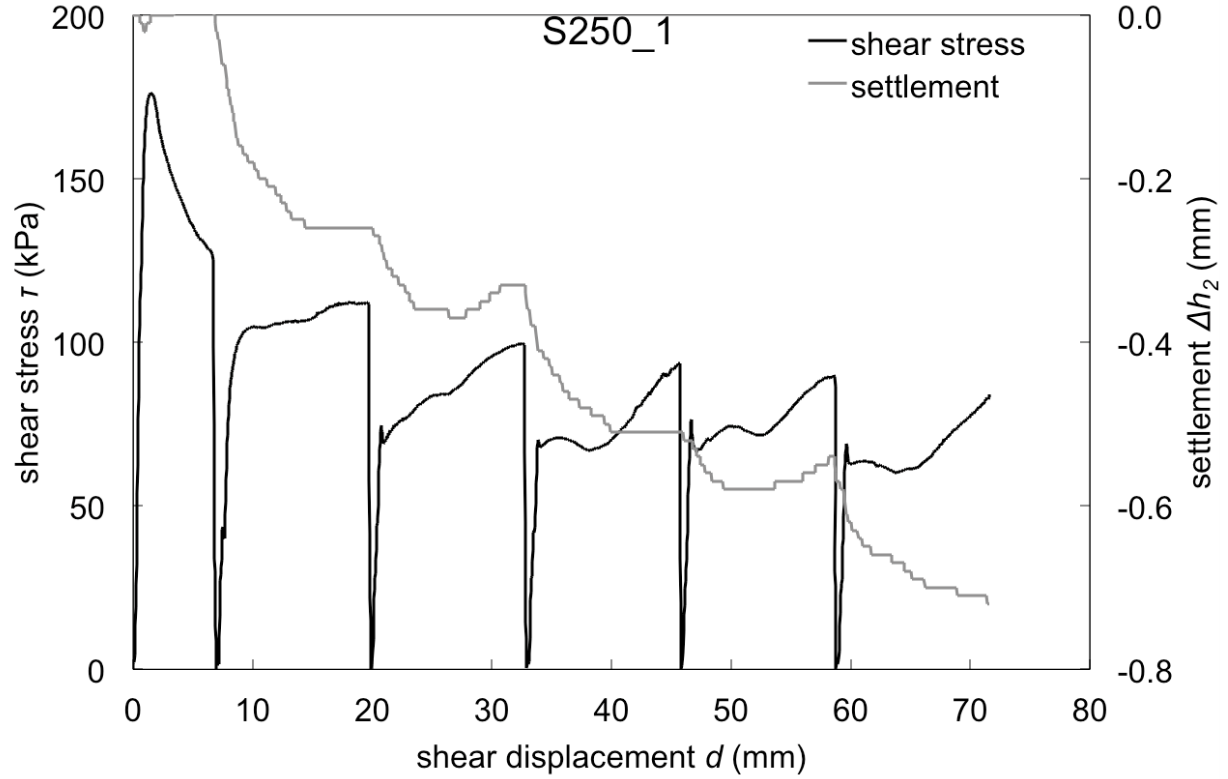

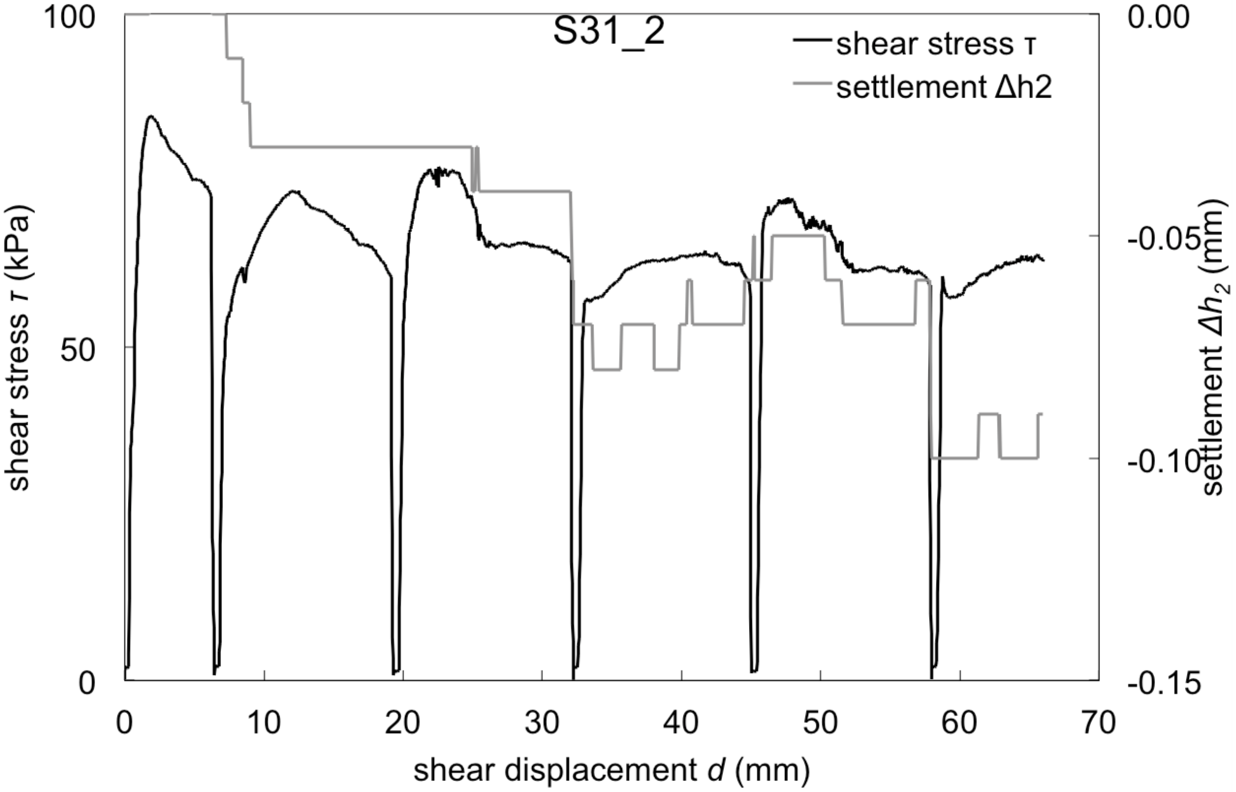
S31_2
shear stress τ
settlement Δh2
shear stress τ (kPa)
settlement Δh₂ (mm)
shear displacement d (mm)
100
50
0
0.00
-0.05
-0.10
-0.15
0
10
20
30
40
50
60
70

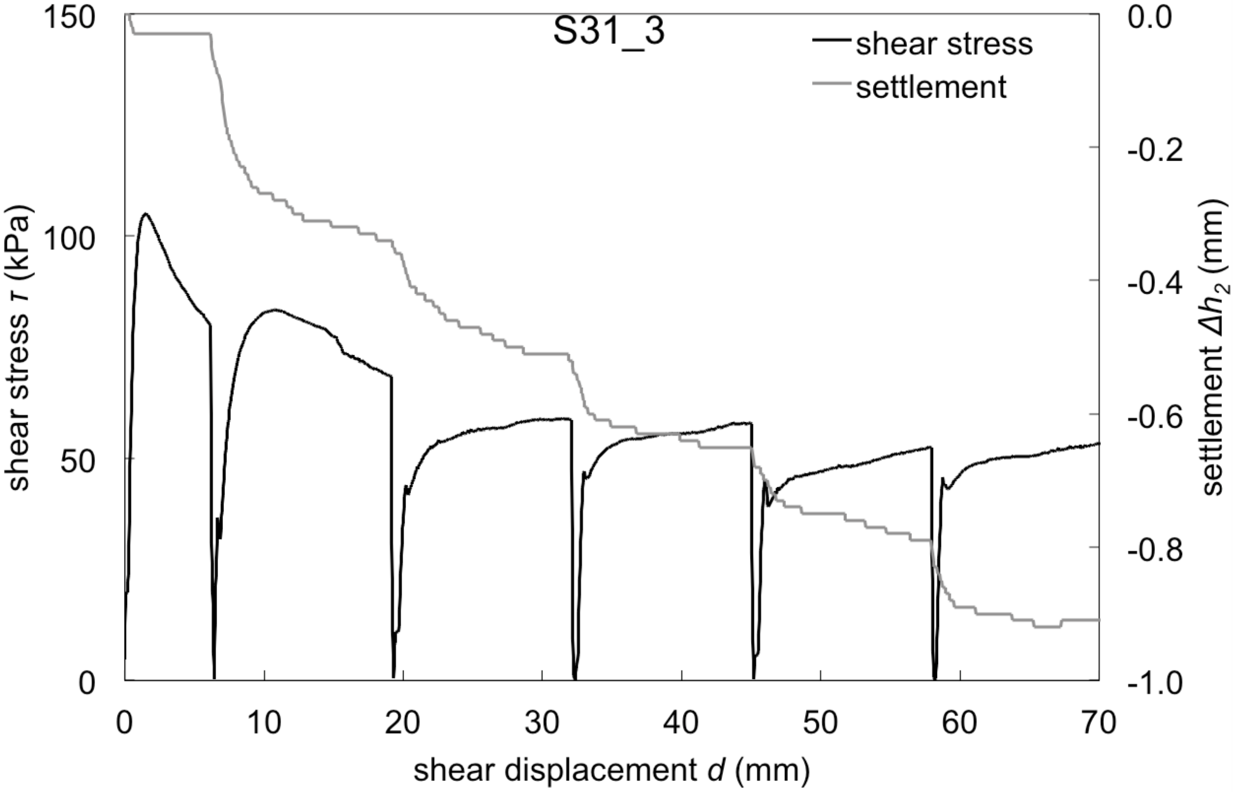
S31_3
shear stress
settlement
shear stress τ (kPa)
settlement Δh₂ (mm)
shear displacement d (mm)
150
100
50
0
0.0
-0.2
-0.4
-0.6
-0.8
-1.0
0
10
20
30
40
50
60
70

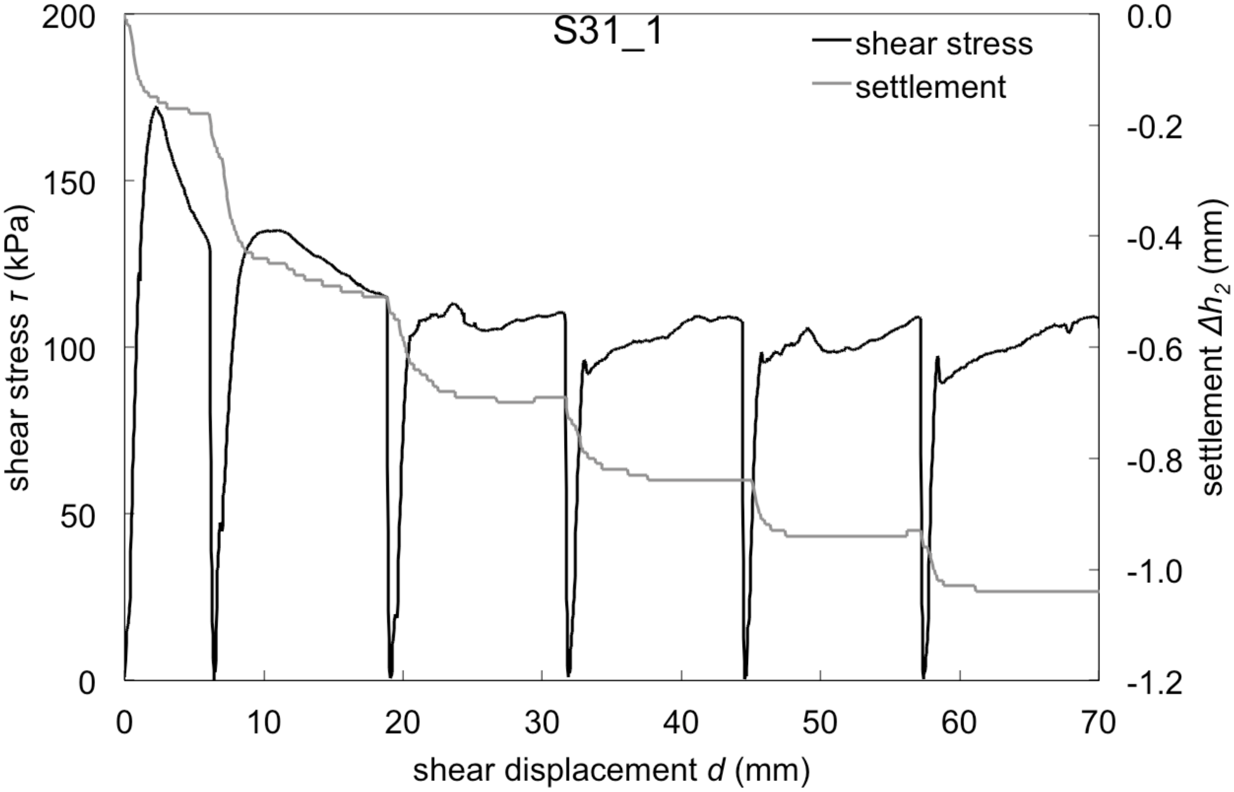
S31_1
shear stress
settlement
shear stress τ (kPa)
settlement Δh₂ (mm)
shear displacement d (mm)
200
150
100
50
0
0.0
-0.2
-0.4
-0.6
-0.8
-1.0
-1.2
0
10
20
30
40
50
60
70

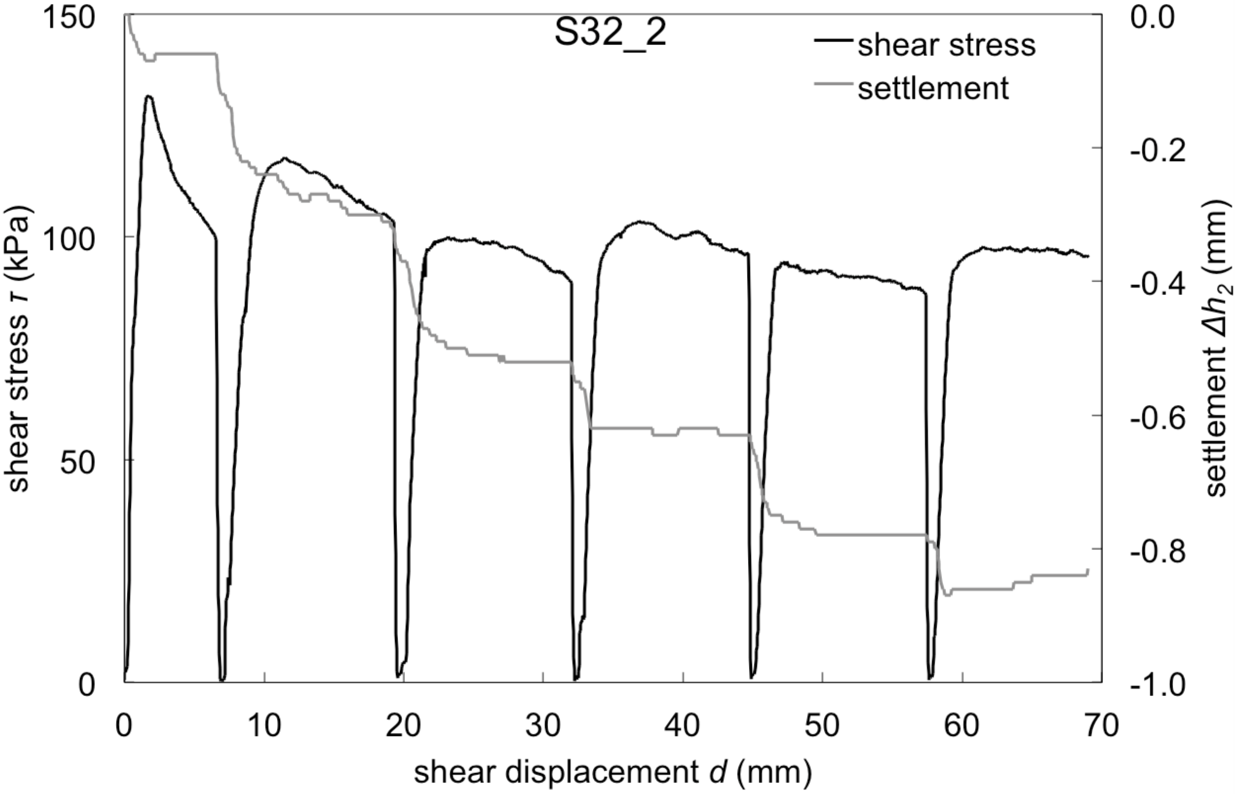
S32_2
shear stress
settlement
shear stress τ (kPa)
settlement Δh₂ (mm)
shear displacement d (mm)
150
100
50
0
0.0
-0.2
-0.4
-0.6
-0.8
-1.0
0
10
20
30
40
50
60
70

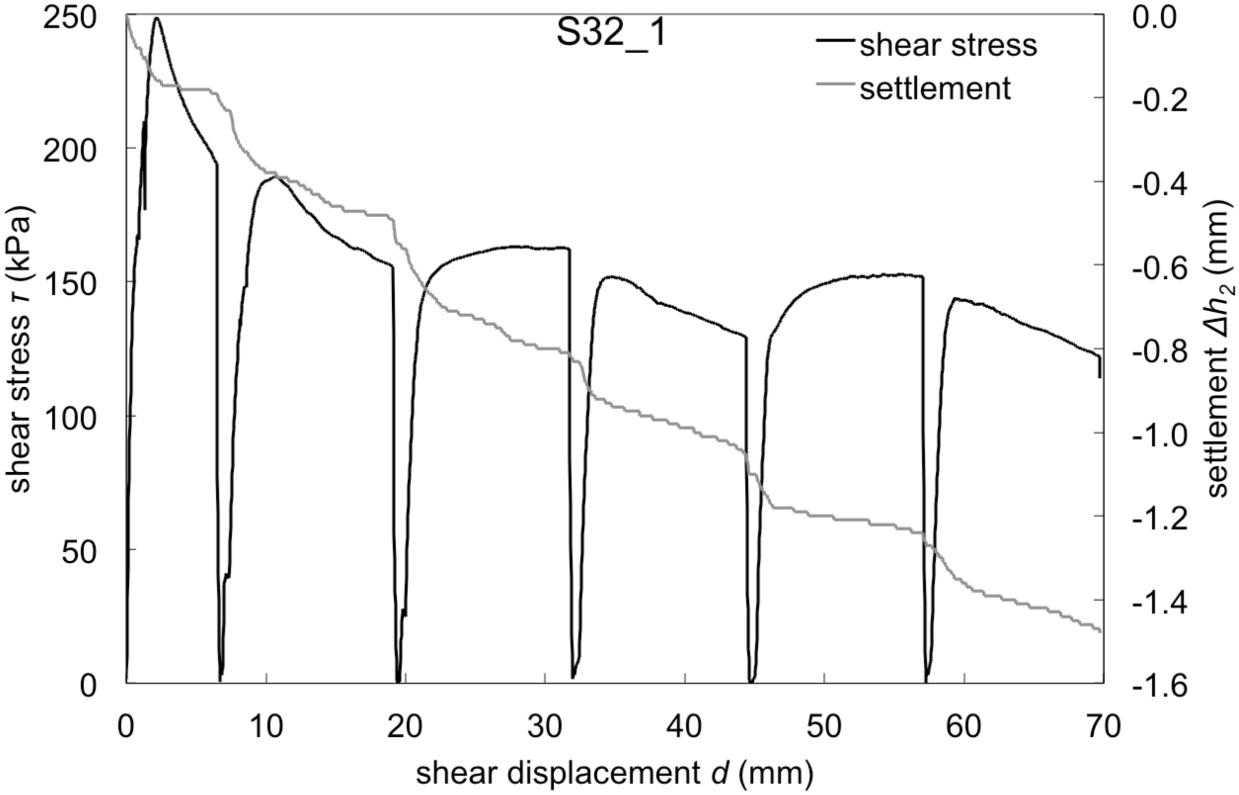
S32_1
shear stress
settlement
shear stress τ (kPa)
settlement Δh_2 (mm)
shear displacement *d* (mm)
0
50
100
150
200
250
0.0
-0.2
-0.4
-0.6
-0.8
-1.0
-1.2
-1.4
-1.6
0
10
20
30
40
50
60
70

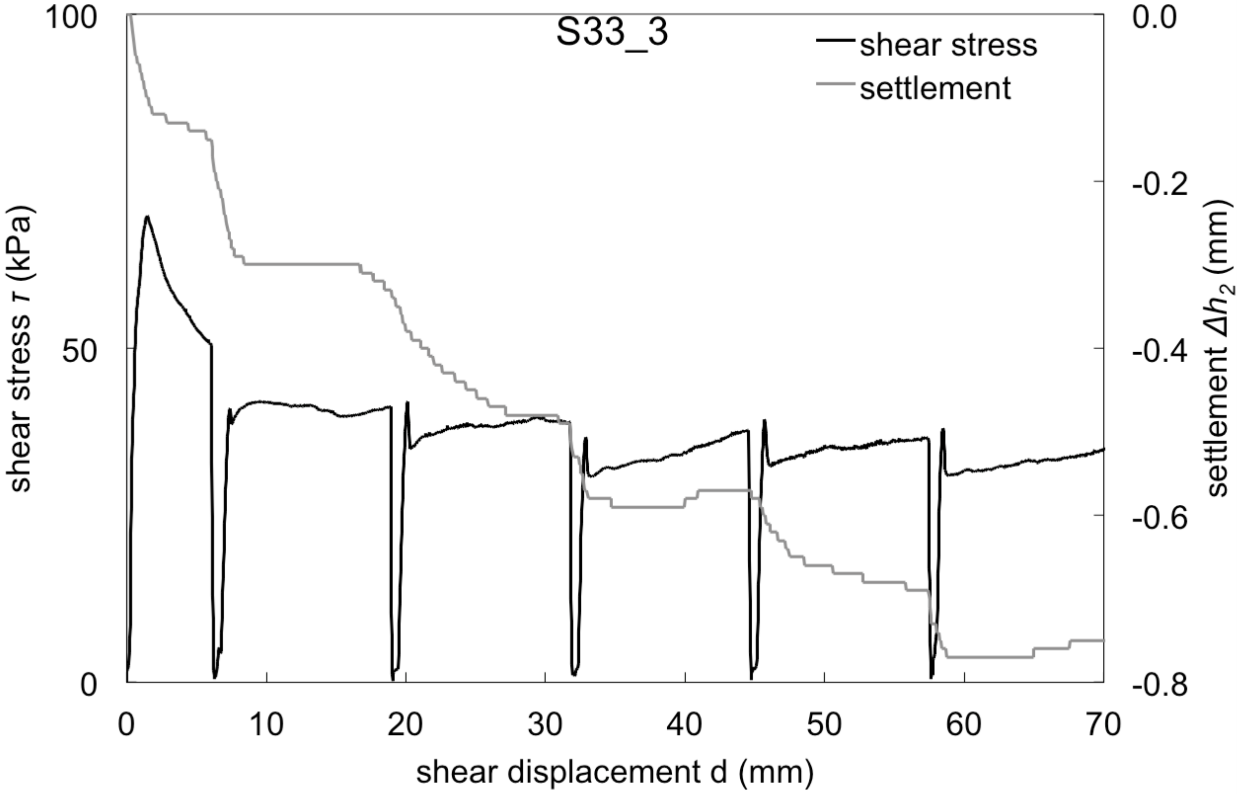
S33_3
shear stress
settlement
shear stress τ (kPa)
settlement Δh_2 (mm)
shear displacement d (mm)
0
50
100
0.0
-0.2
-0.4
-0.6
-0.8
0
10
20
30
40
50
60
70

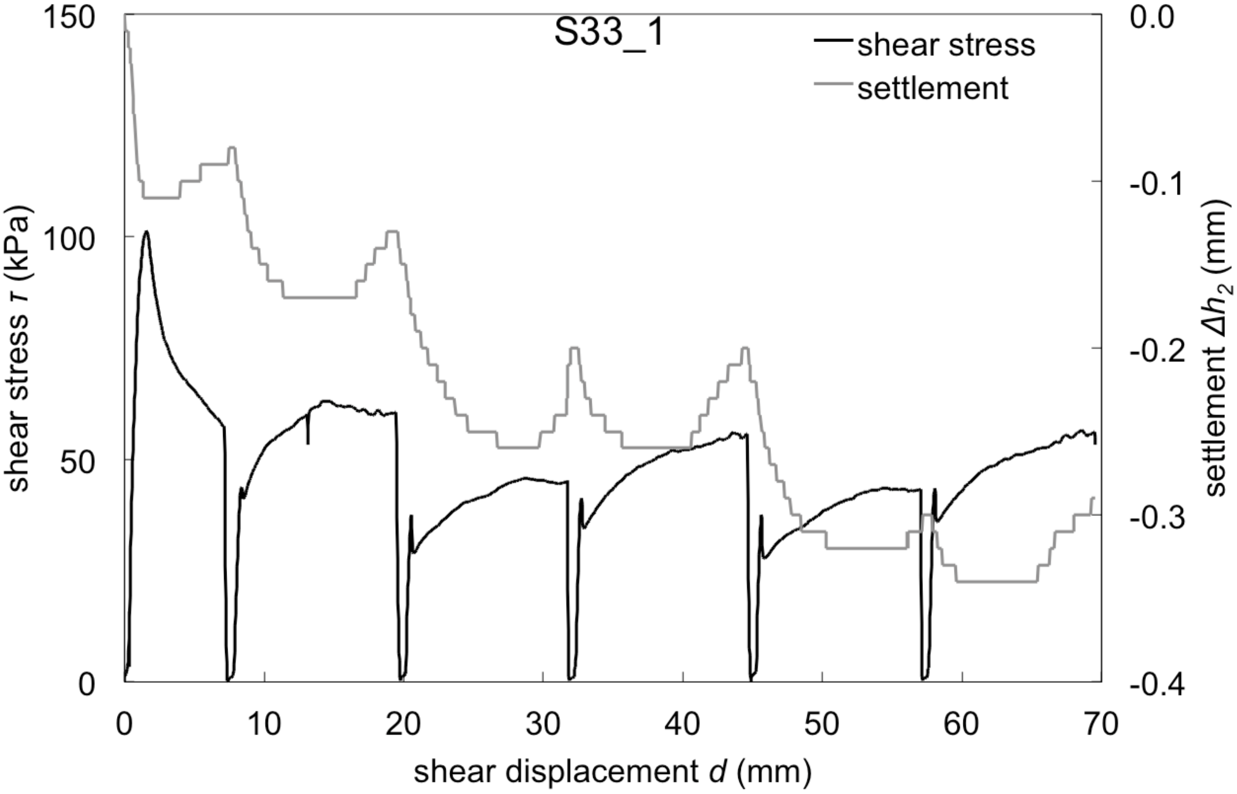
S33_1
shear stress
settlement
shear stress τ (kPa)
settlement Δh₂ (mm)
shear displacement d (mm)
150
100
50
0
0.0
-0.1
-0.2
-0.3
-0.4
0
10
20
30
40
50
60
70

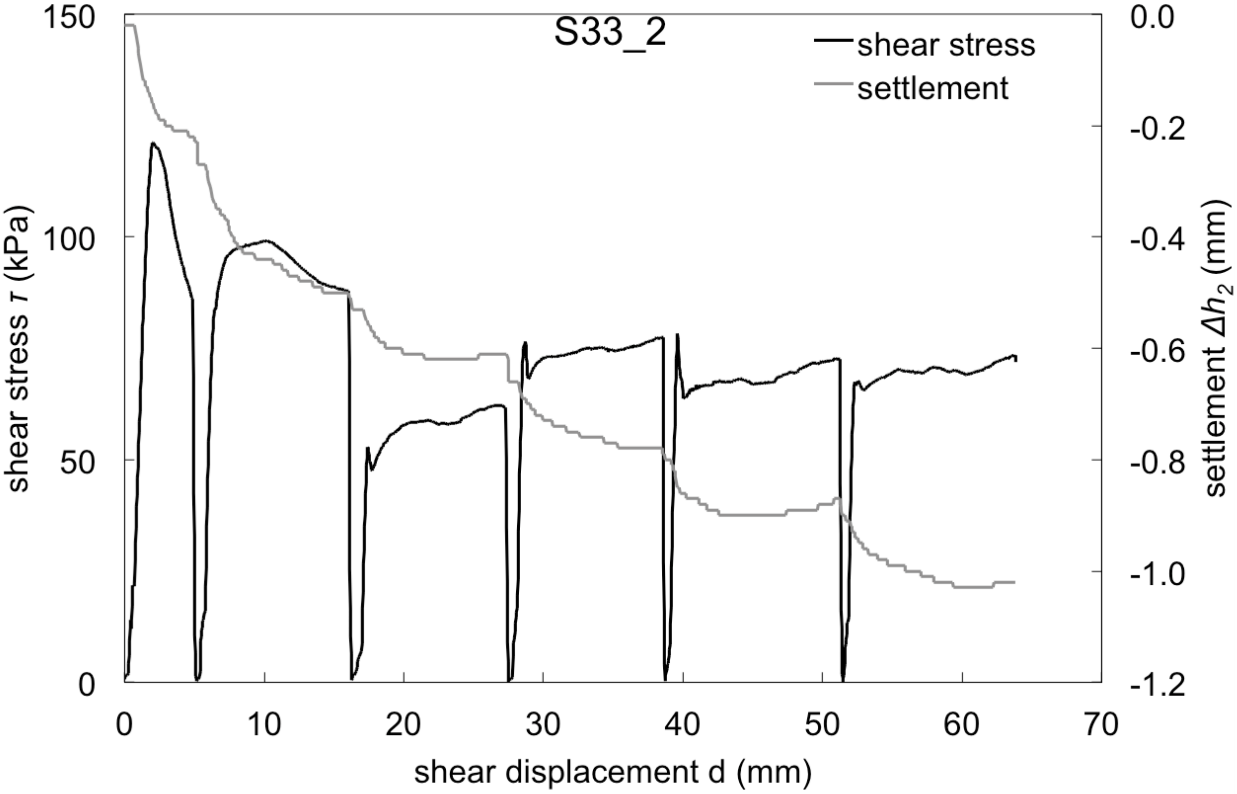
S33_2
shear stress
settlement
shear stress τ (kPa)
settlement Δh₂ (mm)
shear displacement d (mm)
150
100
50
0
0.0
-0.2
-0.4
-0.6
-0.8
-1.0
-1.2
0
10
20
30
40
50
60
70

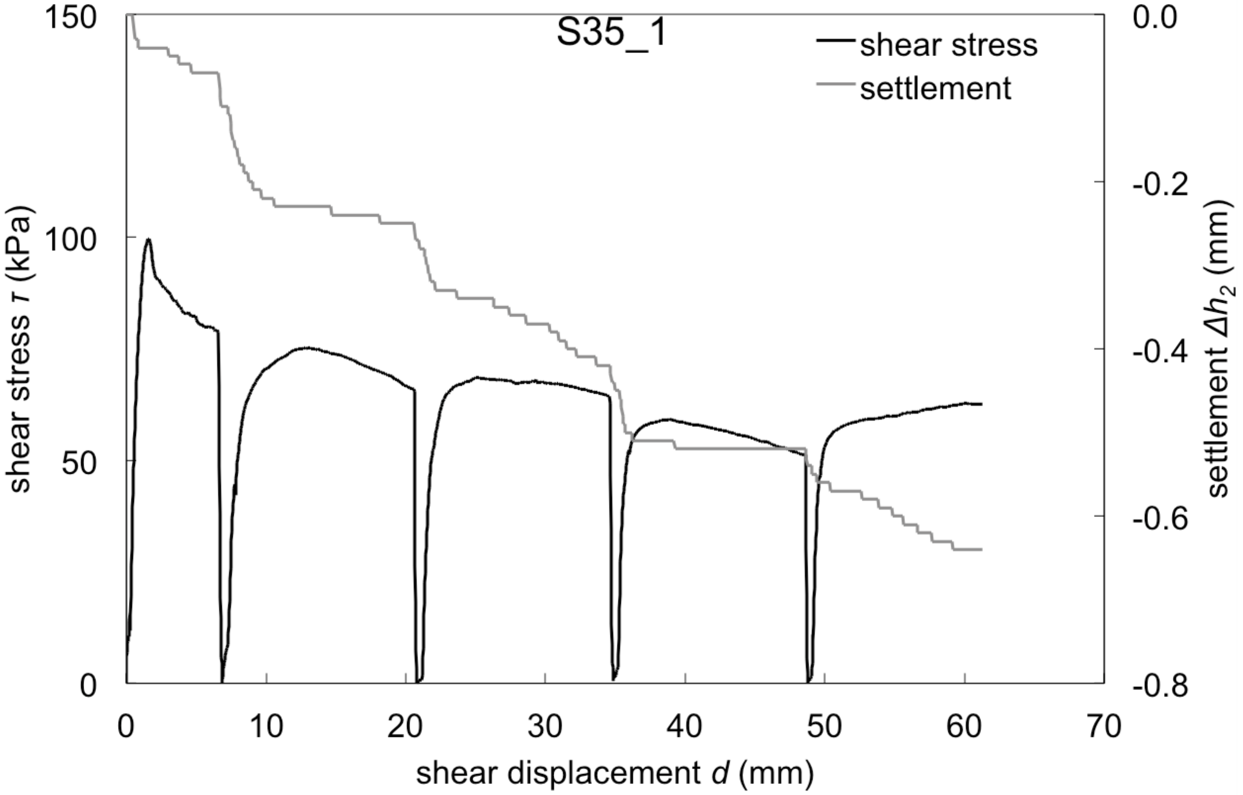

S35_1
shear stress
settlement
150
100
50
0
0.0
-0.2
-0.4
-0.6
-0.8
0
10
20
30
40
50
60
70
shear stress τ (kPa)
settlement Δh_2 (mm)
shear displacement d (mm)

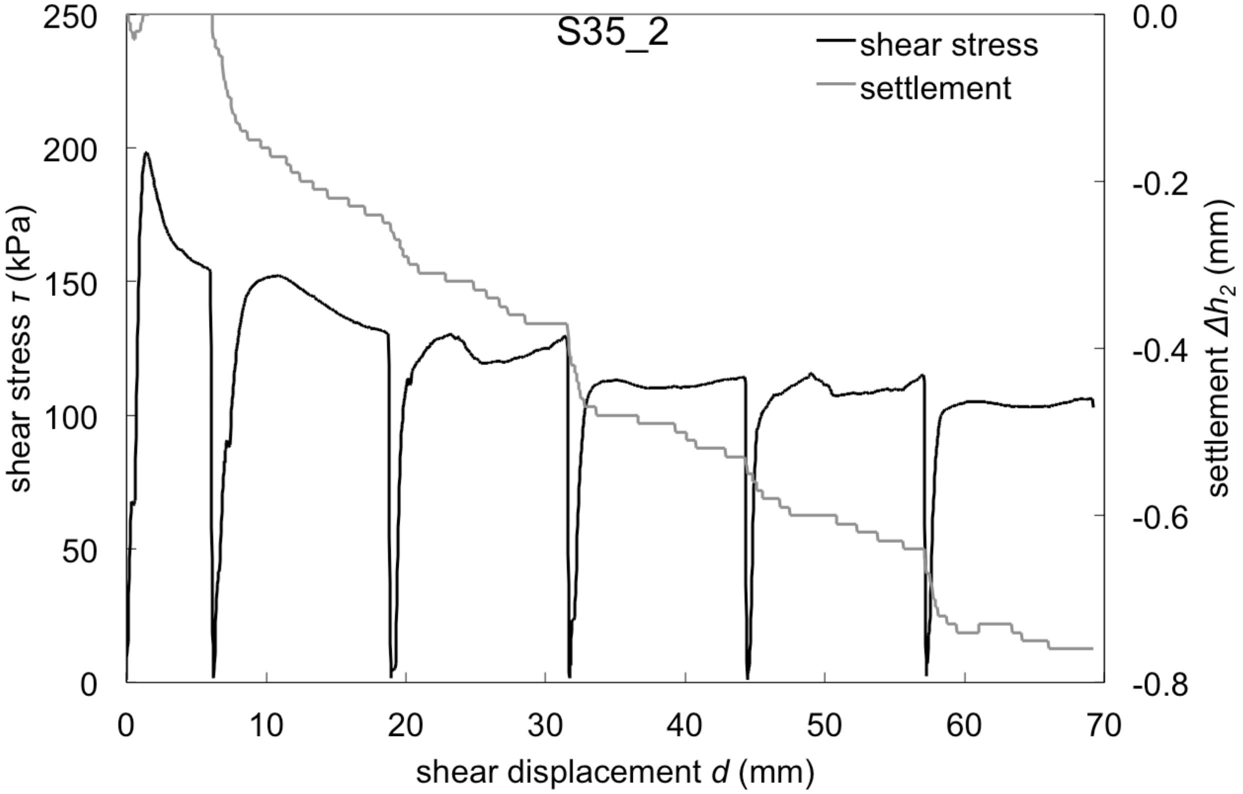

S35_2
shear stress
settlement
250
200
150
100
50
0
0.0
-0.2
-0.4
-0.6
-0.8
0
10
20
30
40
50
60
70
shear stress τ (kPa)
settlement Δh_2 (mm)
shear displacement d (mm)

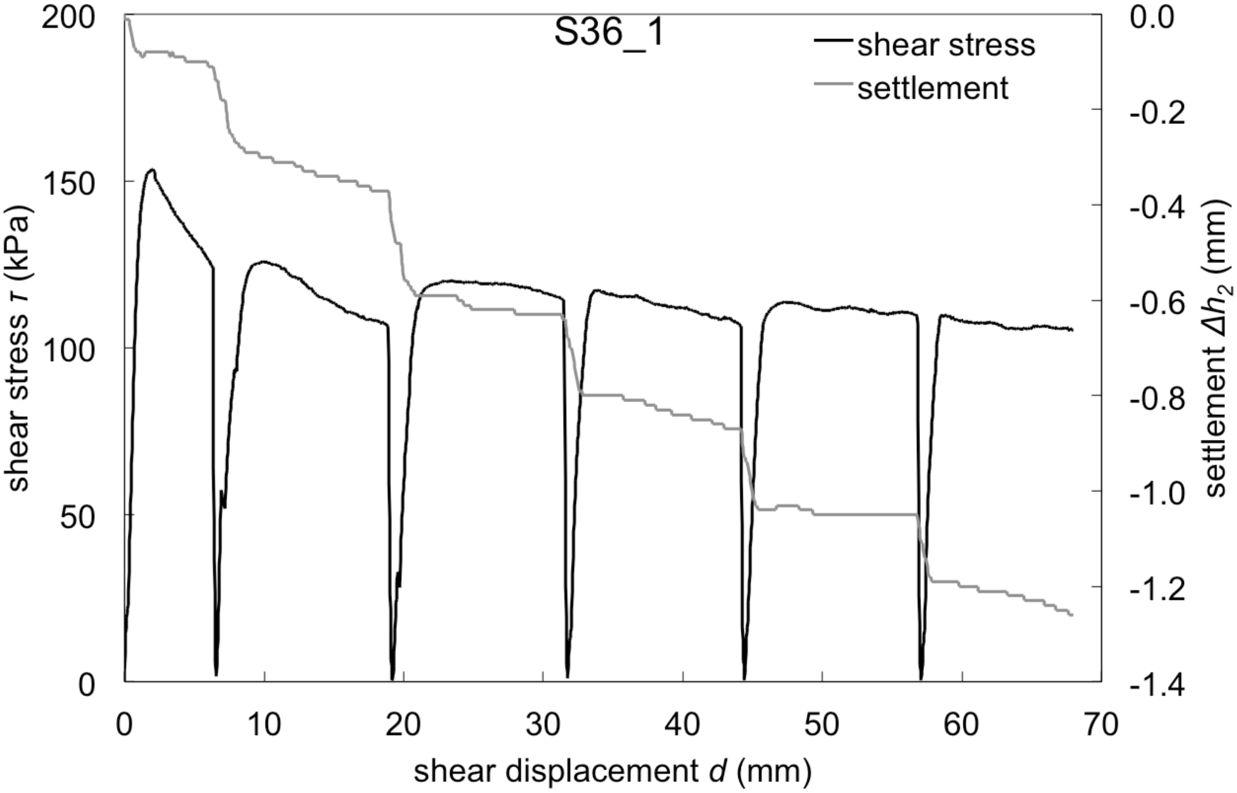
S36_1
shear stress
settlement
shear stress τ (kPa)
200
150
100
50
0
settlement Δh2 (mm)
0.0
-0.2
-0.4
-0.6
-0.8
-1.0
-1.2
-1.4
0
10
20
30
40
50
60
70
shear displacement d (mm)

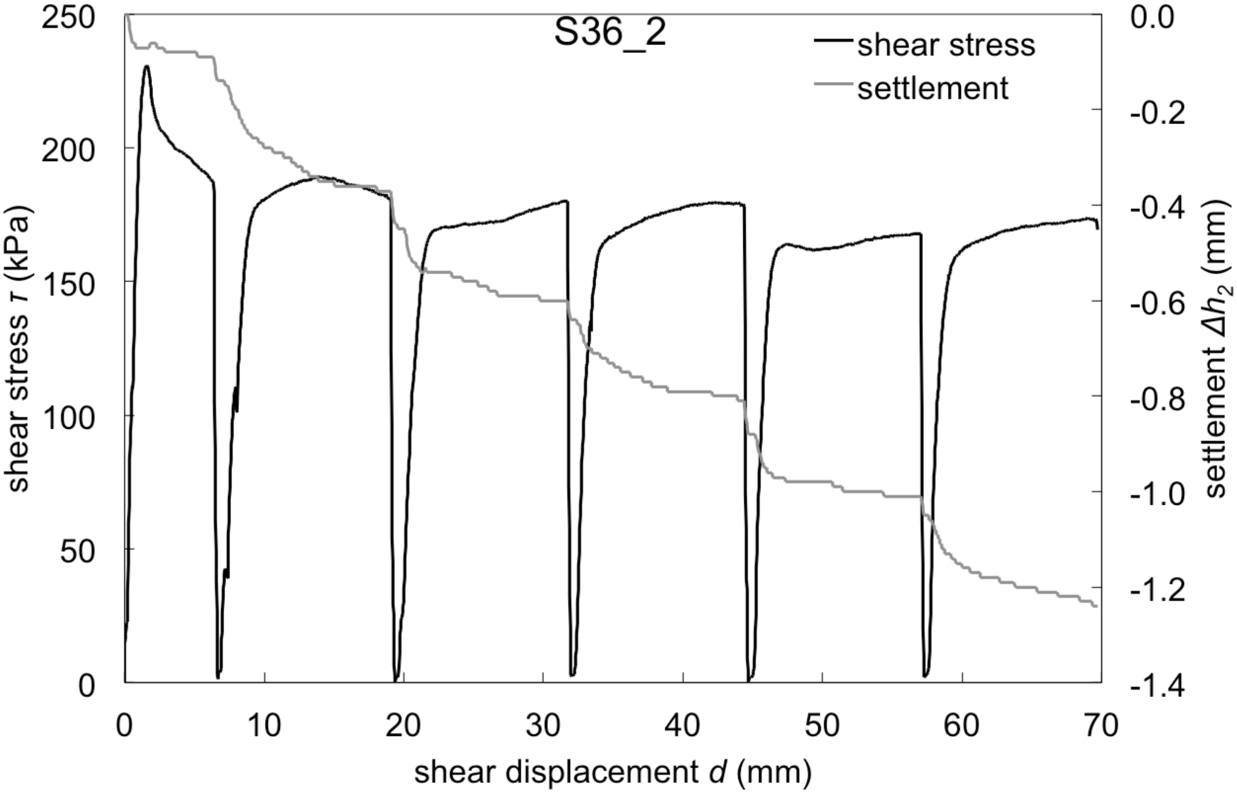
S36_2
shear stress
settlement
shear stress τ (kPa)
250
200
150
100
50
0
settlement Δh2 (mm)
0.0
-0.2
-0.4
-0.6
-0.8
-1.0
-1.2
-1.4
0
10
20
30
40
50
60
70
shear displacement d (mm)

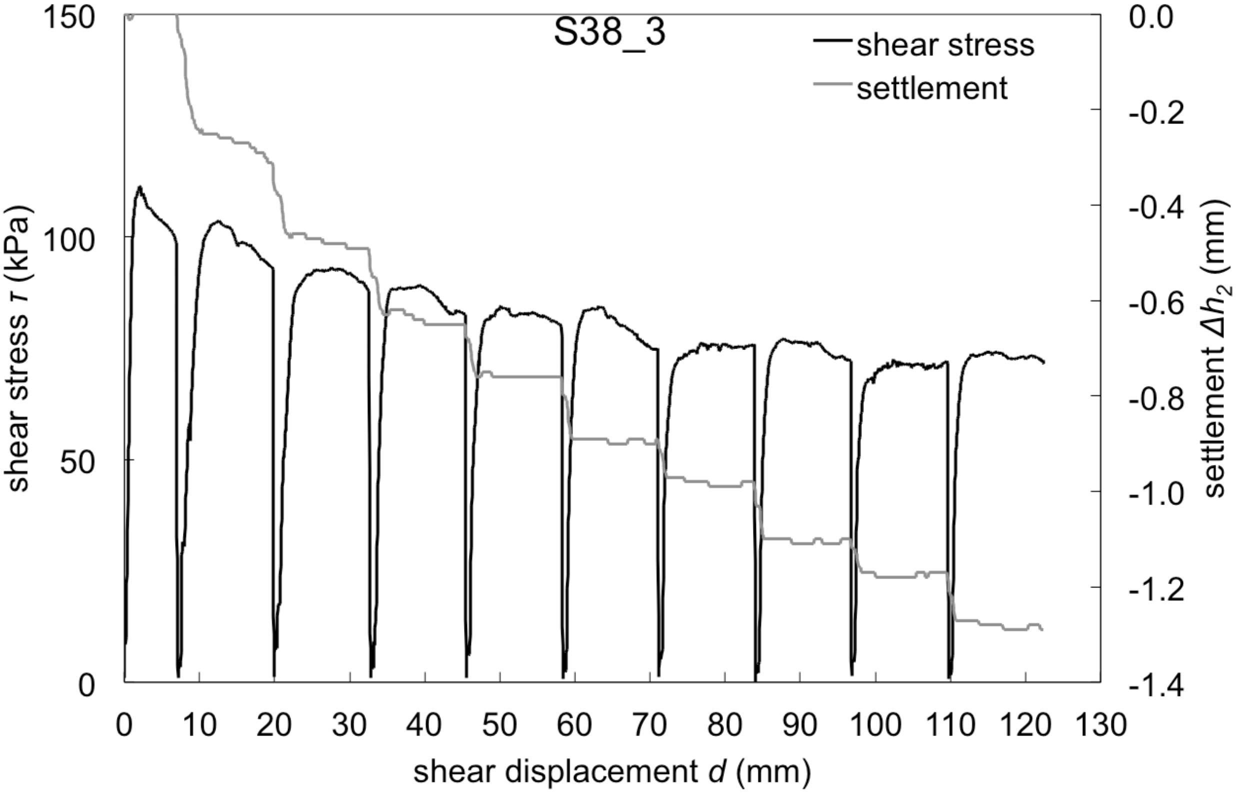
S38_3
shear stress
settlement
shear stress τ (kPa)
150
100
50
0
settlement Δh2 (mm)
0.0
-0.2
-0.4
-0.6
-0.8
-1.0
-1.2
-1.4
0
10
20
30
40
50
60
70
80
90
100
110
120
130
shear displacement d (mm)

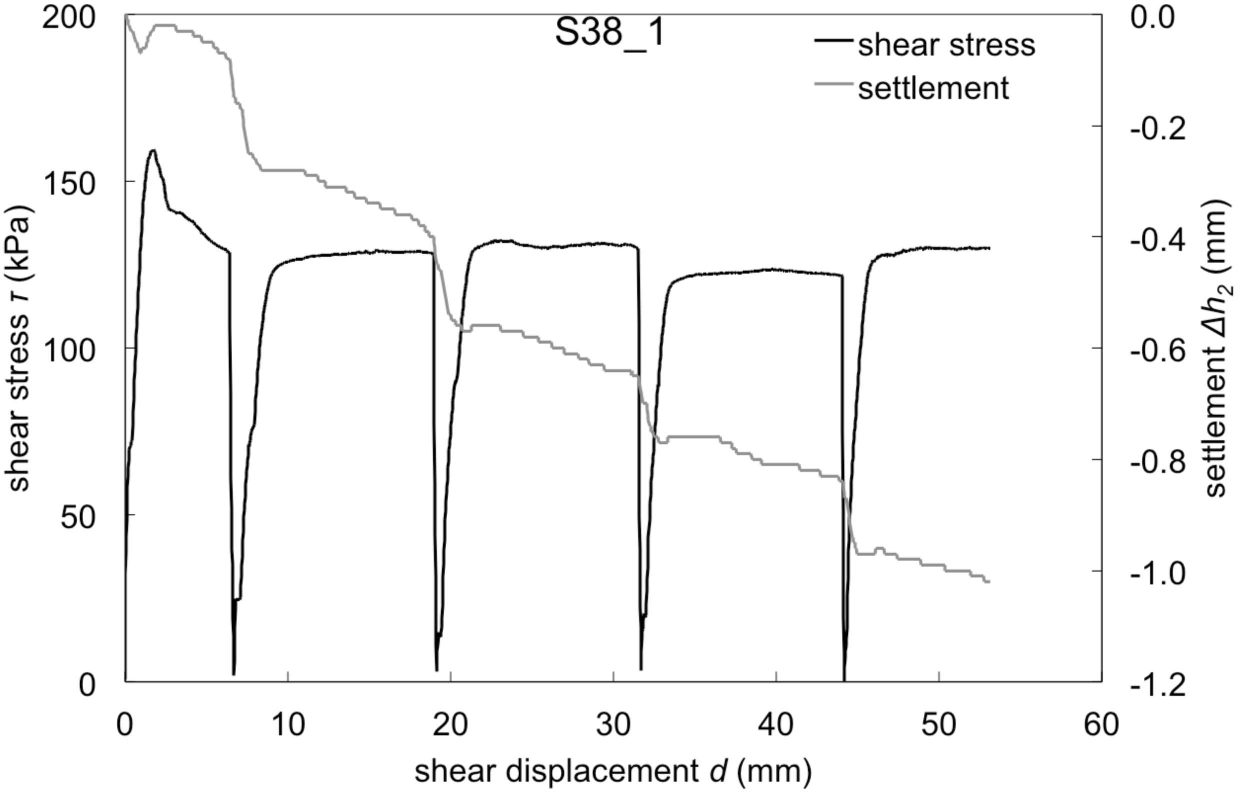
S38_1
shear stress
settlement
shear stress τ (kPa)
200
150
100
50
0
settlement Δh2 (mm)
0.0
-0.2
-0.4
-0.6
-0.8
-1.0
-1.2
0
10
20
30
40
50
60
shear displacement d (mm)

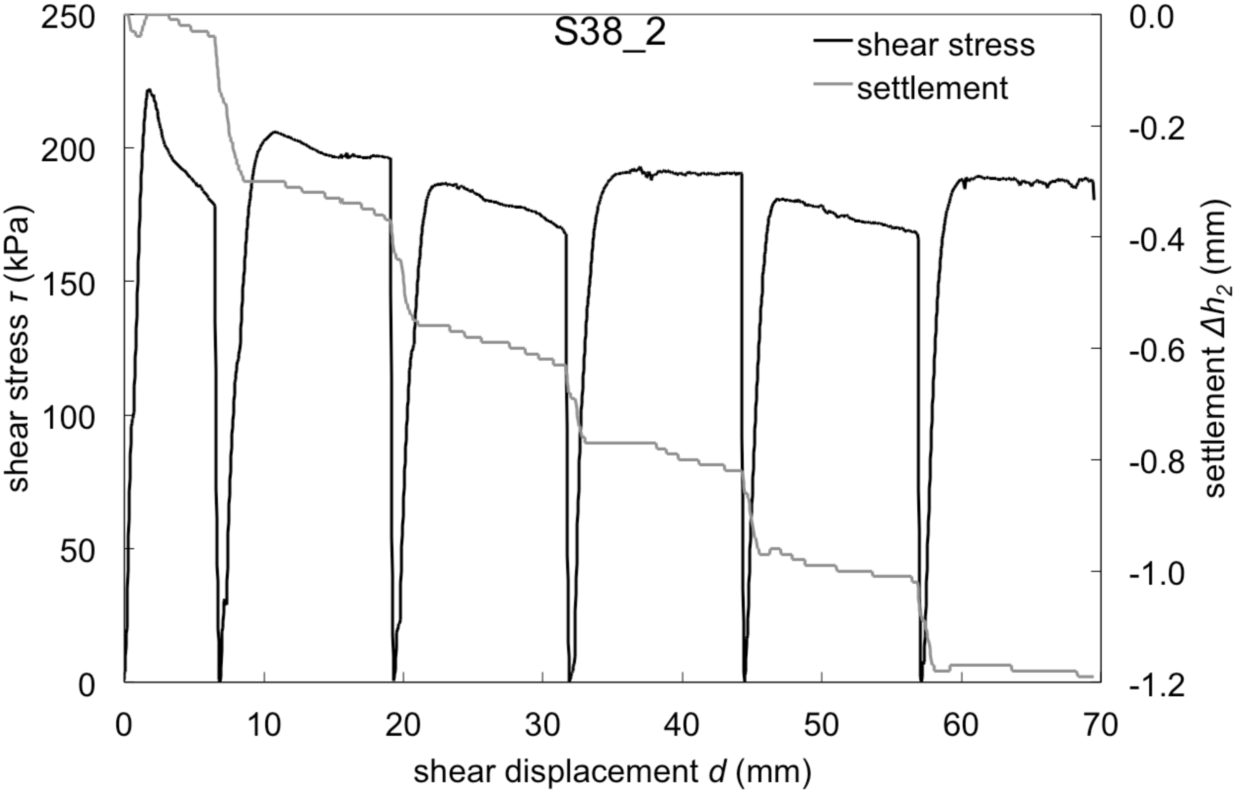
S38_2
shear stress
settlement
shear stress τ (kPa)
settlement Δh2 (mm)
shear displacement d (mm)
250
200
150
100
50
0
0.0
-0.2
-0.4
-0.6
-0.8
-1.0
-1.2
0
10
20
30
40
50
60
70

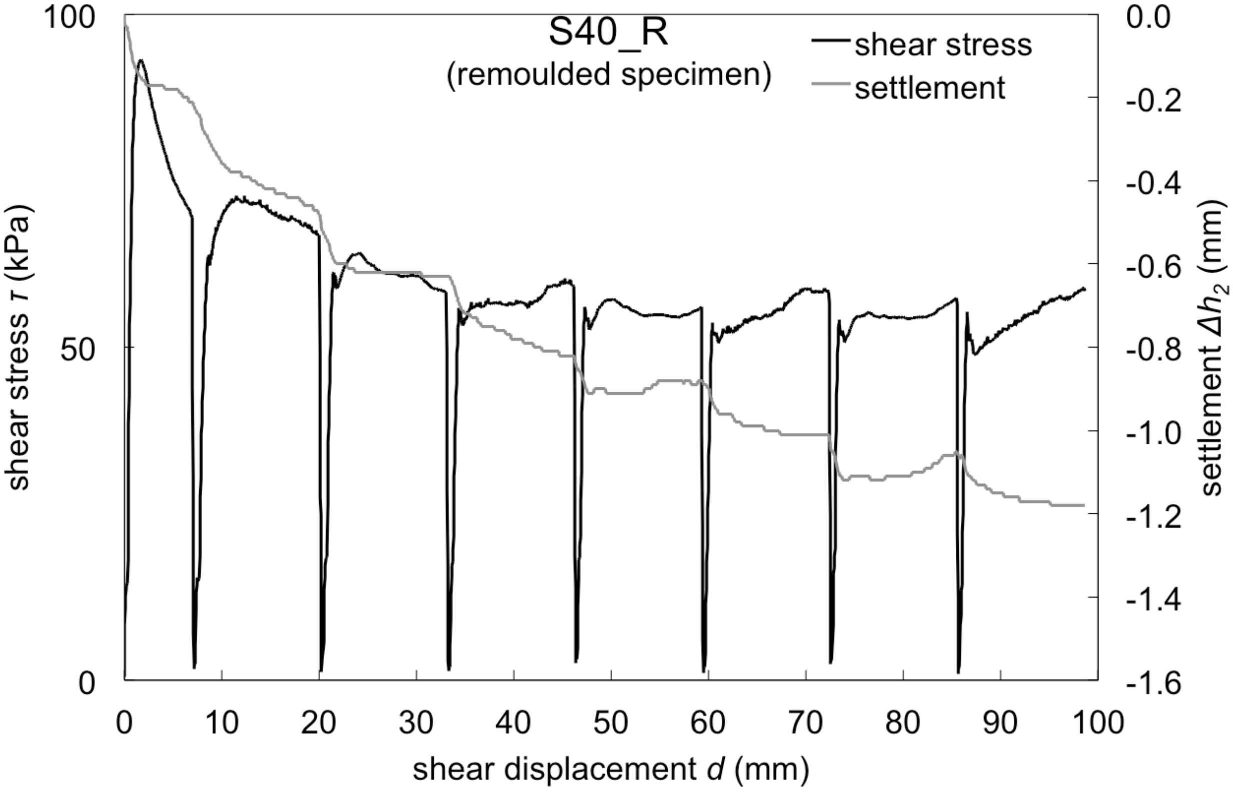
S40_R
(remoulded specimen)
shear stress
settlement
shear stress τ (kPa)
settlement Δh2 (mm)
shear displacement d (mm)
100
50
0
0.0
-0.2
-0.4
-0.6
-0.8
-1.0
-1.2
-1.4
-1.6
0
10
20
30
40
50
60
70
80
90
100

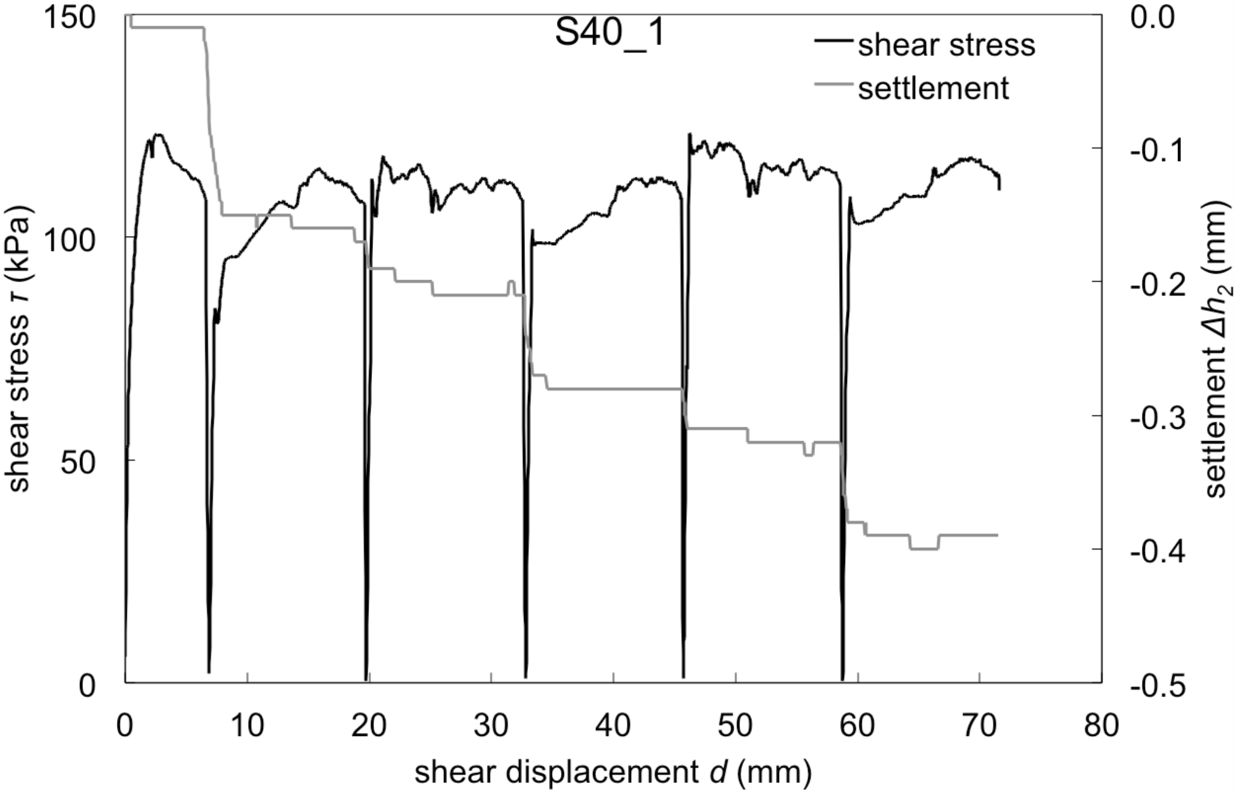
S40_1
shear stress
settlement
shear stress τ (kPa)
settlement Δh2 (mm)
shear displacement d (mm)
150
100
50
0
0.0
-0.1
-0.2
-0.3
-0.4
-0.5
0
10
20
30
40
50
60
70
80

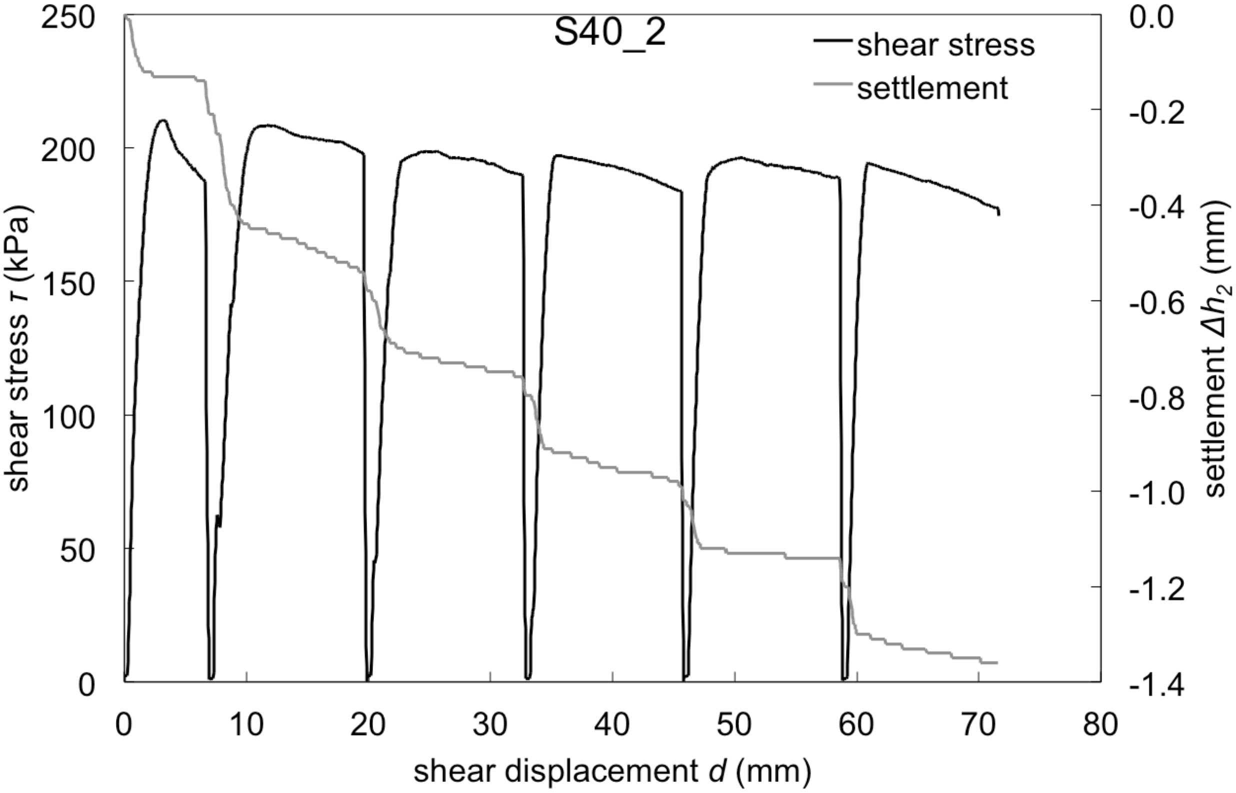
S40_2
shear stress
settlement
shear stress τ (kPa)
settlement Δh2 (mm)
shear displacement d (mm)
250
200
150
100
50
0
0.0
-0.2
-0.4
-0.6
-0.8
-1.0
-1.2
-1.4
0
10
20
30
40
50
60
70
80

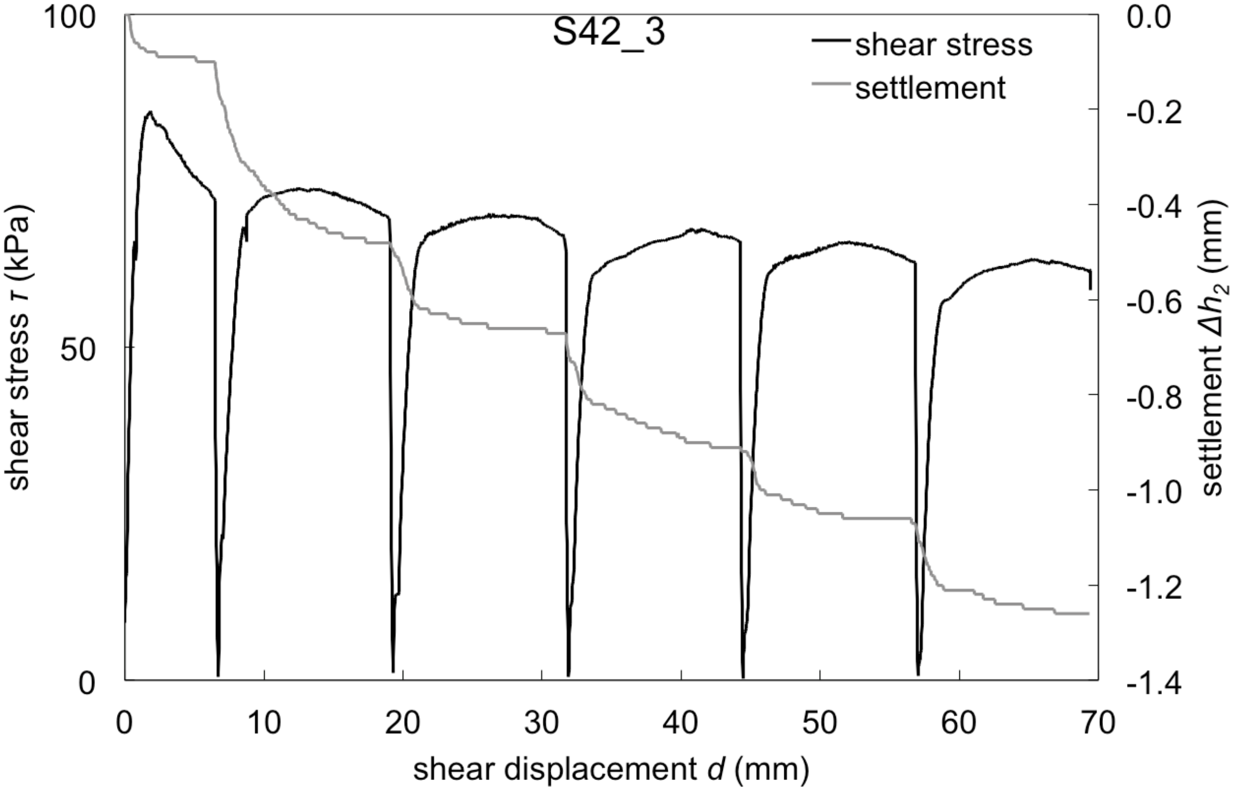
S42_3
shear stress
settlement
shear stress τ (kPa)
settlement Δh2 (mm)
shear displacement d (mm)
100
50
0
0.0
-0.2
-0.4
-0.6
-0.8
-1.0
-1.2
-1.4
0
10
20
30
40
50
60
70

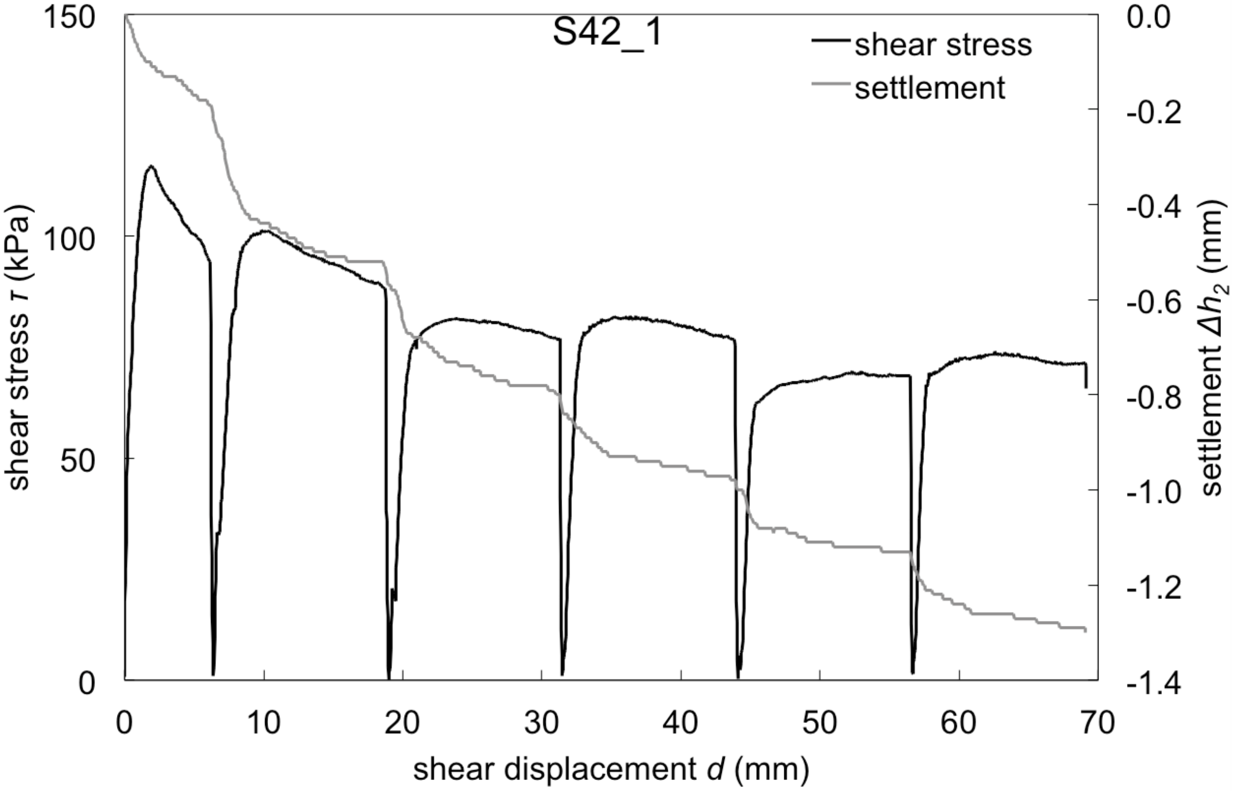
S42_1
shear stress
settlement
shear stress τ (kPa)
settlement Δh2 (mm)
shear displacement d (mm)
150
100
50
0
0.0
-0.2
-0.4
-0.6
-0.8
-1.0
-1.2
-1.4
0
10
20
30
40
50
60
70

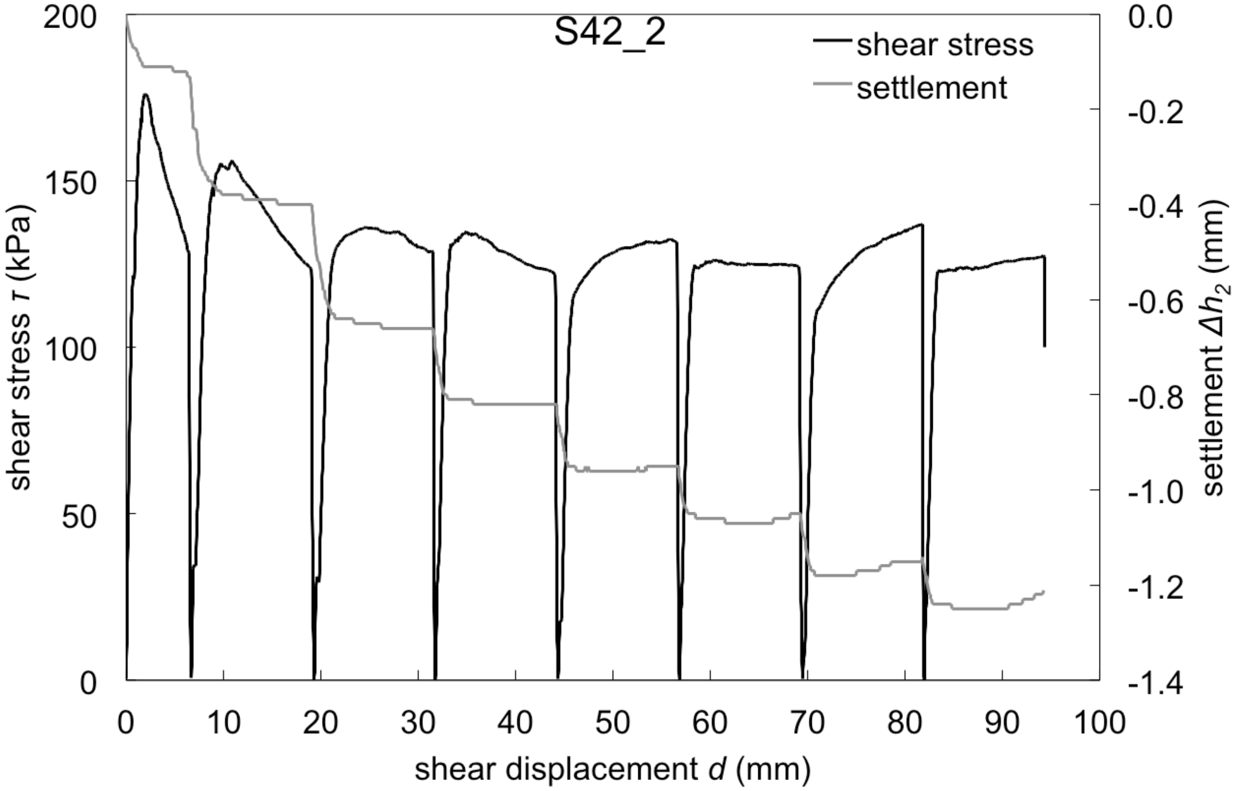
S42_2
shear stress
settlement
shear stress τ (kPa)
settlement Δh2 (mm)
shear displacement d (mm)
200
150
100
50
0
0.0
-0.2
-0.4
-0.6
-0.8
-1.0
-1.2
-1.4
0
10
20
30
40
50
60
70
80
90
100

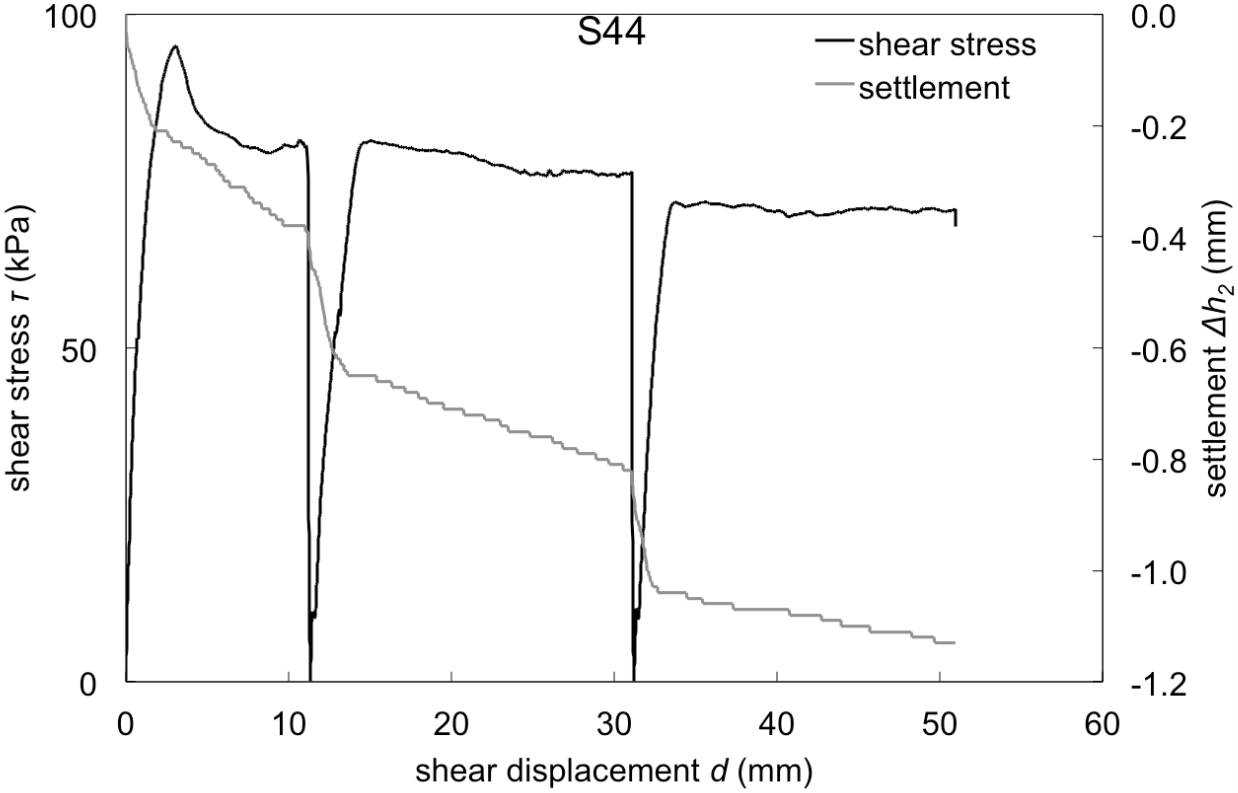
S44
shear stress
settlement
shear stress τ (kPa)
settlement Δh2 (mm)
shear displacement d (mm)
100
50
0
0.0
-0.2
-0.4
-0.6
-0.8
-1.0
-1.2
0
10
20
30
40
50
60

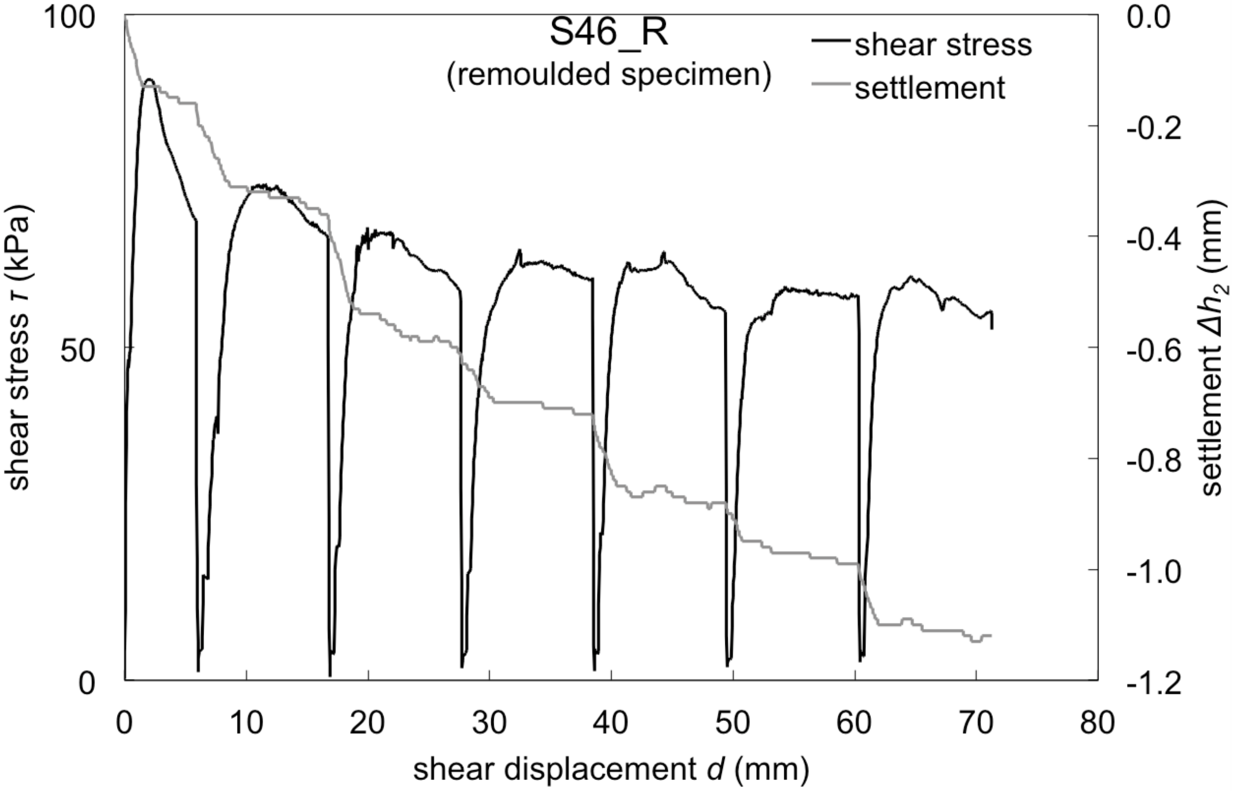
S46_R
(remoulded specimen)
shear stress
settlement
shear stress τ (kPa)
settlement Δh2 (mm)
shear displacement d (mm)
100
50
0
0.0
-0.2
-0.4
-0.6
-0.8
-1.0
-1.2
0
10
20
30
40
50
60
70
80

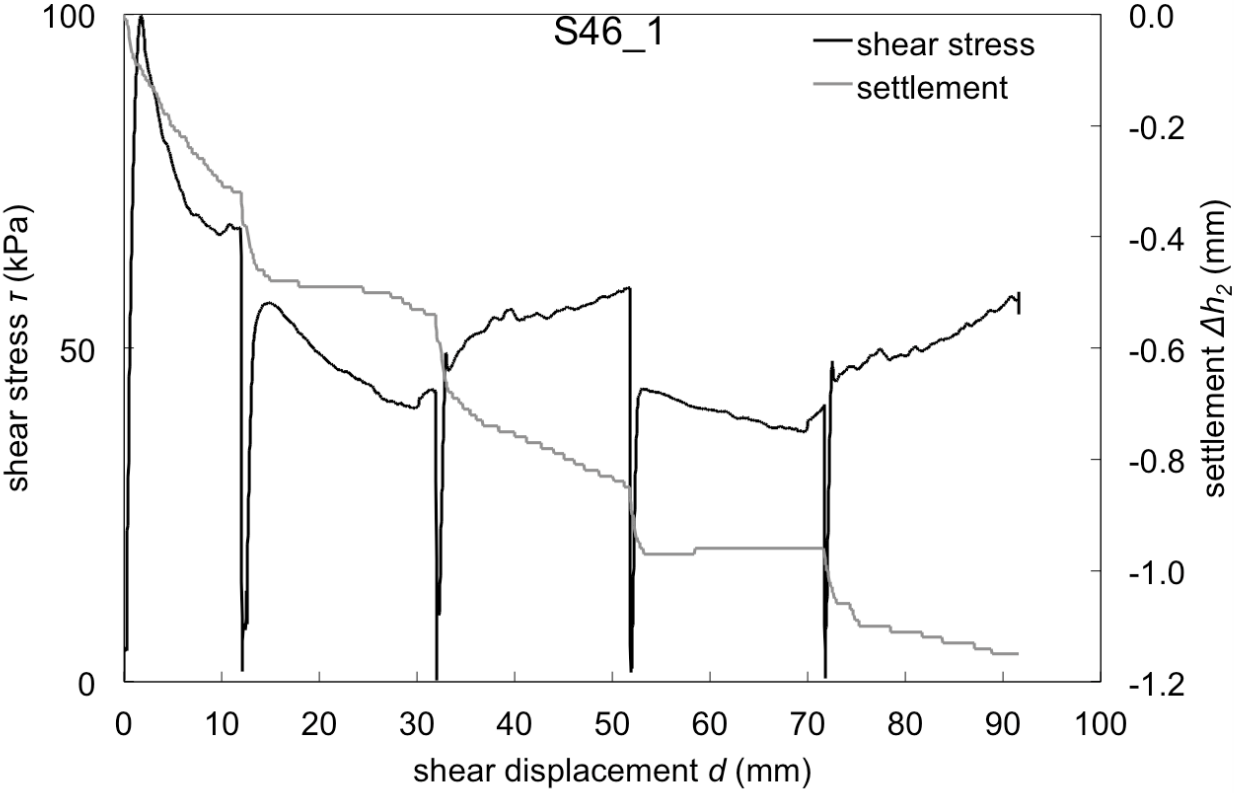
S46_1
shear stress
settlement
shear stress τ (kPa)
settlement Δh2 (mm)
shear displacement d (mm)
100
50
0
0.0
-0.2
-0.4
-0.6
-0.8
-1.0
-1.2
0
10
20
30
40
50
60
70
80
90
100

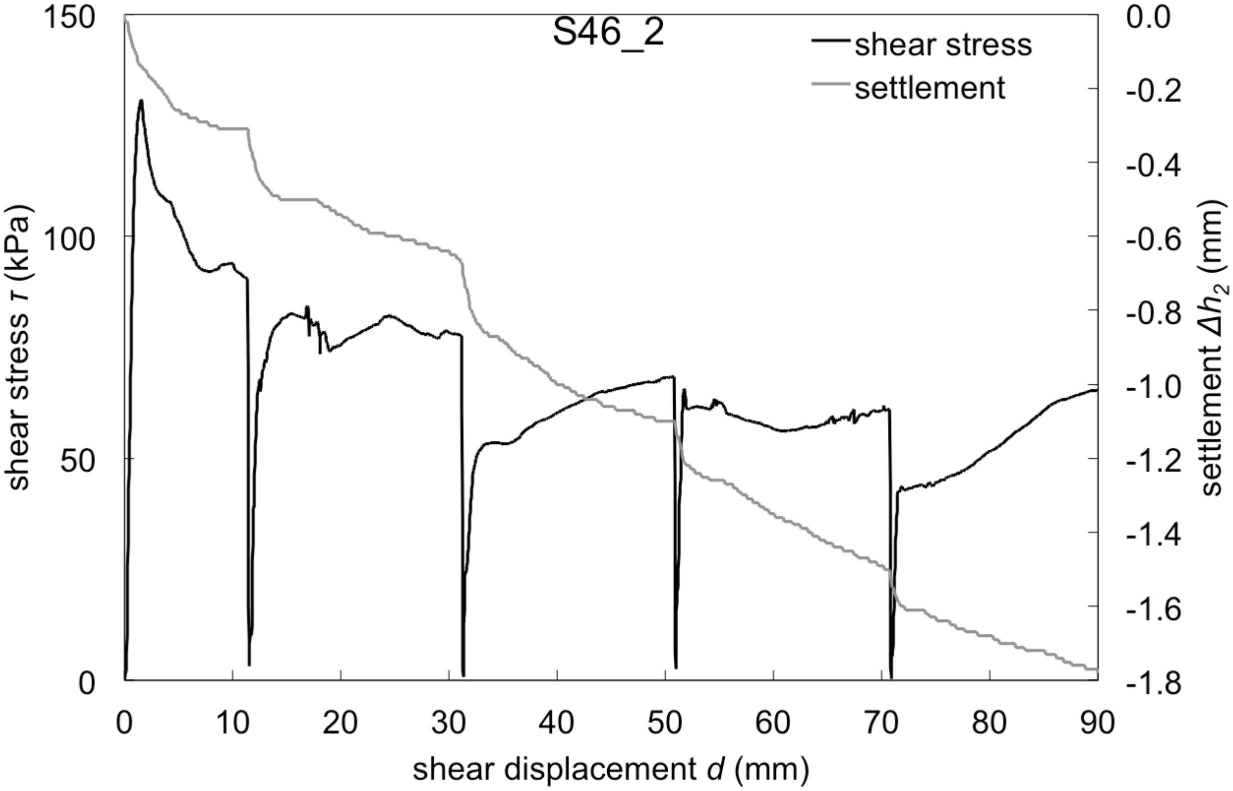
S46_2
shear stress
settlement
shear stress τ (kPa)
settlement Δh2 (mm)
shear displacement d (mm)
150
100
50
0
0.0
-0.2
-0.4
-0.6
-0.8
-1.0
-1.2
-1.4
-1.6
-1.8
0
10
20
30
40
50
60
70
80
90

APPENDIX G. RING SHEAR TEST RESULTS

Table G.1. Ring shear test parameters

Test	Sample depth (m)	Initial water content w_i (%)	Normal stress σ'_n (kPa)	Shear displacement rate $\dot{d}$ (mm/min)	Total shear displacement d (mm)	Consolidation settlement Δh_1 (mm)	Shear settlement Δh_2 (mm)
S250_a	7.6	28	170	0.024	152	0.42	0.59
S31_b	8.4	-	100	multiple	237	0.23	0.63
S31_a	8.4	30	170	multiple	117	0.35	0.47
S32_a	8.9	32	100	0.024	64	0.46	0.39
S32_b	8.9	25	170	multiple	94	0.35	0.59
S33_c	9.1	40	100	multiple	133	0.24	0.49
S33_b	9.1	40	100	0.024	82	0.25	0.48
S33_a	9.1	54	170	0.024	65	0.88	0.35
S40_a	12.8	31	100	0.018	64	0.55	0.37
S40_b	12.8	22	100	0.018	63	0.21	0.27
S40_c	12.8	39	294	0.018	59	1.41	0.39
S42_a	14.2	30	200	0.025	195	0.55	0.60
S44_a	14.9	23	134	0.025	68	0.73	0.26
S46_c	16.2	33	100	0.024	102	0.37	0.46
S46_a	16.2	26	134	0.025	96	0.47	0.49
S46_b	16.2	40	170	0.012	47	0.84	0.31

all specimens: initial height H_0=5 mm; inner diameter *ID*=70 mm;
outer diameter *OD*=100 mm

Table G.2. Multiple-rate ring shear test results

Test	Normal stress σ'_n (kPa)	Shear displacement rate (mm/min)		
		2.4×10^{-3}	2.4×10^{-2}	2.4×10^{-1}
		Residual shear strength τ_r (kPa)		
S31_b	100	27.0	26.9	27.1
S31_a	170	50.7	50.4	51.9
S32_b	170	74.3	74.4	75.0
S33_c	100	20.0	20.1	20.7

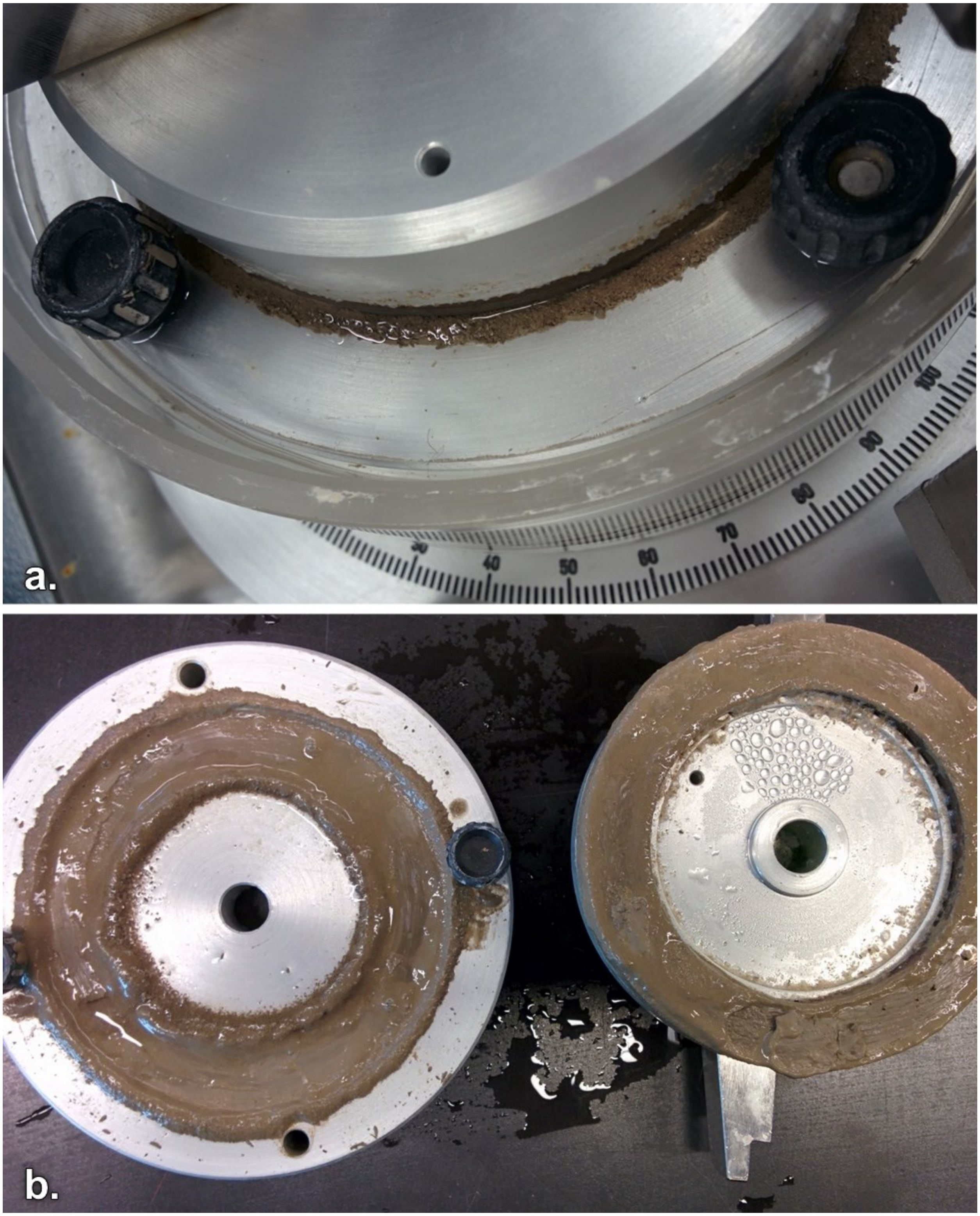
a.
30
40
50
60
70
80
90
100
b.

Figure G.1. Soil extrusion: (a) after consolidation, before shear in Test S33_c; (b) after shear in Test S33_b

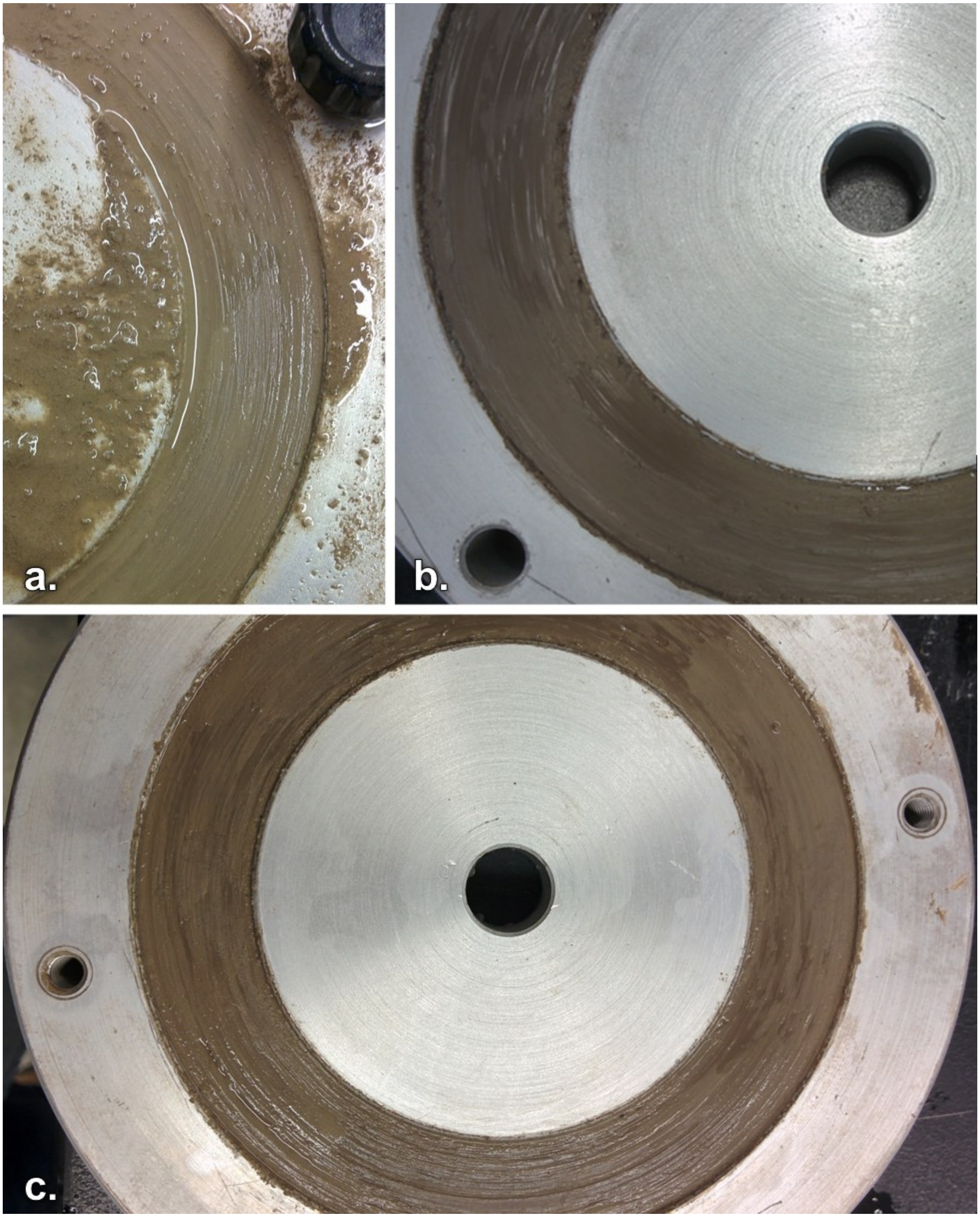

Figure G.2. Shear surfaces: (a) S31_a; (b) S33_c; (c) S250_a

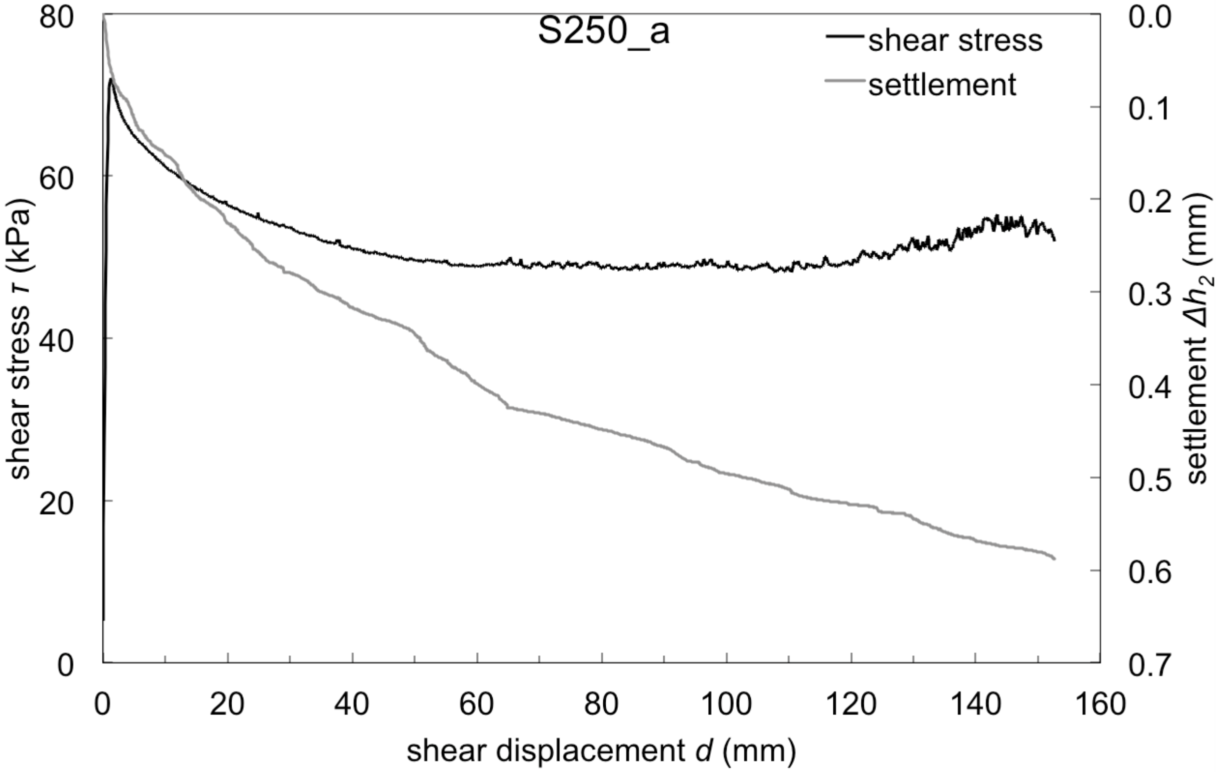
S250_a
shear stress
settlement
shear stress τ (kPa)
0
20
40
60
80
settlement Δh₂ (mm)
0.0
0.1
0.2
0.3
0.4
0.5
0.6
0.7
shear displacement d (mm)
0
20
40
60
80
100
120
140
160

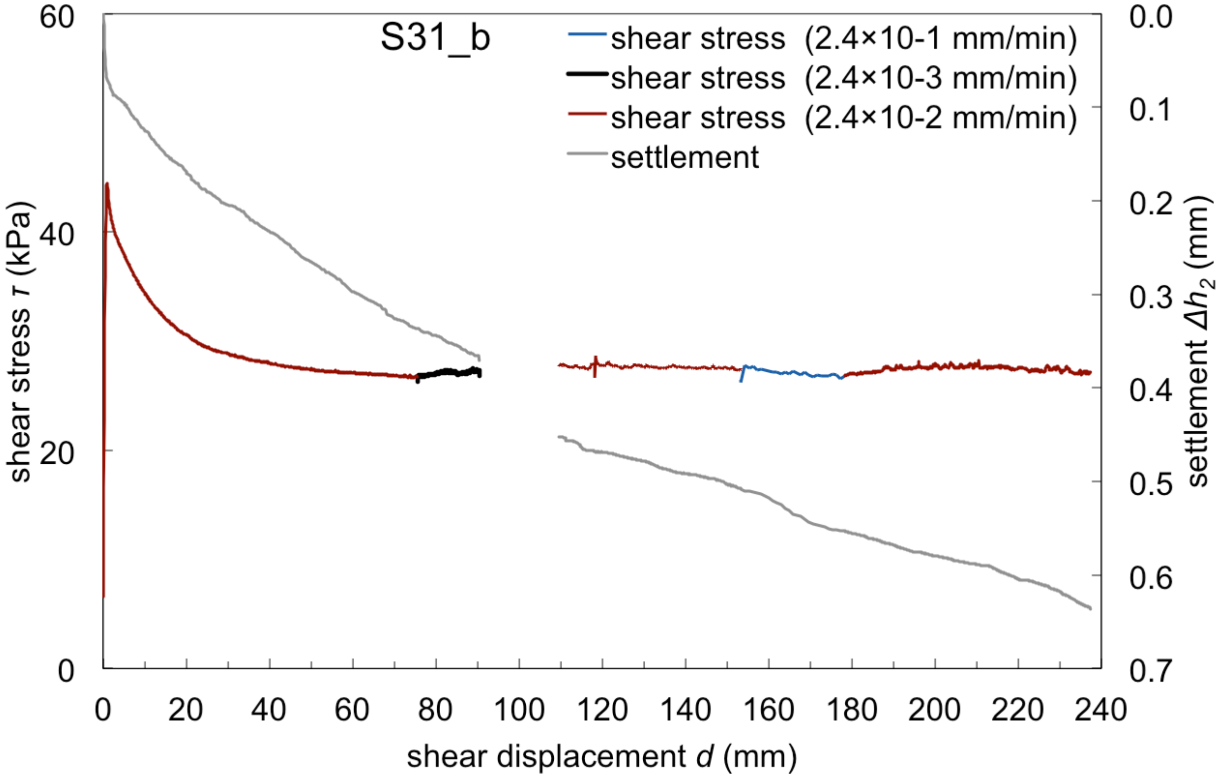
S31_b
shear stress (2.4×10-1 mm/min)
shear stress (2.4×10-3 mm/min)
shear stress (2.4×10-2 mm/min)
settlement
shear stress τ (kPa)
0
20
40
60
settlement Δh₂ (mm)
0.0
0.1
0.2
0.3
0.4
0.5
0.6
0.7
shear displacement d (mm)
0
20
40
60
80
100
120
140
160
180
200
220
240

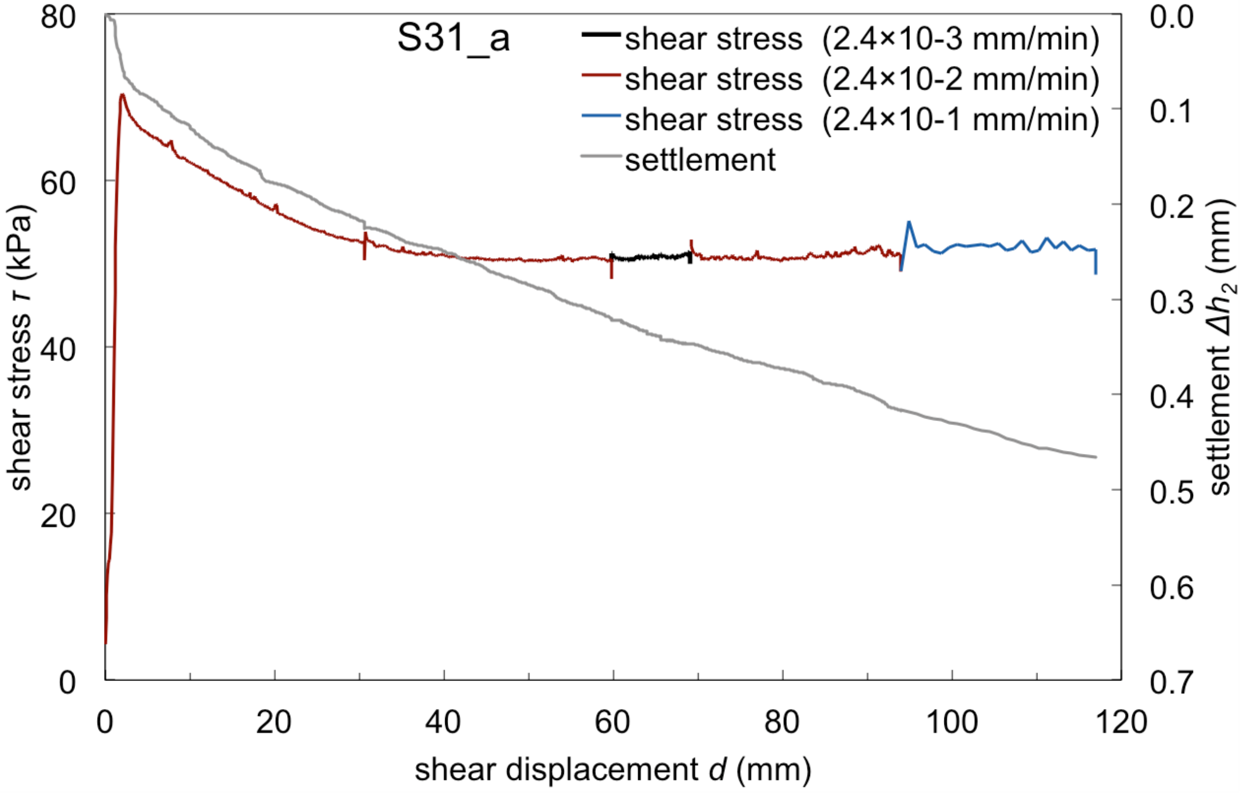
S31_a
shear stress (2.4×10-3 mm/min)
shear stress (2.4×10-2 mm/min)
shear stress (2.4×10-1 mm/min)
settlement
shear stress τ (kPa)
settlement Δh2 (mm)
shear displacement d (mm)
0
20
40
60
80
100
120
0.0
0.1
0.2
0.3
0.4
0.5
0.6
0.7

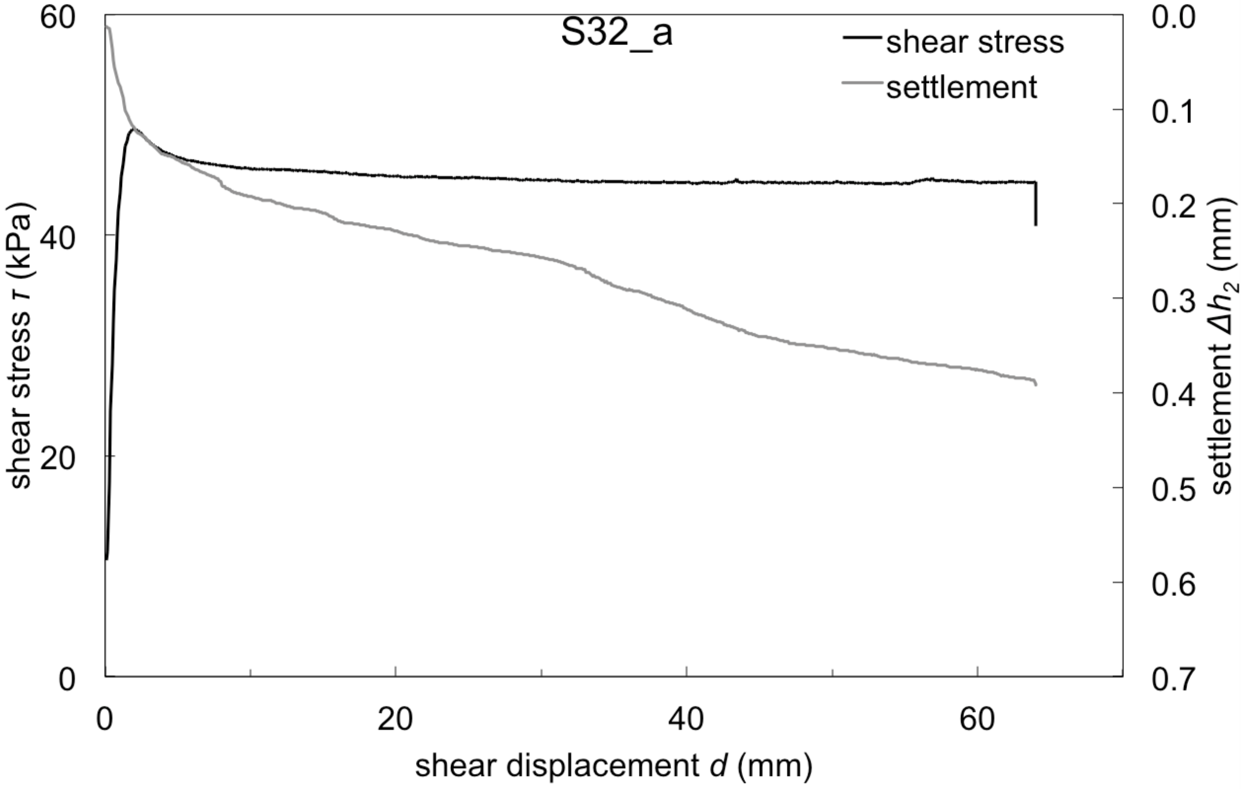
S32_a
shear stress
settlement
shear stress τ (kPa)
settlement Δh2 (mm)
shear displacement d (mm)
0
20
40
60
0.0
0.1
0.2
0.3
0.4
0.5
0.6
0.7

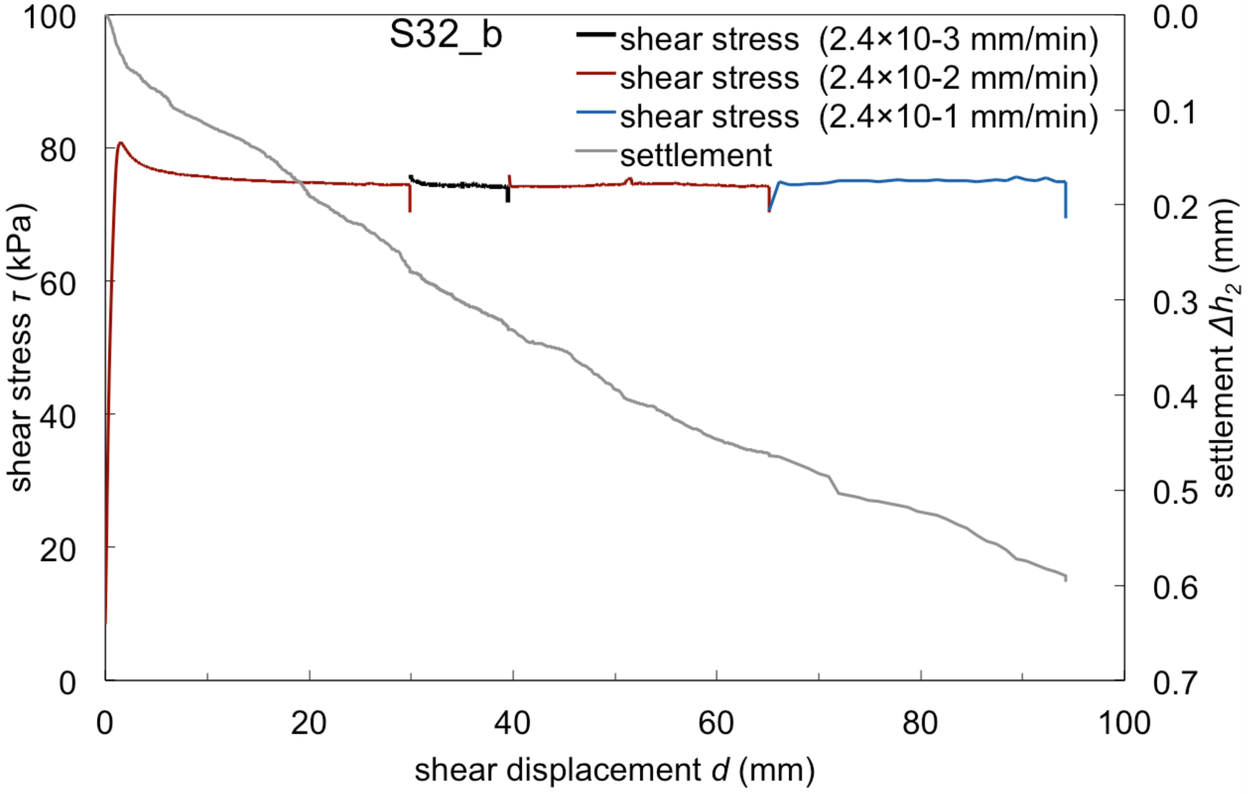
S32_b
shear stress (2.4×10-3 mm/min)
shear stress (2.4×10-2 mm/min)
shear stress (2.4×10-1 mm/min)
settlement
shear stress τ (kPa)
settlement Δh2 (mm)
shear displacement d (mm)
0
20
40
60
80
100
0.0
0.1
0.2
0.3
0.4
0.5
0.6
0.7

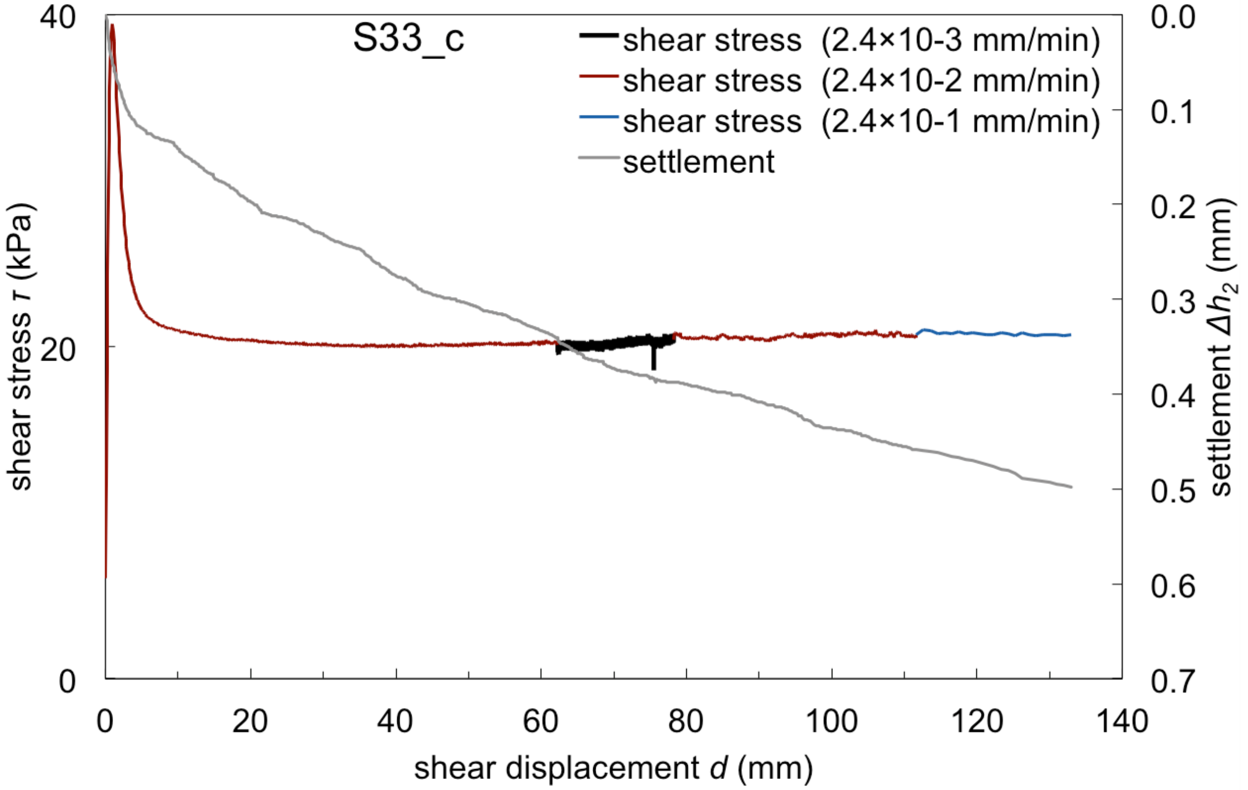
S33_c
shear stress (2.4×10-3 mm/min)
shear stress (2.4×10-2 mm/min)
shear stress (2.4×10-1 mm/min)
settlement
shear stress τ (kPa)
settlement Δh2 (mm)
shear displacement d (mm)
0
20
40
60
80
100
120
140
0.0
0.1
0.2
0.3
0.4
0.5
0.6
0.7

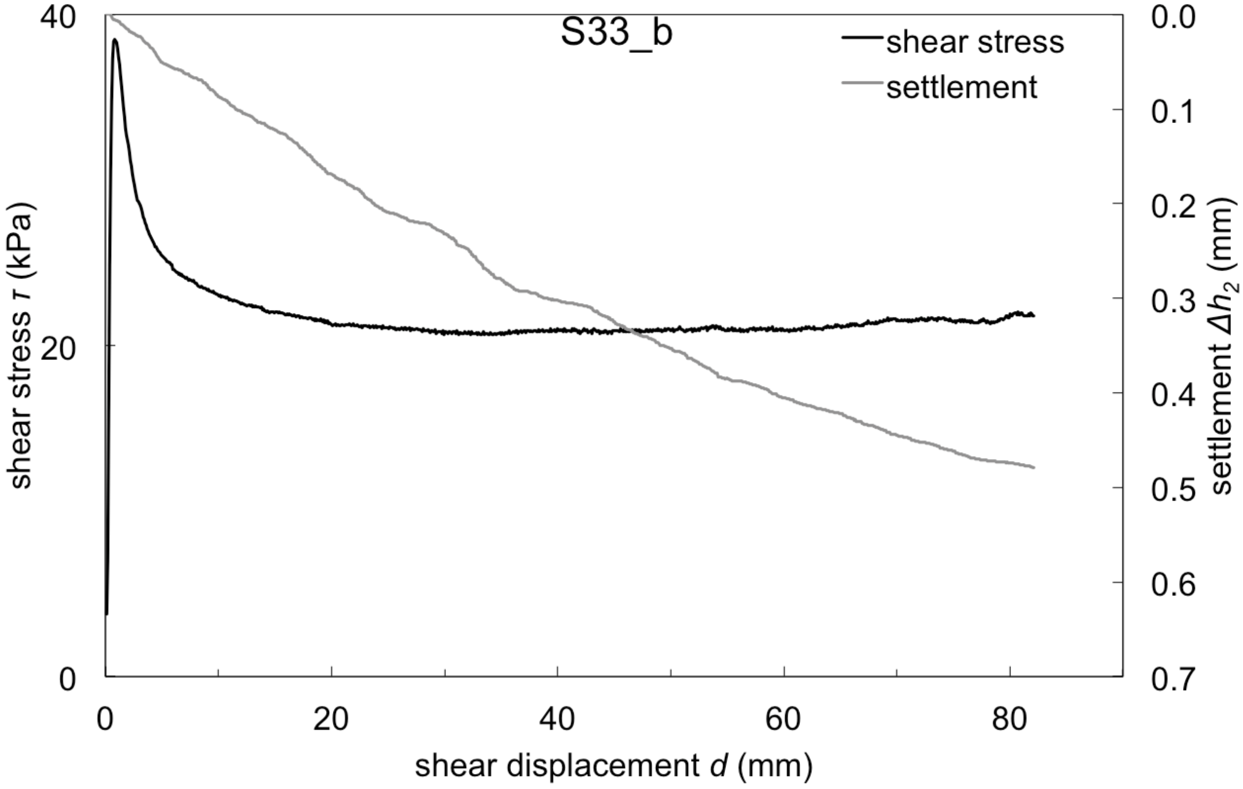
S33_b
shear stress
settlement
shear stress τ (kPa)
settlement Δh_2 (mm)
shear displacement d (mm)
0
20
40
0
20
40
60
80
0.0
0.1
0.2
0.3
0.4
0.5
0.6
0.7

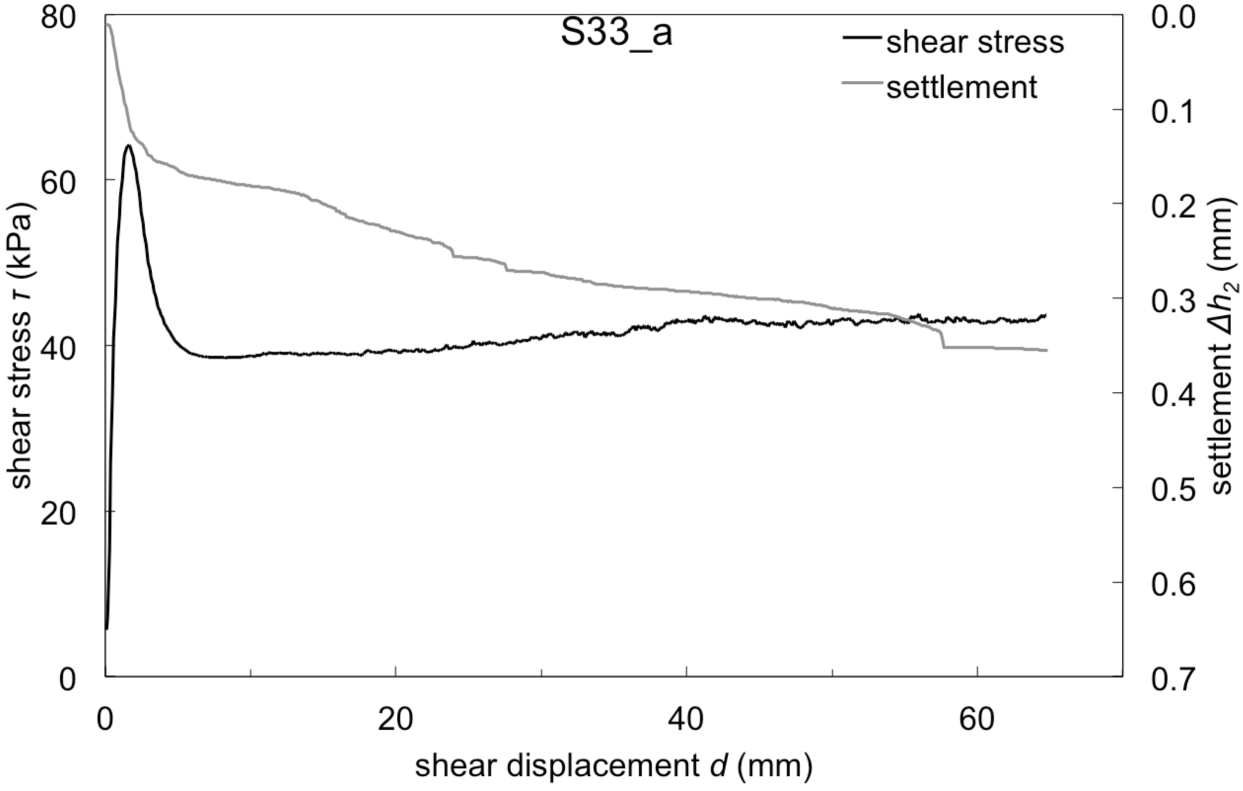
S33_a
shear stress
settlement
shear stress τ (kPa)
settlement Δh_2 (mm)
shear displacement d (mm)
0
20
40
60
80
0
20
40
60
0.0
0.1
0.2
0.3
0.4
0.5
0.6
0.7

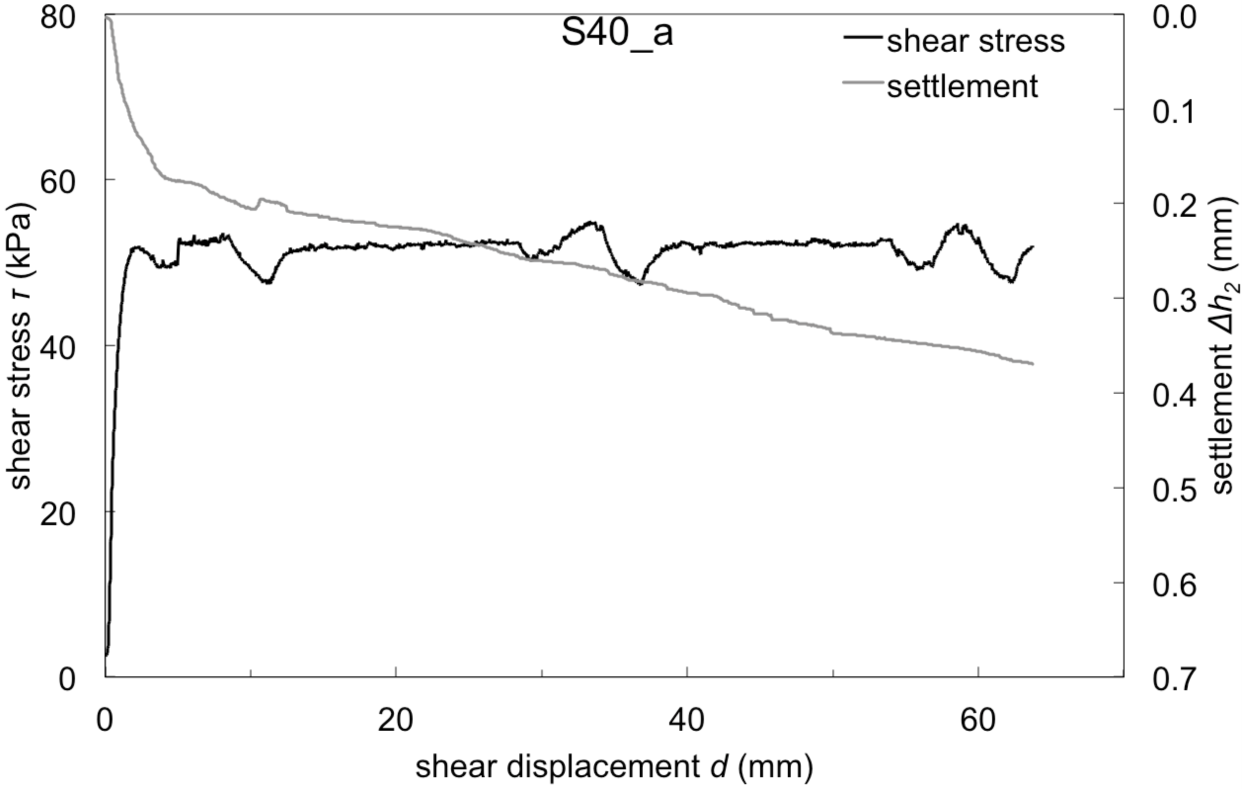
S40_a
shear stress
settlement
shear stress τ (kPa)
settlement Δh₂ (mm)
shear displacement d (mm)
0
20
40
60
80
0.0
0.1
0.2
0.3
0.4
0.5
0.6
0.7
0
20
40
60

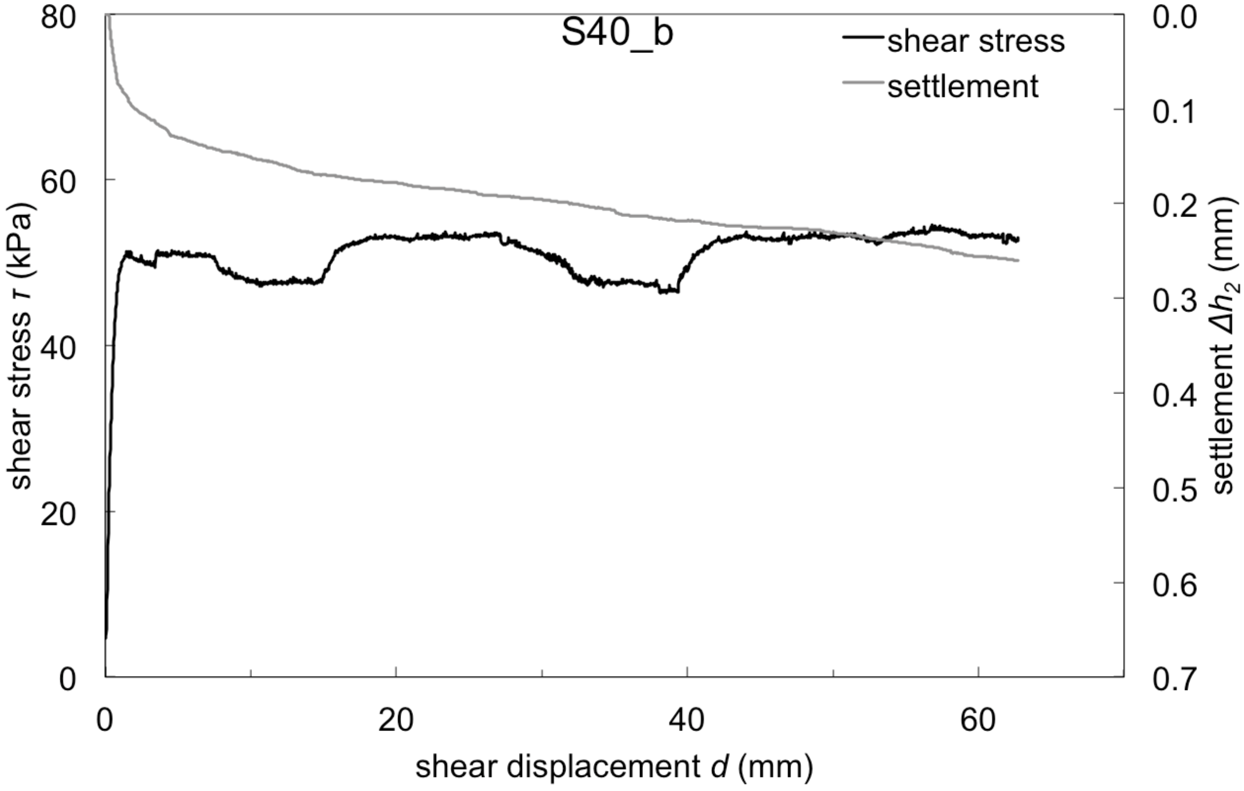
S40_b
shear stress
settlement
shear stress τ (kPa)
settlement Δh₂ (mm)
shear displacement d (mm)
0
20
40
60
80
0.0
0.1
0.2
0.3
0.4
0.5
0.6
0.7
0
20
40
60

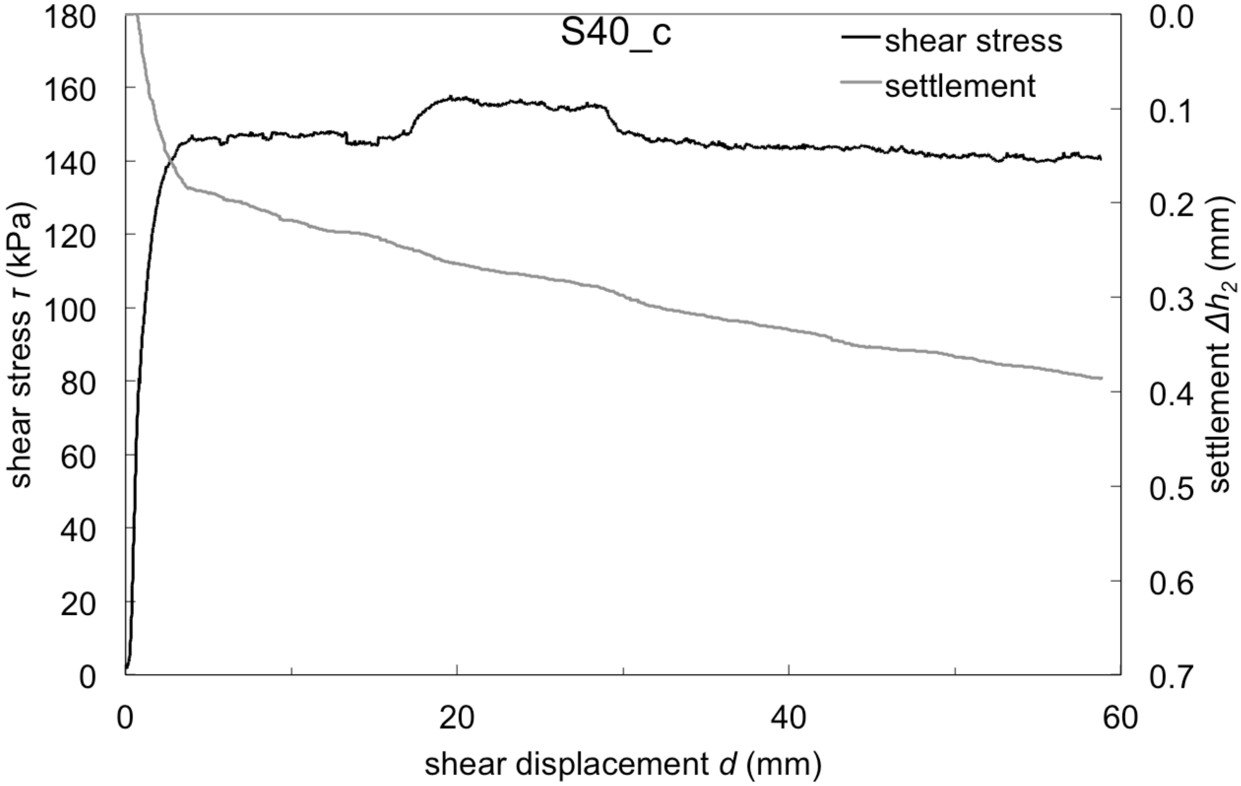
S40_c
shear stress
settlement
shear stress τ (kPa)
settlement Δh2 (mm)
shear displacement d (mm)
180
160
140
120
100
80
60
40
20
0
0.0
0.1
0.2
0.3
0.4
0.5
0.6
0.7
0
20
40
60

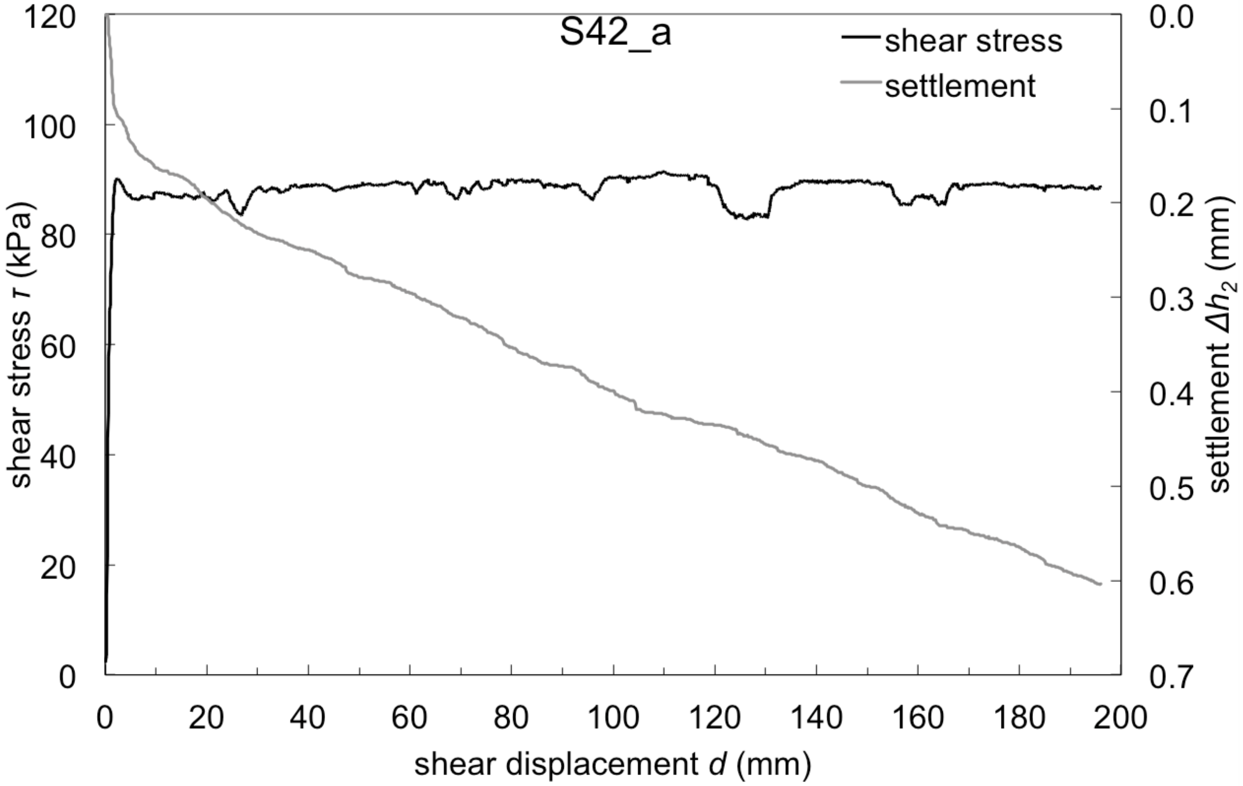
S42_a
shear stress
settlement
shear stress τ (kPa)
settlement Δh2 (mm)
shear displacement d (mm)
120
100
80
60
40
20
0
0.0
0.1
0.2
0.3
0.4
0.5
0.6
0.7
0
20
40
60
80
100
120
140
160
180
200

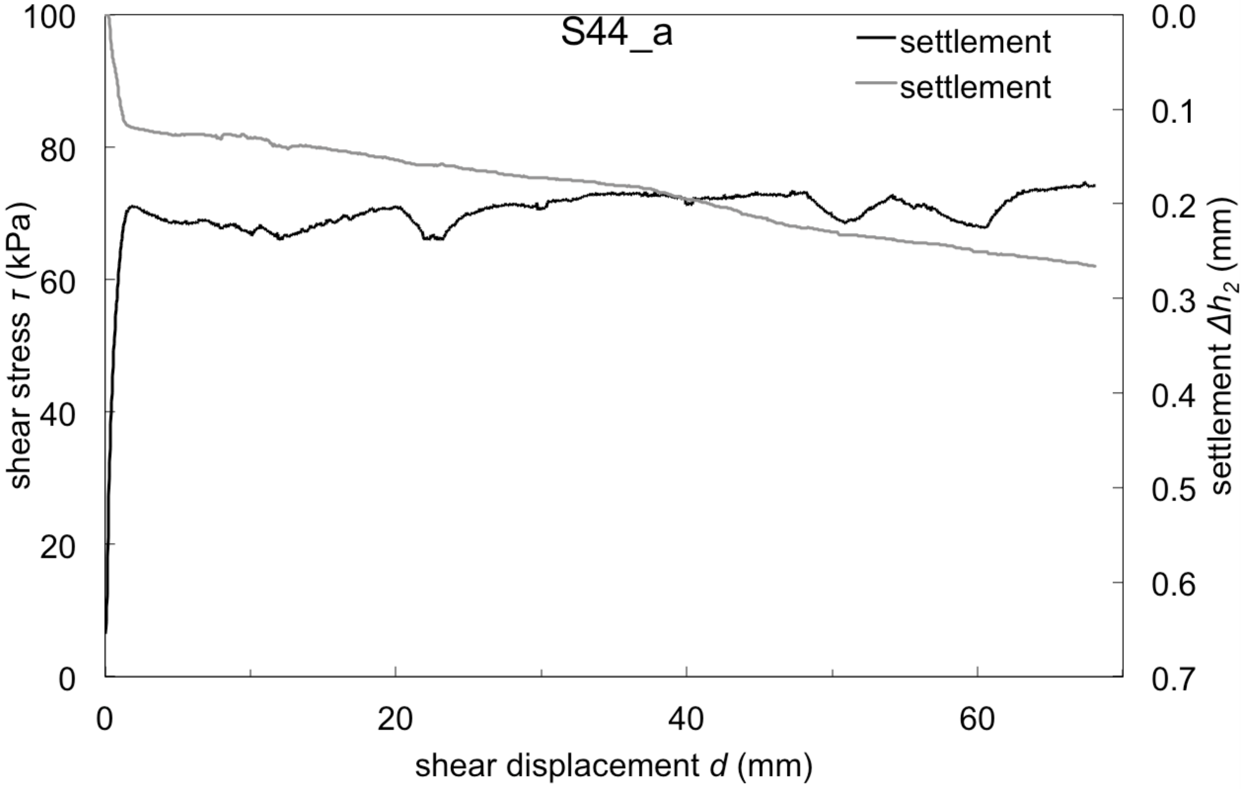
S44_a
settlement
settlement
shear stress τ (kPa)
settlement Δh_2 (mm)
shear displacement d (mm)
0
20
40
60
80
100
0.0
0.1
0.2
0.3
0.4
0.5
0.6
0.7
0
20
40
60

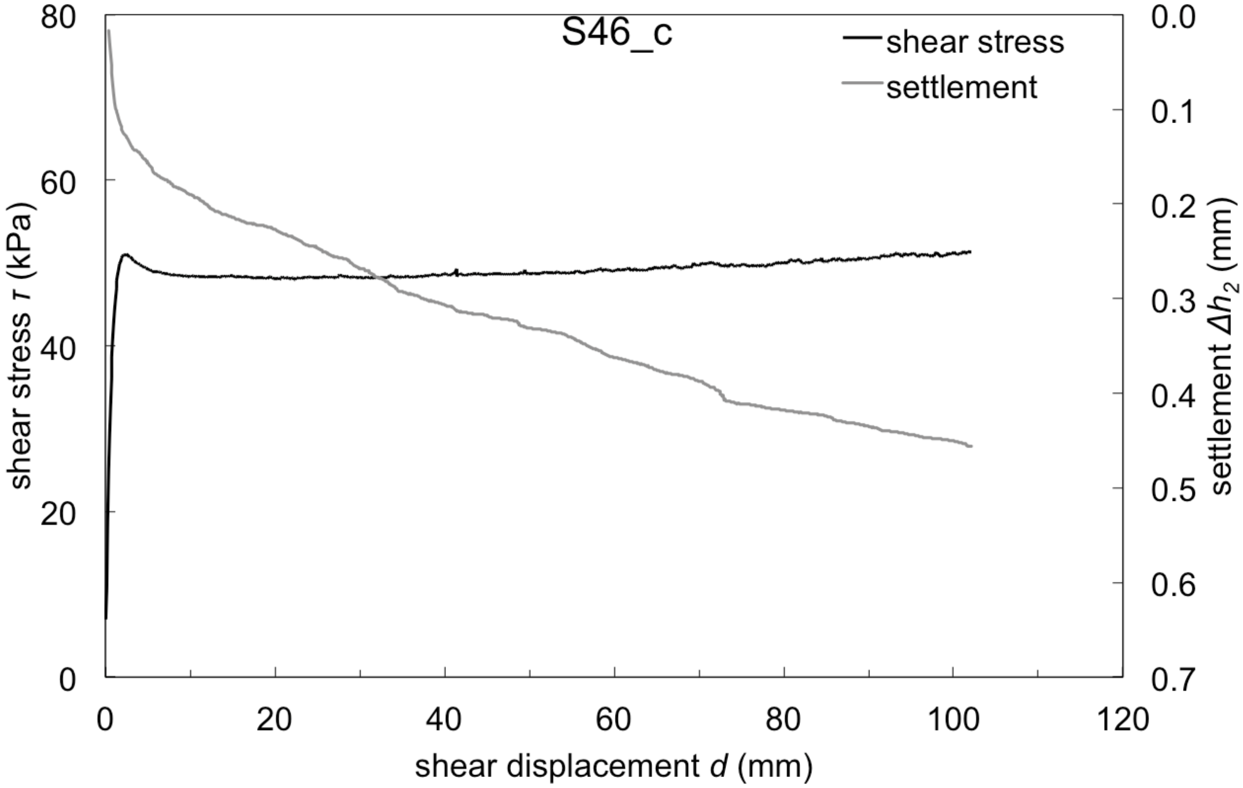
S46_c
shear stress
settlement
shear stress τ (kPa)
settlement Δh_2 (mm)
shear displacement d (mm)
0
20
40
60
80
0.0
0.1
0.2
0.3
0.4
0.5
0.6
0.7
0
20
40
60
80
100
120

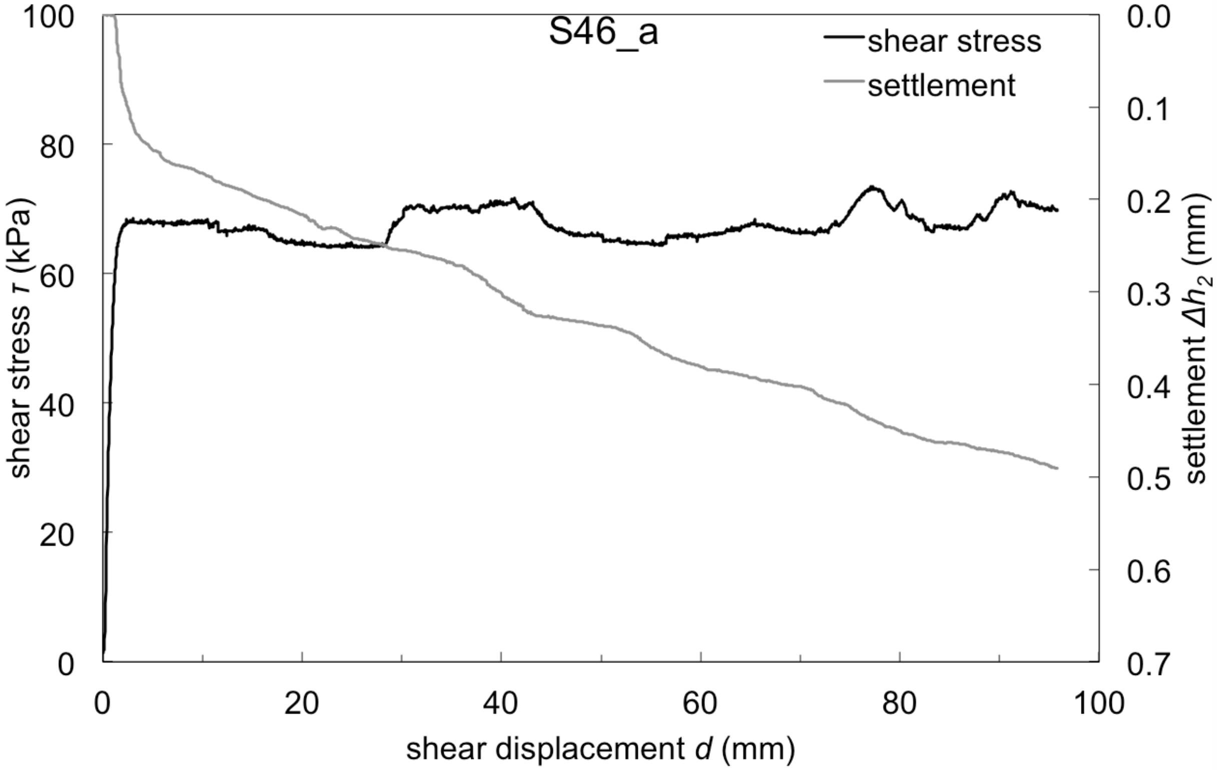
S46_a
shear stress
settlement
shear stress τ (kPa)
settlement Δh₂ (mm)
shear displacement d (mm)
0
20
40
60
80
100
0.0
0.1
0.2
0.3
0.4
0.5
0.6
0.7

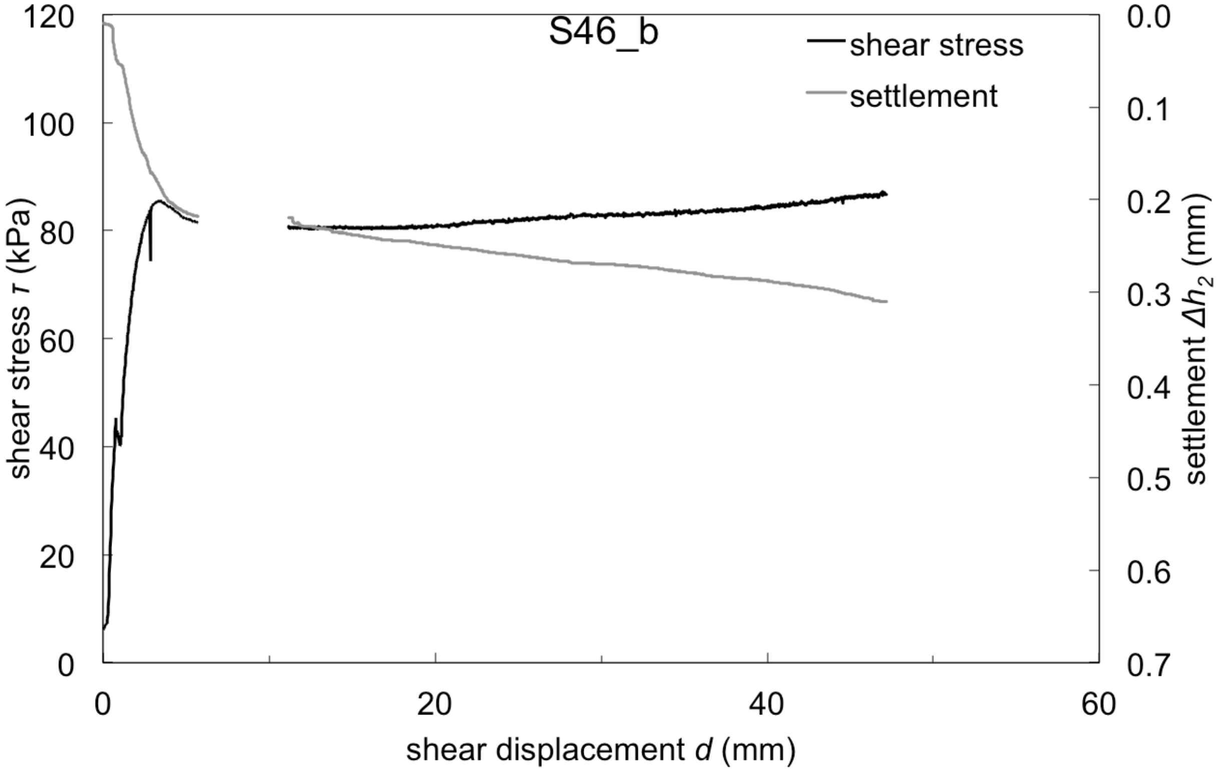
S46_b
shear stress
settlement
shear stress τ (kPa)
settlement Δh₂ (mm)
shear displacement d (mm)
0
20
40
60
80
100
120
0.0
0.1
0.2
0.3
0.4
0.5
0.6
0.7

APPENDIX H. MOHR-COULOMB STRENGTH CRITERIA

Plots. Direct shear and ring shear test results in the τ-σ_n space

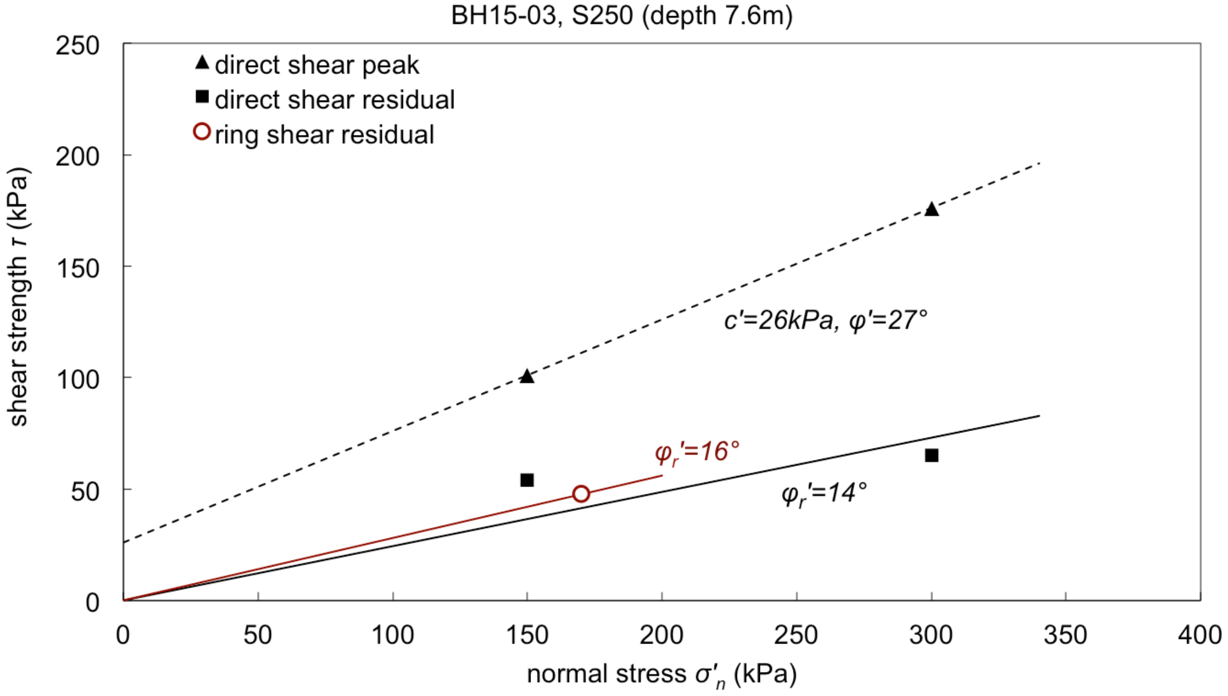

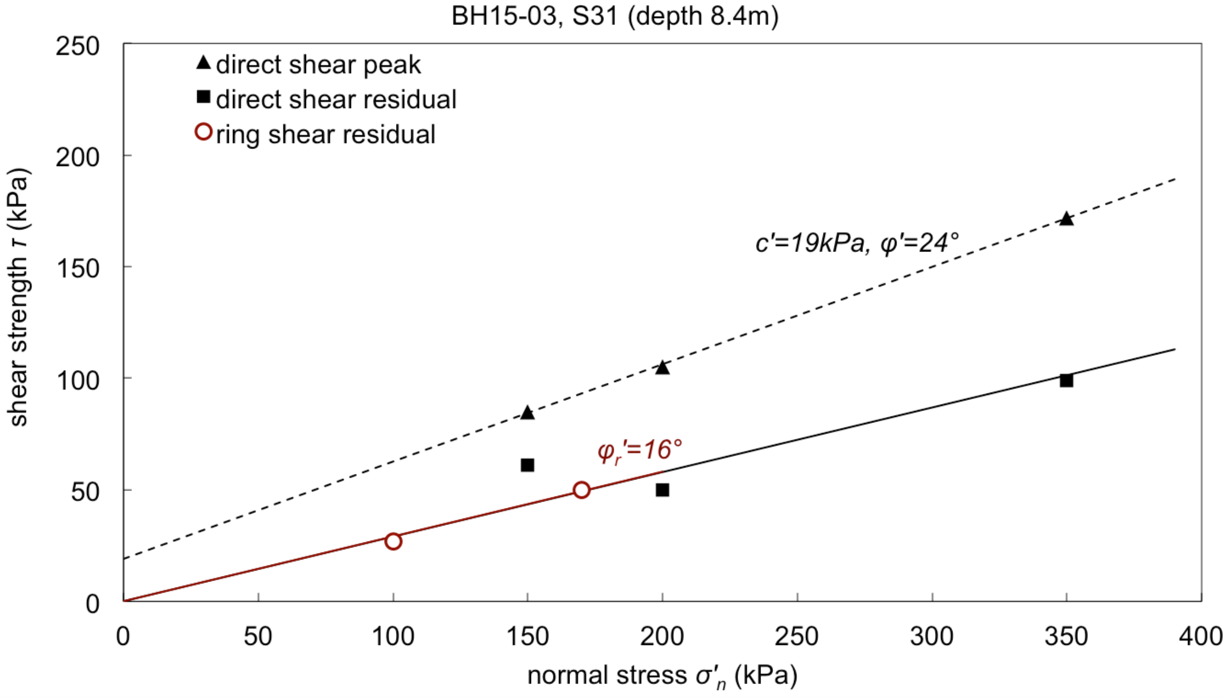

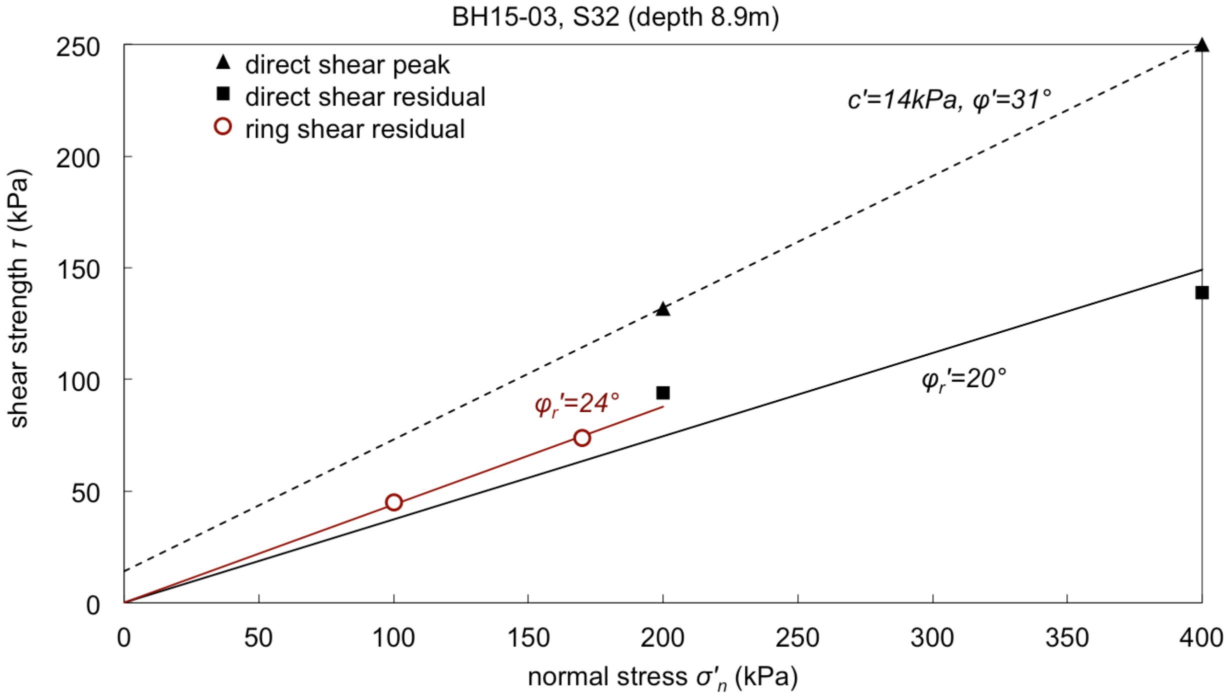
BH15-03, S32 (depth 8.9m)
▲ direct shear peak
■ direct shear residual
○ ring shear residual
c'=14kPa, φ'=31°
φr'=24°
φr'=20°
shear strength τ (kPa)
normal stress σ'n (kPa)
0
50
100
150
200
250
300
350
400

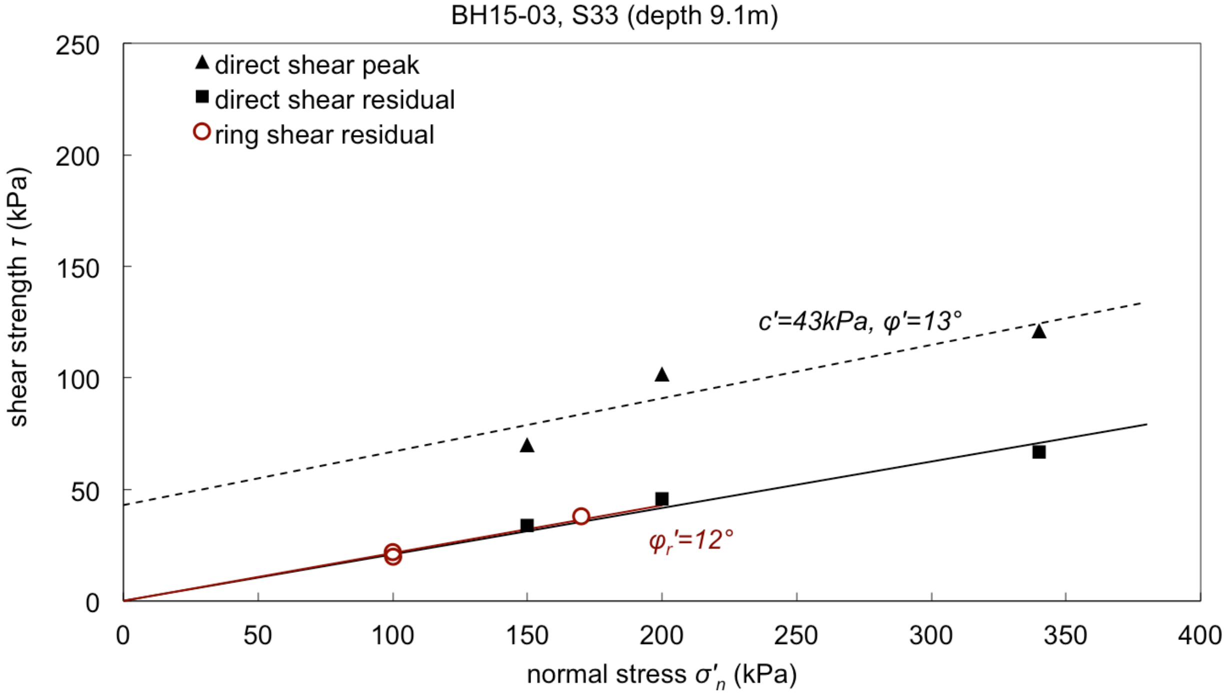
BH15-03, S33 (depth 9.1m)
▲ direct shear peak
■ direct shear residual
○ ring shear residual
c'=43kPa, φ'=13°
φr'=12°
shear strength τ (kPa)
normal stress σ'n (kPa)
0
50
100
150
200
250
300
350
400

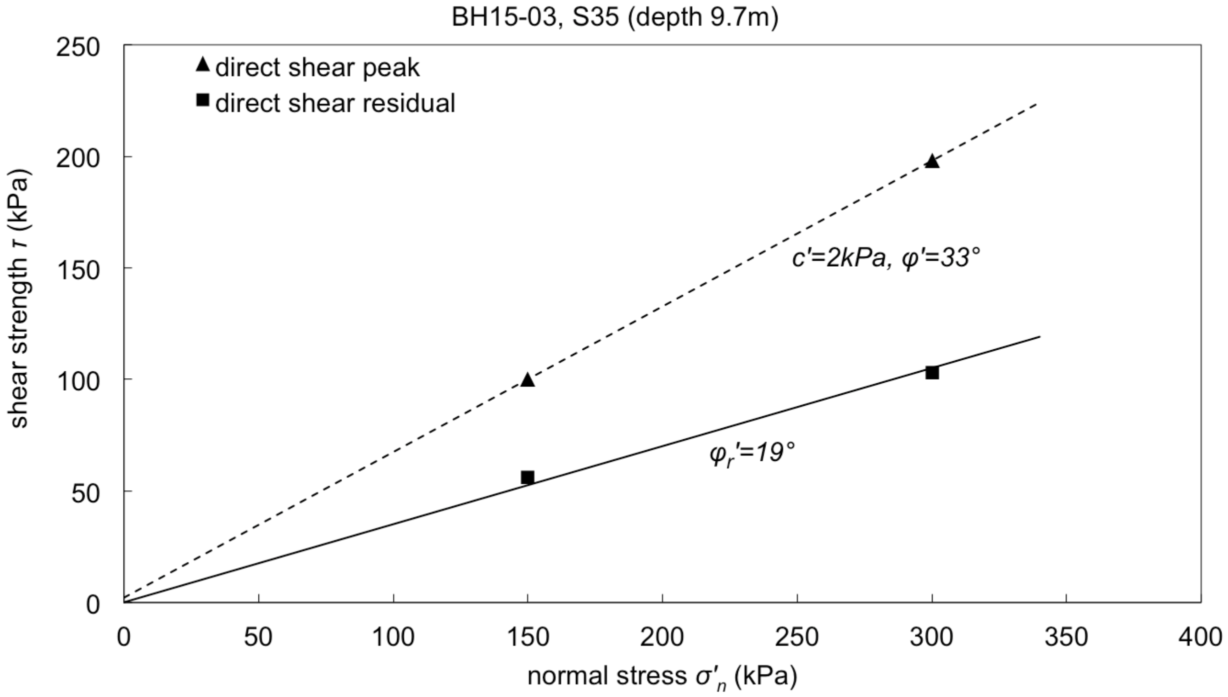
BH15-03, S35 (depth 9.7m)
▲ direct shear peak
■ direct shear residual
c'=2kPa, φ'=33°
φr'=19°
shear strength τ (kPa)
0
50
100
150
200
250
normal stress σ'n (kPa)
0
50
100
150
200
250
300
350
400

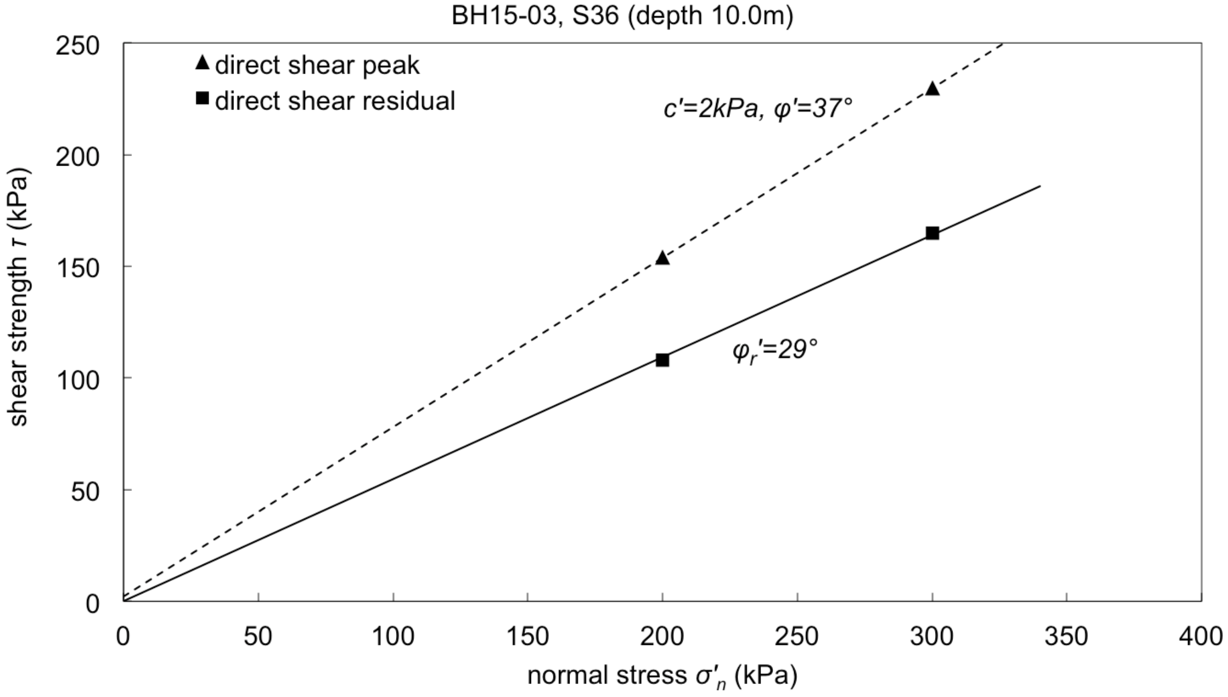
BH15-03, S36 (depth 10.0m)
▲ direct shear peak
■ direct shear residual
c'=2kPa, φ'=37°
φr'=29°
shear strength τ (kPa)
0
50
100
150
200
250
normal stress σ'n (kPa)
0
50
100
150
200
250
300
350
400

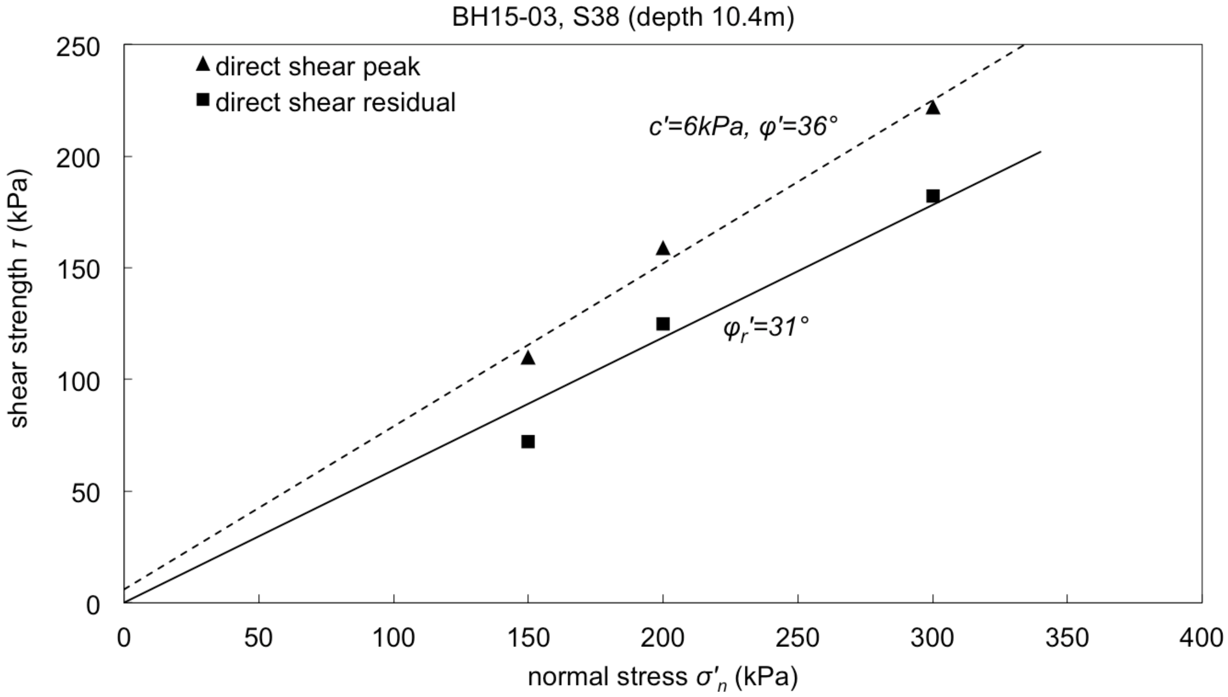

BH15-03, S38 (depth 10.4m)
▲ direct shear peak
■ direct shear residual
c'=6kPa, φ'=36°
φr'=31°
shear strength τ (kPa)
normal stress σ'n (kPa)
0
50
100
150
200
250
0
50
100
150
200
250
300
350
400

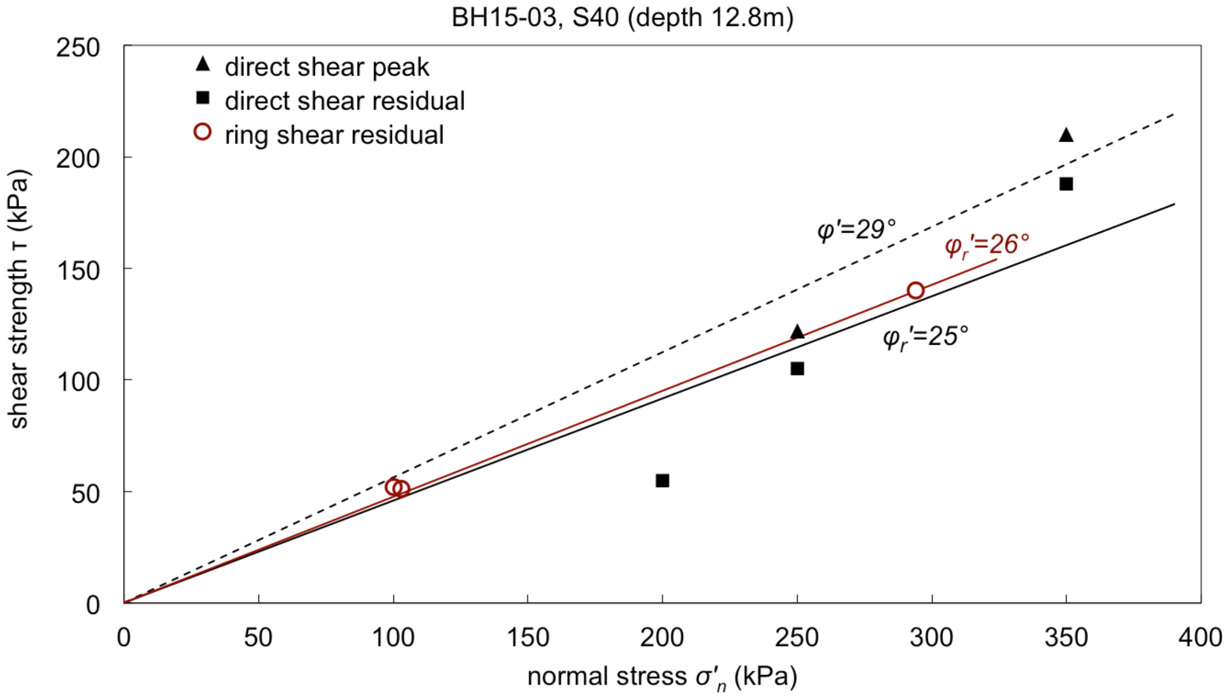

BH15-03, S40 (depth 12.8m)
▲ direct shear peak
■ direct shear residual
○ ring shear residual
φ'=29°
φr'=26°
φr'=25°
shear strength τ (kPa)
normal stress σ'n (kPa)
0
50
100
150
200
250
0
50
100
150
200
250
300
350
400

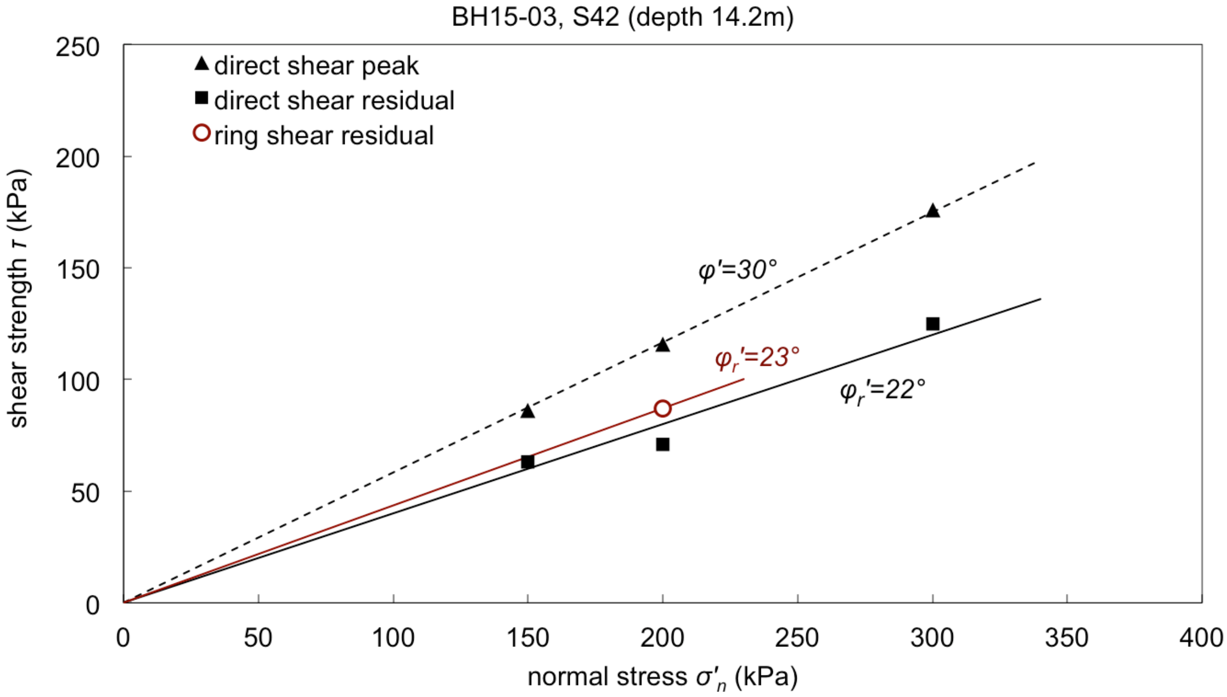

BH15-03, S42 (depth 14.2m)
▲ direct shear peak
■ direct shear residual
○ ring shear residual
φ'=30°
φr'=23°
φr'=22°
shear strength τ (kPa)
normal stress σ'n (kPa)
0
50
100
150
200
250
300
350
400

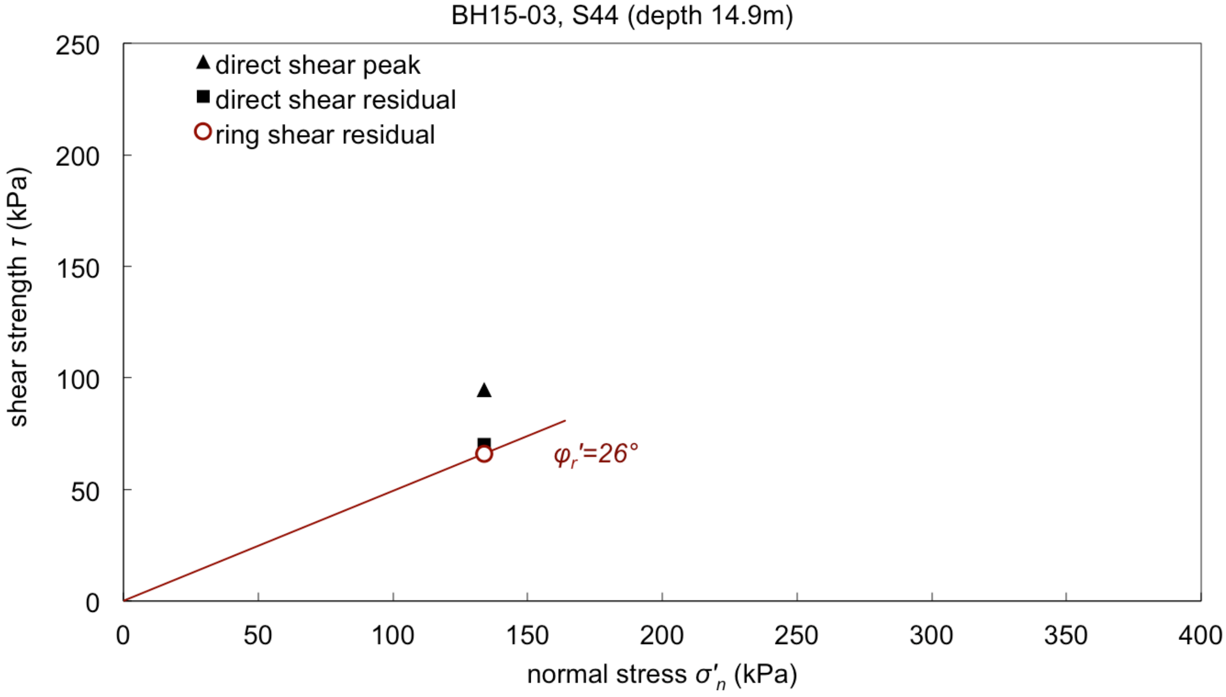

BH15-03, S44 (depth 14.9m)
▲ direct shear peak
■ direct shear residual
○ ring shear residual
φr'=26°
shear strength τ (kPa)
normal stress σ'n (kPa)
0
50
100
150
200
250
300
350
400

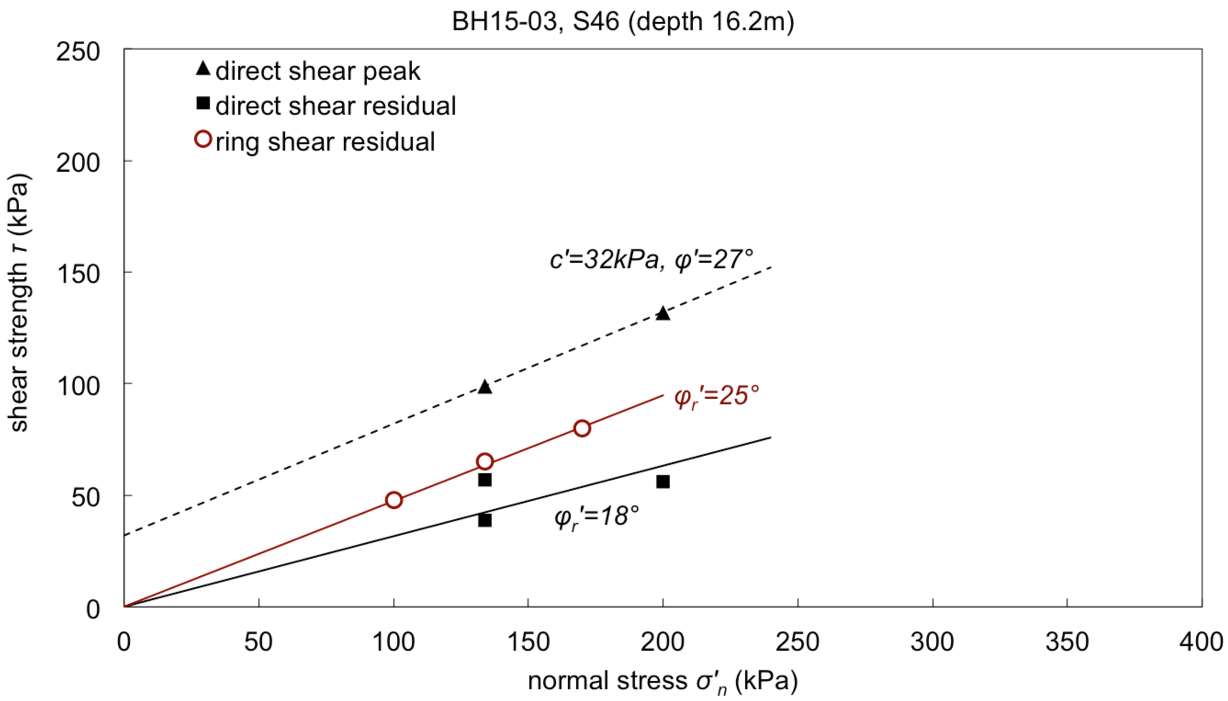
BH15-03, S46 (depth 16.2m)
▲ direct shear peak
■ direct shear residual
○ ring shear residual
c'=32kPa, φ'=27°
φr'=25°
φr'=18°
shear strength τ (kPa)
0
50
100
150
200
250
normal stress σ'n (kPa)
0
50
100
150
200
250
300
350
400

APPENDIX I. DIRECT SIMPLE SHEAR TEST RESULTS

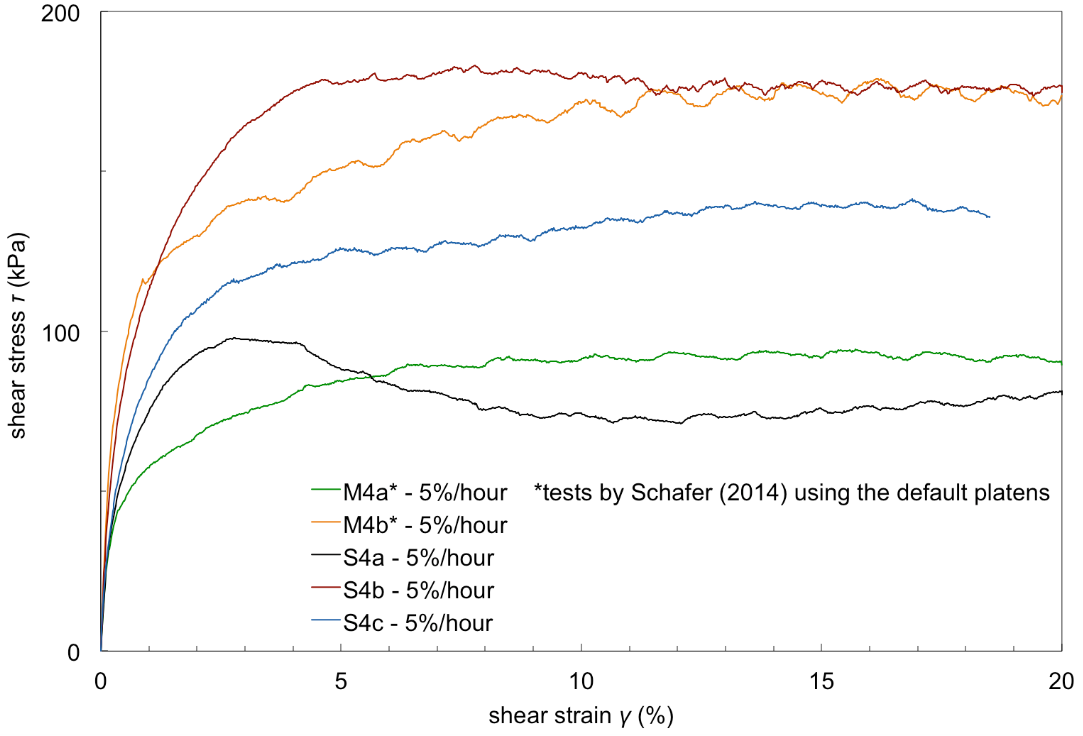

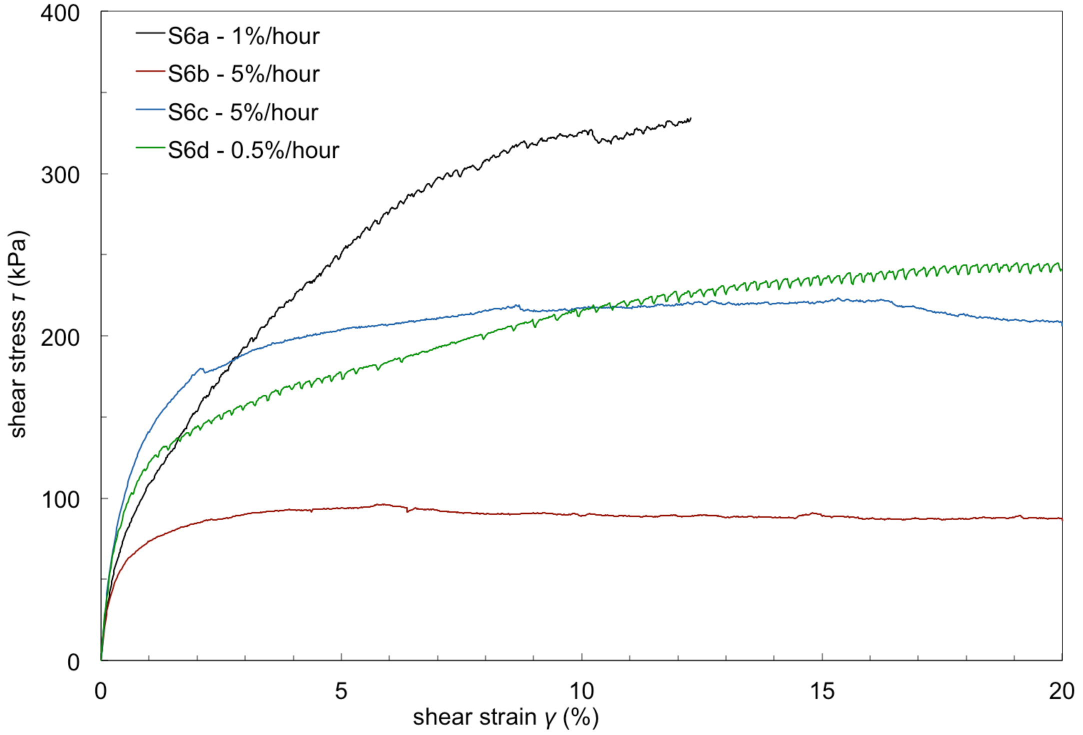

Figure I.1. Stress-strain response of direct simple shear (DSS) tests

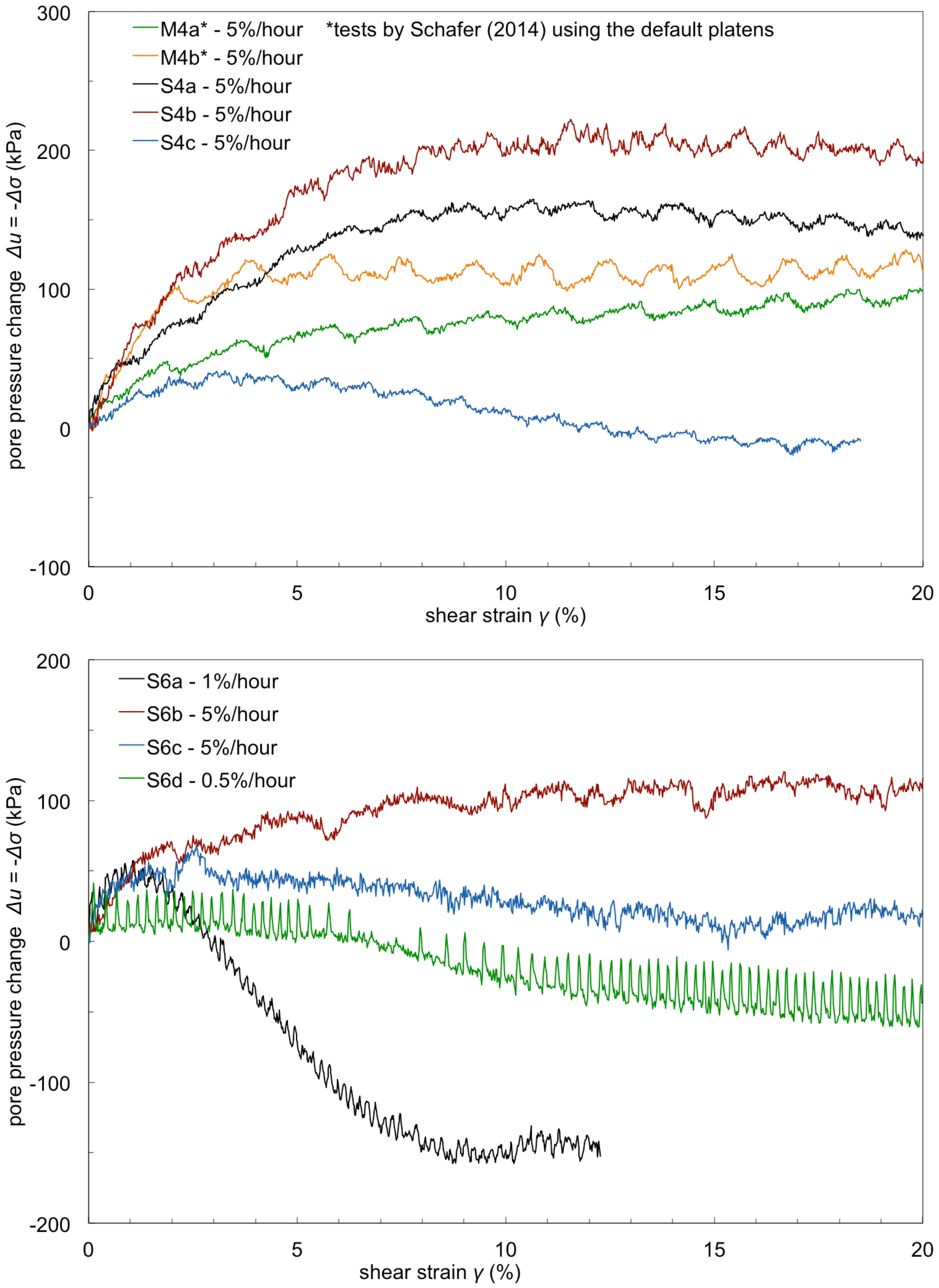

Figure I.2. Pore water pressure change-strain response of DSS tests

Table I.1. DSS test results

	Test	Shear strain rate $\dot{\gamma}$ (%/h)	Initial water content w_i (%)	Consolidation stress σ'_{v0} (kPa)	Undrained shear strength $s_u = \tau_{max}$ (kPa)	Pore water pressure change Δu (kPa)	Issues
S4 (depth 13.4m)	S4a	5	30	300	98	84	boundary zone shear, some slippage
	S4b	5	27	500	179	150	boundary zone shear (Figure I.3.b), some slippage
	S4c	5	32	200	140	-11	excessive slippage (Figure I.3.a)
	M4a[1]	5	29	300	94	76	excessive slippage
	M4b[1]	5	26	500	176	102	excessive slippage
S6 (depth 17.5m)	S6a	1	27	300	327	-157	some slippage
	S6b	5	24	300	96	72	boundary zone shear, some slippage
	S6c	5	27	300	219	23	excessive slippage
	S6d	0.5	25	300	244	-55	excessive slippage

[1] tests by Schafer (2014) using the default platens

all specimens: diameter ø=48.5 mm; height H=16 mm

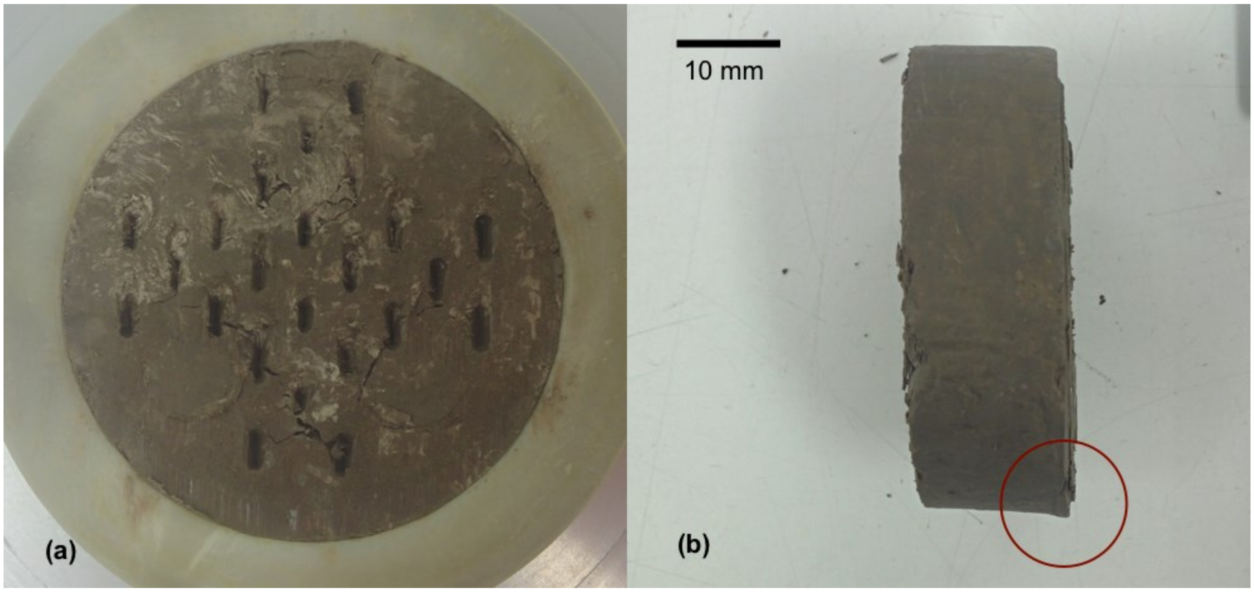

Figure I.3. (a) slippage on the surface of sheared Specimen S4c; (b) strain localized in the boundary zone of sheared Specimen S4b

APPENDIX J. DIRECT SIMPLE SHEAR (DSS) TESTING OF A VERY STIFF GLACIOLACUSTRINE CLAY

A version of this chapter has been published in the 69th Canadian Geotechnical Conference, October 2016, Vancouver:

Le Meil, G., Hendry, M., & Martin, C. (2016). Direct simple shear (DSS) testing of a very stiff glaciolacustrine clay. *69th Canadian Geotechnical Conference, GeoVancouver 2016*.

Abstract

The purpose of the research presented within this paper has been to investigate the impact of undrained loading conditions and the rate of movement on the strength of a heavily overconsolidated Pleistocene glaciolacustrine clay. Shear planes within this clay are implicated in the movement of many large landslides within the Thompson River valley, near Ashcroft, BC. Peak and residual strengths have previously been evaluated with direct shear tests; strength values similar to the residual strength have been back-calculated from several of the meta-stable landslides. Testing of the isotopes within the pore fluid of this clay has been conducted, along with extensive monitoring of pore pressures and displacements of the most active of the landslides within the valley (the Ripley slide). This has allowed for the characterization of the movement of water through the material over geological time, and the quantification of the current pore pressure distribution and rate of movement. Together, these results have shown that this clay is extremely tight and has raised the prospect that the pore pressures generated at the observed rate of shearing may impact the shear strength that can be mobilized.

Direct simple shear (DSS) tests have been conducted on clay specimens retrieved from the Ripley slide in an attempt to mimic the shearing of this clay along the bedding planes under undrained conditions. The use of the conventional NGI-type DSS apparatus for this very stiff clay has been challenging, as it well exceeds the stiffness and strength of soils typically tested with this apparatus. These challenges, the measured strength, and the resulting effective stress paths are presented within this paper.

1. Introduction

A very stiff clay of glaciolacustrine origin is implicated in several large translational landslides in the Thompson River valley near Ashcroft, British Columbia. Active slow-moving landslides such as the Ripley slide (1.0×10^6 m^3) pose a challenge for CN and CP who both operate railway lines through this valley. The exposure of this infrastructure to these landslides has motivated the characterization of the soil implicated in slope instability, as part of an ongoing investigation and monitoring program of the Ripley slide (Hendry et al. 2015, Schafer et al. 2015).

Clague and Evans (2003) have investigated and defined the local geology and stratigraphy relevant to the Thompson River valley landslides. A clayey stratum of glaciolacustrine origin consisting of rhythmically bedded silt and clay has been of particular interest as the landslides rupture surfaces have been systematically located within it (Eshraghian et al. 2007). Clague and Evans (2003) estimate the glaciolacustrine deposit to be of Middle or Early Pleistocene age. Latter glacial advances have consolidated the soil, leaving it very stiff. During both interglacial and postglacial periods the Thompson River has eroded the valley, leaving the clay heavily overconsolidated.

Continuous core samples were retrieved from two drilling campaigns conducted in 2013 and 2015. This core has provided the opportunity to observe and test specimens of this very stiff glaciolacustrine unit. The bedding thickness was observed to vary throughout the deposit, with 1 cm being a representative order of magnitude. Bedding has been observed to be weak or distorted at different depths (Figure J.1). This disturbance has been hypothesised to be the consequence of glacial overriding or early mass wasting. Eshraghian et al. (2007) suspect that the same disturbance processes also created pre-sheared discontinuities, resulting in preferential surfaces for failure to occur.

Down-cutting through the valley fill sediments during deglaciation has unloaded the soils and planar fissility parallel to the bedding has developed. Bedding-parallel fissility and the bedding of silt and clay layers itself are contributors to the strength anisotropy of this glaciolacustrine soil. This anisotropy may affect the shear strength that can be developed along the planar failure surfaces of the translational landslides.

Two main reasons have encouraged the authors to test the clay strength under direct simple shear (DSS):

- A major advantage of simple shear is that it allows for the rotation of the principal stresses during the test. Whereas, triaxial tests only allow for the exchange between the minor and major principal stress directions, thus predetermining the orientation of the stress condition at failure. Simple shear better mimics the in-situ stress condition along a potential failure surface (Figure J.2).

- Constant-volume DSS tests have the potential to measure the undrained response to shear. Dyvik et al. (1987) showed that the change in normal load required to maintain constant volume during a DSS test is equivalent to the change in pore water pressure. Thus, the DSS provides an effective stress path for a constant-load undrained test.

The DSS apparatus deforms the specimen in a simple shear fashion but does not impose a state of simple shear stress (Figure J.3). Resulting non-uniform distributions of shear and normal stress have been addressed several times in the literature (Prevost and Hoeeg 1976, Airey and Wood 1987, Grognet 2011). In spite of the criticism that this has raised against the DSS test (La Rochelle 1981, Saada and Townsend 1981), it is still admitted that the simple shear apparatus is a powerful measuring tool of the soil behaviour (Vucetic and Lacasse 1982). DSS tests have served many geotechnical studies, particularly the characterization of soft soils (Ladd and Edgers 1972, Mayne 1985), often through the use of the NGI-type DSS apparatus that was originally developed by Bjerrum and Landva (1966).

The clay under study well exceeds the stiffness and strength of soil typically tested with the NGI-type DSS apparatus. An issue of concern is slippage along the upper and lower surfaces of the specimen when only part of the shear force is transferred from the apparatus to the upper and lower surfaces of the specimen. Work on stiff soils by Burn (1968, on Leda Clay) and Lau (1988, on Cowden Till and London Clay) shows that addition of protruding pins to the platen surfaces avoids slippage.

The developments presented in this paper aim at identifying the special challenges of DSS tests on a very stiff clay. To this end, an adaptive methodology was used in the laboratory in order to overcome some of these challenges. Other difficulties remain and have been interpreted through laboratory observations, measured strengths and effective stress paths.

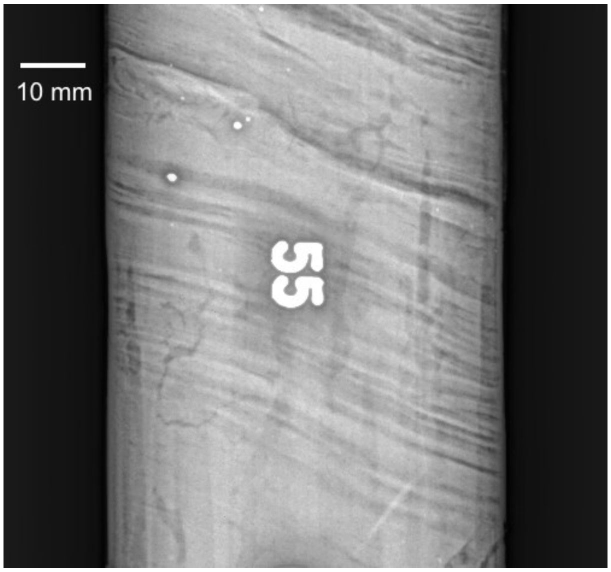

Figure J.1. Tilted lamination of the clay at a depth of 14.5m (x-ray radiography)

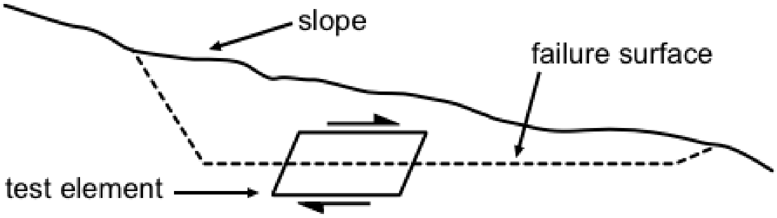
slope
failure surface
test element

Figure J.2. A DSS-relevant problem

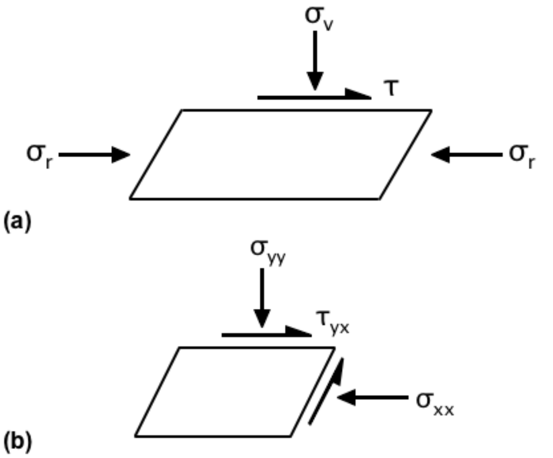
σ_v
τ
σ_r
σ_r
(a)
σ_{yy}
τ_{yx}
σ_{xx}
(b)

Figure J.3. Difference in the stress state between (a) the DSS apparatus and (b) the idealized simple shear

2. Sample characteristics

Soil samples tested with the DSS to produce the result presented within this paper were retrieved in May 2013. The core samples from the glaciolacustrine clay unit were sealed and stored in the moisture-controlled room of the University of Alberta before being tested with a DSS apparatus. The properties of these samples are presented in Table J.1. Samples appear as alternating grey silt and brown to grey clay. Other core samples were used for characterizing index properties (Figure J.4) and preconsolidation stresses (Figure J.5). Clay-size fraction often exceeds 50%. The range of measured preconsolidation stresses (2500-4000 kPa) confirms that the clay is heavily overconsolidated (*OCR* ≥ 10).

Table J.1. Samples selected for DSS tests

	S4	S6
Depth (m)	13.4	17.5
Specific gravity	2.81	2.81
Water content (%)	32	26
Plastic limit (%)	22	25
Liquid limit (%)	55	53
In-situ effective stress	178	220

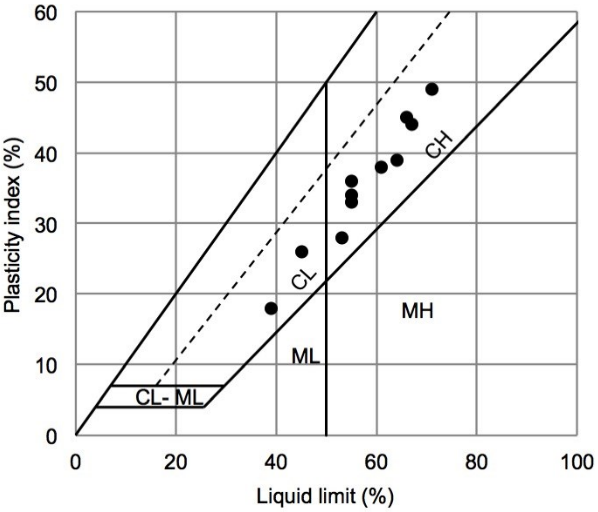

Figure J.4. Plasticity chart

3. Methodology

DSS tests were performed at the MEG Technical Services (Richmond, BC) laboratory. The NGI-type apparatus supplied by GDS Instruments complies with the ASTM standard (2007). Intact clay specimens were trimmed to approximately a height of 16 mm and a diameter of 48.5 mm. It is fitted inside a rubber membrane reinforced by a stack of low-friction rigid rings (Figure J.6). These rings provided lateral confinement so a K_o condition can be attained.

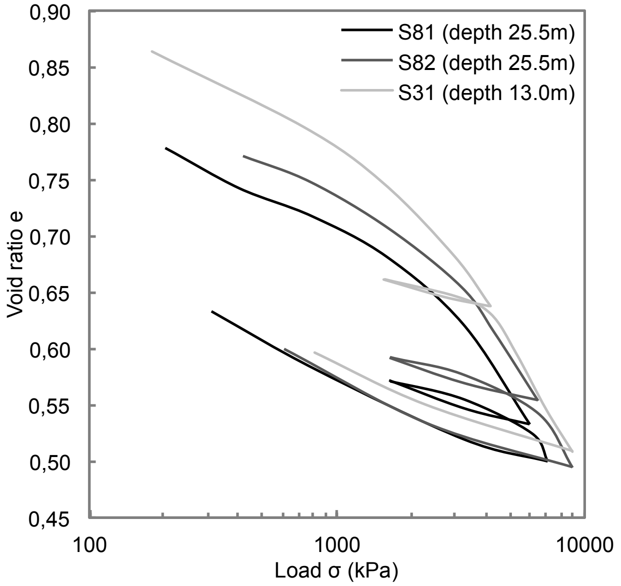

Figure J.5. Consolidation curves

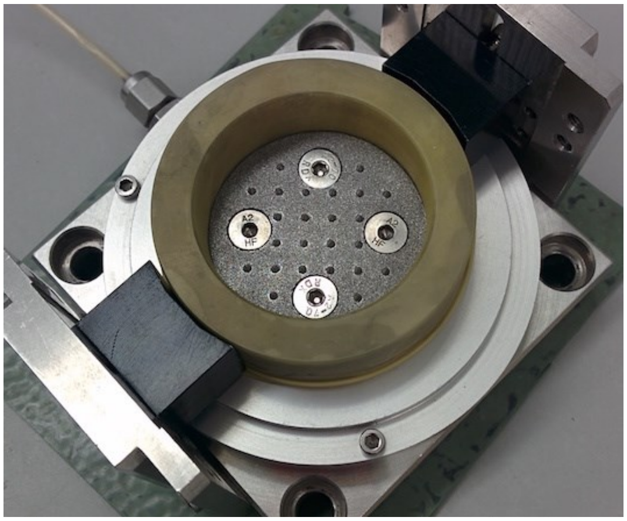

Figure J.6. Pedestal, bottom platen, confining rings stack and membrane (ø48.5 mm)

Schafer (2014) presents a first series of tests conducted on Sample S4 using the standard porous ceramic platens on the top and bottom of the specimens. These platens rely on 1-mm deep and 2-mm wide grooves transverse to the direction of shearing to provide a no-slip boundary condition. While this setup is suited for most soft soils, it was not sufficient for the glaciolacustrine clay from our study site. Under the consolidation load, this very stiff clay did not embed into the grooves to provide enough friction at the soil-platen interface. As a result slippage occurred at the soil-platen interface and little simple shear deformation was achieved. The subsequent testing was conducted with modified platens. These platens have conical pins (height: 1.9 mm; base diameter: 1.9 mm; spaced every 6.0 mm) to provide a better interlock with the clay (Figure J.6). This is similar to work presented by Burn (1968) which found that the use of platens equipped with protruding pins was effective in limiting slippage. The clay is reconsolidated to the estimated in situ vertical stress, as in the Recompression technique (Bjerrum 1973). This consolidation was completed overnight in a single stage. Prior consolidation under higher stresses as in the SHANSEP technique (Ladd 1991) is inappropriate: mechanical overconsolidation would break down inherent structure and misrepresent the natural preconsolidation mechanism of this clay.

The shear strain rate $\dot{\gamma}$ was set to 5%/hour based on ASTM standard D6528 for DSS. Results from this testing raised concern that the observed pore pressure response was a function of the strain rate. To investigate this other tests were conducted at lower strain rates (Table J.2).

Table J.2. Parameters of the DSS tests

Sample	Test	Shear strain rate $\dot{\gamma}$ (%/h)	Consolidation load σ'_{v0} (kPa)	Applied shear strain γ (mm)	Amount of slippage $\gamma_{slippage}$ (mm)
S4	S4a	5	300	3.2	1.8
	S4b	5	500	3.2	1.8
	S4c	5	200	3.0	2.7
	M4a[1]	5	300	3.2	>2.5
	M4b[1]	5	500	3.2	>2.5
S6	S6a	1	300	1.9	1.5
	S6b	5	300	3.2	2.2
	S6c	5	300	3.2	>2.5
	S6d	0.5	300	3.2	>2.5

[1] tests by Schafer (2014) using the default platens

4. Results

Slippage occurred along the lower surface of the specimen except in Test S6a where it was observed along both the lower and the upper surface. It was quantified by measuring the displacement of the bottom most (or topmost) confining ring with respect to the apparatus frame. When this was not achieved slippage was observed to be most of the applied displacement (>2.5 mm). Table J.2 compiles the observed amounts of slippage.

Slippage occurs in all tests but is limited compared to Tests M4a and M4b. Slippage starts after an amount of strain has been already been applied, and when the shear force exceeds the amount of friction that can be mobilized at the soil platen-interface. Protruding pins did increase this strength but was not sufficient to prevent the slippage shown in Figure J.7.a.

After the onset of slippage, the specimen continues deforming. However not all of the displacement imposed by the apparatus turns into actual shear strain of the specimen. This varies depending on the test and is difficult to quantify. For Tests S4a, S4b and S6b observation suggests that strain is focused in the boundary zone, i.e. near the specimen surface affected by slippage (Figure J.7.b). In the boundary zone, the shear strength that can be mobilized changes as the pins cut through the soil. Slippage and shear in the boundary zone are interrelated and simultaneous.

Stress-strain relationships for this mode of failure are illustrated in Figure J.8. These do not exhibit sharp peak strength. They are different from the stress-strain relationship to be expected for stiff heavily overconsolidated clay. The observed response is more reminiscent of a softened and disturbed clay.

The relationship between pore water pressure change and shear strain is equally surprising. The heavily overconsolidated clay exhibits a contractive response whereas this material is typically dilative.

The observation of the pore pressure response within a heavily overconsolidated clay like this raised questions. It must be noted that the pore water pressure is indirectly measured. The drained, constant volume condition simulates the undrained, constant load condition. What is interpreted as the change in pore water pressure actually is the change in normal stress.

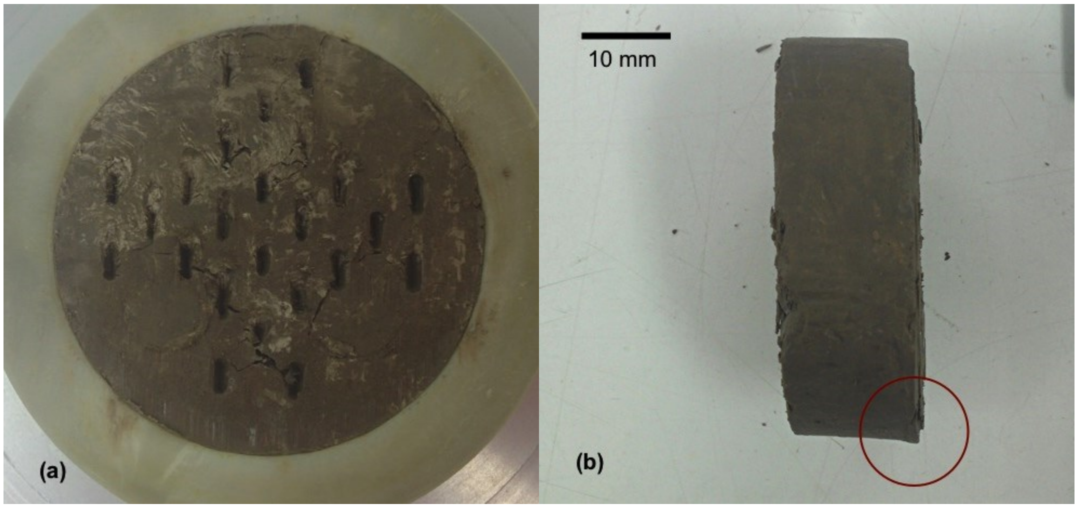

Figure J.7. Evidence of (a) slippage on the surface of sheared Specimen S4c and (b) strain localized in the boundary zone of sheared Specimen S4b

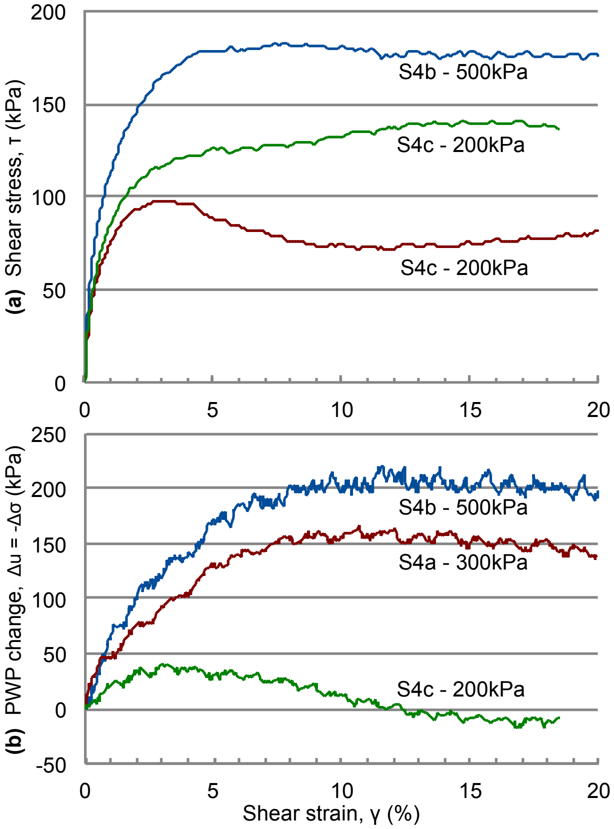

Figure J.8. (a) Stress vs. strain curve and (b) pore water pressure change vs. strain curve

5. Strain rates

The response to undrained constant-load DSS is simulated by a drained constant-volume DSS test. Fully drained conditions are essential to this test. Dissipation of excess pore water pressure is associated with a volumetric response of the soil, resisted by a change in normal stress in the constant volume test. Non-dissipated pore pressures do not create a volumetric response so cannot be measured by the change in normal stress. The test shear strain rate must be low enough to ensure all shear induced pore pressures are dissipated.

Common practice in the DSS test is to set the shear strain rate $\dot{\gamma}$ to 5%/hour or such that the time to failure exceeds twice the time for 90% consolidation t_{90} as determined during the consolidation stage of the test (ASTM D6528 2007). The latter condition appears verified at $\dot{\gamma}$ = 5%/hour, after interpretation of consolidation data. However applied normal stresses are much less than the preconsolidation stress, thus maintaining the clay in the heavily overconsolidated domain. When sheared the overconsolidated clay softens locally. The coefficient of consolidation c_v in the normally consolidated range better represents dissipation of shear induced pore water pressures. For very stiff, overconsolidated clay, the ASTM standard for direct shear (ASTM D3080 2011) suggests c_v is relevant if derived from normal strain versus log time in the normally consolidated range.

Results of complementary oedometer tests make obvious the difference in cv of about one order of magnitude between the normally consolidated (NC) and heavily overconsolidated (HOC) ranges (Figure J.9). The consolidation stage of DSS tests is irrelevant to the choice of a proper strain rate. Given a c_v value of 10^{-8} m^2/s is very low, the commonly used $\dot{\gamma}$ value of 5%/hour may not maintain excess pore water pressures near zero.

The impact of shear strain rate $\dot{\gamma}$ is investigated on Sample S6. Figure J.10 illustrates the comparison between Test S6a ($\dot{\gamma}$ = 1%/hour) and S6b ($\dot{\gamma}$ = 5%/hour). Test S6a yields the behaviour expected for heavily overconsolidated clay. The response is dilative and the undrained shear strength is considerably larger.

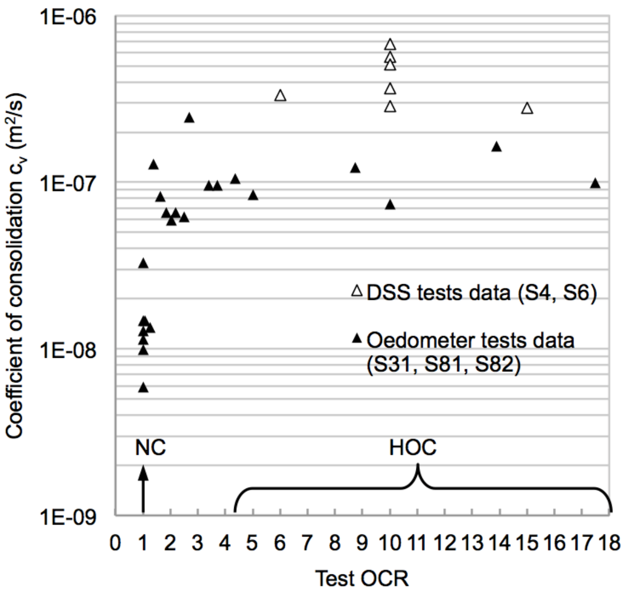

Figure J.9. Consolidation data from oedometer and DSS tests

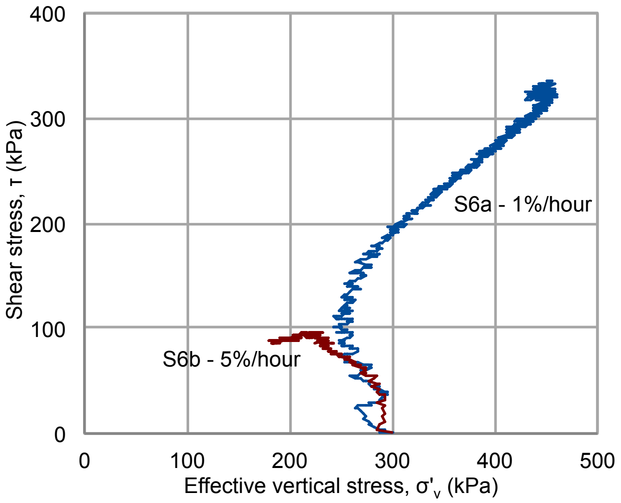

Figure J.10. Effective stress paths for Tests S6a (1%/hour) and S6b (5%/hour)

6. Discussion

Embedment of protruding pins in a very stiff soil is suspected to create uneven stress concentration in the boundary zone. This leads to strain localization, so uniform simple shear strain is not achieved anymore. The boundary zone becomes a preferential shear location.

Slippage itself has little influence on the volumetric response of the soil. Tests S4c, S6c and S6d show that most of the applied displacement results into slippage. The measured pore water pressure exhibits little amplitude ($|\Delta u| \leq 50$ kPa). However slippage means that the protruding pins have to cut through the clay, thus softening it even more. Slippage itself encourages localization of strain in the boundary zone. These issues add to the non-uniformities pointed out by the literature mentioned earlier.

Shear preferentially occurs in the boundary zone (Tests S4a, S4b and S6b), where the soil lost its heavily overconsolidated characteristic. The softened clay is not dilative anymore and subsequent volumetric response is contractive.

Test S6a conducted at a shear strain rate of 1%/hour suggests that the strain rate impacts the measured response. Fast shear strain rate (e.g. 5%/hour) does not allow equalization of the shear induced pore water pressures. Negative pore water pressures generated in the middle of the specimen do not dissipate readily, resulting in higher effective normal stress in the middle of the specimen than in the boundary zone. Fast shear strain rate do not allow for the distribution of effective normal stress to be equilibrated. Such non-uniformities contribute in making the boundary zone a preferential location for failure. However Test S6d ($\dot{\gamma}$ = 0.5 %/hour), shows that a slow shear strain rate does not ensure shear to not localize in the boundary zone.

Tests at a sufficiently small strain rate yield representative undrained conditions. Limited slippage allows the soil shear strength to be measured. However large non-uniformities remain and the soil tends to fail by default in the boundary zone. The response is by no means that of uniform simple shear. The inability to apply the condition of undrained simple shear questions the relevancy of the DSS test.

The DSS test was chosen for its ability to account for strength anisotropy but fails at doing so because non-uniformities control the location of shear failure. Therefore it shows no advantage over the direct shear test, in the case of a very stiff clay tested in its heavily overconsolidated range. Direct shear and ring shear tests will complete the characterization of the shear strength of this soil.

7. Conclusion

DSS tests were motivated by the potential strength anisotropy and undrained behaviour of a very stiff glaciolacustrine clay implicated in slope instability.

The higher strength and stiffness of the materials resulted in difficulties in testing with the DSS apparatus. This included slippage along the soil-platen interface. The platens for the DSS testing apparatus were modified so as to include pins that protrude into the specimens so as to limit the slippage of the specimens along the soil-platen interface. Slippage was limited but not eliminated.

Effective stress paths results showed that the strain rates commonly used in DSS tests are not applicable for this clay of low permeability and high overconsolidation ratio. Consolidation properties relevant to the dissipation of shear induced pore water pressure are those of the normally consolidated range of the soil.

For this very stiff glaciolacustrine clay, uniform simple shear cannot be applied without adverse conditions developing near the soil-platen interface: at this location the soil is softened and loses its heavily overconsolidated characteristics, i.e. brittleness and dilatancy. Slippage and non-equalized pore water pressures are aggravating factors. In consequence tests fail to yield the response of a heavily overconsolidated clay.

In the authors' opinion, DSS testing with the current apparatus is impractical to test the strength of very stiff clays.

References

Airey, D. and Wood, D. 1987. An evaluation of direct simple shear tests on clay, *Géotechnique,* 37(1): 25-35.

ASTM. 2011. *D3080. Standard Test Method for Direct Shear Test of Soils Under Consolidated Drained Conditions,* ASTM International.

ASTM. 2007. *D6528. Standard Test Method for Consolidated Undrained Direct Simple Shear Testing of Cohesive Soils,* ASTM International.

Bjerrum, L. 1973. Problems of soil mechanics and construction on soft clays and structurally unstable soils (collapsible expansive and others), *Proc. Eighth Int. Conf. on Soil Mech. and Found. Engng.,* Moscow, 3: 111-159.

Bjerrum, L. and Landva, A. 1966. Direct simple-shear tests on a Norwegian quick clay, *Géotechnique,* 16(1): 1-20.

Burn, K. 1968. *Direct Simple Shear Tests on Leda Clay. Internal Report No. 363 of the Division of Building Research,* National Research Council of Canada.

Clague, J. and Evans, S. 2003. Geologic Framework of Large Historic Landslides in Thompson River Valley, British Columbia, *Environmental & Engineering Geoscience*, 9(3): 201-212.

Dyvik, R., Berre, T., Lacasse, S. and Raadim, B. 1987. Comparison of truly undrained and constant volume direct simple shear tests, *Géotechnique*, 37(1): 3-10.

Eshraghian, A., Martin, C. and Cruden, D. 2007. Complex Earth Slides in the Thompson River Valley, Ashcroft, British Columbia. *Environmental & Engineering Geoscience*, 13(2): 161-181.

Grognet, M. 2011. *The boundary conditions in direct simple shear tests: development for peat testing at low vertical stress*, M.Sc. thesis, Delft University of Technology.

Hendry, M., Macciotta, R., Martin, C. and Reich, B. 2015. Effect of Thompson River elevation on velocity and instability of Ripley Slide, *Canadian Geotechnical Journal*, 52: 1-11.

La Rochelle, P. 1981. Limitations of direct simple shear test devices, *ASTM Spec. Tech. Publ.,* (740): 653-658.

Ladd, C. 1991. Stability evaluation during staged construction, *Journal of Geotechnical Engineering*, ASCE , 117(4): 540-615.

Ladd, C. and Edgers, L. 1972. *Consolidated-undrained direct simple shear tests on saturated clays,* Research Report R 72-82, Department of Civil Engineering, Massachusetts Institute of Technology.

Lau, W. 1988. *Behaviour of clay in simple shear and triaxial tests,* Ph.D. thesis, The City University, London.

Mayne, P. 1985. A review of undrained strength in direct simple shear, *Soils and Foundations*, 25(3): 64-72.

Prevost, J. and Hoeeg, K. 1976. Reanalysis of simple shear soil testing, *Canadian Geotechnical Journal*, 13(4): 418-429.

Saada, A. and Townsend, F. 1981. State of the art: laboratory strength testing of soils, *ASTM Spec. Tech. Publ.,* (740): 7-77.

Schafer, M. 2014. *Personal communication*, May 21, 2015.

Schafer, M., Macciotta, R., Hendry, M., Martin, C., Bunce, C., Choi, E. and Edwards, T. 2015. Instrumenting and Monitoring a Slow Moving Landslide, *68th Canadian Geotechnical Conference,* Québec City.

Vucetic, M. and Lacasse, S. 1982. Specimen size effect in simple shear test, *Journal of Geotechnical Engineering*, 108(GT12): 1567-1585